2014

QUANTIFICATION OF FACTORS GOVERNING DRUG RELEASE KINETICS FROM NANOPARTICLES: A COMBINED EXPERIMENTAL AND MECHANISTIC MODELING APPROACH

Kyle Daniel Fugit
University of Kentucky, kdfugit@gmail.com

STUDENT AGREEMENT:

I represent that my thesis or dissertation and abstract are my original work. Proper attribution has been given to all outside sources. I understand that I am solely responsible for obtaining any needed copyright permissions. I have obtained needed written permission statement(s) from the owner(s) of each third-party copyrighted matter to be included in my work, allowing electronic distribution (if such use is not permitted by the fair use doctrine) which will be submitted to UKnowledge as Additional File.

I hereby grant to The University of Kentucky and its agents the irrevocable, non-exclusive, and royalty-free license to archive and make accessible my work in whole or in part in all forms of media, now or hereafter known. I agree that the document mentioned above may be made available immediately for worldwide access unless an embargo applies.

I retain all other ownership rights to the copyright of my work. I also retain the right to use in future works (such as articles or books) all or part of my work. I understand that I am free to register the copyright to my work.

REVIEW, APPROVAL AND ACCEPTANCE

The document mentioned above has been reviewed and accepted by the student's advisor, on behalf of the advisory committee, and by the Director of Graduate Studies (DGS), on behalf of the program; we verify that this is the final, approved version of the student's thesis including all changes required by the advisory committee. The undersigned agree to abide by the statements above.

Kyle Daniel Fugit, Student

Dr. Bradley D. Anderson, Major Professor

Dr. Jim Pauly, Director of Graduate Studies

QUANTIFICATION OF FACTORS GOVERNING DRUG RELEASE KINETICS FROM NANOPARTICLES: A COMBINED EXPERIMENTAL AND MECHANISTIC MODELING APPROACH

DISSERTATION

A dissertation submitted in partial fulfillment of the requirements for the degree of Doctor of Philosophy in the College of Pharmacy at the University of Kentucky

By
Kyle Daniel Fugit

Lexington, Kentucky

Director: Dr. Bradley D. Anderson, Professor of Pharmaceutical Sciences

Lexington, Kentucky

2014

ABSTRACT OF DISSERTATION

QUANTIFICATION OF FACTORS GOVERNING DRUG RELEASE KINETICS FROM NANOPARTICLES: A COMBINED EXPERIMENTAL AND MECHANISTIC MODELING APPROACH

Advancements in nanoparticle drug delivery of anticancer agents require mathematical models capable of predicting *in vivo* formulation performance from *in vitro* characterization studies. Such models must identify and incorporate the physicochemical properties of the therapeutic agent and nanoparticle driving *in vivo* drug release. This work identifies these factors for two nanoparticle formulations of anticancer agents using an approach which develops mechanistic mathematical models in conjunction with experimental studies.

A non-sink ultrafiltration method was developed to monitor liposomal release kinetics of the anticancer agent topotecan. Mathematical modeling allowed simultaneous determination of drug permeability and interfacial binding to the bilayer from release data. This method also quantified the effects of topotecan dimerization and surface potential on total amount of drug released from these liposomal formulations. The pH-sensitive release of topotecan from unilamellar vesicles was subsequently evaluated with this method. A mechanistic model identified three permeable species in which the zwitterionic lactone form of topotecan was the most permeable. Ring-closing kinetics of topotecan from its carboxylate to lactone form were found to be rate-limiting for topotecan drug release in the neutral pH region.

Models were also developed to non-invasively analyze release kinetics of actively-loaded liposomal formulations of topotecan *in vivo*. The fluorescence excitation spectra of released topotecan were used to observe release kinetics in aqueous solution and human plasma. Simulations of the intravesicular pH in the various release media indicated accelerated release in plasma was a consequence of increased intravesicular pH due to ammonia levels in the plasma instead of alterations in bilayer integrity. Further

studies were performed to understand the roles of dimerization, ion-pairing, and precipitation on loading and release kinetics obtained from actively-loaded topotecan.

Extension of this type of modeling for other types of nanoparticles was illustrated with doxorubicin-conjugated polymeric micelles. Mathematical modeling of experimental studies monitoring doxorubicin release identified conjugation stability during storage, hydrazone hydrolysis kinetics, and unconjugated doxorubicin partitioning affected micellar doxorubicin release. This work identifies several of the key parameters governing drug release from these liposomal and micellar nanoparticles and lays the framework for future development of *in vivo* release models for these formulations.

KEYWORDS: Drug Release Kinetics, Liposomes, Micelles, Topotecan, Doxorubicin

Kyle D. Fugit
Student's Signature

July 31, 2014
Date

QUANTIFICATION OF FACTORS GOVERNING DRUG RELEASE KINETICS FROM NANOPARTICLES: A COMBINED EXPERIMENTAL AND MECHANISTIC MODELING APPROACH

By

Kyle Daniel Fugit

Bradley D. Anderson
Director of Dissertation

Jim Pauly
Director of Graduate Studies

July 31, 2014
Date

Dedicated To

My wife, parents, and grandparents

Without their love and support, none of this would be possible

ACKNOWLEDGMENTS

While this dissertation is the full body of my own work, contributions from many has strengthened its message. No one more so than my dissertation advisor, Dr. Bradley Anderson, whose insights, thought processes, and wealth of knowledge have molded me into a sound researcher and prepared me for my future career in science. My exponential growth as a scientist during the completion of this dissertation has been in a large part to his exceptional mentoring. I would like to thank my committee members: Drs. Zach Hilt, Paul Bummer, and Markos Leggos, whose expertise, comments, and questions have also improved the quality of my dissertation. I would also like to thank my outside examiner, Dr. Thomas Dziubla for his comments and time reviewing this dissertation. I would also like to thank Drs. Younsoo Bae and Andrei Ponta for the opportunity to collaborate with them on the characterization of their polymeric micelles as well as Drs. Amar Jyoti and Menakshi Upreti whose biological insights were invaluable to our collaborative project examining liposomal drug release in human plasma. And of course, I must thank the funding which provided with the opportunity to conduct. The resources and funding fellowships from the National Science Foundation and National Cancer Institute provided were instrumental in the success of this project.

I have had much encouragement and support during the dissertation process and graduate school. My lab members, Sweta, Dhaval, Michael, Pekka, aided my development through their encouraging words and technical knowledge in many of the experimental methods I used in the completion of this dissertation. I must also thank several summer students: Jill, Erinn, Amy, Laura, NK, and Kim whom I had the privilege of mentoring and whose small projects provided useful information in developing the

path for this dissertation. I must also thank Nico for assisting with data collection during his rotation in our lab. I hope that they benefited from my instruction and teaching as I much as I benefited from my experience mentoring them.

On a more personal note, I must thank all of my friends and family for the emotional support they provided me during my time in graduate school. My fellow friends from graduate school and those I have met during my time here in Lexington have been a true blessing and an immeasurable source of relief during some of the most challenging times I have encountered in my life. But more importantly is the support from my family. The Fugits, Martins, and Wiesners have always believed in me and molded me into the man I am today. No more so than my parents, Dan and Kristi, my sister, Kati, and my grandparents: Jim, Shirley, and Hazel who have shown great love and support throughout my life. I am truly blessed to have such a remarkable family.

Most important of all, I must thank my wife, Ann (the 1st Dr. Fugit). Words cannot begin to explain what the past five years with her has done for me. To say I am a better man for having her in my life is an understatement. The love and support, but most importantly the patience, she has given to me during this process is more than I can comprehend. Luckily, I have the privilege of spending the rest of my life trying to live up to the amazing woman that she is.

TABLE OF CONTENTS

LIST OF TABLES

LIST OF SCHEMES

LIST OF FIGURES

CHAPTER ONE

Statement of Aims

Much has been made of the potential of nanoparticles as drug delivery vehicles due to their unique properties (e.g. size, shape, surface chemistry); however, few nanoparticle formulations have been approved for clinical use. The low percentage of approved nanoparticle formulations is partially due to the current trial-by-error approach generally used in the development of these formulations. Such a haphazard way to develop successful nanoparticle formulations is time-consuming and expensive and must be improved to increase the success of nanomedicines. Furthermore, most *in vitro* characterization studies of nanoparticle release kinetics do not critically evaluate the factors governing observed release let alone provide any idea whether these studies are able to predict release *in vivo*.

The application of mechanistic mathematical models supported by experimental studies is necessary to rationally optimize nanoparticle drug delivery systems and begin the critical task of correlating *in vitro* release characteristics to *in vivo* performance. To this end, the use of mechanistic models to characterize *in vitro* release kinetics must incorporate thermodynamic (e.g. drug ionization state, self-association, interfacial binding) and kinetic (e.g. drug species' permeability and/or kinetics of drug degradation of drug, particle, and/or drug-particle linkages) properties inherent to the drug/particle system. Furthermore, these models must also account for the specific effects of the method used to monitor release, such as drug transport through a dialysis membrane or sink vs. non-sink conditions. This thesis focuses on developing an approach that combines experimental studies with supporting mechanistic mathematical models capable of identifying the factors governing nanoparticle drug release. The aims outlined below were pursued to advance understanding of factors which affect nanoparticle drug release kinetics and provide

examples for future approaches to analyzing drug release kinetics and developing models capable of predicting drug release.

I. **Develop and validate a non-sink method to simultaneously determine both liposomal release kinetics and apparent binding coefficients of topotecan to the lipid bilayer using mathematical modeling.**

An ultrafiltration method was developed and validated to separate encapsulated from free drug to monitor liposomal release kinetics under non-sink conditions. Using a mathematical model that considered both drug permeability and binding to the bilayer-solution interface allowed for both constants to be determined simultaneously from the same experiment. With modification, the model could also describe release kinetics under sink conditions maintained by dynamic dialysis.

II. **A mechanistic model to assess the pH-sensitive release of liposomal topotecan was developed and experimentally validated**

Using the developed non-sink method, experimental studies were conducted to observe the pH-dependent release of passively-loaded liposomal topotecan. Based on these profiles, further studies were conducted to analyze the pKa governing topotecan ionization in the low-to-neutral pH region. The kinetics of reversible, pH-dependent, ring-opening/closing interconversion of the drug between its lactone and ring-opened carboxylate forms was also assessed to clearly determine the contribution of the various topotecan species contributing to drug release.

III. **A non-invasive method was developed to monitor liposomal release kinetics in human plasma and reveal the effect of ammonia levels on intravesicular pH and accelerated release**

A spectroscopic fluorescence method was developed to monitor liposomal release kinetics of topotecan in plasma in real-time. A mathematical model was

developed to compare the release kinetics obtained from this fluorescence method with those determined by HPLC. Lastly, the accelerated release seen in plasma was correlated with the ammonia concentration in plasma using simulations to account for the effects of transbilayer ammonia transport on intravesicular pH.

IV. **Mechanistic mathematical models were developed to identify the factors contributing to experimentally observed loading and release kinetics of actively-loaded liposomal formulations of topotecan**

The kinetics of topotecan active loading was monitored at 37 °C and a mechanistic model was developed which incorporated transport of ion pairs of topotecan with excess chloride in solution. The model was validated with studies that showed slowed release in the absence of excess chloride. Further studies focusing on release from these formulations corroborated these factors using mechanistic models developed to describe release. Lastly, differences in release kinetics between formulations loaded at 37 and 60 °C were assessed. Mechanistic modeling of these release profiles implicated precipitation of a HCl salt of topotecan as the primary cause of the extended release kinetics observed from liposomal topotecan formulations actively-loaded at 60 °C.

V. **A mechanistic model was constructed to characterize the experimental release kinetics of doxorubicin-conjugated polymeric micelles using an approach similar to that used to characterize liposomal drug release kinetics**

The approach used to developed mechanistic models for liposomal drug release was extended to characterize drug release from polymeric micelle nanoparticles. Experimental release studies of doxorubicin conjugated to block copolymers via a pH-sensitive hydrazone linkage were mechanistically modeled. As a result of modeling, instability of the hydrazone linkage during storage and partitioning of

unconjugated doxorubicin into the micellar phase were identified as important factors in the release kinetics as determined by dynamic dialysis.

CHAPTER TWO

Introduction

2.1 Nanotechnology and chemotherapy

Treating cancer with conventional therapeutic agents presents many challenges from both a clinical and physicochemical standpoint. Many chemotherapeutics result in high systemic toxicity due to their nonspecific actions upon DNA repair and/or cell replication.[1] Such toxicity limits the therapeutic doses possible. High systemic clearance and protein binding also limit tumor exposure to many of the anticancer agents already approved or currently under development. Improving clinical efficacy of these chemotherapeutic agents requires increasing tumor exposure while reducing systemic toxicity. From a formulation standpoint, strategies to increase drug solubility, shield drugs from rapid clearance (e.g. extend release), and/or target the tumor vasculature would increase the effectiveness of chemotherapeutic agents. Nanoparticle delivery systems satisfy many of these requirements.

A wide array of nanoparticles has been extensively explored as drug carriers for the treatment of cancer.[2-4] These nanoparticulate systems are attractive for pharmaceutical applications due to their ability to entrap and release drug payloads in a manner capable of altering pharmacokinetics via increased drug solubility or extended release from the particle.[3, 5] Their unique size is also advantageous for passively targeting the particles and their drug payloads to solid tumors due to the enhanced permeation and retention (EPR) effect. This effect is a result of the leaky vasculature within the tumor environment produced by rapid tumor angiogenesis. Fenestrations between endothelial junctions allow nanoparticles that cannot penetrate healthy vasculature to reach tumor tissue.[6-9] In addition to the benefits of nanoparticle size, a multitude of chemical surface modifications may further reduce systemic toxicity through active targeting. Modifying the surface of

these particles with various oligomers that are recognized by receptors overexpressed or unique to cancer cells provides the means to actively target cancer cells.[3-5, 10-13] Active targeting in this context has the potential to increase drug accumulation at the tumor site;[5, 14, 15] it may also allow drugs to bypass efflux transporters overexpressed in drug resistant cancer cells.[7, 16-19]

Many types of nanoformulations have been developed to take advantage of these properties but few have had clinical success.[20] Part of this low success rate may be attributable to differences in release rates observed during *in vitro* characterization studies and those occurring *in vivo*. This is supported by investigations that have shown antitumor efficacy of drug-loaded nanoparticle formulations is linked to drug release rates.[21-24] Many physiological factors (i.e. age, gender, dose regimen, type or location of cancer, mononuclear phagocyte system)[25] have been hypothesized to contribute to a disparity between *in vitro* drug release and the pharmacokinetics (PK) and pharmacodynamics (PD) frequently seen with nanoparticle formulations of anticancer agents. However, correlations between nanoparticle efficacy and these proposed factors remain untested.[26, 27] Understanding the contributions of these various factors to alterations in drug release kinetics from nanoparticles will require a combined approach of experimental techniques and mechanism-based mathematical models. Such an understanding will ultimately aid in the design of models capable of reliably predicting *in vivo* formulation performance and offer insights into ways to minimize these physiological effects on nanoformulations.

2.2 Liposomes

Liposomal formulations offer several potential advantages for the intravenous delivery of antitumor agents due to their ability to increase drug solubility, reduce drug toxicity, and prolong drug release.[3] These liposomes are generally composed of an aqueous core

surrounded by one or more lipid bilayers. Most liposomes range between 50 and 600 nm in diameter. Large unilamellar vesicles (LUV's) (i.e. liposomes with only a single bilayer) typically range between 50 and 200 nm in diameter (Figure 2.1). LUV's are advantageous for developing controlled release strategies and ideal for modeling and studying release kinetics because: 1) a single bilayer provides a single barrier domain as opposed to the heterogeneous barrier properties of multilamellar vesicles;[28] and 2) the bilayer properties are minimally altered by curvature effects that reduce chain order in the bilayer.[28, 29]

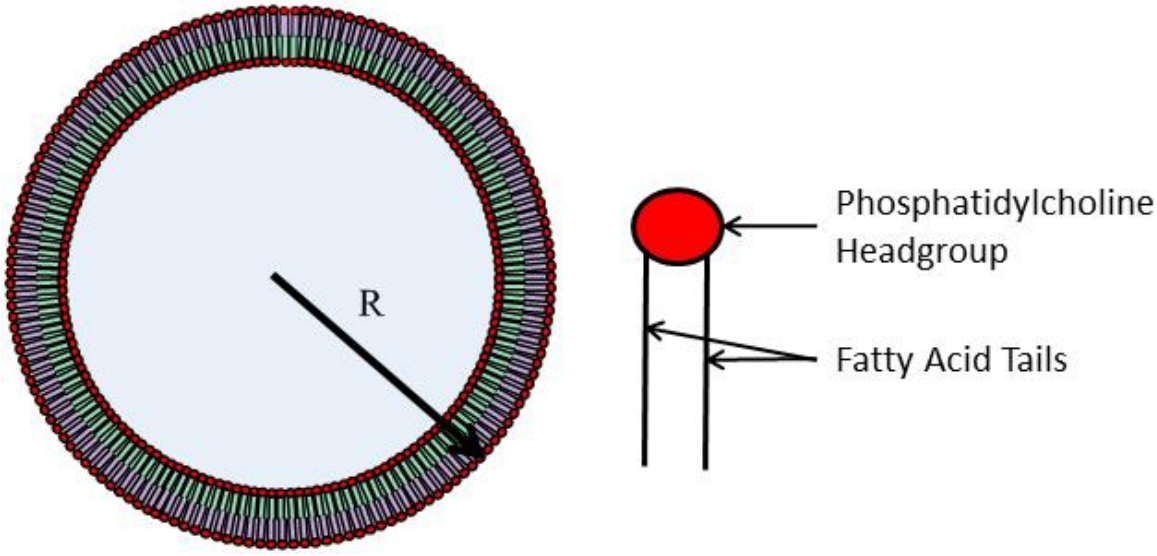

Figure 2.1. An illustration of a liposome used in this thesis. The liposome of radius R forms a single bilayer composed of phospholipids. The phospholipids comprising the inner and outer leaflet of the bilayer (green and purple, respectively) are composed of a hydrophobic fatty acid tail and a hydrophilic phosphatidylcholine headgroup.

Pegylated liposomes have the added benefit of longer systemic circulation due to reduced clearance by the mononuclear phagocytic system. [3, 30-32] This prolonged circulation time when combined with an appropriate particle size provides enhanced delivery of liposomes to solid tumors due to the EPR effect. [3, 8, 31] These properties have led to the FDA-approved liposomal formulation of doxorubicin (DOXIL®) as well as other drug products,

including several currently in clinical trials.[33-40] Functionalization of the liposome surface with specific moieties also makes possible active targeting strategies utilizing receptors that are highly expressed and specific to various cancer types.[3, 7, 16, 40-42]

2.2.1 Factors governing liposomal drug release

The release of drugs from liposomes is dependent upon a multitude of factors. These factors can be divided into two major categories: properties associated with the bilayer structure and those associated with the aqueous compartments.

The structure of the bilayer is quite complex, with various regions of hydrophobicity and 3-dimensional order that may interact with drug molecules in specific ways; however, the hydrophobic domain of the inner bilayer is typically viewed as the rate-limiting barrier governing drug permeability in bilayers.[43-46] The bulk solubility-diffusion model described over a century ago by Overton was one of the earliest attempts to account for the properties of bilayers that govern permeability[47, 48] and is still sometimes used. The model relates permeability, P^m, to the oil-water partition coefficient of the solute, K, the diffusion coefficient of said solute through this oil phase, and the thickness of the bilayer, h. This relationship is illustrated by the equation below.

$$P^m = \frac{KD}{h} \tag{1}$$

This equation clearly illustrates the dependence of permeability upon both the ability of the solute to partition into the bilayer and its diffusivity through the bilayer. The dependence on partitioning qualitatively explains why ionized compounds are generally impermeable to bilayer membranes as the free energy for charged species to partition into the bilayer are much higher than those of neutral compounds.[28, 49-51]

This model is overly simplistic, however. It fails to account for the differences in permeability seen with different bilayer compositions and the drastic reductions in permeability seen as the size of the solute increases. The bulk solubility-diffusion model is unable to capture the effects of the ordered structure of the bilayer's fatty acid tails. This chain ordering effect provides an additional resistance to drug diffusion and an entropic barrier to solute (i.e. drug) partitioning, which is also required for transport across the bilayer.[28, 51, 52] This free-surface-area theory explains why lipids that form rigid gel phases (and higher surface densities) result in lower permeabilities for larger molecules.[49, 52] Even the sudden and large increases seen in transport when the bilayer undergoes a phase transition from its more rigid gel phase to a liquid crystalline environment with increases in temperature may be explained by the more loosely-packed structure of the bilayer..[50, 53] The longer-chain phospholipids used here (see Figure 2.2) exist in the gel phase under physiological conditions and are used to slow release.[49, 50] Further study of the bilayer properties was not a focus of this thesis.

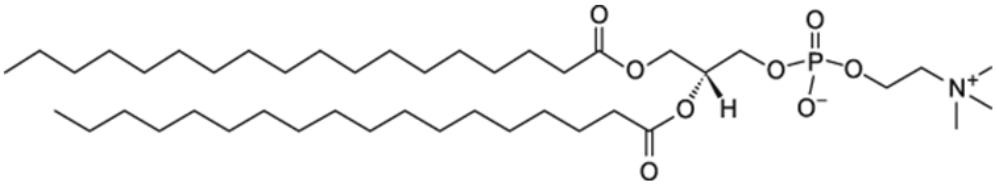

1,2-distearoyl-*sn*-glycero-3-phosphocholine (DSPC)

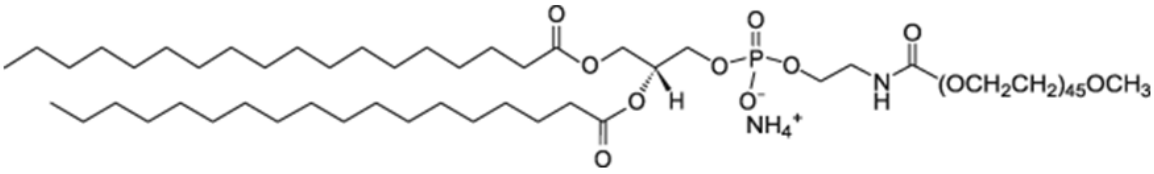

1,2-distearoyl-*sn*-glycero-3-phosphoethanolamine-N-[methoxy(polyethylene glycol)-2000] (ammonium salt) (DSPE-PEG2K)

Figure 2.2 Phospholipids used for liposomal formulations used within this thesis.

When considering release kinetics, determination of the various drug species that are permeable and subsequently their respective permeabilities is crucial. As mentioned previously, the ionization state of drugs and small molecules has been shown to alter release kinetics,[49, 50, 52] Permeability determinations for each ionization state of the drug are therefore crucial to developing mechanistic models governing liposomal drug release. The populations of these ionization states and other equilibria or kinetic events in solution may alter the driving force governing the kinetics of drug release. These factors may include drug self-association, complexation, precipitation, and/or kinetic events which reduce the amount of permeable specie(s) present in solution. The studies conducted in this thesis focus heavily on the physiochemical properties of the drug in the aqueous compartments.

In addition to these physicochemical properties, physiological processes and/or conditions may also affect liposomal drug release. Bilayer integrity may be compromised by the particles' interactions with proteins (e.g. vesicle binding and particle opsonization)[54-57] or osmotic stresses[58, 59] while in circulation or at the tumor site. Other factors such as the influx of other permeable species may alter the conditions of the aqueous compartment *in vivo* and accelerate release.[60] Some of these effects are observed and identified within this thesis.

With a thorough understanding of the physiochemical and biological phenomena that affect liposomal drug release, predictable and tunable drug release may be engineered for these types of formulations. Developing models that incorporate these properties and mechanistically describe their effect on drug release kinetics is vital to a rational development process and one of the principal subjects of this thesis.

2.2.2 Loading Strategies

Implementation of mechanistic models requires an understanding of the loading methods used to entrap drug within the intravesicular compartment. This is important as the environmental conditions dictating drug loading (i.e. loading solution) may have vastly different effects on the intravesicular environment and consequently result in different drug release kinetics. Two of the main methods used to entrap or load drug within a liposome (both used within this thesis) are passive and active loading. Passive loading is quite simple. The lipid films used to form the bilayer are hydrated with a solution containing the drug of interest. Drug loading efficiencies can vary greatly using this method as highly lipophilic drugs will have a great affinity for the bilayer[49, 61] while more hydrophilic drugs will mostly remain within the aqueous phase, leaving much of the drug unencapsulated.[62, 63]

Active loading of drug is more complex, as illustrated in Figure 2.3. Many liposomal formulations of amine-containing (or weakly basic) anticancer agents are actively-loaded by establishing an acidic intravesicular compartment relative to the extravesicular pH of the loading solution. This pH gradient is generated by the release of a small, highly permeable base (ammonia in this case) once it has been removed from the extravesicular solution. As ammonia is released, protons are generated in the intravesicular compartment and the pH is lowered. When a weakly basic drug is exposed to this low intravesicular pH, the drug ionizes and typically becomes impermeable. This maintains the gradient for the permeable form of the drug to continue driving the loading process. This process results in high drug loading efficiencies that often prolong drug retention in aqueous buffers.[23, 62, 64] However, many of these formulations may exhibit accelerated release *in vivo* or *ex vivo*.[23, 62] A mechanistic understanding of the loading process should aid in deciphering the factors that contribute to these differences in release kinetics and are investigated in this thesis.

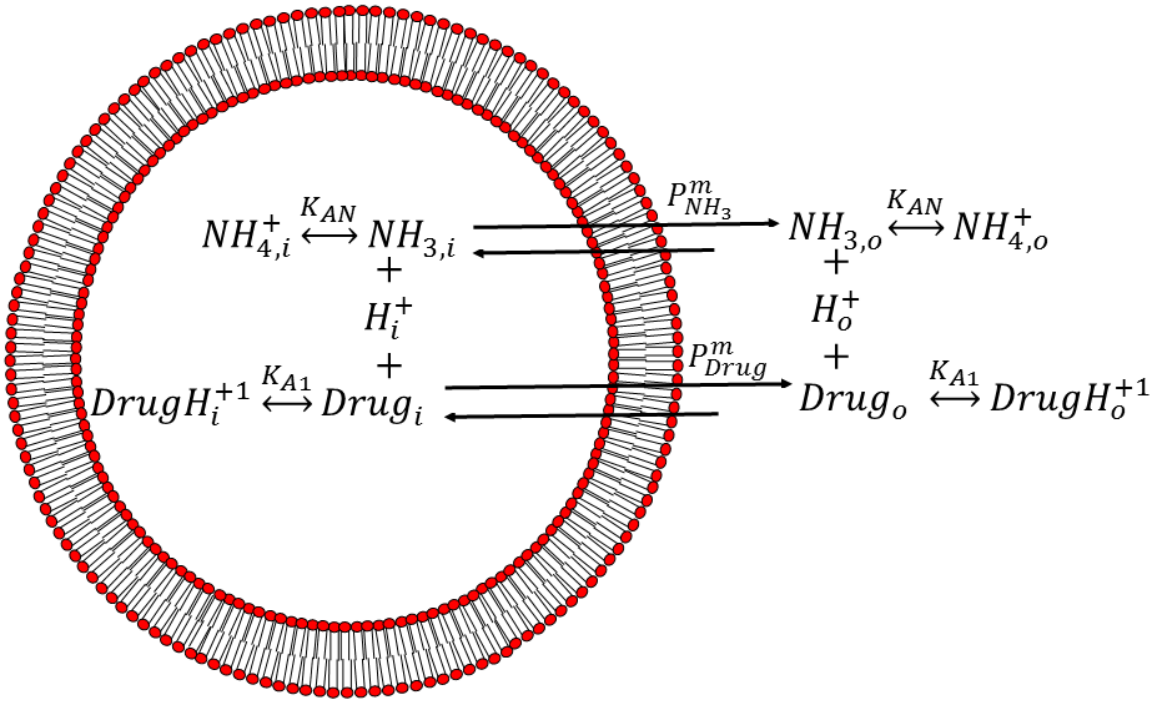

Figure 2.3 An illustration of the active loading process for weakly basic drugs. The rates of drug and ammonia transport are governed by their permeabilities P_{Drug}^m and $P_{NH_3}^m$, respectively.

2.3 Polymeric micelles

Polymeric micelles are amphipathic block copolymers which self-associate to form a hydrophobic core surrounded by a hydrophilic shell when dispersed in aqueous solutions.[5, 65] This is illustrated by Figure 2.4. One of the most common examples of these formulations are Pluronic block copolymer micelles. These triblock copolymers possess a hydrophobic poly(propylene oxide) chain sandwiched between more hydrophilic poly(ethylene oxide) chains.[65, 66] The ratio of these copolymers may be changed to improve the partitioning of a particular drug.[66] These types of micelles are generally between 10-100 nm in diameter, allowing them to take advantage of passive targeting due to the EPR effect[65] and overcome multidrug resistant cancers.[19, 65] These initial polymer micelle formulations primarily focused upon increasing the solubility of many highly lipophilic anticancer agents while

reducing the systemic toxicities encountered using other excipients as solubilizing agents.[67-70]

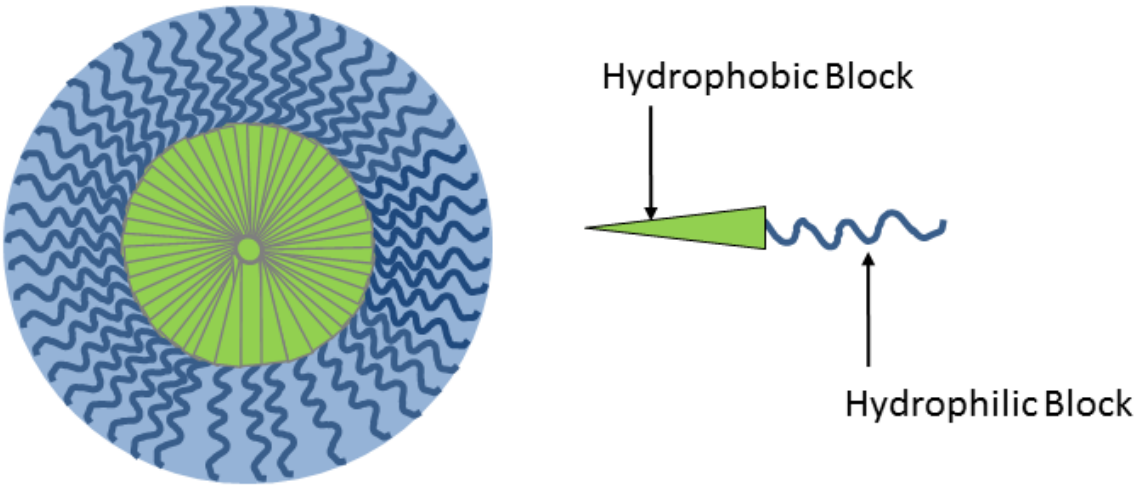

Figure 2.4 An illustration of a polymeric micelle. The nanoparticle forms as the amphipathic block copolymers self-associate in aqueous solution. The more hydrophobic polymer block resides in the core and the more hydrophilic polymer block forms the shell.

Further development of polymeric micelles using more elaborate copolymers has led to many more exotic versions. These more advanced delivery systems are designed to possess unique structures capable of providing a plethora of characteristics exploitable for altering drug release. Some of these designs alter characteristics intrinsic to the formulation (e.g. particle size, charge, hydrophobicity). While these properties may be advantageous for altering drug release kinetics, they may also result in a complicated drug release mechanism. The partitioning of drug payloads may be due to the drug's affinity for a micelle with a highly-charged core rather than the typical hydrophobic core.[5, 65, 66] Over time, drug may be released from these various polymeric micelles due to a combination of kinetic factors (i.e. drug diffusion and/or stability of drug-polymer linkage) and thermodynamic factors (i.e. complexation/absorption to the micelle core, CMC) intrinsic to the drug/polymer system and independent of the release environment.[5, 66] Further complexity

is added when nanoparticles are engineered to respond to external stimuli such as heat, electromagnetic waves, enzymatic activity, or pH[5, 63, 65, 71-79] while active targeting strategies to alter the micelle surface may subsequently alter the mechanism or kinetics of release.[5, 19, 65, 68, 70]

Chemically conjugating drugs to the block copolymers is another way to alter drug release kinetics and adds another dimension to the mechanism of drug release. In several instances, these drug-conjugated micelles exhibit a biphasic drug release pattern (i.e. burst drug release followed by an extremely slow drug release phase) that varies depending upon the pH of the release medium.[80-83] This thesis examines the factors governing release from this type of polymer micelle formulation.

2.4 Topoisomerase inhibitors

2.4.1 Topotecan

Topotecan (TPT) is a topoisomerase I inhibitor currently approved to treat cervical, ovarian, and small cell lung cancers as an oral capsule or an injectable solution. Furthermore, TPT is also used in multiple clinical trials as the sole medication or in conjunction with other medications and/or radiation.[84-88] TPT is one of several camptothecin analogues which stabilize single-strand breaks produced by the DNA-topoisomerase I complex, preventing further DNA replication and eventually resulting in cell death.[89] Due to its dimethylethylamine group, TPT is also weakly basic and subsequently its active lactone conformation is highly soluble under mildly acidic conditions.[90] As such, an injectable solution of the hydrochloride salt is readily made and approved for use;[88, 91] however, TPT undergoes pH-dependent ring-opening hydrolysis from its active lactone to a less-active carboxylate form as pH is increased (see scheme 2.5).[92] This results in the carboxylate form dominating at physiological pH. The ring-opening

combined with base-catalyzed degradation and binding of the carboxylate to serum albumin[90, 91, 93] significantly lowers TPT's effectiveness upon systemic administration.

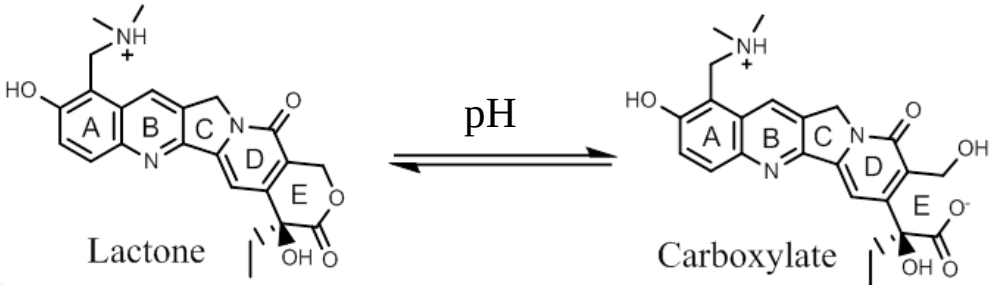

Figure 2.5. TPT undergoes reversible, pH dependent interconversion between its lactone (left) and carboxylate (right) forms that results in the lactone form dominating under acidic conditions while the carboxylate form dominates at neutral or basic pH.

These issues may be circumvented upon TPT encapsulation in liposomes with a low intravesicular pH.[94] Like other weakly basic drugs, TPT can achieve high encapsulation efficiency in liposomal formulations utilizing active loading strategies to generate a transbilayer gradient of lower intravesicular pH relative to the extravesicular loading solution.[21, 42, 61, 73, 95-97] Considerable work has focused on such loading strategies for TPT; however, the subsequent release of TPT from these formulations is poorly understood.[24, 42, 62, 64, 97] Moreover, observations of accelerated release from studies conducted in plasma have not been explained.[62] Part of the work in this thesis focuses on mechanistically determining the critical parameters attributable to liposomal TPT loading and release kinetics.

2.4.2 Doxorubicin

Doxorubicin (DOX) is a topoisomerase II inhibitor currently approved to treat several hematological malignancies in addition to many solid tumors including gastric, ovarian, thyroid, and small cell lung cancers as an injectable solution.[98] DOX is also extensively used

in preclinical and clinical trials with a wide array of nanoparticle formulations.[36, 40, 99-104] The weakly basic anthracycline stabilizes the topoisomerase II cleavage complex (Top2cc) formed during unwinding of supercoiled DNA during replication. In the case of DOX, both single and double strand breaks formed by the Top2cc prevent DNA replication and eventually triggers cell death.[105] At higher DOX concentrations, DOX may suppress Top2cc altogether by altering DNA structure.[105, 106] DOX may be administered as its hydrochloride salt as a soluble injection due to the weakly basic nature (pKa ~ 8.2)[107] of the anthracycline's aminogylcosidic side chain (see Scheme 2.6); however, cardiotoxicity typically occurs in over half the patients that receive chronic treatment.[108] The generation of free oxygen radicals in response to DOX is the likely cause[108-110] (although the mechanisms leading to this are numerous and still debated).[108]

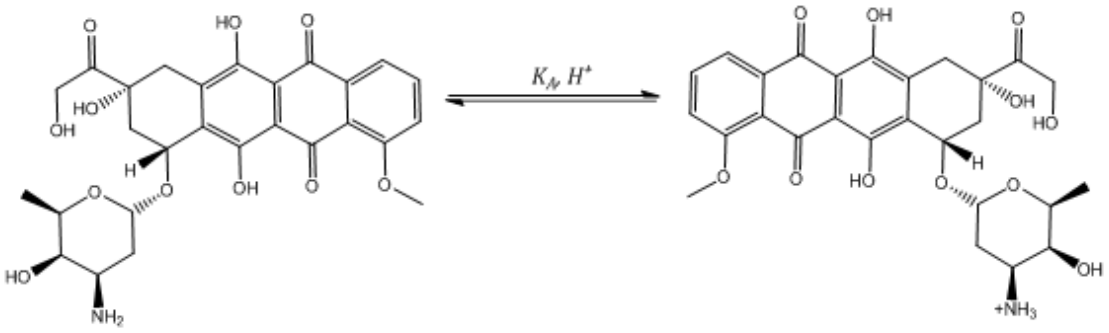

Figure 2.6. The ionization states of DOX are governed by its acid dissociation constant (K_A) and the pH of the solution. At higher pH, the neutral base form dominates (left) while its cationic form (right) dominates at lower pH.

Reducing this cardiotoxicity through formulation is of great clinical interest.[110] The nanoparticle formulation marketed as DOXIL (liposomal doxorubicin) reduces DOX's cardiotoxicity due to its slow release from liposomes and preferential accumulation of these nanoparticles in solid tumors.[30, 73, 111-113] Even so, the liposomal formulations have led to other side effects including hand-foot syndrome (i.e. blistering and skin necrosis typically in

the extremities), likely due to a combination of the prolonged circulation and slow DOX release from the liposome delivery vehicle in combination with the rich capillary beds of the skin.[30, 114] This has led to much research on other nanoparticle formulations with various release rates in an attempt to find formulations which may not share in this same toxicity. The factors governing DOX release from a polymeric micelle formulation are explored as part of this thesis.

2.5 Characterization of nanoparticle drug release

The characterization of nanoparticle drug release requires methods to monitor either the loss of drug from the nanoparticle or the accumulations of drug in the release media. There are many methods employed to monitor nanoparticle drug release under these constraints;[115-117] however, few consider the impact of environmental conditions (particular to the selected characterization method) which may alter observed *in vitro* drug release kinetics. One popular method used to monitor *in vitro* drug release from nanoparticles that exhibits several of these method-specific effects is dynamic dialysis. Dynamic dialysis uses a large reservoir in an attempt to provide the sink conditions necessary to drive release to completion. Meanwhile, the nanoparticles remain concentrated within a small volume compartment separated from the reservoir by a semi-permeable membrane.[19, 60, 63, 64, 118-120] A large reservoir volume, however, does not necessarily ensure sink conditions within the dialysis chamber itself. Depending on the nanoparticle release kinetics and the extent of drug binding to the nanoparticle, transport across the dialysis membrane may become rate-limiting.[3,8] Corrections for drug binding to the nanoparticles and the barrier properties of the dialysis membrane are therefore crucial when interpreting kinetic data collected with dynamic dialysis.[49, 61, 63, 118]

Most other methods used to monitor nanoparticle drug release typically use a physical separation (e.g. size-exclusion chromatography, ultrafiltration)[51, 121] or spectral differences[78, 79] between free and entrapped drug. Validation of the separation efficiency/recovery or spectral deconvolution[63] is obviously required for interpretation of release kinetics using these methods. Just as important as this validation and frequently overlooked during release characterization is evaluation of "sink" or "non-sink" conditions. If non-sink conditions are present, evaluation of release kinetics becomes problematic. For example, changes in the extent of release from nanoparticle formulations due to changes in pH or temperature do not necessarily translate into differences in release rates (i.e. thermodynamics vs. kinetics).[81, 122, 123] Figure 2.7 provides a general illustration of this effect. Without a way to quantify these distinctions, assessing the eventual *in vivo* performance becomes challenging.

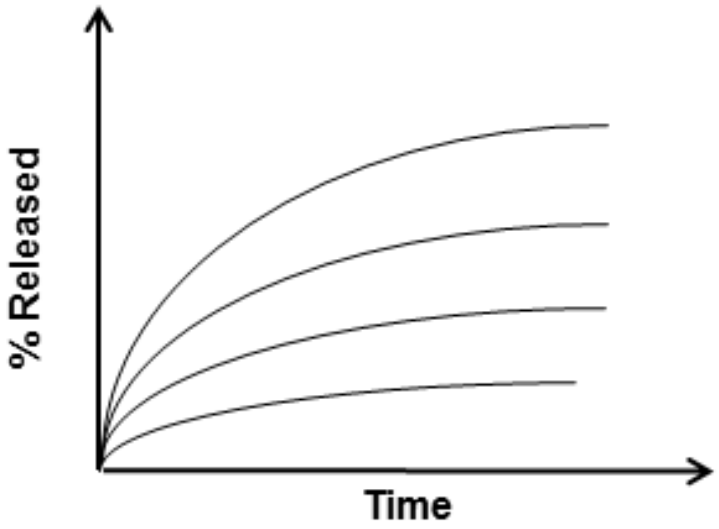

Figure 2.7 An illustration of the effect of non-sink conditions on release profiles. In this illustration, the initial rate of release is the same; however, the final % of drug released is different due to a different equilibrium. Interpreting both factors during nanoparticle release characterization is necessary to evaluate the effect of different conditions (e.g. pH and/or temperature) on altering the rate of release rather than the equilibrium.

Mathematical modeling of release profiles obtained from these methods may provide the ability to validate such release methods and subsequently determine release parameters intrinsic to the drug/nanoparticle system of interest. At a minimum, these models can distinguish the kinetic and thermodynamic quantities intrinsic to the drug/particle system and those from the experimental environment contributing to the observed release profiles.[49, 60, 63, 124-126] This thesis provides validation of several non-sink methods with the aid of mathematical models capable of quantifying the kinetics and approach to equilibrium exhibited by release studies conducted with such methods.

With validated methods, studies that systematically examine release kinetics under a variety of conditions can be used for the development of mechanistic models which will provide insights on further optimization and control of drug release from these nanoparticle drug delivery systems. These mechanistic models will contain the physicochemical principles governing drug release from the nanoparticle of interest. They may require other studies in conjunction with release studies to validate the physicochemical principles affecting release kinetics.[49, 53, 60, 63, 124]

Once these mechanistic models are capable of describing nanoparticle drug release *in vitro*, the incorporation of *in vivo* conditions will be possible and ultimately lead to accurate *in vitro/in vivo* correlations. Such correlations would reduce much of the costs incurred during preclinical development due to extensive animal testing and unguided formulation optimization. Mathematical models for assessing *in vitro* drug release and predicting *in vivo* drug release from nanoparticle formulations would be useful both in the design phase and during preclinical testing where avoiding the extensive use of animals would be highly desirable. Such models would facilitate the design of formulations with adjustable and predictable drug release rates for patient-specific treatment regimens. The work within

this thesis is intended to develop mechanistic models that are adequate enough to describe drug release kinetics from nanoparticle formulations *in vitro*. The approach used here along with its subsequent findings will guide the design of future studies used to characterize nanoparticle drug release kinetics, optimize the loading and release of the formulations studied, and explore the mechanistic changes in release kinetics due to various physiological factors.

CHAPTER THREE

Dynamic Non-sink Method for the Simultaneous Determination of Drug Permeability and Binding Coefficients in Liposomes

3.1 Introduction

Mathematical models for assessing drug permeability and predicting in vivo drug release from nanoparticle formulations would be useful both in the design phase and during preclinical testing where avoiding the extensive use of animals would be highly desirable. Such models would facilitate the design of formulations with adjustable and predictable drug release rates for patient-specific treatment regimens. Mechanism-based models applicable to liposomal systems would need to account for three main factors affecting drug release: 1) the escaping tendency or effective concentration of the entrapped (permeable) drug species which serves as the driving force for liposomal release; 2) drug speciation and species permeability-area products for lipid bilayer transport;[44, 49, 52, 53, 63, 127, 128] and 3) the environmental conditions in which drug release occurs both during the in vitro release characterization and in vivo.[49, 118] The intraliposomal driving force for transport likely depends on such factors as pH-dependent drug speciation, self-association, complexation, precipitate formation, membrane binding, and drug degradation/interconversion kinetics. The driving force for liposomal release and the membrane permeability-area product are closely linked and dependent on which drug species account for the release.[49, 60, 129, 130] The environmental conditions (e.g., temperature, pH, sink conditions or lack thereof, presence of permeable buffer species, lipid-bilayer perturbing components, etc.) also impact both the driving forces and permeability coefficients. Thus, robust mechanism-based models for predicting liposomal drug release may be quite complex. Translation of release parameters generated in vitro to the prediction of drug release in vivo may be particularly challenging.

The necessary corrections will likely vary depending on the in vitro method employed to study drug release.

A number of methods currently exist to monitor in vitro drug release from nanoparticles[115, 117, 131] but extrapolation to predict in vivo release often requires an adjustment for the absence of sink conditions in the in vitro experiments as well as other possible environmental differences. For example, one popular method to monitor in vitro drug release from nanoparticles is dynamic dialysis. Dynamic dialysis uses a large reservoir in an attempt to provide the sink conditions necessary to drive the process to completion. Meanwhile, the nanoparticles remain concentrated within the small volume compartment and separated from the reservoir by a semi-permeable membrane.[19, 60, 63, 64, 118-120] Unfortunately, a large reservoir volume does not ensure sink conditions within the dialysis chamber itself. Depending on the nanoparticle release kinetics and the extent of drug binding to the nanoparticle, transport across the dialysis membrane may become rate-limiting.[3,8] Corrections for drug binding to the nanoparticles and the barrier properties of the dialysis membrane are therefore crucial when employing dynamic dialysis for predictive modeling.[49, 61, 63, 118] In some cases, incomplete release has been observed even though approximate sink conditions (based on overall drug concentration gradients) were maintained due to factors such as pH differences or drug binding phenomena. Such factors reduce the thermodynamic activity gradient for the permeable species, resulting in the achievement of equilibrium and subsequently incomplete release.[72, 132-134] Finally, even if the above concerns relating to sink conditions are properly taken into account, a separate set of experiments in addition to dynamic dialysis would be needed. These additional experiments would be required to quantify the species-dependent membrane binding of the drug and its influence on observed release kinetics for the construction of a mechanism-based release model. [63, 119]

A method to evaluate drug release kinetics under well-defined non-sink conditions when combined with the appropriate mechanistic release model would allow simultaneous determination of the kinetic and thermodynamic parameters governing release kinetics. This method would also provide a more robust assessment of nanoparticle formulations. This study demonstrates the utility of a novel ultrafiltration method to analyze drug release from nanoliposomal formulations under non-sink conditions using the model anti-cancer agent topotecan (TPT). With the appropriate mathematical models, the liposomal drug release parameters generated under non-sink conditions were shown to be comparable with those obtained from dynamic dialysis. This non-sink method was also used to simultaneously characterize membrane binding of the drug and its dependence on both drug and lipid concentrations in suspension.

3.2 Experimental

3.2.1 Materials

Powders of 1,2-distearoyl-sn-glycero-3-phosphatidylcholine (DSPC, >99% purity) and 1,2-distearoyl-sn-glycero-3-phosphoethanolamine-N-[methoxy(polyethyleneglycol)-2000] (m-PEG DSPE, MW = 2806, >99% purity) were purchased from Avanti Polar Lipids (Alabaster, AL). Topotecan hydrochloride was purchased from AK Scientific (Union City, CA). Float-A-Lyzer® G2 dialysis tubes (100,000 MWCO) were purchased from Spectrum Labs (Rancho Dominguez, CA). Millipore semi-micro ultrafiltration centrifugation devices (regenerated cellulose, NMWL: 30,000), 100 nm pore size Nuclepore polycarbonate membranes, solvents, and buffer salts were purchased from Fisher Scientific (Florence, KY). All solvents were HPLC grade.

3.2.2 Preparation and characterization of DSPC/m-PEG DSPE liposomes

Large unilamellar vesicles were formed using a film hydration and extrusion process as reported previously with slight modifications.[28, 49, 62] Briefly, DSPC and m-PEG DSPE (95:5 mol:mol) lipids were weighed, dissolved in chloroform, and aliquots of the resulting solutions were distributed into separate vials. Chloroform was subsequently evaporated under a stream of nitrogen gas and the residue was vacuum-dried at 40°C for 6 hours. For release studies, TPT was passively loaded into liposomes by hydrating the dried lipid film with TPT solutions (0.25 mM in pH 4.0, 50 mM formate buffer adjusted to an ionic strength of 0.3 with NaCl) to achieve 40 or 90 mg lipid/mL suspensions. These suspensions were extruded 10 times through two stacked 100 nm pore size Nuclepore® polycarbonate membranes using a Liposofast® extrusion device at 60°C to obtain unilamellar vesicles with encapsulated TPT in the intra-vesicular solution. Blank liposome suspensions (40 mg lipid/mL) used in spiking experiments for dynamic dialysis and ultrafiltration validation were made under the same conditions as passively loaded liposomes without TPT present in the hydrating solution.

Liposome characterization included particle size measurements by dynamic light scattering (DLS) and lipid content analyses using HPLC with evaporative light scattering detection (ELSD) as previously reported.[130] Particle size data were used to monitor liposome stability and in combination with information on the number of vesicles in suspension (based on lipid content) and bilayer surface density data from the literature to calculate liposomal volumes necessary for the mathematical models.[49, 50, 84, 135]

3.2.3 Release of TPT from DSPC/m-PEG DSPE liposomes

All release studies were conducted in a water-jacketed incubator maintained at 37 °C.

3.2.3.1 Sephadex® column removal of unencapsulated drug from passively loaded liposome suspensions

To compare release studies using dynamic dialysis (sink conditions) and ultrafiltration (non-sink conditions), 0.7 mL of 40 mg lipid/mL suspensions was passed through a Sephadex® PD-10 column to separate liposomes from unencapsulated drug. The first 4.75 mL was collected and diluted to 15 mL of suspension using the same buffer used for lipid hydration (without drug). Next, 4.5 mL of this suspension was either transferred to dialysis tubes or 7 mL glass vials with a rubber stopper. Release studies under either sink or non-sink conditions were performed in triplicate. Additional studies of the concentration dependence of binding to the DSPC bilayer utilized 90 mg lipid/mL suspensions and 0.25 or 0.7 mL aliquots passed through a Sephadex® column. In these instances, the first 1.5 mL of eluent was discarded and the next 3.25 mL containing the liposome suspension was collected and transferred to 7 mL glass vials with a rubber stopper.

3.2.3.2 Non-sink release studies measured by ultrafiltration

Glass vials containing the liposome suspensions were placed on a Thermo Cimerac iPoly 15 multipoint stirrer insulated with 1.5 inches of Styrofoam® to minimize heating from the stir plate and subsequently maintained a suspension temperature of 37.4 ± 0.6 °C. Liposome suspensions were stirred at 200 rpm over the time course of the release study (~ 96 hours) using 10 x 5 mm Teflon® stir bars. Encapsulated drug was monitored by ultrafiltration of 100 µL samples taken throughout the duration of the release studies.

Ultrafiltration was chosen as it has been used in previous studies with liposomes as a method in which encapsulated drug may be separated from released drug.[121, 130] Each sample was diluted with chilled (4 °C) buffer to 450 µL to quench drug release and ultrafiltered using an Amicon® Ultra 0.5 mL centrifugal filter device with a 30,000 MWCO Ultracel® membrane. Samples were centrifuged in these cartridges at 14,000 rpm for 10 minutes in an

Eppendorf 5417R maintained at 4 °C. During centrifugation, liposome integrity was maintained as suspensions were concentrated but not dried completely due to the conical geometry of the ultrafiltration membrane. Concentrated suspensions (26 ± 2 µL) were recovered by inverting and centrifuging the cartridge at 2000 rpm for another 2 minutes. After recovery of the concentrate, 400 µL of chilled buffer was added and the process was repeated to ensure complete removal of membrane-bound extravesicular drug. The final concentrate from this second cycle was analyzed by HPLC after dilution into the calibration range of TPT standards. Chilled methanol (-20 °C) was used to disrupt the vesicles and minimize solvent evaporation during sample dilution. Samples that had not been ultrafiltered (20–100 uL) were also taken and immediately diluted in chilled methanol to determine the total amount of TPT and any extravesicular drug present at the beginning of the release study.

3.2.3.3 Dynamic dialysis under sink conditions

Dialysis tubes (Float-A-Lyzer® G2, 100,000 MWCO) containing 4.5 mL of liposome suspension were placed in 900 mL reservoirs containing pH 4.0 formate buffer pre-equilibrated at 37 °C. Aliquots (20 uL) were removed from the dialysis tube over a 48 hour period and immediately diluted in chilled methanol for TPT analysis by HPLC.

3.2.4 Dialysis tube swelling studies

Changes in the suspension volume within the dialysis tube during release studies may produce errors in the observed loss of drug during dynamic dialysis. To correct for this, the rate of swelling as measured by the volume of sample within the dialysis tubes at equilibrium must be determined. Fresh dialysis tubes of the same make as those used in dynamic dialysis studies were filled with 4 mL of the same buffer as that in the reservoir. These tubes were then allowed to sit in reservoirs at the same conditions used in dynamic

dialysis studies. The volume in these tubes was monitored over time using a 10 mL graduated cylinder.

3.2.5 TPT dimerization

Several reports have indicated that TPT self-associates to form dimers,[136-138] the tendency of which may be pH dependent.[138] Self-association of TPT may result in liposomal membrane binding coefficients that are concentration dependent if only the monomeric form is involved in binding. Since previous characterization of TPT self-association has been in the neutral pH range,[136-138] studies were conducted to assess TPT dimerization at the conditions release studies were performed. Apparent extinction coefficients were calculated for varying concentrations of TPT (1 – 250 μM) dissolved in the same buffer employed for release studies. Absorbance was measured at wavelengths of 360, 376, 378, 380, 382, 384, 386, and 388 nm using a Varian Cary 50 UV-Vis spectrophotometer. NSG quartz cuvettes (NSG Precision Cells, Farmingdale, NY) with 2 and 10 mm path lengths were used to stay within the analytical range of the instrument.

3.2.6 HPLC analyses

Samples from release and validation studies were analyzed for TPT and lipid concentration by HPLC as reported previously.[49, 130] TPT samples were analyzed with a previously developed HPLC method utilizing fluorescence detection.[130] TPT lactone standards were prepared in chilled, acidified methanol over a concentration range of 20-200 nM. Samples were diluted to within this concentration range using chilled methanol. Samples were either immediately injected or stored at -20 °C for no more than 48 hours before analysis.

Lipid analysis was performed using an HPLC coupled to an ELSD (Sedere, Inc., Lawrenceville, NJ) as previously reported.[49, 130] DSPC standards and samples were dissolved

in 80% chloroform:19.5% methanol:0.5%(v/v) of 30% (vol) NH_4OH solution. Standards spanned the concentration range of 0.05 – 0.3 mg DSPC/mL. Lipid samples from release studies (50 – 150 µL) were dried at room temperature under N_2. Once dried, samples were redissolved in the above-mentioned solvent mixture to be within the calibration range of DSPC standards.

3.2.7 Model Development and Data Analysis

Previously, mechanistic models for liposomal release have been developed to account for the additional resistance contributed by the dialysis membrane in dynamic dialysis studies.[49, 60, 118] The general concepts applicable to liposomal systems are depicted in Scheme 3.1. By developing appropriate models, the rate of drug release applicable to sink conditions can be extracted from a variety of release methods. Such a case is illustrated here by using mathematical models to analyze and compare the kinetics of liposomal release of TPT under sink and non-sink conditions. All fitting of release kinetics and dimerization data was performed using Micromath® Scientist® non-linear regression software utilizing a weighting factor of two.

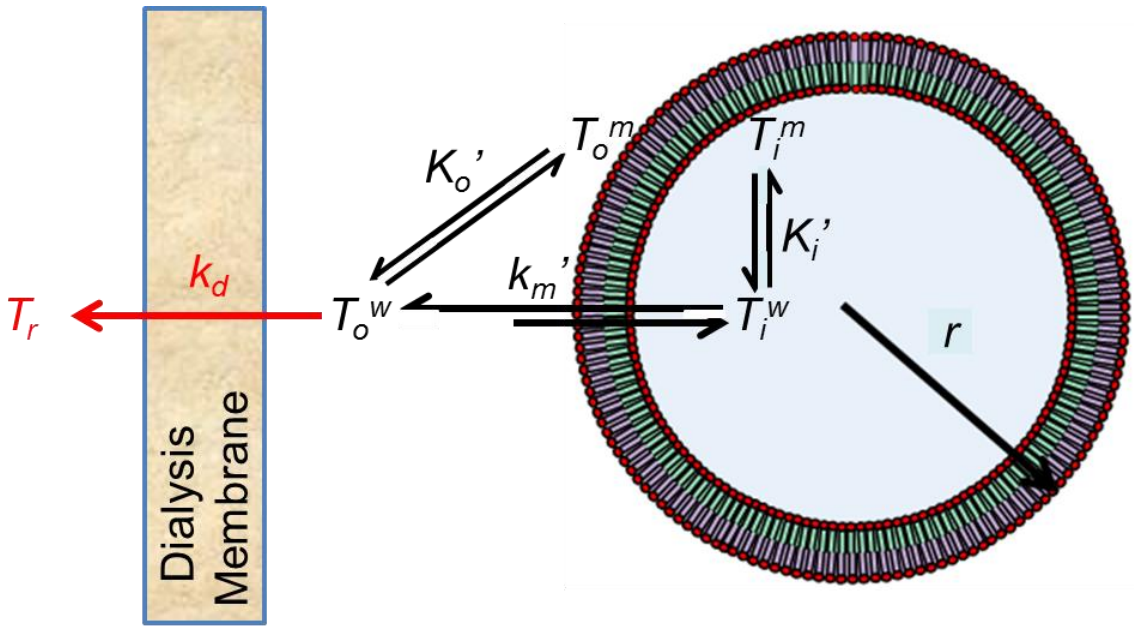

Scheme 3.1. Illustration of the relevant kinetic and equilibrium processes applicable in developing a mathematical model for liposomal drug release as determined by dynamic dialysis. The volume compartments of a liposome with radius, *r*, are highlighted along with the kinetic and binding components governing drug release. The blue core is the inner aqueous volume, $\boldsymbol{V_i^w}$, while the green and purple sections refer to the inner, $\boldsymbol{V_i^m}$, and outer, $\boldsymbol{V_o^m}$, membrane volumes, respectively. The rate of liposomal drug release depends on the rate constant, k_m', and the difference in the unbound inner and outer aqueous drug concentrations, T_i^w and T_o^w, respectively, while the apparent intravesicular, K_i', and extravesicular, K_o', binding coefficients govern the equilibrium between drug bound to the inner or outer lipid membrane, T_i^m and T_o^m, respectively, and the corresponding unbound drug in the intravesicular or extravesicular compartments, respectively. The rate constant k_d reflects the diffusion of drug across the dialysis membrane driven by the concentration gradient $T_o^w - T_r$. All notations in red refer to aspects unique to dynamic dialysis conditions.

3.2.7.1 Mathematical model of TPT release from unilamellar liposomes: non-sink conditions

A mechanistic, mathematical model is required to obtain both drug permeability and membrane- binding from release studies. Several models describing drug loading and release have already been developed;[49, 60, 124, 127, 128, 139, 140] however, only a few have been tested and these studies have only examined release under sink conditions.[49, 60, 124]

The apparent rate constant governing drug release from a liposome is a function of the drug's apparent permeability coefficient, P_m', through the bilayer and the radius, *r*, of the particle. This is shown below in equation 1.[49, 50]

$$k_m' = \frac{3}{r} P_m' \tag{1}$$

While k_m' may be dependent on the respective permeabilities of each species of drug present in solution, such a distinction cannot be made here as multiple conditions (e.g. pH) must be explored to determine each specie's contribution. Therefore, the k_m' determined

here applies to the specific pH chosen for these experiments (which is satisfactory for comparing these different release methods).

Liposomal drug release is dependent on the driving force developed by the effective concentration gradient between unbound, intra- and extra-vesicular drug concentrations (T_i^w and T_o^w, respectively). This is expressed by equations 2a and b.

$$\frac{dT_i}{dt} = -k'_m(T_i^w - T_o^w) \tag{2a}$$

$$\frac{dT_o}{dt} = \frac{nV_i^T}{V_0^T}k'_m(T_i^w - T_o^w) = f_v k'_m(T_i^w - T_o^w) \tag{2b}$$

These differential equations describe bilayer-limited Fickian diffusion at a pseudo steady-state. The term f_v symbolizes the ratio of total entrapped volume (the product of the total number of vesicles, n, and intravesicular volume of a single liposome, V_i^T) to total extravesicular volume, V_0^T, thus accounting for the difference in volumes of the inner and outer compartments. Derivation of the concentrations of unbound drug in the intra- and extra-vesicular compartments in terms of total intra- and extra-vesicular drug concentrations (T_i and T_o, respectively) will be described in a later section.

For non-sink release studies, both the initial concentrations of intra- and extra-vesicular drug were determined by analyzing total suspension concentration of drug, T, and drug concentration after ultrafiltration of suspension when the release study began, $T_{i,0}$. This is shown by the equations below:

$$T_i(0) = T_{i,0} \tag{3a}$$

$$T_o(0) = T_{o,0} = T - f_v T_{i,0} \tag{3b}$$

3.2.7.2 Dynamic dialysis model of drug release from unilamellar liposomes: sink conditions

Dynamic dialysis is advantageous for maintaining sink conditions as it provides a large reservoir capable of maintaining the driving force for drug release. Because nanoparticles cannot cross the dialysis membrane, significant dilution of the nanoparticle suspension

during drug release is avoided and the concentration of drug remaining in the suspension versus time can be quantified. This is depicted in Scheme 1. Mathematically, the differential equation governing transport in the vesicle is the same as equation 2a, where T_o^w refers to the unbound extravesicular TPT within the dialysis tube. A release rate constant for transport of liposomally-released drug from the dialysis tube, k_d, must be added to eqn. 2b to describe transport from the extravesicular compartment of the dialysis tube into the reservoir compartment. This is expressed by equation 4 with portions in red identifying the term unique to dynamic dialysis.

$$\frac{dT_o}{dt} = k'_m f_v (T_i^w - T_o^w) - k_d T_o^w \tag{4}$$

In these studies, the suspension concentration of TPT within the dialysis tube at any time (T_d) is sampled. This concentration would naturally be composed of intra- and extravesicular TPT as shown by equation 5.

$$T_d = f_v T_i + T_o \tag{5}$$

Derivation of the unbound drug concentrations in dynamic dialysis is the same as in the non-sink condition case (see next section).

For sink conditions using the dynamic dialysis method, the initial conditions are dependent on the loading condition of the liposome suspension. For passively-loaded liposomes, the initial conditions are as follows:

$$T_i(0) = \frac{S}{f_v} \tag{6a}$$

$$T_o(0) = 0 \tag{6b}$$

where S is the initial suspension concentration of TPT within the dialysis tube. To accurately discern the rate of transport of drug through the dialysis membrane, a suspension of blank liposomes spiked with free TPT was used. While the rate equations are the same as for passively-loaded drug, the initial conditions are not and are expressed below:

$$T_i(0) = 0 \tag{7a}$$

$$T_o(0) = S \tag{7b}$$

3.2.7.3 Derivation of unbound drug concentration for modeling of release studies at sink and non-sink conditions

Binding of drug to the phospholipid membrane interface has been reported previously with other chemotherapeutics and lipophilic drugs.[49, 53, 61, 63, 118, 141] Such binding will reduce the driving force for drug transport, resulting in the need for a mathematical model that includes this effect on release kinetics. Such a model was developed based on previous models (which account for drug binding) to describe the concentration of unbound drug in terms of total intra-and extravesicular drug concentration and its subsequent effect on release kinetics.[49, 60] The relationship is the same for release studies conducted under non-sink and sink conditions and is derived below.

The total amount of drug inside ($M_{i,T}$) and outside ($M_{o,T}$) the vesicle can be expressed in terms of the contributions of aqueous and membrane bound components. Equations 8a and b express these mass balances.

$$M_{i,T} = M_{i,T}^{w} + M_{i,T}^{m} \tag{8a}$$

$$M_{o,T} = M_{o,T}^{w} + M_{o,T}^{m} \tag{8b}$$

In these equations and from this point on, the superscripts "w" and "m" represent unbound drug in the aqueous compartment and membrane bound drug, respectively; the subscripts *i*, and *o*, refer to the intra- and extra-vesicular compartments. These mass balance equations can be expressed in terms of concentrations using the ratios of the aqueous to membrane volume in the inner and outer compartments defined in equations 9a-e (see Scheme 1)

$$a = \frac{V_i^w}{V_i^T}, b = \frac{V_i^m}{V_i^T}, c = \frac{V_o^w}{V_o^T}, d = \frac{nV_o^m}{V_o^T}, f_v = \frac{nV_i^T}{V_o^T} \tag{9a-e}$$

thus producing equations 10a & b for total drug concentration within, T_i, and outside, T_o, the vesicles:

$$T_i = a(T_i^w) + b(T_i^m) \quad (10a)$$

$$T_o = c(T_o^w) + d(T_o^m) \quad (10b)$$

Next, the concentration gradient of aqueous, unbound drug must be solved in terms of total drug encapsulated. This is done by incorporating an apparent volume-normalized membrane binding coefficient describing the equilibrium between TPT bound at the interface of the bilayer membrane and that in solution for the intravesicular, K_i', and extravesicular, K_o', compartments. These binding constants may differ if there are differences in the intra- versus extra-vesicular environments (e.g. pH gradients, ionic strength differences, etc.) or prior to equilibrium when drug concentrations may differ dramatically between the inner and outer compartments. In the present study of passively loaded liposomes, the intravesicular and extravesicular compartments were at the same pH and buffer concentration throughout the experiment. At equilibrium both compartments contained the same drug concentration. Under these conditions we found that a single K' could be assumed ($K_i' = K_o'$) without diminishing the quality of the fit of the model to the data.

With this assumption, the model may refer to both as K' and, T_i^w and T_o^w may be described by equations 11a and b

$$T_i^w = f_i^w T_i;\ f_i^w = \frac{1}{a+bK'} \quad (11a)$$

$$T_o^w = f_o^w T_o;\ f_o^w = \frac{1}{c+dK'} \quad (11b)$$

with $K' = T^m/T^w$. Using these substitutions, equations 2a, 2b, and 4 can be rewritten in terms of total intra- and extra-vesicular drug concentration.

3.2.7.4 Concentration corrections for ultrafiltration recovery and dialysis compartment volume

For non-sink release studies, the recovery of intra- and extra-vesicular drug after ultrafiltration must be accounted for to accurately assess release kinetics. In dialysis experiments under sink conditions, the volume of the nanoparticle suspension within the dialysis tubes may fluctuate.

The concentration of TPT determined by HPLC analysis of ultrafiltered samples, while mostly composed of intravesicular TPT, may require corrections due to the ultrafiltration process. The observed concentration obtained from ultrafiltration, T_u, must be interpreted correctly to accurately model drug release. This can be accomplished by expressing T_u with equation 12.

$$T_u = \omega \frac{T_i}{f_v} + \varphi T_o \tag{12}$$

Here, the % of intravesicular (ω) and extravesicular drug (φ) recovered in the ultrafiltrate were determined with validation studies.

Ideally, the concentration in samples from dynamic dialysis studies at any sample time, n, would be dependent upon only diffusive transport process. This suspension concentration, $T_{d,n}$, can be determined from the observed concentration within the dialysis tube, $T'_{d,n}$, by accounting for volume changes due to sample removal and dialysis bag shrinking/swelling. These effects are expressed by equation 13.

$$T_{d,n} = x_{v,n} x_{s,n} T'_{d,n} \tag{13}$$

The factors $x_{v,n}$ and $x_{s,n}$ correct for volume swelling in the dialysis tube and the mass removed due to sample collection since the previous time point, respectively.

The correction factor for volume change in the dialysis tube, $x_{v,n}$, is:

$$x_{v,n} = \frac{V_{n-1}}{V_n} \tag{14}$$

where V_n is the volume present in the dialysis tube at sample time, n, and V_{n-1} is the volume present after removing sample for analysis at the previous time point (*n-1*). The following equation describes the volume change occurring between time points:

$$V_n = V_{n-1} + \left(V_{eq} - V_{n-1}\right)(1 - e^{-k_v t_{\Delta n}}) \quad (15)$$

where k_v is the rate constant and V_{eq} is the volume in the dialysis tube at hydrostatic equilibrium. V_{n-1} is the volume at the previous sampling time and $t_{\Delta n}$ is the time interval between the samples.

In addition to swelling, the mass removed with each sample, while small, could cumulatively result in a substantial amount of lipid removal and subsequently encapsulated drug removed from the dialysis tube. Because of volume swelling, the amount of mass taken from the previous sampling must be accounted for at each sampling. The correction factors for the first, second, and any later sample ($x_{s,1}$, $x_{s,2}$, and $x_{s,n}$, respectively) are:

$$x_{s,1} = \frac{L_0}{L_0} \quad (16a)$$

$$x_{s,2} = \frac{L_0}{L_0} - \frac{L_{s,1}V_{s,1}}{L_0V_0} \quad (16b)$$

$$x_{s,n} = \frac{L_0}{L_0} - \left(\frac{L_{s,1}V_{s,1}}{L_0V_0} + \frac{L_{s,2}V_{s,2}}{L_0V_0} + \cdots \frac{L_{s,n-1}V_{s,n-1}}{L_0V_0}\right) \quad (16c)$$

Here, L_0 is the lipid concentration in the initial suspension in the dialysis tube, L_s and V_s are the lipid concentration and volume of sample taken, respectively (at the denoted sample number), and V_0 is the initial volume of suspension added to the dialysis chamber.

3.2.7.5 Determination of TPT dimerization constant (K2)

Self-association of TPT in solution has been previously reported[137, 138] and may affect observed binding due to the different binding affinities of the drug in its monomeric (T_1) and dimeric (T_2) forms and the effects of binding on the bilayer surface charge. The two forms of TPT in solution can be related by a dimerization constant, K_2, as shown by equation 17.

$$K_2 = \frac{T_2}{{T_1}^2} \quad (17)$$

The two forms may also be related by mass balance in which the total concentration of TPT in solution, *T*, may be written as the sum of these species as shown in equation 18.

$$T = T_1 + 2T_2 \quad (18)$$

Using these equations, the fraction of monomer present in solution, f_1, can be solved as expressed by equation 19.

$$f_1 = \frac{-1+\sqrt{1+8K_2T}}{4K_2T} \quad (19)$$

In solution, both monomeric and dimeric forms of TPT have their own unique extinction coefficients ($\varepsilon_{1,i}$ and $\varepsilon_{2,i}$, respectively) at any wavelength, *i*, which contribute to the apparent extinction coefficient, ε_{app}. This is shown by equation 20.

$$\varepsilon_{app,i} = f_1\varepsilon_{1,i} + f_2\varepsilon_{2,i} = f_1\varepsilon_{1,i} + (1 - f_1)\varepsilon_{2,i} \quad (20)$$

Using equations 19 and 20, the concentration dependence of $\varepsilon_{app,i}$ was fit at multiple wavelengths simultaneously to determine K_2, $\varepsilon_{1,i}$ and $\varepsilon_{2,i}$.

3.3 Results

3.3.1 Validation of Analytical Methods and Liposome Particle Characterization

TPT concentrations were analyzed using a previously validated HPLC method with fluorescence detection.[130] A linear response for TPT lactone (4.5 min retention time) was observed between 20 and 200 nM using excitation and emission wavelengths of 380 nm and 550 nm, respectively. TPT concentrations in samples taken from release studies and size exclusion experiments ranging from 0.2 - 2 μM were determined by diluting samples with chilled methanol into the concentration range of standards.

Phospholipid content was determined using an HPLC method previously developed and validated.[49, 130] ELSD was employed due to the lack of a chromophore/fluorophore in the lipid molecules. A peak retention time of 7.9 minutes and a linear relationship between the logarithm of peak area and DSPC concentration was observed from 0.05 – 0.3 mg DSPC/mL,similar to that previously reported.[49, 130]

Separation of passively-loaded TPT liposomes from unencapsulated drug was achieved with a Sephadex® size exclusion column. Figure 3.1 compares the elution profiles of an aqueous solution of TPT in the absence of liposomes and a suspension of passively-loaded TPT-containing liposomes. Both TPT and liposomes detected using HPLC and DLS, respectively, were present in the peak eluting in the 2.5- 5mL range while the solution of TPT in the absence of liposomes did not produce a peak in this range.

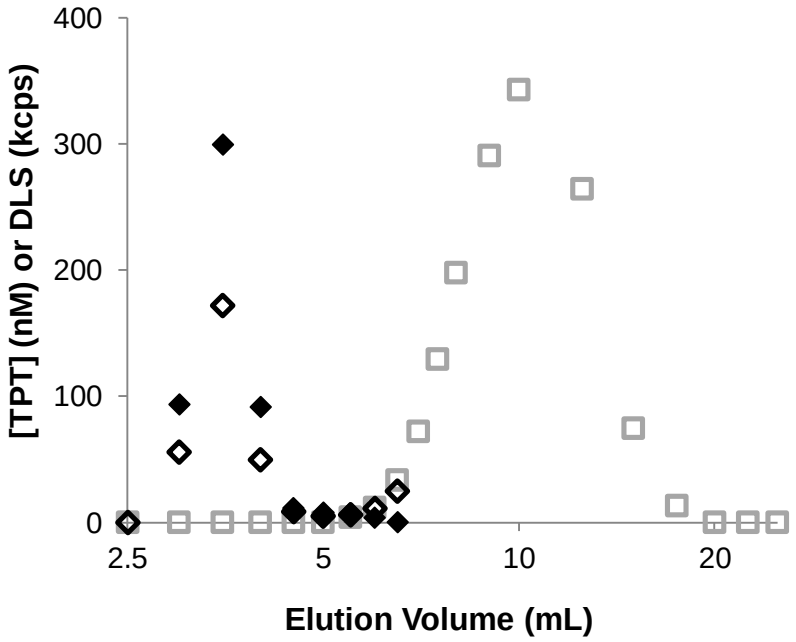

Figure 3.1. Elution profiles of free (□) or liposomal TPT (◇) analyzed by HPLC. The DLS intensity profile generated by liposomes (◆) is also shown to indicate separation of free from entrapped drug.

Particle size was determined by DLS for the liposomes before and after the conclusion of release studies. The average particle size in five independent release studies (with 95 % confidence interval) was 98 ± 2 nm before studies began and 100 ± 3 nm after release studies were concluded. Because phospholipids undergo acid-catalyzed ester hydrolysis, [142-144] the stability of the phospholipid bilayer under acidic conditions for extended periods of time could lead to lipid loss during the release study and alter release kinetics.[143] Lipid stability was evaluated by monitoring lipid content in solution using HPLC with an ELSD. Figure 3.2 demonstrates that liposomal suspensions employed in release studies conducted under non-sink conditions exhibited no lipid loss during the 96 hour period in which release was monitored.

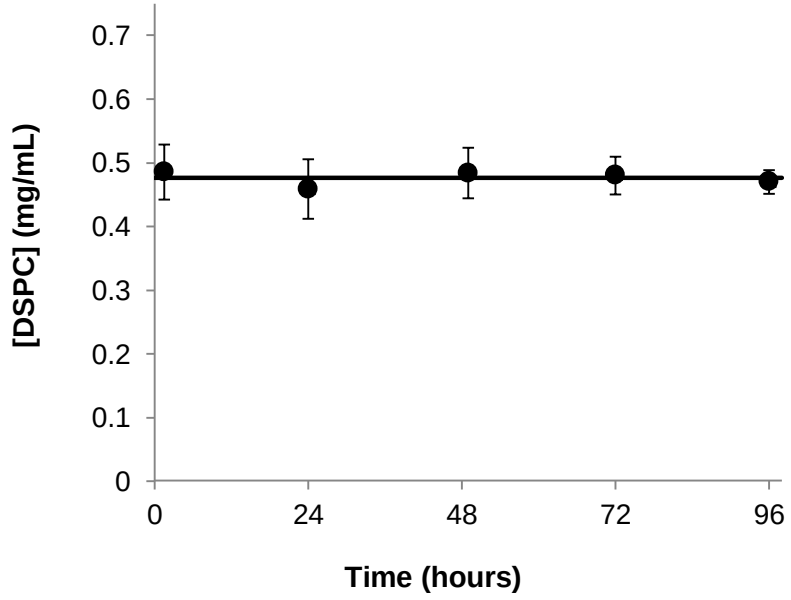

Figure 3.2. Lipid content was monitored during non-sink release studies. The line indicates the average of all measured lipid concentrations and shows lipid content remained constant throughout the release experiments. Error bars represent 95% confidence intervals.

3.3.2 Recovery from ultrafiltration and volume changes in dynamic dialysis

Corrections were required to obtain the true release profiles from changes in drug concentration observed by both ultrafiltration and dynamic dialysis methods. Values for the % of TPT and lipid recovered after ultrafiltration have been reported previously under similar conditions.[130] The % of lipid recovered was used to determine the actual amount of intravesicular drug present in samples as trace amounts of extravesicular TPT still present after separation by Sephadex®[118] would lead to a lower % of TPT recovered.[130]

Additionally, any extravesicular drug still present after ultrafiltration could also lead to an overestimation in the binding coefficient observed. To determine the % of extravesicular drug present in the retentate after ultrafiltration, blank liposome suspensions were spiked with TPT followed by immediate ultrafiltration. Using similar drug and lipid concentrations as those employed in release studies, the % of extravesicular TPT recovered during ultrafiltration was determined to be 1.5 ± 0.2 %. This recovery was similar to the 1.4 % that would be expected based on the 26 μL of ultrafiltrate suspension that was retained after ultrafiltration. For non-sink release studies, the initial concentration of extravesicular drug was never more than 0.2% of the drug concentration used to load the liposomes.

Dynamic dialysis studies also required corrections in drug concentration due to increases or decreases in volume within the dialysis tube. Additionally, the effect of sample removal also needed to be taken into account. For these dynamic dialysis studies, 4.5 mL of solution was initially observed to fill the dialysis tubes to the top of the dialysis membrane. However, these tubes swelled during release studies. To correct for the effect of observed volume changes on drug concentration, the rate of volume swelling was determined. This was achieved by filling a fresh set of dialysis tubes initially with 4 mL (V_o) of buffer solution, then monitoring volume changes over 72 hours at the same conditions used in dynamic

dialysis release studies. The rate of swelling, k_v, and tube volume at equilibrium, V_{eq}, could be determine using the equation below.

$$V = V_0 + (V_{eq} - V_0)(1 - e^{-k_v t}) \quad (21)$$

The resulting swelling profile of the dialysis tubes is shown by Figure 3.3a and resulted in a k_v of 0.13 ± 0.02 hr^{-1} while V_{eq} varied greatly between dialysis tubes (ranging from 4.8 – 5.3 mL. Using this rate constant and the V_{eq} determined for each dialysis tube, the loss of lipid observed in dynamic dialysis studies could be accounted for using the correction factors described by equations 13 – 16 and is illustrated by Figure 3.3b. These equations were then applied to TPT concentrations obtained during dynamic dialysis studies to reflect drug loss due only to liposomal release.

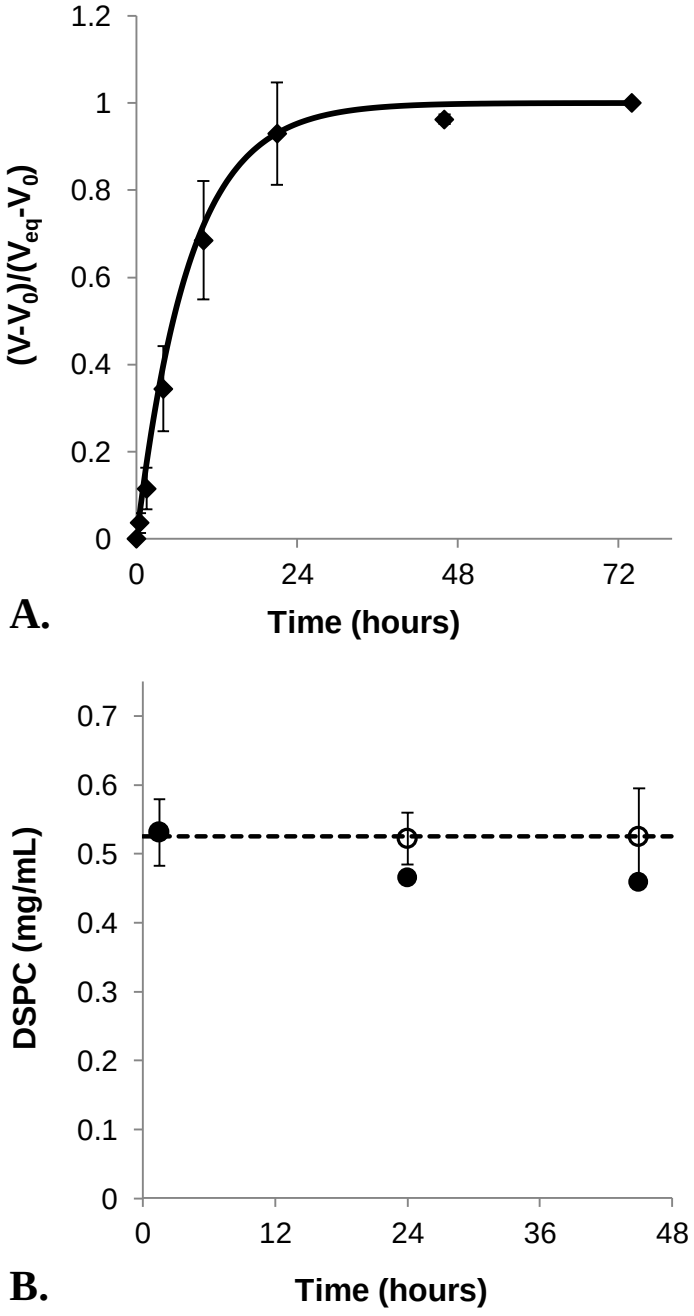

Figure 3.3. The rate of dialysis tube swelling was monitored and used to determine a swelling rate constant for the dialysis tubes used in dynamic dialysis studies (A). Using this swelling rate and accounting for the volume of sample removed over time, the loss in lipid observed over time in dynamic dialysis studies (●) could be accounted for (O) (B).

3.3.3 Comparison of release studies under non-sink and sink conditions

In addition to these corrections, the parameters calculated in Table 3.1 which describe the ratio of aqueous and membrane volumes for the intravesicular compartment (a and b respectively) and the extravesicular compartment (c and d respectively) along with the ratio of entrapped and external volume (f_v) were required for model fitting (see Appendix for a more detailed explanation) and calculated using previously reported values and equations.[50, 135] With this information, the kinetic parameters for drug release under non-sink and sink conditions could be compared. For simplicity and because equilibrium is nearly reached in these non-sink studies, K_i' and K_o' are assumed to be equivalent at the end of these studies and thus referred to from this point on as K'. Fitting of release profiles from 0.48 mg lipid/mL suspensions under non-sink conditions as shown in Figure 3.4a resulted in a k'_m of 0.51 ± 0.05 hr^{-1} and K' of 73 ± 2. For dialysis studies, drug transport across the dialysis membrane may affect observed drug release.[49, 118] As such, release profiles from passively loaded liposome suspensions and blank liposome suspensions spiked with TPT were simultaneously fit to determine both k'_m and the rate constant for TPT transport across the dialysis membrane (k_d). Because K' cannot be determined from dynamic dialysis studies, it was held constant at the value determined from the non-sink studies. Using this value and the parameters listed in Table 1, k'_m and k_d were simultaneously fit as shown by Figure 3.4b, resulting in values of 0.50 ± 0.04 hr^{-1} and 0.79 ± 0.13 hr^{-1} respectively. The release profile of passively-loaded liposomes in Figure 3b also exhibits a lag time consistent with accumulation of released drug within the dialysis tube caused by the non-instantaneous rate of drug transport across the dialysis membrane.[49, 118] The values of k'_m determined from both methods are nearly identical and show that non-sink studies can simultaneously provide accurate release rate constants along with drug binding information.

Table 3.1. Volume parameters used when comparing release studies of liposome suspensions under non-sink and sink-conditions

Lipid Suspension Concentrations	a	b	c	d	f_v
0.48 mg/mL (non-sink)	0.85	0.15	0.99982	0.00018	0.00122
0.51 mg/mL (dialysis)	0.85	0.15	0.99980	0.00020	0.00135

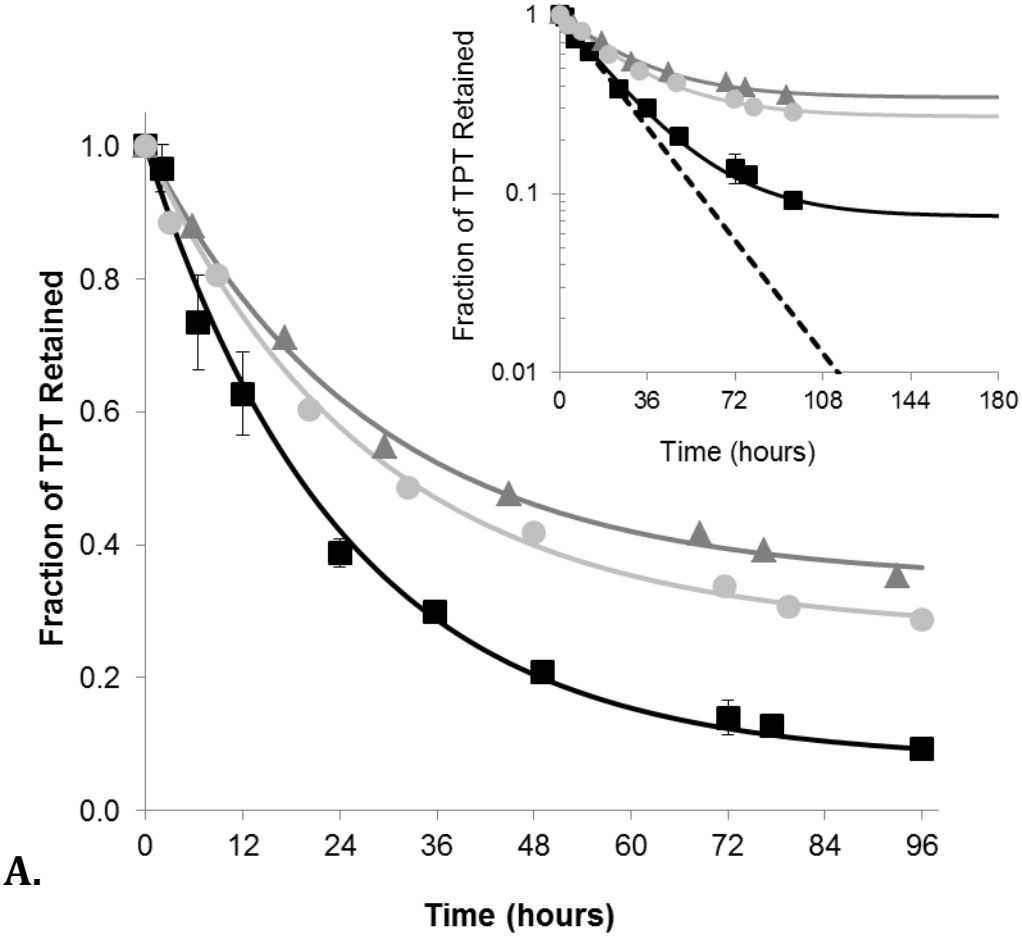

A.

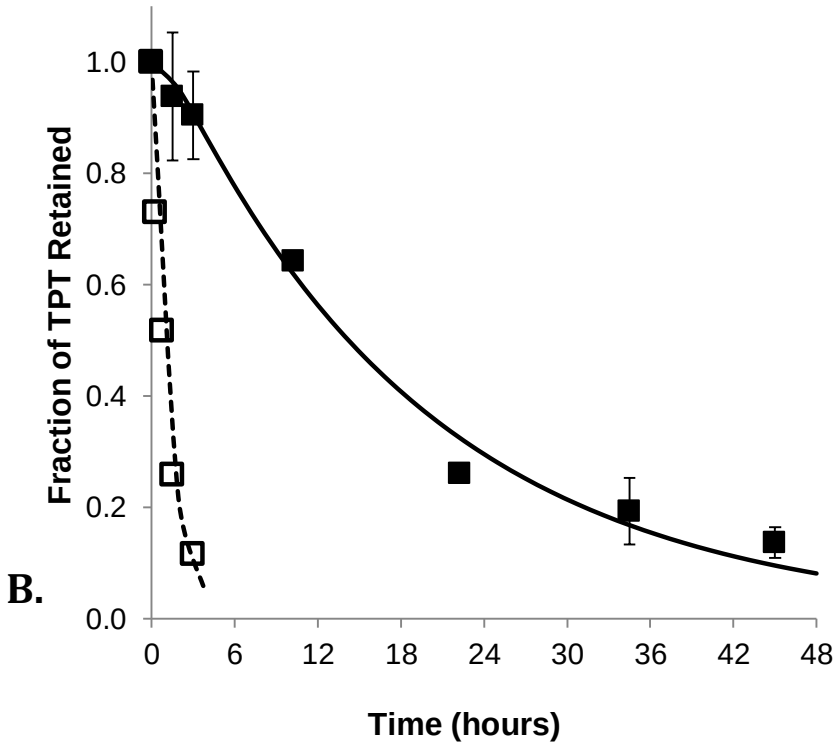

Figure 3.4. A comparison of the release profiles of TPT from DSPC/mPEG-DSPE liposomes obtained from ultrafiltration (A) and dynamic dialysis (B) methods at pH 4.0, 37 °C. A) The release profiles of TPT under non-sink conditions are shown for suspensions of 0.48 (■), 5.44 (●), and 15.3 (▲) mg lipid /mL along with the fits of these data to the mathematical model describing release under non-sink conditions (represented by the lines of corresponding color). The inset at the top right compares the approach to equilibrium occurring under non-sink conditions to a simulated profile of release under sink conditions (▬ ▬). B) The release profiles of TPT using dynamic dialysis. After correcting for volume swelling and sampling of the dialysis tube, TPT release from passively loaded liposomes (■) and blank liposome suspensions spiked with free drug (□) were fit simultaneously, producing their respective release profiles (▬ and ▬ ▬). Error bars indicate the standard deviation at each time point of triplicate release experiments.

3.3.4 Drug and lipid concentration effects on drug partitioning probed by non-sink method

Further validation of the non-sink method to examine release kinetics was performed by varying the suspension concentration of lipid. For these studies, the same initial concentration of TPT was used to passively load the three different lipid suspensions. This was done to avoid drug self-association effects on release kinetics (i.e., to maintain the same intravescicular driving force between the studies).

Because equilibrium is achieved with a different extent of drug released due to changes in membrane binding of drug, the effects of membrane binding (K') in addition to TPT permeability (k'_m) on release may be observed by calculating the half-life to equilibrium ($t_{1/2}$) from these non-sink release studies. This calculation starts by solving for $t_{1/2}$ with the rearrangement of equation 2a and substituting for T_o using the mass balance $T_o = f_v(T_{i,0} - T_i)$.

$$-\frac{dT_i}{dt} = k'_m T_i(f_i^w + f_o^w f_v) - k'_m f_o^w f_v T_{i,0} \quad (22)$$

Next, the term $k'_m f_o^w f_v T_{i,0}$ may be solved for by assuming equilibrium where $\frac{dT_i}{dt} = 0$ and $T_i = T_i^{eq}$ and 22 becomes equation 23.

$$k'_m f_o^w f_v T_{i,0} = k'_m T_i^{eq}(f_i^w + f_o^w f_v) \quad (23)$$

Substituting 23 back into 22 and rearrangement provides equation 24.

$$\frac{dT_i}{dt} = -(k'_m f_i^w + k'_m f_o^w f_v)(T_i - T_i^{eq}) \quad (24)$$

Equation 24 takes on the general form of a first order reaction. Upon integration and substituting equations A11a & b for f_i^w and f_o^w respectively, equation 25 is produced by solving for $t_{1/2}$ as the time at which the amount of drug encapsulated is halfway to equilibrium ($T_i - T_i^{eq} = 0.5(T_{i,0} - T_i^{eq})$).

$$t_{1/2} = \frac{\ln(2)}{k'_m\left(\frac{1}{a+bK'} + \frac{f_v}{c+dK'}\right)} \tag{25}$$

The fitted release profiles for the three suspensions at varying lipid concentration in Figure 3.4a resulted in similar release half-lives (see Table 3.2), indicating this method is useful over a wide range of lipid concentrations. Altering the suspension concentration of lipid to validate the non-sink method's ability to determine release kinetics also allowed critical evaluation of the membrane binding coefficient determined from these release studies. The apparent binding coefficients (*K'*) were observed to vary depending on the lipid concentration (spanning a 30-fold range). The resulting fits of *K'* were 73 ± 2, 46 ± 6, and 23 ± 3 for the 0.48, 5.44, and 15.3 mg lipid/mL suspensions, respectively.

Because this release model accounts for the differences in aqueous and membrane volumes encountered under the various conditions studied, the apparent binding coefficients should not be different between these studies. However, the cationic charge of TPT at pH 4.0 in conjunction with the varying suspension concentrations of TPT may have an effect on observed binding coefficients. Both of these variables may be accounted for with the consideration of drug self-association and the change in bilayer surface potential due to binding of cationic drug. To assess whether either or both effects contribute toward the variation in *K'* observed experimentally, TPT dimerization in solution and the varying surface potential at the lipid membrane-solution interface were evaluated and used to determine intrinsic binding coefficients for the monomeric and dimeric forms of TPT binding to the DSPC/m-PEG DSPE bilayer.

In general, the intrinsic binding coefficient, K_i^0, for any species "*i*" (in this case TPT) capable of binding to the lipid membrane may be expressed by equation 26.

$$K_i^0 = \frac{T_{i\to 0}^m}{T_{i\to 0}^w} \tag{26}$$

Essentially, K_i^0 represents the equilibrium partition coefficient at infinitely dilute concentrations within the membrane and aqueous phases ($T_{i\to 0}^m$ and $T_{i\to 0}^w$, respectively) when the membrane surface charge is zero. These intrinsic partition coefficients can be related to the observed partition coefficient at higher TPT concentrations as illustrated by equation 27.

$$K' = f_1\delta_1 K_1^0 + f_2\delta_2 K_2^0 = f_1\delta_1 K_1^0 + (1 - f_1)\delta_2 K_2^0 \quad (27)$$

Here, f_1 and f_2 account for the fractions of total TPT in the monomeric and dimeric forms, respectively, as defined by equation 19. Values of f_1 corresponding to the conditions at the end of each release study were calculated from the dimerization constant (K_2) obtained by fitting the dependence of the TPT extinction coefficient on concentration (Figure 3.5a) to the dimer model described by equations 19 and 20. The estimated value of K_2 is 6700 ± 600 M^{-1}.

Table 3.2. Values used to calculate the intrinsic DSPC bilayer/water partition coefficients for TPT species at pH 4 and 37 °C.

Parameters	Lipid suspensions		
	0.48 mg/mL	5.44 mg/mL	15.3 mg/mL
Total TPT (μM)	0.94	4.99	15.44
$t_{1/2}$ (hrs)	17 ± 2	19 ± 2	19 ± 3
K'	73 ± 2	46 ± 4	23 ± 3
f_1	0.99	0.95	0.83
$\sum_i C_i$	0.6	0.6	0.6
δ_1	1.3 ± 0.1	1.8	2.3
δ_2	1.6 ± 0.3	3.2	5.3

95% confidence intervals are shown where applicable

The δ values account for the effects of changes in membrane surface potential on species binding with increasing drug concentration. Because TPT is primarily cationic at pH 4, its

ability to bind to the bilayer surface will also depend on the membrane surface potential. Using the Gouy-Chapman theory as previously described by Austin and coworkers,[141] this effect may be calculated for any partitioned species with charge *z* using the correction factor δ_z. This correction factor is calculated with the following equation.[141]

$$\delta_z = \left[\frac{\alpha+\sum_i C_i+\sqrt{\alpha^2+2\alpha\sum_i C_i}}{\sum_i C_i}\right]^z \quad (28)$$

Here, $\alpha = \sigma/(2000RT\epsilon_0\epsilon_r)$ where σ is the surface charge density due to the concentration of TPT bound to the bilayer, ϵ_0 is the permittivity of a vacuum and ϵ_r is the relative permittivity of water. This correction is also dependent upon the bulk concentration of all electrolytes in solution, $\sum_i C_i$, and the charge of the TPT species of interest as both monomer (1^+) and dimer (2^+) forms are present in the concentration range studied.[138]

Using the values reported in Table 3.2 to account for dimerization and the membrane surface potential, K_1^0 was determined to be 80 ± 20 while the partition coefficient for the dimer, K_2^0, was found to be negligible. In Figure 3.5b, the profile generated by equation 27 using the fitted value of K_1^0 along with the dimer constant, K_2, correlates well with the experimentally-observed apparent binding constants, *K'*. The inset in 4b also demonstrates the non-linearity observed in the plot of bound drug-to-lipid ratio, T^m/L, versus unbound monomeric drug concentration conforms to the Gouy-Chapman theory.

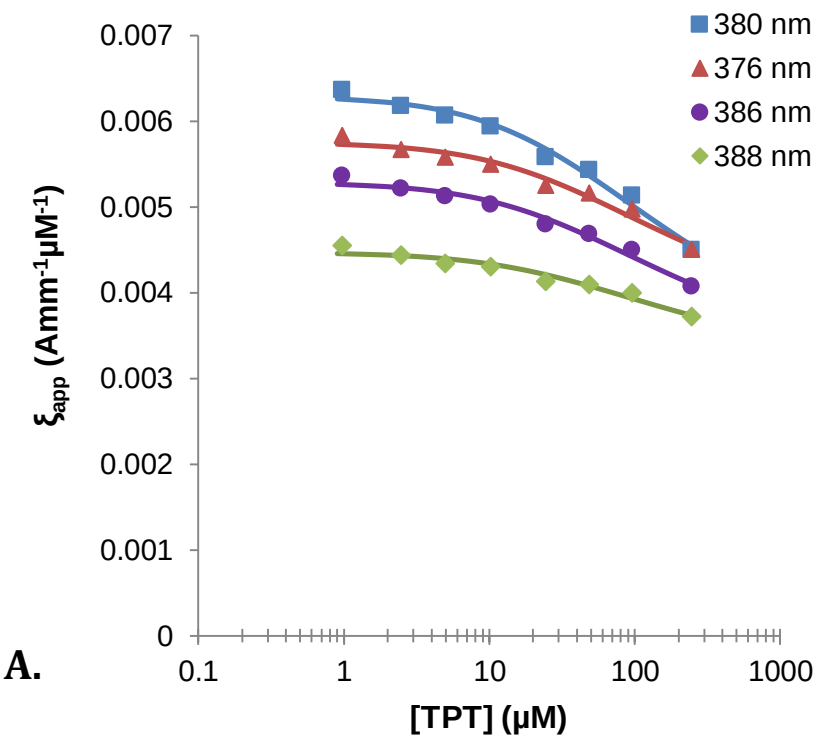
380 nm
376 nm
386 nm
388 nm
0.007
0.006
0.005
0.004
0.003
0.002
0.001
0
ξ_{app} ($Amm^{-1}\mu M^{-1}$)
0.1
1
10
100
1000
[TPT] (μM)

A.

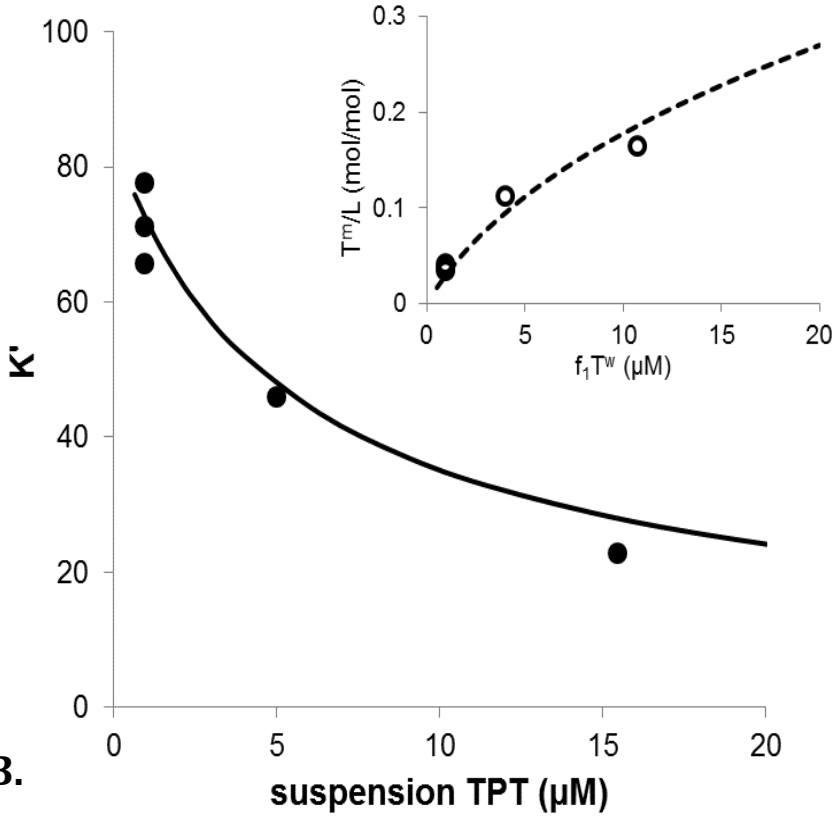
100
80
60
40
20
0
K'
0
5
10
15
20
suspension TPT (μM)
0.3
0.2
0.1
0
T^m/L (mol/mol)
0
5
10
15
20
f_1T^w (μM)

B.

Figure 3.5. A) The apparent extinction coefficients of TPT as a function of concentration at pH 4 were simultaneously fit to the dimer equations (19 and 20) to determine a dimerization constant, K_2. The plot shows extinction coefficients at 380 (blue), 376 (red), 386 (purple), and 388 (green) nm wavelengths along with lines of the corresponding color to represent the fit of the data to the dimerization model. Only four of the eight wavelengths used are shown above for clarity. B) Using K_2 and correcting for the changes in bilayer surface potential described by the Gouy-Chapman theory, the apparent binding coefficient, K', observed at the three lipid concentrations used in non-sink release studies (●) was used to determine the intrinsic binding coefficient, K_1^0 with equation 27, and the values provided in Table 3.2. The resulting fit of K' to equation 27 is shown (solid line) and correlates with the reduction in binding experimentally observed with the three TPT suspension concentrations studied. The inset to the top right compares the non-linear relationship of bound drug-to-lipid ratio, T^m/L, with increasing concentration of unbound, monomeric drug, f_1T^u, predicted by the Gouy-Chapman equation (dotted line) with that determined from non-sink release studies (O).

3.4 Discussion

3.4.1 Effect of experimental parameters on extent of drug release under non-sink conditions

For the non-sink experiments, the extent of drug release is highly dependent upon two primary factors: fraction of volume encapsulated (f_v) and the apparent membrane binding of drug to the liposomal bilayer (K'). The effect of these factors can be appreciated by examining the percentage of total drug released as defined by the following equation.

$$X = \frac{M_{o,\infty}}{M_T} \times 100\% \tag{29}$$

Here, $M_{o,\infty}$ refers to the total mass of extravesicular drug at equilibrium and M_T is the total mass of drug in the suspension.

Using the non-sink model, X can be simulated under a variety of experimental conditions (e.g. different lipid concentrations, particles sizes, drug binding coefficients etc.). Figures 3.6a and b illustrate two of the main experimental parameters affecting the total amount of drug released. Here simulations were conducted to determine the expected % of drug released, X, for varying values of binding coefficients, K', in Figure 3.6a and as a function of the ratio of entrapped volume, f_v (i.e. liposome concentration), in Figure 3.6b. In Figure 3.6a, the plot shows that increasing values of K' result in less drug released into the extravesicular compartment due to a higher amount bound to the membrane leaflet. For Figure 3.6b, the increasing values of f_v result in less drug released because a larger fraction of the total volume is within the intravesicular compartment.

It would also be convenient to generalize these relationships so that the extent of drug release from liposomes under non-sink conditions could be estimated for a wide array of experimental conditions. Such a relationship is illustrated by Figure 3.6c. This nomograph was constructed by noting that at equilibrium, the concentrations of unbound, aqueous drug in the intra- and extra-vesicular solution will be equal.

$$T_i^w = T_o^w \tag{30}$$

This relationship can then be rewritten in terms of total concentration of intra- and extra-vesicular drug using the previous derived fraction of unbound intra- and extra-vesicular drug (eqns. 11a & b) and rearranged to the following ratio.

$$\frac{T_i}{T_o} = \frac{f_o^w}{f_i^w} = \frac{a+bK'}{c+dK'} \tag{31}$$

Furthermore, one can specify the percent of drug released, X, in terms of the total suspension concentration of drug present in solution, T, for T_i and T_o as expressed by equations 32a and b.

$$T_i = \frac{(100-X)T}{E} \tag{32a}$$

$$T_o = (1 - E)XT \tag{32b}$$

Here, the fraction of total volume entrapped, E, may be expressed in terms of the previously defined ratio of entrapped to external volume, $E = f_v/(1 + f_v)$. These equations can be substituted into equation 31 and rearranged into the following equation.

$$\frac{(100-X)}{X} = \left[\frac{a+bK'}{c+dK'}\right]\frac{E}{1-E} \tag{15}$$

This relationship is linear as shown in Figure 3.6c with $E/(1 - E)$ providing the slope. Here, the slopes of lines are shown based on varying values of *E,* and the horizontal lines indicate the percent of drug which would be released at equilibrium.

The above calculations and simulations assumed that all released drug, whether membrane-bound or free in extravesicular solution, was removed during ultrafiltration due to the low binding observed in these studies. This assumption can be assessed based on the dilutions made during ultrafiltration and drug binding coefficients. Based on the highest binding coefficient obtained during these experiments (73), there would be less than a 2.5% change in the total amount of drug removed over the range of lipid concentrations (0.48 – 15.3 mg lipid/mL) used in these studies. For drugs with higher membrane binding, a similar analysis shows that a 0.5 mg lipid/mL suspension would have less than a 3% change in the amount of drug removed for a lipophilic compound having a binding coefficient of 2400.

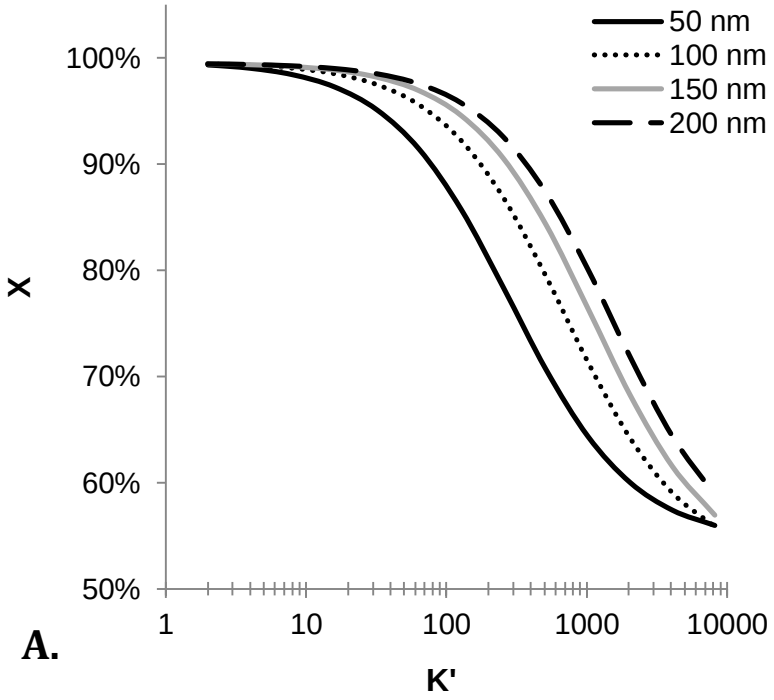
50 nm
100 nm
150 nm
200 nm
100%
90%
80%
70%
60%
50%
X
1
10
100
1000
10000
K'

A.

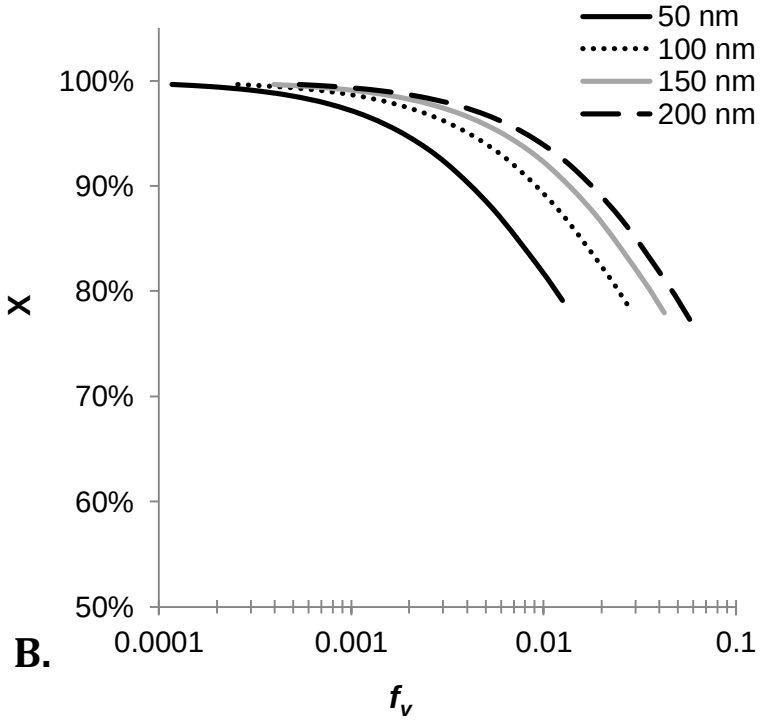
50 nm
100 nm
150 nm
200 nm
100%
90%
80%
70%
60%
50%
X
0.0001
0.001
0.01
0.1
f_v

B.

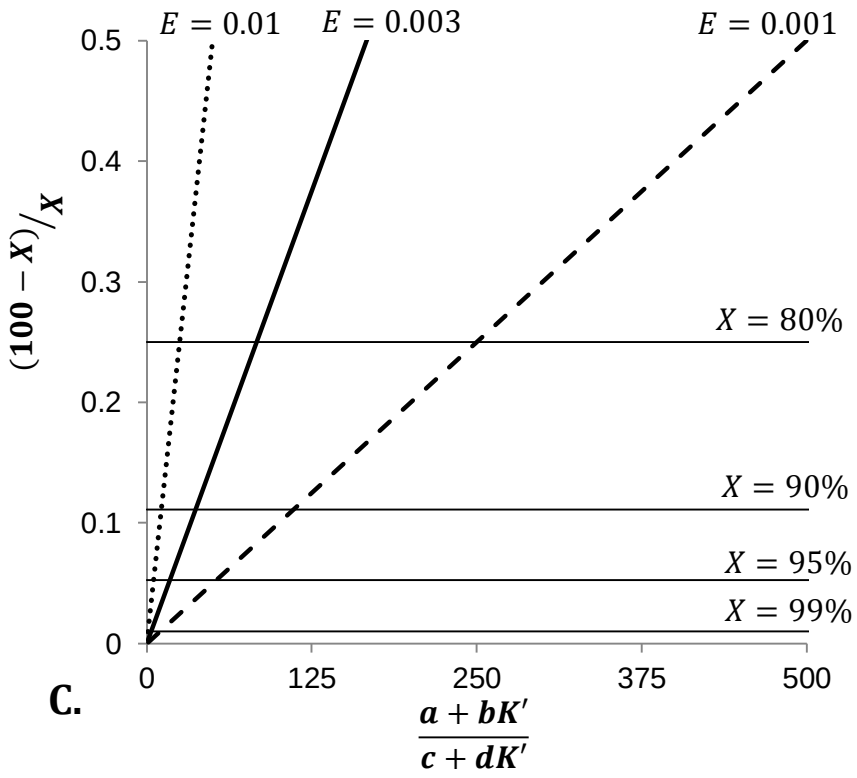

Figure 3.6. The effect of experimental parameters on total drug release at equilibrium. A) Keeping the suspension concentration constant at 0.5 mg/mL, simulations using the equations describing the non-sink model were used to determine the % of released drug, ***X***, as a function of varying values of drug binding coefficients, *K'*. These simulations are plotted for several common diameters of liposomes. B) To illustrate the effect entrapped volume, f_v , has on the amount of drug released under non-sink conditions, simulations were conducted in which *K'* was held constant at 90. The plot shows increasing f_v (i.e. increasing amount of liposomes) reduces the amount of drug released as the volume fraction entrapped increases (i.e. the number of liposomes in the suspension increase). The lines illustrate this trend for liposomes of different diameters indicated by the legend in the upper right corner of plot. C) This nomograph provides a general method for estimating the amount of released drug. The plot relates all experimental conditions affecting the amount of drug released during a non-sink release study including the drug binding coefficient, *K'*, and the volume compartments present in the suspension (*a* and *b* for intravesicular aqueous and membrane compartments, and *c* and *d* for

extravesicular aqueous and membrane compartments), to ***X*** (as indicated by the labeled, horizontal lines). This relationship is highly dependent upon the fraction of entrapped volume, *E*, as the slope steepens dramatically with increasing *E* (and subsequently higher lipid concentration).

3.4.2 Applicability to drug release characterization for other drugs and/or nanoparticle formulations

The mathematical model described here should be adaptable to other drugs and nanoparticle formulations. For every drug-nanoparticle combination, careful consideration should be given to which components of the current model are relevant and whether additional terms are necessary. For example, an evaluation of the effect of pH on release requires consideration of drug speciation as the ionization of the drug may have an effect on observed release.[49, 130] Other effects such as drug precipitation, complexation, or degradation may be taken into account by including relevant equilibrium equations to solve for the fraction of total drug free to permeate the membrane or by adding relevant kinetic terms (e.g. degradation/ineterconversion[130] or dissolution rate constant) into the rate equation. More generally, the non-sink method and model may be applicable to other agents as well as other types of nanoparticles (e.g., a current application of similar methodology underway in this laboratory involves doxorubicin-conjugated polymeric micelles).

Validation of the % recovery and % of free drug removed is critical when considering the use of ultrafiltration to isolate drug remaining within the nanoparticle. Significant binding of drug to the ultrafiltration membrane may interfere with removal of released drug by a washing step. In such cases, other methods that can separate (e.g. size-exclusion) or distinguish (e.g. spectroscopic techniques) entrapped from released drug may be more appropriate yet still amenable to the non-sink mathematical model used here.

3.5 Conclusions

The liposomal release kinetics and lipid bilayer partitioning of the anticancer agent TPT were simultaneously determined by ultrafiltering liposomal suspensions under non-sink conditions at various times. . Dynamic dialysis was used to validate these findings by providing a nearly identical release rate constant. The non-sink method was also able to probe the concentration dependence of TPT binding to the bilayer and revealed that binding was dependent on the surface potential at the bilayer interface and TPT dimerization. The non-sink method provides a reliable way to obtain both kinetic and thermodynamic descriptors. This method may also be useful in future mechanistic studies of liposomal drug release kinetics where dynamic dialysis studies are complicated by drug binding to the dialysis membrane or observed release is rate-limited by drug transport through the dialysis membrane. The parameter values and methodology provided may have utility in the development of models capable of providing *in vitro* - *in vivo* correlations; however, environmental *in vivo* factors that may alter release rates would have to be investigated and incorporated into mechanistic models to yield useful, predictive relationships for liposomal formulations.

CHAPTER FOUR

The Role of pH and Ring-opening Hydrolysis Kinetics on Liposomal Release of Topotecan

4.1 Introduction

Liposomal formulations offer several potential advantages for the intravenous delivery of antitumor agents due to their ability to increase drug solubility, reduce drug toxicity, and prolong drug release.[3] Pegylated liposomes have the added benefit of longer systemic circulation due to reduced clearance by the mononuclear phagocytic system. [3, 30-32] This prolonged circulation time when combined with an appropriate particle size provides preferential delivery of liposomes to solid tumors, a result of the well-known enhanced permeability and retention of nanoparticles in tumors. [3, 8, 31] These properties have led to the FDA-approved liposomal formulation of doxorubicin (DOXIL®) as well as other drug products, including several currently in clinical trials.[33-40]

When investigated systematically, the antitumor efficacy of drug-loaded liposomal formulations has been closely linked to the drug release rate.[21-24] Such investigations imply that the ability to tailor liposomal drug release rates could enable clinicians to optimize efficacy for a specific tumor by selecting the delivery system that produces the optimal tumor concentration profile. Protracted or metronomic dosing regimens have shown such promise with enhanced antitumor agent efficacy,[1, 145, 146] but these approaches are unable to take advantage of the localized intratumoral drug release afforded by liposomes and other nanoparticulate systems. Liposomal systems that provide predictable drug release rates would reduce the frequent visits and monitoring currently necessary due to the narrow therapeutic window and rapid clearance of many chemotherapeutics.

While many models have been developed to describe drug loading,[124, 127, 139, 140] few have considered release kinetics [49, 60, 128] and even fewer have been validated experimentally. [49, 60, 124] Mechanistic models that incorporate physicochemical properties of the drug in solution including the drug species present as a function of intraliposomal pH, their interactions with the lipid bilayer, and their membrane permeabilities would be essential to release rate design and optimization.

Liposomal formulations of topotecan (TPT) serve as a prime example of the need for mechanistic models to reliably predict drug release rates under a variety of loading and release conditions. TPT is a topoisomerase I inhibitor currently approved to treat cervical, ovarian, and small cell lung cancers as an injectable solution and in multiple clinical trials as the sole medication or in conjunction with other medications and/or radiation.[84-88] Like other weakly basic drugs, TPT exhibits high encapsulation efficiency in liposomal formulations utilizing active loading strategies.[21, 42, 61, 73, 95-97] Previous work with liposomal TPT has mainly focused on encapsulation strategies, while the emphasis on controlled or extended release has been limited.[24, 42, 62, 64, 97]

Studies that systematically examine various formulation and releasing-media parameters are necessary to develop a model capable of understanding and controlling release. Since the generation of a low-intravesicular pH is a prerequisite for active loading of weak bases while drug release occurs under physiological conditions near a neutral pH, [64, 73, 96] evaluating the sensitivity of TPT release to both the intra- and extravesicular pH is critical to the development of a mechanistic model having practical utility. Over this pH range, TPT is assumed to exist in solution as one of four major species as illustrated in Scheme 4.1.

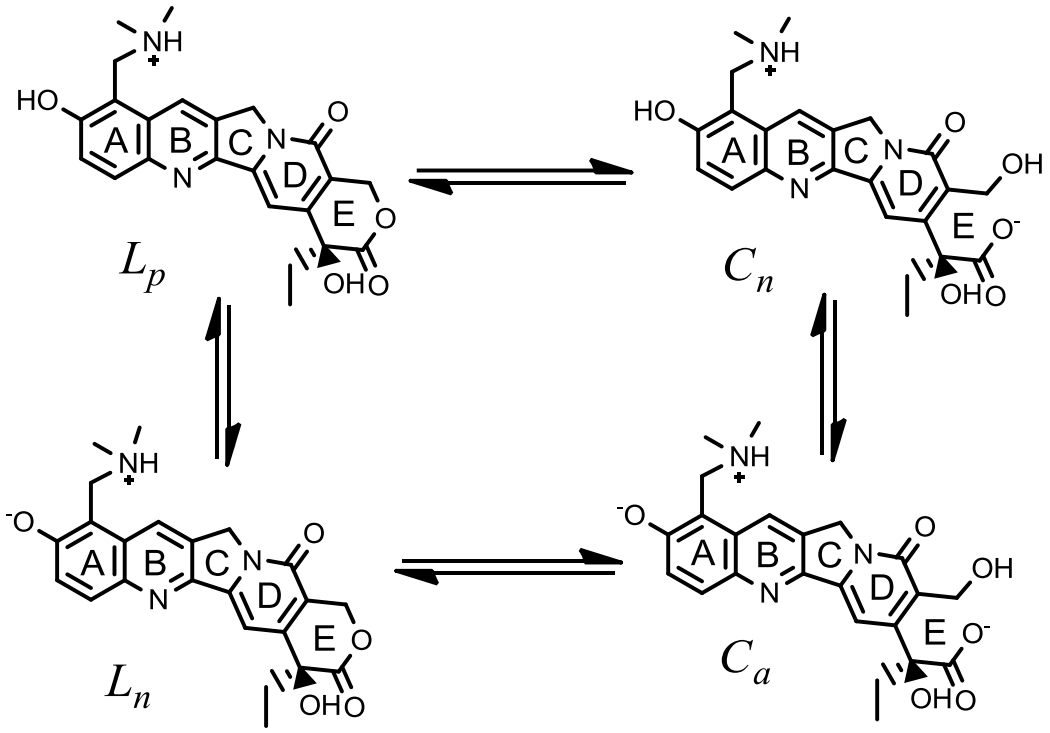

Scheme 4.1. The major species of TPT in solution in the low to neutral pH range. Two lactone forms are present ($L_p$and L_n) differing in the state of ionization of the phenol on ring A. Reversible hydrolysis of the lactone E-ring may transform these species to their carboxylate counterparts (C_n and C_a respectively).

The aim of the present work was to determine the pH sensitivity of TPT release from unilamellar liposomes and develop a mechanism-based mathematical model to account for the observed transport rates. To completely account for the pH-permeability profiles obtained experimentally, the mathematical model had to include the effects of TPT speciation via ionization, membrane-binding equilibria, drug species' permeability coefficients, and the kinetics and pH dependence of TPT lactone ring-opening/closing.

4.2 Materials and Methods

4.2.1 Materials

Powders of 1,2-Distearoyl-sn-glycero-3-phosphatidylcholine (DSPC, >99% purity) and 1,2-distearoyl-sn-glycero-3-phosphoethanolamine-N-[methoxy(polyethyleneglycol)-2000] (m-PEG DSPE, MW = 2806, >99% purity) were purchased from Avanti Polar Lipids (Alabaster, AL). Topotecan hydrochloride was purchased from AK Scientific (Union City, CA). Millipore ultrafiltration cartridges (Amicon® Ultra 0.5 mL centrifugal filter device with 30,000 MWCO Ultracel® membrane), Nuclepore polycarbonate membranes (0.1 μm), solvents, and buffer salts were purchased from Fisher Scientific (Florence, KY). All solvents were HPLC grade.

4.2.2 Preparation and characterization of DSPC/m-PEG DSPE liposomes for lactone-carboxylate interconversion and release studies

Large unilamellar vesicles were formed using the film hydration and extrusion process described in several previous reports with slight modifications.[49, 62] Briefly, DSPC and m-PEG DSPE (95:5 mol:mol) lipids were weighed into borosilicate vials, then dissolved in chloroform. The chloroform was subsequently evaporated under a stream of N_2 and the residue was vacuum-dried at 40°C for 6 hours to form a thin lipid film. Films were hydrated and passed 10 times through two stacked Nuclepore polycarbonate membranes (100 nm pore) using a Liposofast® extrusion device at 60°C to obtain unilamellar vesicles. All solutions for film hydration were made with a buffer concentration of 50 mM and adjusted to an ionic strength of 0.3 with NaCl. The reported pH was measured at 37 °C. Liposomes used in lactone-carboxylate interconversion studies were composed of lipid films hydrated with pH 6.33 (2-(*N*-morpholino)ethanesulfonic acid (MES)) and pH 7.67 (Tris) to achieve a final lipid concentration of 50 mg/mL. Liposomes for release studies were hydrated with

solutions of pH 3.35 (chloroacetate), 4.01 (formate), 5.01 (acetate), 5.92 and 6.33 (MES), 7.04 and 7.39 (phosphate), and 7.67 (Tris) containing 50 μM TPT, yielding a lipid concentration of 40 mg/mL.

For the calculation of vesicle volume parameters, particle size and lipid content were determined. Liposome particle size was analyzed using a Beckman Delsa™ Nano C Particle Sizer with a 70 second accumulation time. Particle size before and after release studies was determined using Cumulants analysis. Liposome suspensions were diluted by a factor of 10 before analysis to obtain intensity readings within the detection range of the instrument. To avoid interference from dust and other artifacts during size analysis, the buffers used in liposome hydration and subsequent release studies were filtered with a 0.22 μm nitrocellulose filter. Samples were stored at 4°C until analysis. Lipid content was determined using HPLC and is described in further detail in the analyses section.

4.2.3 Fluorescence measurements of aqueous TPT solutions

The acid dissociation constant of the TPT A-ring phenol was determined using changes in fluorescence excitation spectra with pH. Solutions of 500 nM TPT were prepared at various pH with buffers of formate (pH 3.50), acetate (4.50 and 5.50), MES (pH 6.00 and 6.27) and phosphate (pH 6.50, 6.80, 7.20, and 7.50) at concentrations of 50 mM while ionic strength was kept at 0.3 by adjustment with sodium chloride. Solutions were scanned with a FluoroMax-3 (Jobin Yvon Inc., Edison, NJ). Excitation scans were made over a range of 300 – 470 nm using an emission wavelength of 560 nm. The temperature of the sample chamber was maintained at 37 °C, and fluorescence intensity was recorded using a 0.5 second integration time and a 3 nm band pass width.

4.2.4 TPT interconversion studies

Kinetic studies of the reversible and pH dependent ring-opening/closing of TPT were conducted with 0.4-0.6 μM TPT solutions at pH 5.92, 6.33, 7.04, 7.39, and 7.67 using the same buffers used to hydrate liposomes. At pH 5.92 and 6.33, solutions were spiked with a 50 μM stock solution of the ring-opened TPT carboxylate dissolved in 0.1 N NaOH. Studies at higher pH used a 50 μM stock of lactone TPT in DMSO. To determine the effect (if any) of TPT binding to the bilayer, interconversion studies were also conducted in 50 mg/mL liposome suspensions at pH 6.33 and 7.67 and compared with profiles obtained in aqueous solution.

At various times, 150 μL samples were withdrawn and interconversion was quenched using 300 μL of a chilled (-20 °C) 2:1 (v:v) acetonitrile: methanol solution. Samples were immediately injected and analyzed by HPLC for both ring-opened carboxylate and lactone content. All studies were conducted in a water-jacketed incubator maintained at 37 °C and stirred at 200 rpm with a 10 x 5 mm Teflon stir bar using a Thermo Cimerac iPoly 15 multipoint stirrer.

4.2.5 Release of TPT from DSPC/DSPE-PEG-2K liposomes

Release studies were conducted in a similar manner as reported previously.[147] Unencapsulated TPT present in passively loaded liposome suspensions was removed by passing suspensions through a Sephadex G-25 column equilibrated with the same buffer as the liposome suspension. Aliquots of liposome suspension (0.2–0.5 mL) were passed through the column and the drug-loaded liposome fraction eluting between 2.5–5 mL was collected, yielding liposome suspensions for release studies having lipid concentrations of 1.0-4.5 mg/mL. Liposome suspensions were transferred to glass vials capped with a rubber stopper and stirred at the same conditions used for interconversion studies within a water-

jacketed incubator maintained at 37 °C. Suspension temperature was monitored daily using a digital thermometer over the time span of release studies.

Encapsulated drug was monitored by ultrafiltration of 50–150 μL aliquots of liposome suspension taken at various time points. Each aliquot was diluted with chilled (4 °C) buffer to 425 μL and ultrafiltered using an Amicon® Ultra 0.5 mL centrifugal filter device with 30,000 MWCO Ultracel® membrane. Cartridges were then centrifuged at 14,000 rpm for 10 minutes in an Eppendorf 5417R maintained at 4 °C. The concentrated suspension (50 μL) was recovered by inverting the cartridge and centrifuging at 2000 rpm for another 2 minutes. Recovered concentrate was resuspended in another 400 μL of chilled buffer and the process was repeated. The final concentrate was dissolved in acidified methanol and diluted within the calibration range for HPLC analysis.

4.2.6 HPLC analyses

Samples from interconversion studies were analyzed for TPT concentration by HPLC.[148] A Waters Alliance 2695 separation system coupled to a Waters fluorescence detector (M474) was employed with excitation and emission wavelengths at 380 and 560 nm, respectively. Interconversion studies measured both lactone and carboxylate forms of TPT using a Supelcosil™ ABZ+ column (250 x 4.6 mm, 5 μm) and guard column (20 x 4.0 mm, 5 μm) with a mobile phase (14% acetonitrile: 86% (v/v) of 5% (pH = 5.5) triethylamine acetate, 50 mM tetrabutylammonium hydrogen sulfate (TBAHS) buffer) flow rate of 1.5 mL/min. Lactone TPT standards were prepared in chilled, acidified methanol (-20 °C) and carboxylate standards were prepared in 10 mM sodium carbonate buffer (pH 10.1) at 20-200 nM concentrations. Lactone and carboxylate retention times were 5.5 and 2.1 min, respectively.

For release studies, samples were diluted in chilled, acidified methanol (0.001 N HCl for studies at pH ≤ 5.01 and 0.02 N HCl for studies conducted at higher pH) to convert all TPT to its lactone form. Samples were stored at -20 °C until analysis. TPT lactone was then analyzed using a Waters Symmetry® C18 column (4.6×150 mm, 5 μm) and guard column (3.9 x 20 mm) with a mobile phase (16% acetonitrile: 84% (v/v) of 5% (pH = 5.5) triethylamine acetate buffer) flow rate of 1 mL/min. Sample compartment and column were kept at ambient temperature. The retention time for TPT lactone was 4.5 min and response was linear between 20 and 200 nM.

Lipid analysis was performed with HPLC using an evaporative light scattering detector (ELSD, Sedere, Inc., Lawrenceville, NJ) based on a previously described method using an Allsphere (Alltech Associates, Inc., Deerfield, IL) silica column (4 x 150 mm, 5 μm) and guard column (20 x 4.0 mm, 5 μm). The elution method employed a linear gradient composed of 100% mobile phase A (80% chloroform:19.5% methanol:0.5%(v/v) NH4OH) changing to 80% mobile phase A and 20% mobile phase B (80% methanol:19.5% water:0.5% (v/v) NH_4OH) at 3 min which was maintained until 7 min, and returned to 100% mobile phase A at 14 min at a flow rate of 1 mL/min.[49] Samples (100 μL) were dried at room temperature under N_2, then dissolved in chilled mobile phase A before analysis.

4.2.7 Mechanism-based mathematical model development

4.2.7.1 Mathematical model for liposomal TPT release including kinetics of lactone ring-opening/closing

Scheme 4.2 depicts the equilibria and rate constants that influence the rate of liposomal release of TPT as a function of pH. While the mechanistic approach is similar to those employed previously for other compounds,[49, 60, 124] the species present and parameter values will obviously differ. Using this scheme, a mathematical model that accounted for

the various species of TPT as a function of pH was developed and described in the following section.

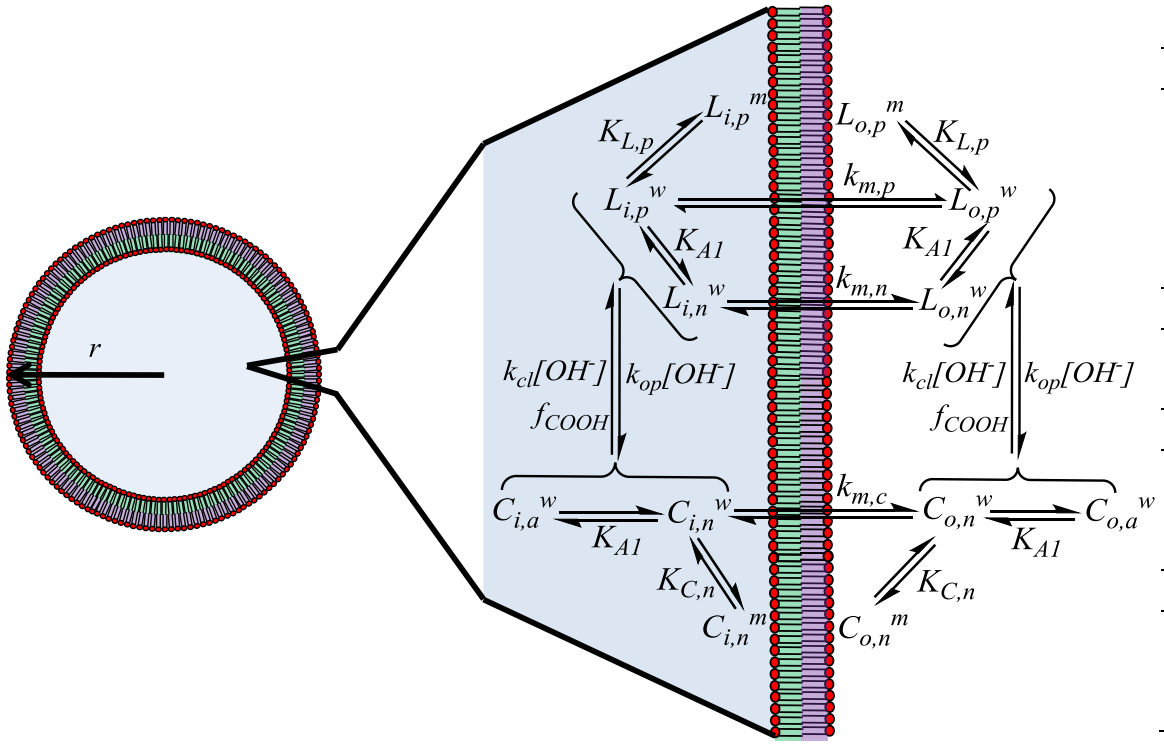

Symbols and description	
K_{A1}	Phenol ionization
w	Aqueous species
m	Membrane-bound species
i	Intravesicular
o	Extravesicular
Partition coefficients	
$K_{L,p}$	Binding for species L_p
$K_{C,n}$	Binding for species C_n
Release constants (hr^{-1})	
$k_{m,p}$	For species L_p
$k_{m,n}$	For species C_n
$k_{m,c}$	For species C_n
Interconversion kinetics	
k_{cl}	Ring-closing rate constant (hr^{-1})
k_{op}	Ring-opening rate constant (hr^{-1})
f_{COOH}	Carboxylate fraction

Scheme 4.2. A schematic of the associated equilibria and kinetics governing liposomal release of TPT. The liposome depicted with radius, *r*, highlights the volume compartments described in the mathematical model. The different volume compartments are color coded with blue highlighting the inner aqueous volume, V_i^w, while the green and violet sections refer to the inner, V_i^m, and outer, V_o^m, membrane volumes, respectively. The transport pathways and binding/ionization equilibria for all species illustrated in Scheme 4.1 are also depicted and described in the accompanying table (right).

Based on Scheme 4.2, the total amount of drug inside and outside liposomes consists of various solution and membrane-bound species (Equations 1a and b):

$$M_i = M_{i,L}^u + M_{i,L}^m + M_{i,C}^u + M_{i,C}^m \quad (1a)$$

$$M_o = M_{o,L}^u + M_{o,L}^m + M_{o,C}^u + M_{o,C}^m \quad (1b)$$

In these equations and from this point on, the superscripts *u* and *m* represent unbound species in the aqueous compartment and phospholipid membrane bound species, respectively; the subscripts, *i*, and, *o*, refer to the intra- and extravesicular compartments, respectively; and and L and C refer to the lactone and carboxylate TPT species, respectively. These mass balance equations can be transformed to concentrations using volume ratios of the aqueous and membrane volumes of the inner and outer compartments. These are expressed below in Equations 2a-e using the same annotations for volume as in Scheme 4.2.

$$a = \frac{V_i^w}{V_i^T}, b = \frac{V_i^m}{V_i^T}, c = \frac{V_o^w}{V_o^T}, d = \frac{nV_o^m}{V_o^T}, f_v = \frac{nV_i^T}{V_o^T} \quad (2a\text{-}e)$$

Combining the mass balance equations with Equations 2a-d produced equations for total drug concentration within, T_i, and outside, T_o, the vesicles as described below.

$$T_i = a(L_i^u + C_i^u) + b(L_i^m + C_i^m) \quad (3a)$$

$$T_o = c(L_o^u + C_o^u) + d(L_o^m + C_o^m) \quad (3b)$$

Total drug release within a liposome suspension may be described by the total rate of change for both intra- and extravesicular concentrations of TPT ($\frac{dT_i}{dt}$ and $\frac{dT_o}{dt}$, respectively). This total rate of change is the sum of the rates of change for both the lactone, $\frac{dL_i}{dt}$ & $\frac{dL_o}{dt}$, and carboxylate, $\frac{dC_i}{dt}$ & $\frac{dC_o}{dt}$, forms of TPT in the intra- and extravesicular compartments. This is expressed in Equations 4a and b.

$$\frac{dT_i}{dt} = \frac{dL_i}{dt} + \frac{dC_i}{dt} \tag{4a}$$

$$\frac{dT_o}{dt} = \frac{dL_o}{dt} + \frac{dC_o}{dt} \tag{4b}$$

The driving force governing liposomal drug release is the concentration gradient between the unbound, intra- and extra-vesicular concentrations of the permeable species. In the case of TPT, pH-dependent ring-closure may become the rate-limiting step for drug release under certain conditions. Thus, the rates of change of the intravesicular lactone and carboxylate concentrations are determined by both diffusive and chemical kinetic contributions as depicted in Equation 5.

$$rate = diffusion + interconversion \tag{5}$$

These terms can be explicitly written for the rates of both the lactone and carboxylate forms of TPT as shown by Equations 6a-d.

$$\frac{dL_i}{dt} = -k'_{m,L}(L_i^u - L_o^u) - k_{cl}K_0L_i + k_{cl}f_{COOH}C_i \tag{6a}$$

$$\frac{dC_i}{dt} = -k'_{m,C}(C_i^u - C_o^u) + k_{cl}K_0L_i - k_{cl}f_{COOH}C_i \tag{6b}$$

$$\frac{dL_o}{dt} = k'_{m,L}f_v(L_i^u - L_o^u) - k_{cl}K_0L_o + k_{cl}f_{COOH}C_o \tag{6c}$$

$$\frac{dC_o}{dt} = k'_{m,C}f_v(C_i^u - C_o^u) + k_{cl}K_0L_o - k_{cl}f_{COOH}C_o \tag{6d}$$

The colors highlighting the various terms in Equations 6a-d correspond to those in Equation 5. In these equations, the rates of change of intravesicular lactone and carboxylate (highlighted green) are composed of diffusive (yellow) and chemical kinetic components (blue) describing interconversion of TPT between its lactone and carboxylate forms. The diffusive term describes bilayer-limited Fickian diffusion using a pseudo steady-state

approximation (based on the absence of a lag time in the observed drug release profiles). The two terms to the right reflect the reversible kinetics of TPT lactone ring opening and closing. The term f_v accounts for the ratio of total entrapped volume to total volume as defined by Equation 2e.

In the *diffusion* term, $k'_{m,L}$ and $k'_{m,C}$ are effective transport rate constants for the lactone and carboxylate species, respectively. These constants are pH dependent, as determined by the various ionization states of the lactone and carboxylate species (Scheme 4.1) and their permeability coefficients. The superscript, u, indicates that only lactone and carboxylate species not bound to the membrane contribute to the diffusive driving force governing release.

The transport rate constants for the lactone and carboxylate forms of TPT are dependent upon their ionization states and will vary depending upon the pH. These factors are accounted for by Equations 7a and b for both the lactone, $k'_{m,L}$, and carboxylate, $k'_{m,C}$, respectively:

$$k'_{m,L} = f_{L_p}^{u} k_{m,L_p}^{0} + f_{L_n}^{u} k_{m,L_n}^{0} \tag{7a}$$

$$k'_{m,C} = f_{C_n}^{u} k_{m,C_n}^{0} + f_{C_a}^{u} k_{m,C_a}^{0} \tag{7b}$$

Lactone transport is a function of the fraction of the protonated species and its transport coefficient, k_{m,L_p}^{0}, and the fraction of zwitterionic phenolate and its transport coefficient, k_{m,L_n}^{0}. Similarly, carboxylate transport is governed by the fraction of the zwitterionic form and k_{m,C_n}^{0}, and the anionic phenolate fraction and k_{m,C_a}^{0}. The lactone and carboxylate forms were assumed to have the same phenol group pK_a because of the separation of the A-ring phenolic –OH from the lactone ring. Therefore,

$$f_{L_p}^u = f_{C_n}^u = \frac{H^+}{H^+ + K_{a1}}; f_{L_n}^u = f_{C_a}^u = \frac{K_{a1}}{H^+ + K_{a1}} \quad (8a;b)$$

Next, the concentration gradient of aqueous, unbound drug must be solved in terms of total drug encapsulated for both lactone and carboxylate. This is accomplished by incorporating the apparent volume-based membrane partition coefficients for the lactone, K_L', and the carboxylate, K_C', as shown in Equations 9a and b.

$$L_i^u = f_{i,L}^u L_{i,T};\ f_{i,L}^u = \frac{1}{a + bK_L'} \quad (9a)$$

$$C_i^u = f_{i,C}^u C_{i,T};\ f_{i,C}^u = \frac{1}{a + bK_C'} \quad (9b)$$

Similar substitutions can be made for the extra-vesicular fraction unbound for lactone, $f_{o,L}^u$, and carboxylate, $f_{o,C}^u$, using the ratios for extra-vesicular membrane, *c*, and aqueous, *d*, volume.

As before with permeability, ionization of these species may also affect binding. The apparent partition coefficients may then be written in terms of the intrinsic partition coefficients of each ionization state.

$$K_L' = f_{L_p}^u K_{L_p}^0 + f_{L_n}^u K_{L_n}^0 \quad (10a)$$

$$K_C' = f_{L_p}^u K_{C_n}^0 + f_{L_n}^u K_{C_a}^0 \quad (10b)$$

By substituting the expressions in Equations 7 and 9 into Equations 6a-d, the differential equations may be solved in terms of total intra- and extra-vesicular concentrations of lactone and carboxylate species.

$$\frac{dL_i}{dt} = -\left(f_{L_p}^u k_{m,L_p}^0 + f_{L_n}^u k_{m,L_n}^0\right)\left(f_{i,L}^u L_i^u - f_{o,L}^u L_o^u\right) - k_{cl} K_0 L_i + k_{cl} f_{COOH} C_i \quad (11a)$$

$$\frac{dC_i}{dt} = -(f_{L_p}^u k_{m,C_n}^0 + f_{L_n}^u k_{m,C_a}^0)\left(f_{i,L}^u C_i^u - f_{o,L}^u C_o^u\right) + k_{cl}K_0 L_i - k_{cl}f_{COOH}C_i \quad (11b)$$

$$\frac{dL_o}{dt} = f_v(f_{L_p}^u k_{m,L_p}^0 + f_{L_n}^u k_{m,L_n}^0)\left(f_{i,L}^u L_i^u - f_{o,L}^u L_o^u\right) - k_{cl}K_0 L_o + k_{cl}f_{COOH}C_o \quad (11c)$$

$$\frac{dC_o}{dt} = f_v(f_{L_p}^u k_{m,C_n}^0 + f_{L_n}^u k_{m,C_a}^0)\left(f_{i,L}^u C_i^u - f_{o,L}^u C_o^u\right) + k_{cl}K_0 L_o - k_{cl}f_{COOH}C_o \quad (11d)$$

While this provides a valid set of equations to solve, initial conditions must include the initial fractions of lactone and carboxylate. These were determined from the pH, assuming initial equilibrium between the two forms. Because the fraction of ring-opened carboxylic acid is negligible due to the dominance of lactone at low pH for camptothecins,[92] an apparent acid dissociation constant, K_{a2}, relating the lactone to carboxylate form can be described in terms of the ring-opening constant (K_0) and the ionization constant for the carboxylic acid (K_{COOH}). This relationship is expressed by Equation 12.

$$K_{a2} = \frac{[H^+][C_T^W]}{[L_T^W]} = K_{COOH}K_0 \quad (12)$$

Using Equation 12, the initial concentrations of lactone and carboxylate were solved as shown below.

$$L_i(0) = \frac{T_i H^+(a+bK_L')}{H^+(a+bK_L')+K_{a2}(a+bK_C')} \quad (13a)$$

$$C_i(0) = \frac{T_i K_{a2}(a+bK_C')}{H^+(a+bK_L')+K_{a2}(a+bK_C')} \quad (13b)$$

$$L_o(0) = \frac{T_o H^+(c+bK_L')}{H^+(c+bK_L')+K_{a2}(d+bK_C')} \quad (13c)$$

$$C_o(0) = \frac{T_o K_{a2}(d+bK_C')}{H^+(c+bK_L')+K_{a2}(d+bK_C')} \quad (13d)$$

Additionally, observed suspension concentrations obtained from HPLC samples after ultrafiltration, T_i', were related to the total intravesicular concentration of entrapped TPT as only a small fraction of total suspension volume was encapsulated. The ratio of entrapped to extra-vesicular volume is f_v.

$$T_i' = f_v T_i \tag{14}$$

To avoid over-estimation of binding from release studies, any extra-vesicular drug at the beginning of the experiment was incorporated into the initial conditions when solving the model. Determination of the extra-vesicular concentration (if any), T_o, at the beginning of the experiment was done with the following equation:

$$T_o = T - T_i' \tag{15}$$

where T is the total TPT concentration in suspension before ultrafiltration. The equations above were then used to fit the release data obtained at pH 3.35 – 7.67. By incorporating pK_{a1},k_{cl}, and K_o (constants previously determined in other experiments), all release data were fit simultaneously to determine the partition coefficients and rate constants of each TPT species in solution.

Using this mechanistic model to obtain release rate constants for each TPT species from transport studies also required separate experiments to generate parameters governing the ionization state of the TPT A-ring phenol and the lactone-carboxylate interconversion kinetics. These determinations are described in the following sections.

4.2.7.2 Spectrometric determination of the TPT A-ring phenol (pKa1)

The ionization state of drugs and small molecules has been shown to alter release kinetics, typically due to the likelihood that the neutral form is more permeable than charged species.[49, 50, 52] In the case of TPT, the phenolic -OH group *ortho* to the dimethyl-aminomethyl substituent on the A ring may ionize and alter the charge of TPT as depicted in Scheme 4.3.

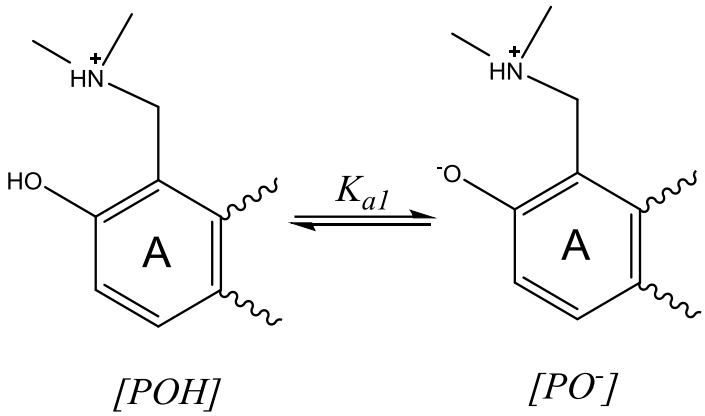

Scheme 4.3. Phenol ionization on the A ring of TPT is governed by the acid dissociation constant, K_{a1}.

The relationship between the phenol and the phenolate depicted in Scheme 4.3 and its pH dependence is governed by the acid dissociation constant, K_{a1}, as expressed in Equation 16.

$$K_{a1} = \frac{[H^+][PO^-]}{[POH]} \tag{16}$$

where $[PO^-]$ is the total concentration of TPT species with an ionized phenolate moiety and $[POH]$ is the concentration of all TPT species with the unionized phenol moiety.

At any given excitation wavelength, *j*, the fluorescence intensity in aqueous solution emitted at wavelength, I_j, can be described as the sum of the phenol species, $I_{j,OH}$, and phenolate species, I_{j,O^-} (Equation 17).

$$I_j = I_{j,OH} + I_{j,O^-} \quad (17)$$

These intensities can be related to the concentrations of each species by their respective specific intensities, ϵ_{OH}, and ϵ_{O^-}, and the fractions of the phenol, f_{OH}, and phenolate, f_{O^-}, forms in solution containing a total concentration, T. Equation 17 can be rewritten in terms of the fractions of each species present.

$$I_j = T[f_{OH}\epsilon_{j,OH} + f_{O^-}\epsilon_{j,O^-}] \quad (18)$$

Here, the fraction of drug in each form may be expressed by mass balance and rearrangement of Equation 16 as illustrated below in Equations 19a and b.

$$f_{OH} = \frac{H^+}{H^+ + K_{a1}}; f_{O^-} = \frac{K_{a1}}{H^+ + K_{a1}} \quad (19a; b)$$

For spectrometric determination of K_{a1}, fluorescence emission at 560 nm was fitted to the above equations at varying pH (3.5 – 7.5) and a constant TPT concentration of 500 nM to determine K_{a1} and ϵ_{j,O^-} at excitation wavelengths of 335, 365, 380, and 410 nm. The determination of $\epsilon_{j,OH}$ was accomplished using the fluorescence intensity at pH 3.5 by assuming I_{j,O^-} was negligible at this pH.

4.2.7.3 TPT lactone-carboxylate interconversion kinetics in solution and in the presence of liposomes

The lactone E-ring in TPT can undergo reversible, base-catalyzed hydrolysis to form its ring-opened, carboxylate form via deprotonation of the carboxylic acid intermediate, C_{COOH} (Scheme 4.4). This process is pH-dependent, similar to other camptothecin analogues, with the lactone form, L, dominating at low pH. As pH is increased, both ring-opening and closing rate constants are base-catalyzed; however, ionization of the ring-opened carboxylic acid to form C_{COO-} shifts the equilibrium toward the ring-opened species.[92, 148]

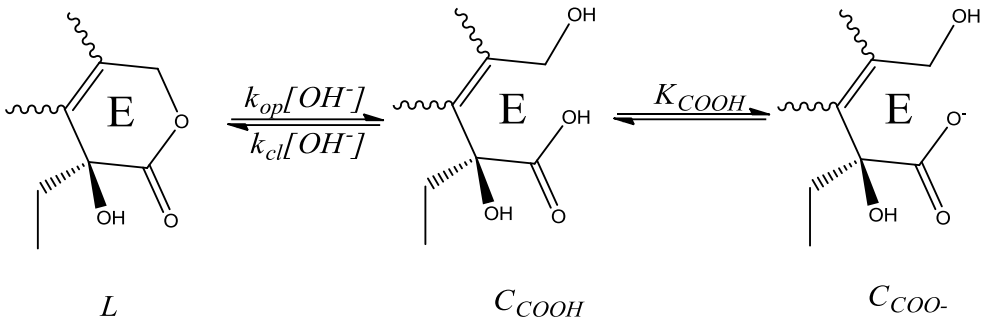

Scheme 4.4. The proposed mechanism for reversible, pH dependent ring opening of TPT from its lactone, L, to carboxylate, C_{COO-}, form. Because ring opening proceeds through the carboxylic acid species, C_{COOH}, ring opening increases as more carboxylate is formed at higher pH, as governed by the acid dissociation constant for the E-ring carboxylic acid, K_{COOH}.

Because of its location and the molecule's rigidity, it is unlikely that the ionization state of the phenol would have any effect on the lactone-carboxylate interconversion kinetics. With this assumption, the rate equations for ring opening and closing can be expressed in terms of total lactone, L, and carboxylic acid, C_{COOH}, concentrations in solution as shown below.

$$\frac{dL}{dt} = k_{cl}[OH^-]C_{COOH} - k_{op}[OH^-]L \tag{20a}$$

$$\frac{dC}{dt} = -k_{cl}[OH^-]C_{COOH} + k_{op}[OH^-]L \tag{20b}$$

Solving for C_{COOH} in terms of total ring-opened species, C, is needed. The fraction of total ring-opened species present as carboxylic acid at a particular pH, f_{COOH}, can be determined from the pKa of the carboxylic acid (Equation 21).

$$f_{COOH} = \frac{H^+}{H^+ + K_{COOH}} \tag{21}$$

In previous studies, the pK_{COOH} for TPT, camptothecin, and other analogues has been assumed to be 3.8 or 4.0.[92, 148] Based on those studies and the pKa value of 3.86 for glycolic acid, a value of 3.9 was assumed for model fitting.

To reduce the correlation between the ring-opening, k_{op}, and ring-closing, k_{cl}, rate constants during model fitting, the equilibrium constant between the ring-opened carboxylate acid and ring-closed lactone forms, K_0, was used. As seen in Equation 22b, k_{op} can be rewritten in terms of k_{cl} and K_0.

$$K_0 = \frac{C_{COOH}}{L} = \frac{k_{op}}{k_{cl}}; k_{op} = k_{cl}K_0 \quad (22a; b)$$

Substituting Equations S21 and 22b into rate Equations 20a and b,

$$\frac{dL}{dt} = k_{cl}[OH^-]f_{COOH}C - k_{cl}K_0[OH^-]L \quad (23a)$$

$$\frac{dC}{dt} = -k_{cl}[OH^-]f_{COOH}C + k_{cl}K_0[OH^-]L \quad (23b)$$

To determine K_0 and k_{cl} at the same conditions used for release studies, TPT interconversion studies were first performed at varying pH (6.33 – 7.67) in the absence of liposomes. These studies were fit simultaneously to rate Equations 23a and S8b. Studies in the presence of liposome suspensions (50 mg/mL) prepared in pH 6.33 and pH 7.67 buffers were also conducted. The lactone and carboxylate concentration versus time profiles were compared to those obtained at the same pH in the absence of liposomes to evaluate whether membrane binding had an effect on the interconversion kinetics.

4.2.7.4 Mathematical model for liposomal TPT release assuming equilibrium for lactone ring-opening/closing

To evaluate the need for lactone/carboxylate interconversion kinetics in the release model, the half-life profile of that model was compared to a half-life profile generated by

fitting TPT release profiles at varying pH to an equilibrium model. To determine the half-life profile for the equilibrium model, $t_{1/2}$ may be expressed by Equation 24.

$$t_{1/2} = \frac{\ln(2)}{k_m f^u} = \frac{\ln(2)(a+bK')}{k_m} \quad (24)$$

Here, the overall release constant, k_m, and total fraction of unbound intravesicular drug, f^u, are considered. Both parameters are a function of pH. In equation 24, k_m accounts for the fraction of each permeable species found in solution along with their respective transport rate constants, where k^0_{m,L_p} is the transport rate constant for the protonated lactone, k^0_{m,L_n} is for the zwitterionic phenolate form of the lactone, and k^0_{m,C_n} is for the ring-opened carboxylate zwitterion.

$$k_m = \frac{H^+\left(f^u_{L_p} k^0_{m,L_p} + f^u_{L_n} k^0_{m,L_n}\right) + K_{A2} f^u_{L_p} k^0_{m,C_n}}{H^+ + K_{A2}} \quad (25)$$

The unbound fraction (f^u) in Equation 24 varies with pH as it is a function of the apparent membrane binding constant, *K'*, as illustrated by Equation 25. The binding constants obtained previously using the mathematical model for liposomal TPT release that included the kinetics of lactone ring-opening/closing were inserted as constants into Equation 25.

$$K' = \frac{f^u_{L_p}\left(H^+ K^0_{L_p} + K_{A2} K^0_{C_n}\right)}{H^+ + K_{A2}} \quad (25)$$

The release profiles were simultaneously fit to the equilibrium model described by Equations S22-24 where the rate constants (k^0_{m,L_p}, k^0_{m,L_n}, k^0_{m,C_n}, and k^0_{m,C_a}) and membrane binding constants ($K^0_{L_p}$, $K^0_{L_n}$, $K^0_{C_n}$, and $K^0_{C_a}$) were fitted using non-linear regression.

4.2.7.5 Regression Analysis

Data fitting for constants describing the A-ring phenol pKa, ring-opening interconversion kinetics, and release kinetics was performed using Scientist® non-linear least squares regression software with a weighting factor of two.

4.3 Results

4.3.1 Validation of analytical methods and liposome characterization

TPT concentrations were analyzed by HPLC with fluorescence detection using excitation and emission wavelengths of 380 nm and 550 nm, respectively. Peak areas varied linearly with concentration between 20 and 200 nM for both lactone and carboxylate standards. Release studies monitored total TPT concentration by converting all drug to its lactone form by diluting samples with chilled acidified methanol into the concentration range of standards. Coefficients of variation for response factors of standards were ±1.4% intraday and ±2.6% interday. Initial TPT concentrations ranged from 0.2-1.0 μM for these experiments. Studies monitoring TPT interconversion kinetics were performed with initial concentrations of 0.4-0.6 μM and coefficients of variation for response factors were ±2.0% intraday and ±7.1% interday for carboxylate standards and ±1.5% intraday and ±2.1% interday for lactone standards. Phospholipid content was determined by a previously validated HPLC method with slight modifications.[49, 60] ELSD, necessary due to the lack of chromophore/fluorophore in the lipid molecules, provided linear log-log plots of the peak areas versus DSPC concentration between 0.025 – 0.3 mg/mL and a peak retention time of 7.9 minutes, similar to that previously reported.[49]

To validate the ultrafiltration procedure as a reliable technique to analyze drug release kinetics, the recovery efficiency of TPT and phospholipid after ultrafiltration was determined. Sephadex separation of liposomally entrapped TPT from unencapsulated drug

was used as previously reported[147] to determine this recovery value. By analyzing TPT concentrations in liposomal fractions collected immediately after Sephadex purification, the percentage of TPT recovered after the ultrafiltration procedure was determined to be 88.0 ± 2.4%; however, this value may be an underestimation if trace amounts of unentrapped TPT were present after Sephadex separation. To further explore this as a possible source of error, phospholipid content was also determined in liposome samples after ultrafiltration. Phospholipid recovery was determined to be 94.0 ± 3.9%. The slightly higher recovery of phospholipid in comparison to TPT after ultrafiltration of freshly purified drug-loaded liposomes provides evidence for the presence of a small percentage of unentrapped drug. Consequently, phospholipid and TPT recovery were compared at the start of a release experiment to estimate the initial amount of TPT in the extra-vesicular solution. During these experiments, the initial extra-vesicular TPT was never more than 2.5% of the initial intra-vesicular TPT. As a final validation, suspensions of liposomes containing no drug were spiked with TPT and then ultrafiltered. Ultrafiltration of these spiked solutions showed only trace amounts of TPT present well, below the limit of quantitation (less than 0.3% of initial TPT). Because passive loading was used to conduct these experiments, encapsulation efficiency was not determined as it was expected to be low (< 3%) and not germane to the goals of this study.

Volume parameters (Table 1) used in model fitting were calculated from particle sizes and phospholipid contents determined during release studies. Particle size was determined at each pH (8 measurements) for the suspensions before and after the conclusion of release studies. The average particle size before release studies (with 95 % confidence interval) was 96 ± 2 nm and 98 ± 3 nm after release studies were finished, indicating no statistically significant change in particle size during the experiments. Because of the narrow particle size distribution, average particle size was used to determine the aqueous/total entrapped

volume ratio (a) and membrane/total entrapped volume ratio (b), parameters that were necessary for the analysis of the transport data (see Supplementary Data). Extra-vesicular volume ratios (c and d) analogous to a and b were also required for the determination of membrane binding constants and subsequently release rate constants because these studies were not performed under sink conditions. The entrapped/unentrapped volume ratio (f_v) calculated from the lipid content present in suspension was varied in release studies by altering the lipid concentration to avoid possible systematic errors in estimation of membrane binding constants from release profiles. Thus, the lipid content determined for each release study was used rather than the average of values for all experiments. The values in Table 1 reflect the parameter ranges explored.[50, 135, 149]

Table 4.1. Volume parameters used in TPT release studies

Parameter	Average	Range
a	0.855	NA
b	0.145	NA
c	0.9997	0.9995 – 0.9999
d	0.0003	0.0001 – 0.0005
f_v	0.0067	0.0024 – 0.0110

Phospholipids undergo acid-catalyzed ester hydrolysis[142-144] that could lead to hydrolysis-induced changes in bilayer integrity over longer periods of time. This possibility was examined by monitoring lipid content in solution using HPLC with an ELSD. No loss of lipid was detected in release studies at pH 4.01 over 72 hr but >10% lipid loss was found after 48 hr at pH 3.35 (Figure 4.1) which is qualitatively consistent with literature data [150]. Previous literature reports have shown compromised bilayer integrity when 15% or more

phospholipid has degraded.[143] Consequently, only samples taken before 36 hours from the pH 3.35 release study were used in data fitting.

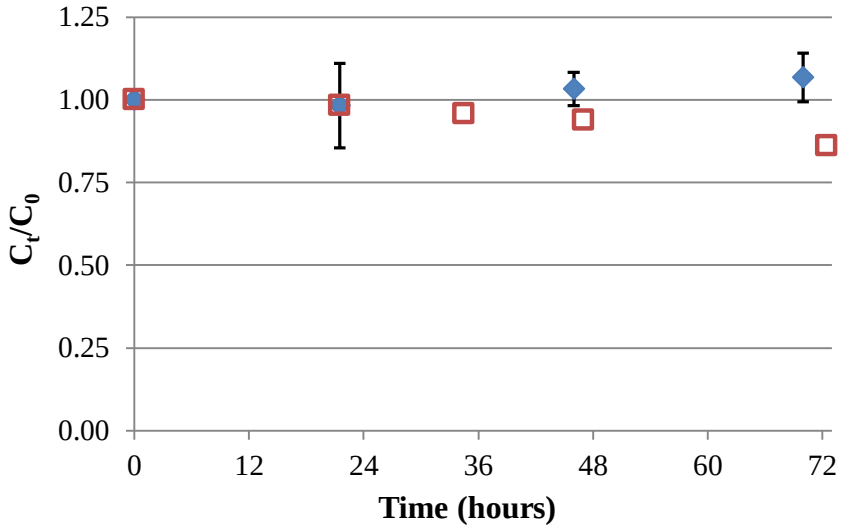

Figure 4.1. The fraction of DSPC remaining during release studies conducted at pH 3.35 ☐ and 4.01 ◆. Error bars at pH 4.01 are the 95 % confidence intervals determined by samples taken from four independent experiments.

4.3.2 Spectrometric determination of the TPT A-ring phenol (pKa1)

Because of the high dependency of bilayer permeability on permeant charge,[3, 50, 52, 60, 73] the pKa of the phenolic -OH on the A ring was determined at 37 °C from changes in the TPT fluorescence excitation spectra with pH as seen in Figure 4.2a. Spectral changes as a function of pH (Fig. 2b) were used to determine pK_{a1} to be 6.56 ± 0.12. This value is similar to those previously reported at lower temperatures.[90, 92, 138, 151]

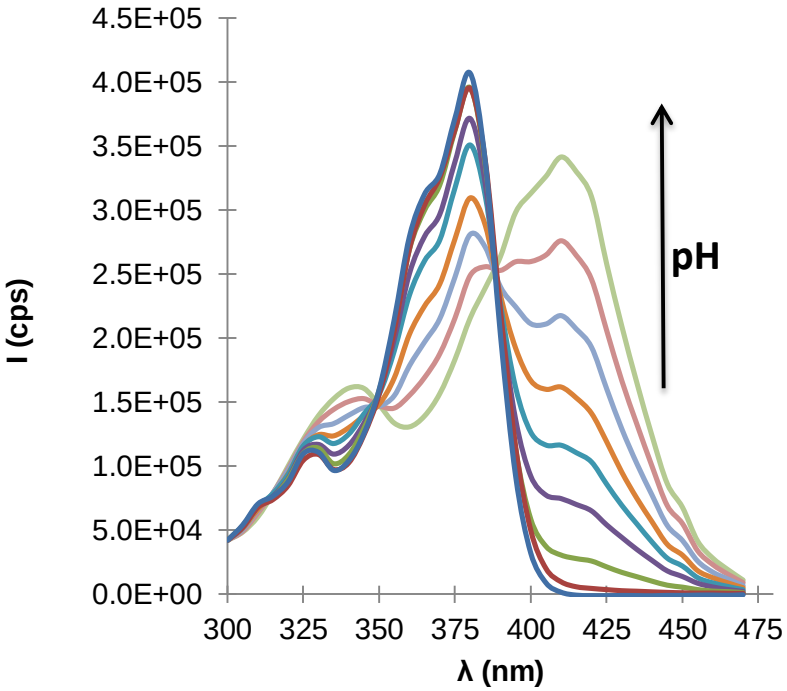

A.

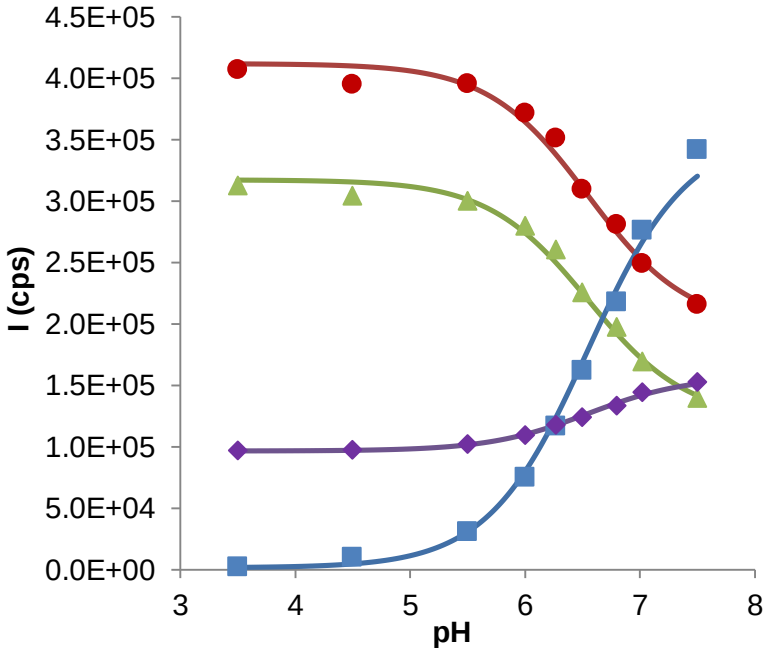

B.

Figure 4.2. A) TPT excitation spectra at varying pH (3.50, 4.50, 5.50, 6.00, 6.27, 6.50, 6.80, 7.10, and 7.50) obtained at an emission wavelength of 560 nm. As pH is increased, a red shift occurs with maximum excitation shifting from 380 nm to

410 nm. B) Fluorescence intensities at an emission wavelength of 560 nm and at excitation wavelengths of 380 (●), 365 (▲), 335 (♦), and 410 nm (■) from TPT solutions at varying pH and fit to Equations S3 & S4 to determine pK_{a1}. The lines represent the simultaneous fit of intensities at all wavelengths vs. pH.

4.3.3 TPT lactone-carboxylate interconversion kinetics

The kinetics of interconversion of TPT between its lactone and carboxylate forms was monitored as a function of pH by following both carboxylate and lactone species (Figure 4.3a). A kinetic model based on a ring opening/closing mechanism previously described in the literature,[92] was able to account for the pH-dependence, resulting in a base-catalyzed ring-closing rate constant ($k_{c,OH}$) of 7.4 ± 0.3 x 10^8 $mol^{-1}hr^{-1}$ and a carboxylic acid/lactone equilibrium constant (K_0) of 1.98 ± 0.07 x 10^{-3}. Combining the pKa of the ring-opened carboxylic acid assumed to be 3.9 (based on values previously assumed for camptothecin and its analogues and a pKa of 3.86 for the α-hydroxy acid glycolic acid)with K_0 gave an effective pKa for the ring-opening/ionization reaction (pK_{a2}) of 6.60. This value is similar to that reported for camptothecin and other analogues.[92, 148]

Interconversion studies conducted in liposomal suspensions at high lipid content revealed no significant changes in the kinetic parameters or value of K_0 from those obtained at the same pH in aqueous solutions (Figures 4.3b and c). This supports the negligible effect of membrane binding on interconversion kinetics and the use of k_{cl} and K_0 to describe inter-conversion kinetics of total intravesicular TPT.

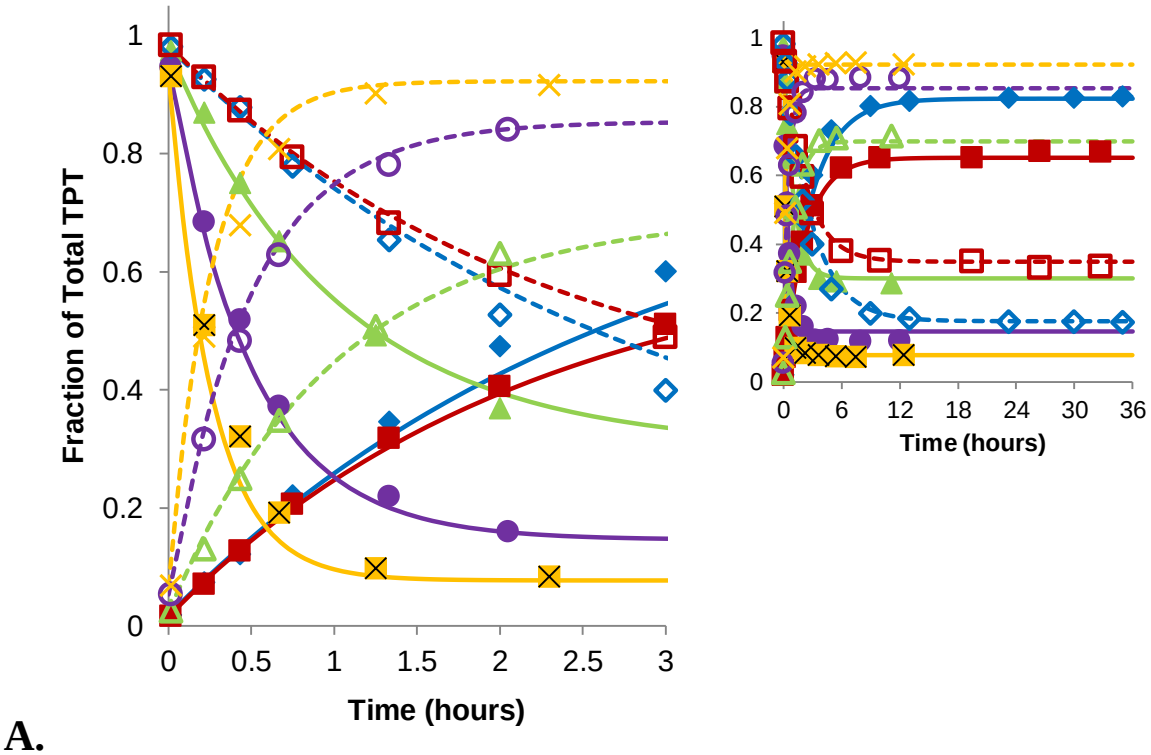

A.

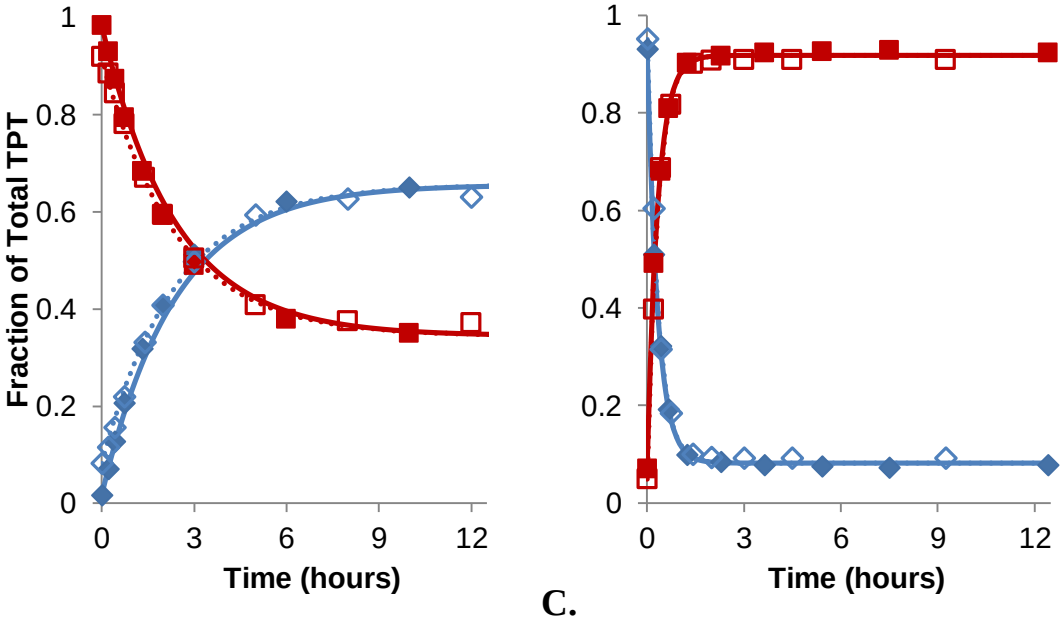

B.

C.

Figure 4.3. Ring opening/closing kinetics of TPT as a function of pH. A) The plots display the fractions of total TPT in the lactone form (closed symbols) or carboxylate form (open symbols) versus time at the same pH of 5.92 (◆,◇), 6.33(■, □), 7.04 (▲,△), 7.39 (●,○), or 7.67 (x, x). The curves of matching

color represent simultaneous fits of the kinetic interconversion model to the lactone (solid lines) and carboxylate (dashed lines) data. Most interconversion occurred within the first three hours (left) while equilibrium was achieved for all studies (right). Interconversion of TPT in liposome suspensions (50 mg/mL) at pH 6.33 (B) and pH 7.67 (C) is also shown. The fractions of total TPT in the lactone ◆ and carboxylate ■ form are shown in aqueous solution while the open symbols represent studies conducted in liposomal suspensions. Solid and dotted lines indicate the simulated interconversion profiles for both aqueous and liposome studies simulated by the kinetic parameters previously determined from aqueous solution studies.

4.3.4 pH Sensitive release of TPT

Transport experiments were performed at varying pH and at a recorded average temperature of 38.7 ± 0.1 °C during the time period of the studies. The fractions of TPT retained in DSPC/DSPE-PEG2K liposomes versus time at varying pH are shown in Figure 4.4. The curves displayed in Figure 4.4 represent simultaneous fits to the mechanism-based mathematical model for TPT release developed in the Supplementary Data using the equilibria and chemical kinetic constants determined from spectrometric and interconversion studies. From these data, transport rate constants and partition coefficients were obtained for the various ionization states of the lactone and carboxylate species (see Scheme 4.1). Transport rate constants of 0.51 ± 0.07 hr^{-1} and 33.9 ± 4.6 hr^{-1} were found for the cationic lactone species (L_p) and the zwitterionic lactone (L_n), respectively, while the ring-opened carboxylate zwitterion (C_n) had a rate constant of 5.7 ± 0.5 hr^{-1} and its anionic form (C_a) was found to be impermeable.

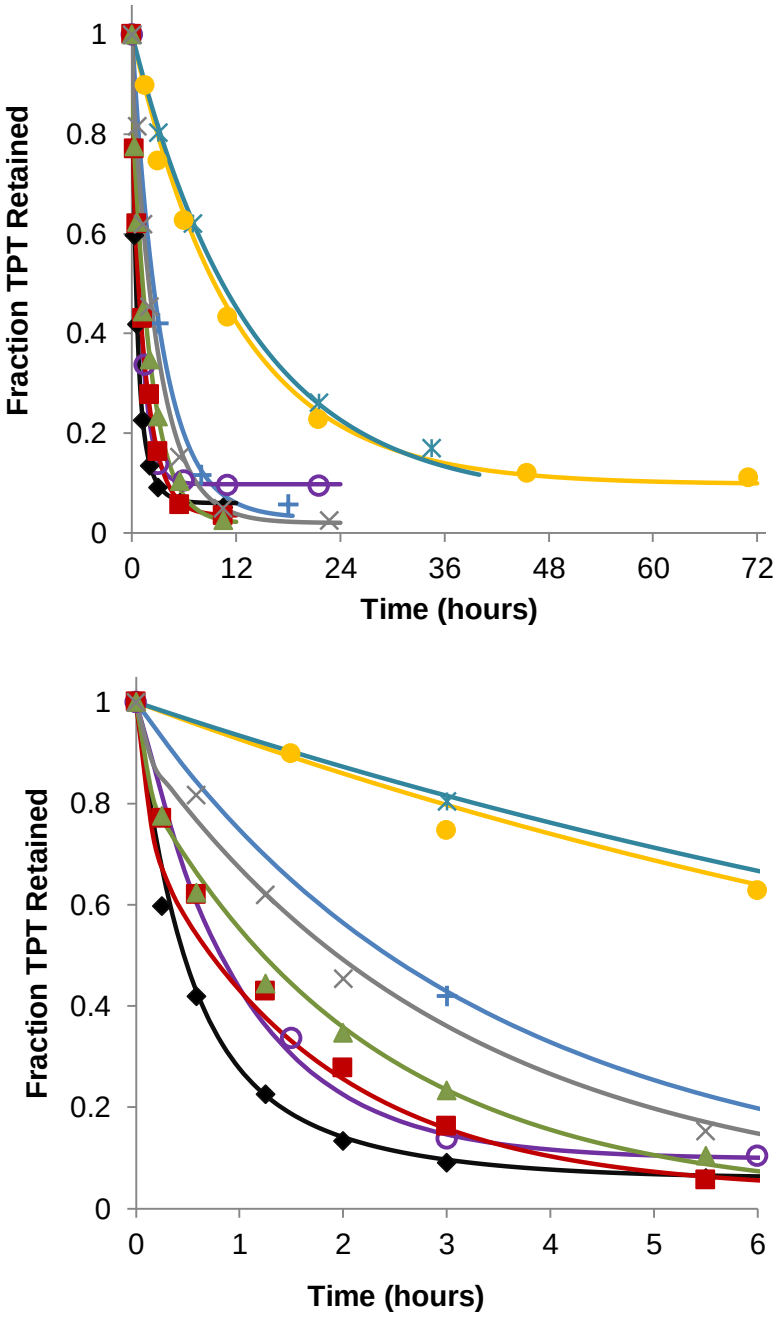

Figure 4.4. Fraction of TPT retained in DSPC/DSPE-PEG2K liposomes vs. time at varying pH (right panel displays only the first 6 hrs). Release studies were conducted at pH 3.35 ✳, 4.10 ●, 5.10 +, 5.93 ○, 6.33 ◆, 7.04 ■, 7.39 ▲, and 7.67 x. The solid curves of the same color represent the simultaneous fit of the mechanism-based mathematical model developed in this paper to the entire data set.

The same analysis also indicated that the zwitterionic lactone (L_n) and anionic carboxylate form C_a exhibited negligible binding to the phospholipid bilayer. Both of these species have in common a phenolate moiety that evidently disfavors interaction with the bilayer. This and the similar partition coefficients of 62 ± 6 and 42 ± 6 for the lactone and carboxylate species in which the phenol is unionized (L_p and C_n, respectively) suggest that binding likely occurs with preferential orientation of the TPT A-ring toward the hydrophobic region of the phospholipid bilayer. Opening of the lactone ring had a negligible effect on membrane binding.

4.4 Discussion

4.4.1 Effect of TPT ring-opening on pH sensitive release kinetics

The significantly greater permeability of the zwitterionic lactone species (L_n) than any of the other TPT species present in the pH range explored (Scheme 4.1) raises the possibility that, under certain pH conditions, this species might be depleted from the intravesicular compartment due to its slow regeneration from the ring-opened form. Simulated profiles of the concentrations of carboxylate and lactone species at pH 6.33 (where the lactone fraction is greater) and pH 7.04 (where the carboxylate fraction is greater) are shown in Figure 4.5 along with the profile of total drug released in Figure 4.4. Because interconversion is not instantaneous, the more permeable lactone zwitterion was depleted at a faster rate than its carboxylate counterpart, resulting in biphasic release profiles at certain pH values such as within the first 30 min of release at pH 7.04 (Figure 4.5b, see also Figure 4.5b).

The ratio of lactone to carboxylate species, *R*, during release is also depicted in Figure 4.5. The profile of *R* initially shows a rapid decrease as the more permeable lactone species are depleted during the early phase of release. During the later phase of release, R

approaches its initial equilibrium value as the less permeable carboxylate specie continues to release. Similar trends of R are evident for release studies conducted in the neutral pH range (Figure 4.5c)

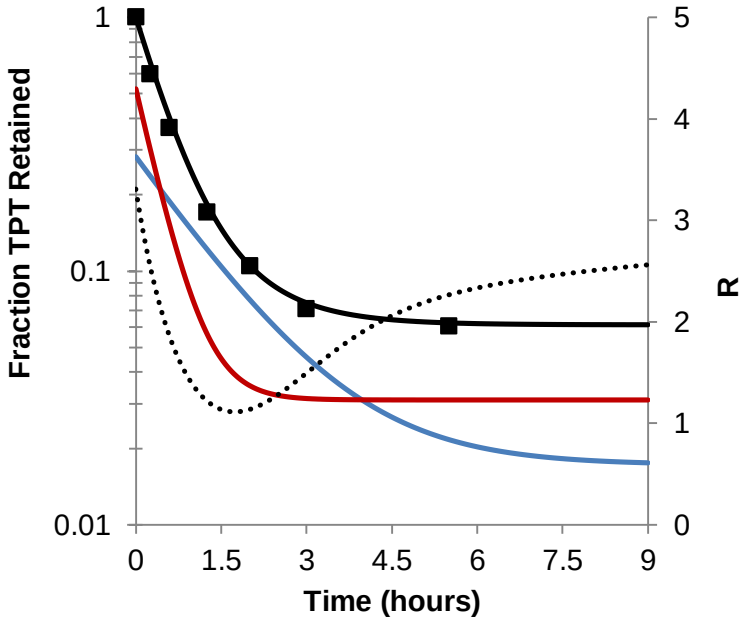

A.

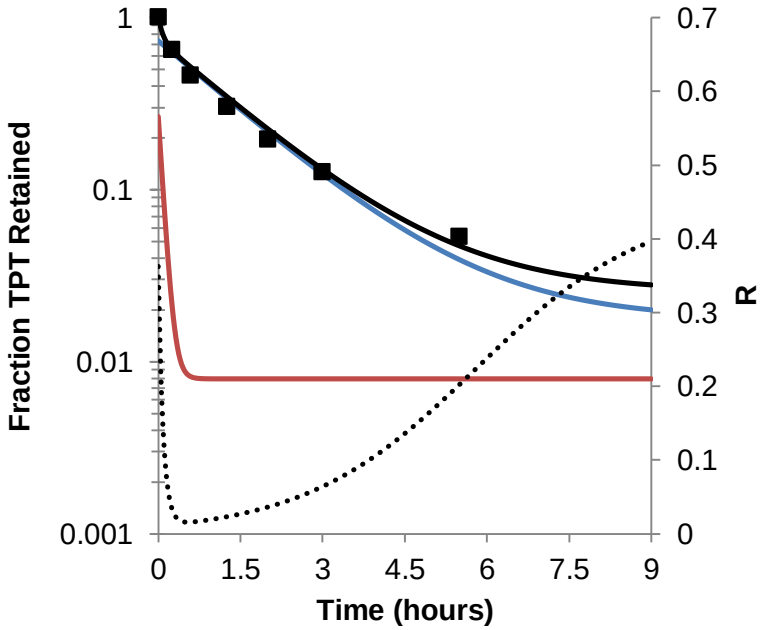

B.

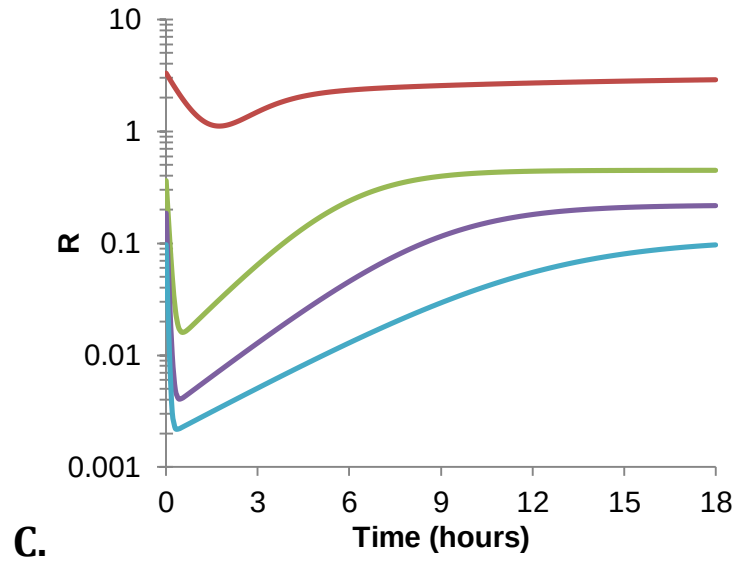

Figure 4.5. Liposomal TPT release profiles at pH 6.33 (A) and 7.04 (B). The observed fraction of total TPT retained ■ and the resulting fit to the model described within this paper (—) are shown. The simulated profiles of the lactone (—) and ring-opened (—) forms are also displayed to illustrate the rapid depletion of the lactone. The lactone to carboxylate ratio, R (.....), is also shown to highlight the role of slow carboxylate-> lactone conversion during TPT release. C) Changes in ***R*** during liposomal TPT release studies for all pH studied where interconversion kinetics were not instantaneous (pH 6.33 (—), 7.04 (—), 7.39 (—), and 7.67 (—)) were also simulated. All profiles show a decrease in ***R*** as the more permeable lactone is depleted, thus indicating non-instantaneous interconversion between the two species.

4.4.2 Comparison of kinetic and equilibrium models of lactone ring-opening/closing

In previous pH-dependent release studies with the camptothecin analogue AR-67, ring-opening kinetics could be assumed to be instantaneous because the high membrane-binding constant for the lactone form reduced the driving force for release and provided a reservoir of the lactone species.[49, 60, 63] Both of these factors minimized the depletion of lactone. In contrast, the low membrane-partitioning observed for TPT required such an assumption to

be tested. To compare the release model that incorporated the kinetics of ring-opening with one that assumed ring-opening/closing equilibrium, the pH profiles for the release half-lives ($t_{1/2}$) generated by the two models as a function of pH were compared in Figure 4.6 along with the experimentally-observed half-lives.

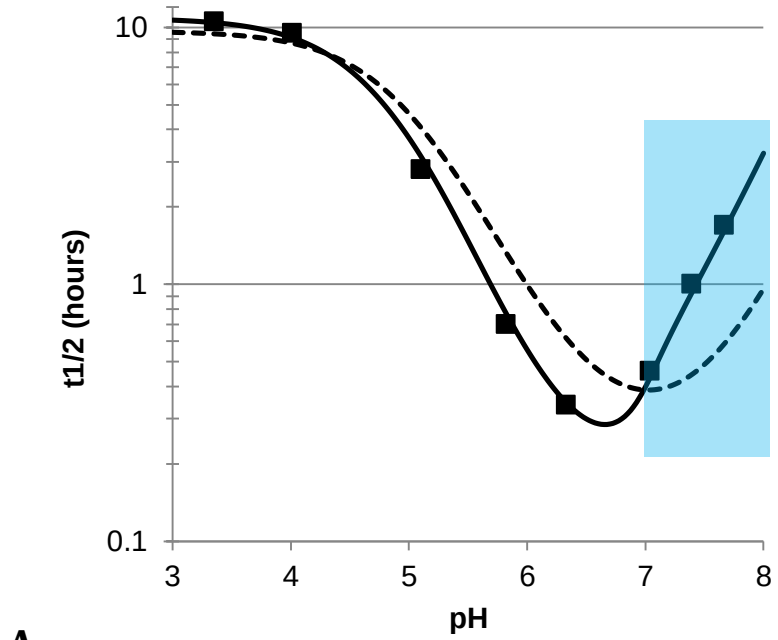

A.

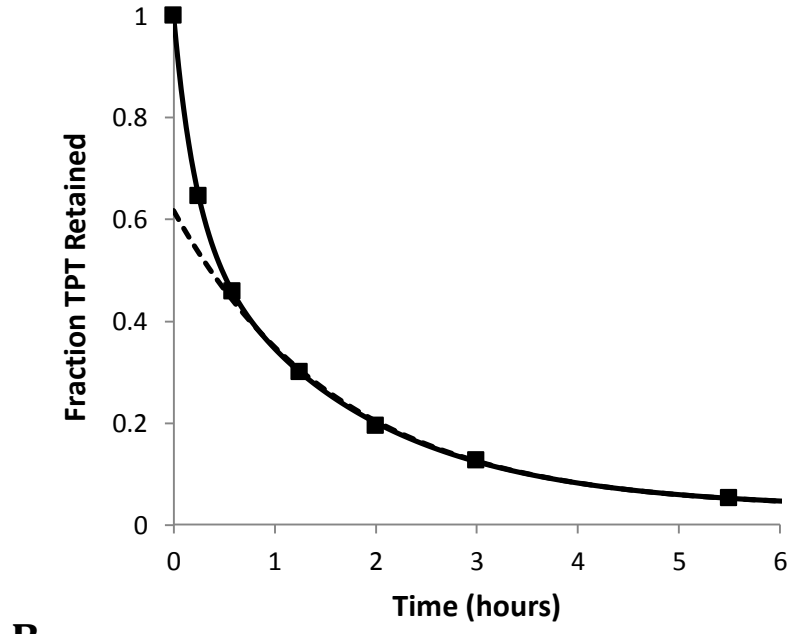

B.

Figure 4.6. (A) Comparison of the experimental pH profile of TPT release half-lives (■) to model fits that account for the kinetics of lactone-carboxylate interconversion (—) or assume lactone-carboxylate equilibrium (.....). The equilibrium model was unable to account for the steep changes in half-life in the neutral pH region. The blue section highlights the pH region in which release was slowed by greater than 25% due to rate-limiting ring-closure. (B) The biphasic release profile observed at pH 7.04 and the fits of models that either include interconversion kinetics (—) or assuming interconversion equilibrium (.....).

Because the equilibrium model does not account for interconversion kinetics, it tries to compensate for the steep change in half-life (resulting from rate-limited ring-closing) seen at neutral pH (6.8 – 8.0) by overestimating release in the acidic region and underestimating release at higher pH. Figure 4.6 also demonstrates the inadequate fit of the equilibrium model to a single release profile. Here, the equilibrium model underestimated the initial phase of drug release as it could not account for biphasic kinetics. In contrast, the model incorporating interconversion kinetics is able to account for the rapid initial phase of drug release that leads to lactone depletion followed by subsequent slower release limited by intravesicular regeneration of lactone from the carboxylate.

4.4.3 Determination of species permeability coefficients

The apparent permeability coefficient, P_m^0, is related to the apparent transport rate constant at a given pH and the radius of the particle, r, as expressed by Equation 26.

$$P_m^0 = \frac{r}{3} k_m^0 \tag{26}$$

Using the release model that included the kinetics of ring-opening/closing, three TPT species were determined to contribute to the liposomal transport. From these release rate constants, permeability coefficients could be calculated for these species.

Based on the 100 nm liposomes used in these studies, the cationic and zwitterionic lactone permeability coefficients were $2.4 \times 10^{-10}\, cm/s$ and $1.5 \times 10^{-8}\, cm/s$ while TPT carboxylate zwitterion permeability coefficient was $3.0 \times 10^{-9}\, cm/s$. Generally, neutral, non-ionized species are orders-of-magnitude more permeable than charged species; however, few zwitterions have been explored.[49, 50, 52] The permeability coefficient for the lactone zwitterion determined from this work is similar to one obtained for the neutral, unionized lactone species of another camptothecin analogue.[49] This is likely due to an intramolecular interaction between the A-ring phenolate and dimethyl-ammonium substituents. Because of their close proximity and orientation, the free energy required for bilayer partitioning of this specie may be lower due to an electrostatic interaction or an intramolecular hydrogen bond between the heteroatoms. This is supported by the large pKa shifts observed in aqueous solution for the phenolic –OH (i.e., from 10.0 in phenol to 6.56 in TPT) and dimethyl-aminomethyl substituent (from 8.93 in benzyldimethylamine to 10.5 in TPT), respectively. These shifts in pKa are a direct consequence of the stabilization of the zwitterionic form in Scheme 4.3. A similar effect has also been reported for other compounds with this same feature,[92, 152] and recent studies of TPT fluorescence lifetimes in aqueous solution have distinguished intramolecular and bulk solution contributions to phenol deprotonation.[151] These interactions may help explain the small but significant permeability of the cationic species, L_p, seen in this study. Partial shielding of the cationic charge of L_p may be through hydrogen bonding with the phenol which may be further stabilized by resonance forms that delocalize the charge throughout TPT's conjugated ring structure.

Unlike the lactone zwitterion, the carboxylate form, C_n, does not offer the possibility of such intramolecular interactions between adjacent charged residues. Without this feature,

the observed permeability may reflect the minor fraction of unionized neutral species, C_0, as depicted in Scheme 4.5.

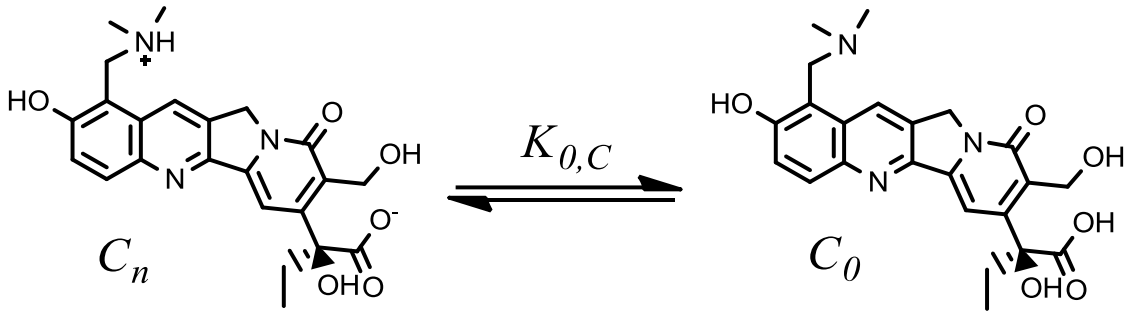

Scheme 4.5. The equilibrium between TPT's carboxylate zwitterion and neutral, unionized form is governed by $\boldsymbol{K_{0,C}}$.

To ascertain whether the observed permeability for the carboxylate could be attributable to C_0, the equilibrium constant between C_n and C_0, $K_{0,C}$, must be determined. This may be written in terms of the fraction of the zwitterion, $f_{z,C}$, and non-ionized, $f_{0,C}$, species as expressed in Equation 26.

$$K_{0,C} = \frac{C_0}{C_n} = \frac{f_{0,C}}{f_{z,C}} = \frac{K_{a3}}{K_{COOH}} \tag{26}$$

Using this ratio, a maximum permeability for C_0 may be determined if one assumes C_0 is the sole specie contributing to the observed permeability of the carboxylate. Using this assumption and a pK_{a3} of 10.5 for the dimethyl-amino group,[92] the maximum permeability coefficient is estimated to be $9.3 \times 10^{-3}\ cm/s$ for C_0.

To assess the significance of this permeability coefficient, comparison to the theoretical maximum permeability, P_{max}, is needed. P_{max} can be described by diffusion-limited transport through the boundary layer of a spherical particle. This is given by Equation 27.

$$P_{max} = \frac{D_{TPT}}{r} \tag{27}$$

Here, the diffusivity of TPT, D_{TPT}, was determined by the Stokes-Einstein equation for diffusivity in water at 37 °C and a molecular volume of 366.8 Å^3 (ACD labs). Based on this information, D_{TPT} was calculated to be $7.52 \times 10^{-6}\ cm^2/s$ and P_{max} was estimated to be $1.50\ cm/s$. While the estimated permeability coefficient of C_0 necessary to account for the experimental data is below P_{max}, it is still several orders of magnitude higher than that of TPT's lactone zwitterion and another neutral, non-ionized camptothecin of similar size.[49] This analysis suggests transport of the neutral, unionized ring-opened species is unlikely to fully account for the transport observed. Other mechanisms that may stabilize the ring-opened carboxylate zwitterion as it traverses the bilayer include: long-range intramolecular substituent effects on membrane partitioning, formation of water bridges through the bilayer, or ion-pairing within the barrier domain during TPT transport.[45, 129, 153-155]

4.5 Conclusions

The pH dependent release of TPT from DSPC/m-PEG DSPE liposomes was characterized and the contribution of the kinetics of the pH-dependent ring-closure reaction to this process was assessed. These factors were incorporated into a mechanism-based mathematical model to describe TPT release. Based on this model, three TPT species were determined to be permeable to the membrane with the A-ring zwitterion form being the most permeable species. Within a defined pH region lactone depletion resulted in ring-closure of the ring-opened carboxylate form becoming at least partially rate-determining. A mathematical model that assumed equilibrium between the lactone and ring-opened species was inadequate in accounting for the complete profile for the dependence of $t_{1/2}$ on pH and the biphasic release kinetics observed at certain pH values. The mechanism-based model developed in these studies will provide a basis for understanding the loading and release kinetics of actively-loaded formulations of TPT.

CHAPTER FIVE

Insights Into Accelerated Liposomal Release of Topotecan in Plasma Monitored by a Non-invasive Fluorescence Spectroscopic Method

5.1 Introduction

Many physiological factors (i.e. age, gender, dose regimen, type or location of cancer, mononuclear phagocyte system[25]) have been proposed to influence the pharmacokinetics (PK) and pharmacodynamics (PD) of nanoparticle formulations of anticancer agents. Unfortunately, the correlation between these factors and nanoparticle efficacy remain largely unknown.[26, 27] In liposomal formulations, bilayer integrity may be compromised by the particles' interactions with proteins (e.g. vesicle binding and particle opsonization)[54-57] or osmotic stresses[58, 59] while in circulation or at the tumor site. Other factors may also accelerate release of actively-loaded drug by destabilizing the pH gradient in vivo.[60] Actively-loaded liposomal formulations of anticancer agents are numerous[21, 42, 62, 73, 95, 156] and would share in these susceptibilities. Reports describing the effects of such physiological phenomena on release kinetics in vivo have been limited due to the lack of available in-situ methods to monitor and distinguish entrapped from free drug. Methods to determine the release kinetics of drug from circulating liposomes and/or at the tumor site are crucial to optimizing the efficacy of liposomal-based drug delivery systems.

Validation of such a method to quantify release kinetics requires parallel development of a mathematical model to interpret observed release profiles. The model must distinguish physicochemical release characteristics intrinsic to the drug/particle system from artifacts of the release environment (i.e. kinetic or thermodynamic effects attributable to the particular medium within which release is determined).[49, 60, 63, 124-126] With such models, the in vivo factors that lead to variability in liposomal formulation performance may be identified and mechanistically understood.

Topotecan (TPT) is a camptothecin analogue known for its topoisomerase-I inhibitory activity and regulation of genes associated with angiogenesis.[157] Several preclinical studies have demonstrated increased anti-tumorigenic efficacy of liposomal formulations of TPT that have reduced systemic clearance, allowing greater uptake and extended tissue exposure in murine solid tumors.[62, 158, 159] Many of the liposomal formulations of TPT are actively loaded by establishing an acidic intravesicular compartment relative to the extravesicular pH of the loading solution. This process provides high drug loading efficiencies while ensuring the pharmacologically active lactone form of TPT is delivered to the tumor. While actively loaded liposomal formulations have often shown prolonged retention in aqueous buffers,[23, 62, 64] the same formulations may exhibit accelerated release in plasma.[23, 62]

While the low intravesicular pH persists after active drug loading, [62, 64, 159-161] to the authors' knowledge it has never been used to differentiate between entrapped and free TPT during drug release. Because the fluorescence of TPT is pH-dependent,[156, 162] changes in TPT fluorescence in aqueous liposomal suspensions and in plasma were explored as a potential means of non-invasively monitoring liposomal release in real-time. Analyses of fluorescence spectra confirmed that free TPT exhibits a red shift in its excitation spectrum as pH is increased. Due to this red shift, release of TPT from actively loaded liposomal TPT (ALLT) formulations could be monitored using fluorescence at higher wavelengths (410-430nm) where entrapped drug at low intravesicular pH does not fluoresce.

The initial aim of this study was to validate a fluorescence method to non-invasively monitor liposomal release of TPT in tissue samples. During the course of comparing apparent liposomal release profiles in different media including PBS buffer, plasma, and plasma ultrafiltrate using either the fluorescence method or HPLC it became evident that: a)

TPT release is dramatically accelerated in human plasma as initially reported by Liu et al.;[62] and b) similar release kinetics were obtained in plasma ultrafiltrates. Recognizing that a non-filterable plasma component must be responsible for the accelerated release and that normal human plasma contains low levels of ammonia,[163, 164] additional studies were conducted to probe the concentrations of ammonia in the plasma samples and the effect of ammonia on TPT release. To mechanistically rationalize differences in release profiles using different analytical methods and media, mathematical models were developed to account for the effects of liposome concentration, intravesicular pH, TPT ionization, and ammonia concentration on release kinetics.

5.2 Materials and Methods

5.2.1 Materials

Powders of 1,2-distearoyl-sn-glycero-3-phosphatidylcholine (DSPC, >99% purity) and 1,2-distearoyl-sn-glycero-3-phosphoethanolamine-N-[methoxy(polyethyleneglycol)-2000] (DSPE-PEG2K, MW = 2806, >99% purity) were purchased from Avanti Polar Lipids (Alabaster, AL). Topotecan hydrochloride was purchased from AK Scientific (Union City, CA). Heparinized human plasma samples from three individual donors of different ethnicity were purchased from Innovative Research (Novi, MI), aliquoted and stored at -20°C. Benzene sulfonic acid sodium salt (sodium besylate) was purchased from Spectrum Chemicals (New Brunswick, NJ). Millipore ultrafiltration cartridges (Amicon® Ultra 0.5 mL centrifugal filter device with 3,000 MWCO Ultracel® membrane), Nuclepore polycarbonate membranes (0.1 μm), Dowex 50Wx8-200 resin in the H^+ form, solvents, and buffer salts were purchased from Fisher Scientific (Florence, KY). All solvents were HPLC grade.

5.2.2 Liposome preparation

Large unilamellar liposomes were prepared based on previously reported methods.[49, 50, 60, 118, 124, 125] Briefly, powders of DSPC and DSPE-PEG2K were dissolved in chloroform at a molar ratio of 95:5, then dried under nitrogen, and finally under vacuum (- 30 in Hg) at 35 °C for 6 hours. After drying, the films were hydrated in either 0.3 M ammonium besylate, 1 mM TPT in 50 mM pH 3.75 formate buffer, or pH 7.4 phosphate buffered saline (PBS) solutions to produce 30 mg/mL lipid suspensions. These suspensions were vortexed at 60 °C, then extruded through two 100 nm polycarbonate membranes 10 times at 40 psig and 60 °C to yield suspensions of ammonium besylate-loaded liposomes (ABLs), passively-loaded TPT-containing liposomes, or blank liposomes, respectively.

The ammonium besylate solutions (0.3 M) used for liposome hydration were prepared in a manner similar to that previously used to make other amino-based salts.[21, 42] Solutions of sodium besylate (0.6 M) were passed through an ion exchange column loaded with Dowex 50Wx8-200 resin in the H+ form. The eluted solutions were subsequently titrated with ammonium hydroxide (3.0 M) to the equivalence point and diluted to the desired concentration.

5.2.3 Active loading of TPT into ammonium besylate liposomes

Previous studies have shown that active-loading of weakly basic drugs results in high encapsulation efficiency and possibly longer drug retention in vitro and in vivo.[62, 159] Actively- loaded liposomal suspensions of TPT were prepared with the aim of evaluating a fluorescence method to analyze drug release in vivo or ex vivo. Active loading was performed by generating a low intravesicular pH via an ammonia gradient.[62, 73] This gradient was established when extravesicular ammonium besylate was removed by passing the suspension through a Sephadex G-25 column similar to previous reports.[62] In this case,

0.4 mL of the ABL suspension was passed through the column equilibrated with 100 mM 2-(N-morpholino) ethanesulfonic acid (MES) pH 5.5 buffer and the first 5 mL of eluted suspension was collected for loading studies. Next, 1.5 mL of the eluted suspension was added to an equal volume of TPT dissolved in the same pH 5.5 buffer to achieve a total TPT suspension concentration of 50 or 200 μM and a lipid concentration of 0.92 mg lipid/mL. Loading occurred over a 72 hour period within a 37 °C incubator.

Actively-loaded liposomal TPT (ALLT) suspensions were prepared for release studies by removing extravesicular buffer and any remaining unloaded drug by applying 0.5 mL of ALLT to a Sephadex G-25 column equilibrated with PBS similar to previous reports.[60, 63] The first 2.5 mL fraction eluted from the column was discarded. ALLT eluted in the next 2.5 mL fraction and was collected for use in release studies monitored by fluorescence or HPLC.

5.2.4 Liposome characterization

Particle size was determined for ALLT and PLLT using dynamic light scattering (DLS) using a Beckman Delsa™ Nano C Particle Sizer as previously reported.[125, 126] Lipid content was monitored by HPLC using an evaporative light scattering detector (ELSD). A Waters Alliance 2695 separations module equipped with an Allsphere (Alltech Associates, Inc., Deerfield, IL) silica column (4 x 150 mm, 5 μm) and guard column (20 x 4.0 mm, 5 μm) and a mobile phase consisting of 80% of solvent A (80% chloroform:19.5% methanol:0.5%(v/v) NH_4OH) and 20% of solvent B (80% methanol:19.5% water:0.5% (v/v) NH_4OH) flowing at 1 mL/min was used to quantify DSPC in conjunction with an ELSD (Sedere, Inc., Lawrenceville, NJ) operated at 40 psig and 40 °C. Standards of DSPC were dissolved in mobile phase A (0.05 – 0.3 mg DSPC/mL). Log-log plots of peak area versus concentration were linear over this concentration range. Samples (100 – 250 μL) were dried at room temperature under N2, then dissolved in chilled solvent A before analysis.

5.2.5 Fluorescence method development and validation

5.2.5.1 TPT Excitation Spectra

Samples and standards from validation and release studies were placed in 1 ml quartz cuvettes (NSG Precision Cells, Inc. Farmingdale, NY) for spectrometric analysis. Fluorescence excitation spectra (290-500nm) were collected with a FluoroMax-3 spectrofluorometer (Jobin Yvon Inc. Edison, NJ) operating at a constant emission wavelength of 550 nm, slit width of 1.5 nm, and a 0.5 second integration time. The temperature of the sample chamber was maintained at 37 °C.

Excitation spectra of free TPT (2.5 μM) and PLLT (2.5 μM total suspension concentration of TPT after Sephadex removal of unentrapped drug) in pH 3.75 formate buffer were analyzed to compare the excitation spectra of free and entrapped TPT under acidic conditions. Excitation spectra were obtained by Dr. Amar Jyoti. These spectra were compared to excitation spectra of free TPT (2.5 μM) at pH 7.4 and ALLT suspensions in pH 7.4 PBS (2.5 μM suspension TPT, 37 ug lipid/mL) to determine if ALLT spectra were indicative of an acidic intravesicular environment and whether spectra of entrapped and unentrapped drug were different.

5.2.5.2 TPT release studies by fluorescence

Release of liposomal TPT in the presence of extravesicular ammonia may be particularly important, as it is present in physiological fluids and tissues and may have an effect on intravesicular pH and subsequently on release kinetics. To observe these effects, release studies of ALLT were conducted at 37 °C in pH 7.4, phosphate buffered saline (PBS) solution and in PBS containing 60 μM of NH_4Cl.

For release studies monitored by fluorescence, 100 uL aliquots of the liposomal suspension collected after Sephadex purification were diluted to 1 mL with either PBS, human plasma (from three individual donors), or plasma ultrafiltrate (obtained from the donors' plasma used in release studies) to achieve suspension concentrations of 19.2 μg/mL lipid and 3.2 μM TPT (as determined by HPLC). Excitation spectra were collected over time and compared to spectra for TPT standards (0.5-5 μM) in the same sample matrix analyzed at the same time to quantify the accumulation of free TPT released into the extravesicular solution.

TPT release was monitored by Dr. Jyoti using the increase of fluorescence intensity at an excitation wavelength of 410 nm for PBS and plasma ultrafiltrate while intensities at 420 nm were used for human plasma studies. TPT standard calibration curves were constructed using Equation 14 to adjust for fluctuations in lamp intensity at each sample time, $I_0(t)$, and TPT dimerization in solution:[137, 138]

$$I(t) = (i_1 T_1 + i_2 T_2) I_0(t) \tag{14}$$

where T_1 and T_2 are the solution concentrations of TPT monomer and dimer, respectively, and i_1 and i_2 are the corresponding response factors for these species. Using a mass balance equation for total TPT in solution ($T_o = T_1 + 2T_2$), the TPT dimerization constant ($K_2 = T_2/{T_1}^2$), and Equation 11, fitted values for i_1, i_2, $I_0(t)$, and K_2 were obtained from these calibration curves and used to calculate the concentration of extravesicular TPT at each time point.

5.2.6 TPT release by HPLC

TPT release was monitored by HPLC in suspensions prepared by diluting 0.2 mL of the suspension collected after Sephadex to 4 mL with pH 7.4 PBS containing either no added

ammonia or 60 μM NH_4Cl. The resulting TPT and lipid suspension concentrations were 240 nM and 6.4 μg/mL, respectively. Aliquots (150 μL) withdrawn at various times were diluted with chilled methanol (-20 °C) to disrupt the liposomes and quench the lactone/carboxylate interconversion of TPT. Samples were immediately analyzed by HPLC to quantify both the lactone and carboxylate forms of TPT. A previously published HPLC method was employed with slight modifications.[125] Briefly, a Waters Alliance 2695 separation system with a Waters Symmetry® C18 column (3.9×150 mm, 5 μm) and guard column (3.9 x 20 mm) was used to separate lactone and carboxylate TPT using a mobile phase of 11.5% acetonitrile: 88.5% (v/v) of a 5% (pH = 5.5) triethylamine acetate, 50 mM tetrabutylammonium hydrogen sulfate (TBAHS) buffer at a flow rate of 1 mL/min. TPT lactone and carboxylate standards (20-200 nM) were prepared in chilled, acidified methanol (-20 °C) and 10 mM sodium carbonate buffer (pH 10.1), respectively. Lactone and carboxylate retention times were 6.1 and 2.7 min, respectively. A Waters M474 fluorescence detector (operating at excitation and emission wavelengths of 380 and 560 nm, respectively) was used to analyze the fractions of lactone and carboxylate TPT after separation.

5.2.7 TPT degradation kinetics in the presence/absence of ammonia

Significant TPT degradation would affect the observed concentration of extravesicular TPT and must be incorporated into models describing liposomal TPT release. TPT (0.5 - 5 μM) degradation was assessed in pH 7.4 PBS with or without 60 μM NH_4Cl at 37°C. Degradation of TPT was measured by Dr. Jyoti in the presence of ammonia due to its presence in release studies and previous reports indicating that increasing concentrations of ammonia promote TPT degradation via formation of 9-amino methyl degradants.[91] Aliquots (25 - 40μL) of TPT solutions taken over a 5 day period were diluted to a final volume of 1 mL with acidified methanol (0.001 N HCl) to convert all TPT to its lactone form

and analyzed by the HPLC method used to monitor release. TPT concentrations versus time (t) were fit to a first-order kinetic model as shown below in Equation 12 where k_d is the first-order degradation rate constant and X is the fraction of initial TPT remaining in solution.

$$X = e^{-k_d t} \tag{12}$$

5.2.8 Ammonia analyses

Potentiometric measurements of ammonia content in plasma were performed before and after release studies by Dr. Jyoti using an Orion ammonia electrode in conjunction with a Thermo Scientific Orion Star A214 pH, ISE, mV, temperature meter. Ammonia standards were prepared between 0.01-0.3 ppm in Milli-Q H2O. Immediately before ammonia analysis, 100 µL of NaOH reagent was added to 10 mL of standards to raise pH and convert any ammonium to ammonia. Solutions were allowed to equilibrate for 3-5 minutes under mild stirring and the final voltage was recorded. A Nernst relationship between ammonia concentrations and electric potential (mV) was observed and used to make a standard curve for the estimation of total ammonia in solution. Plasma samples (100µL) were analyzed after ultrafiltration and subjugation to the same dilution and addition of NaOH as standards to obtain ammonia concentrations within the sample.

5.2.9 General mathematical model for actively-loaded liposomal TPT release under non-sink conditions

Because of the low intravesicular pH established during the active loading process, encapsulated TPT exists solely in its lactone form.[62, 97, 165] Under physiological pH, TPT undergoes pH-dependent conversion to its carboxylate counterpart as it is released (Scheme 5.1A).[62, 165] TPT's ionization state also changes upon release as the unionized phenol dominates at low intravesicular pH (pKa = 6.56) while the phenolate anion is the

major species at physiological pH (Scheme 5.1B).[92, 125, 138] By applying the appropriate mathematical model, it is possible to extract the critical release parameters from either the time-dependent profiles of TPT lactone and carboxylate generated by HPLC or changes in fluorescence excitation spectra.

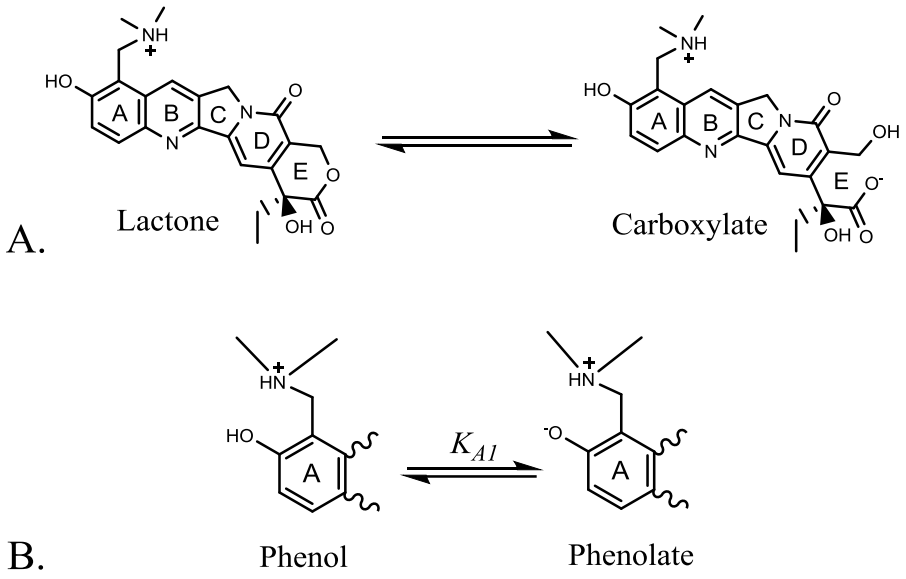

Scheme 5.1. Physicochemical properties of TPT considered in modeling liposomal release kinetics. TPT undergoes pH-dependent interconversion between its lactone and ring-opened carboxylate forms which can be monitored by HPLC (A). Ionization of the A-ring phenol causes a shift in the fluorescence excitation spectrum of TPT which occurs only when drug is exposed to a physiological pH upon liposomal release (B).

A simple kinetic model describing drug release proceeding to equilibrium under non-sink conditions was used to quantify the release profiles obtained by both HPLC and fluorescence methods. Because previous studies have shown the lactone form of TPT to be the most permeable, this model assumes the intra- and extravesicular lactone species (Li and Lo, respectively) govern the rates of change of total intra- and extra-vesicular TPT ($\frac{dT_i}{dt}$ and $\frac{dT_o}{dt}$, respectively).

$$\frac{dT_i}{dt} = -k_m L_i + k_m K L_o \quad (1a)$$

$$\frac{dT_o}{dt} = k_m L_i - k_m K L_o - k_d T_o \quad (1b)$$

where k_m is the rate constant for bidirectional TPT transport, K is the ratio Li /Lo at equilibrium, and kd is the first-order degradation constant for TPT released into the extravesicular solution.

Once released, lactone TPT undergoes reversible, pH-dependent lactone hydrolysis to form its ring-opened, carboxylate counterpart. This process may be assumed to be fast relative to release and thus in equilibrium. Assuming this pH-dependent equilibrium, an apparent acid dissociation constant (K_A') may be used to solve for the fraction of extravesicular TPT in the lactone form ($f_L = \frac{H^+}{H^+ + K_A'}$). This expression allows L_o to be written in terms of T_o, and $L_i \cong T_i$ due to the low intravesicular pH resulting from active loading. Using this information, the rate equations can be rewritten as shown below.

$$\frac{dT_i}{dt} = -k_m(T_i - f_L K T_o) \quad (2a)$$

$$\frac{dT_o}{dt} = k_m(T_i - f_L K T_o) - k_d T_o \quad (2b)$$

T_o was directly monitored by fluorescence while the fractions of total drug remaining in the suspension in the lactone and carboxylate forms were monitored by HPLC. Ti and To could be obtained from the total lactone and carboxylate fractions ($L(t)$ and $C(t)$, respectively) and the total suspension concentration of TPT measured at each time point, $T(t)$:

$$L(t) = \frac{T_i + f_L T_o}{T(t)} \quad (3a)$$

$$C(t) = \frac{(1 - f_L) T_o}{T(t)} \quad (3b)$$

Initial conditions were required to accurately solve and fit the above differential equations to release data. In fluorescence studies, extravesicular drug present at the beginning of the release study (T_o^0) was directly analyzed by fluorescence; however, the initial intravesicular drug could not be determined directly from fluorescence. The initial concentration of intravesicular drug was determined after subtracting T_o^0 from the total initial suspension concentration (T^0) obtained by HPLC analysis. These initial conditions are expressed by the equations below.

$$T_o(0) = T_o^0 \tag{4a}$$

$$T_i(0) = T^0 - T_o^0 \tag{4b}$$

HPLC studies had similar initial conditions. Assuming that any carboxylate in the suspensions was attributable to extravesicular drug, the initial fraction of carboxylate present in the release suspension (C_0) could be related to T_o^0 and subsequently be used in conjunction with the initial fraction of lactone (L_0) to solve for the initial intra- and extra-vesicular conditions as shown below.

$$T_o(0) = T_o^0 = \frac{C_0}{(1-f_L)} \tag{5a}$$

$$T_i(0) = L_0 - \frac{C_0}{(1-f_L)} \tag{5b}$$

5.3 Results

5.3.1 Differences in fluorescence spectra and quantitation of extravesicular TPT

Increases in pH result in a red shift in TPT excitation spectra in aqueous solution.[125, 138] Such a shift suggests TPT release from actively-loaded liposomes into a pH 7.4 buffer or plasma could be distinguished from entrapped drug. This hypothesis was confirmed by comparing the fluorescence excitation spectra obtained for various aqueous solutions and liposomal suspensions of TPT. In Figure 5.1, the excitation spectra of TPT under acidic conditions (either in solution or encapsulated) were nearly identical to the excitation spectrum obtained for ALLT suspended in pH 7.4 PBS with maximum excitation occurring at 380 nm. These results are indicative of a low intravesicular pH environment remaining after the active loading process.[21, 42, 62, 64, 73, 95] The red shift observed for free or extravesicular TPT in PBS at pH 7.4 resulting in maximum excitation at 410 nm is not altered in the presence of blank liposomes (Figure 5.1). Determination of extravesicular TPT is possible without significant interference from encapsulated drug because TPT under these more acidic conditions is not excitable at this higher wavelength.

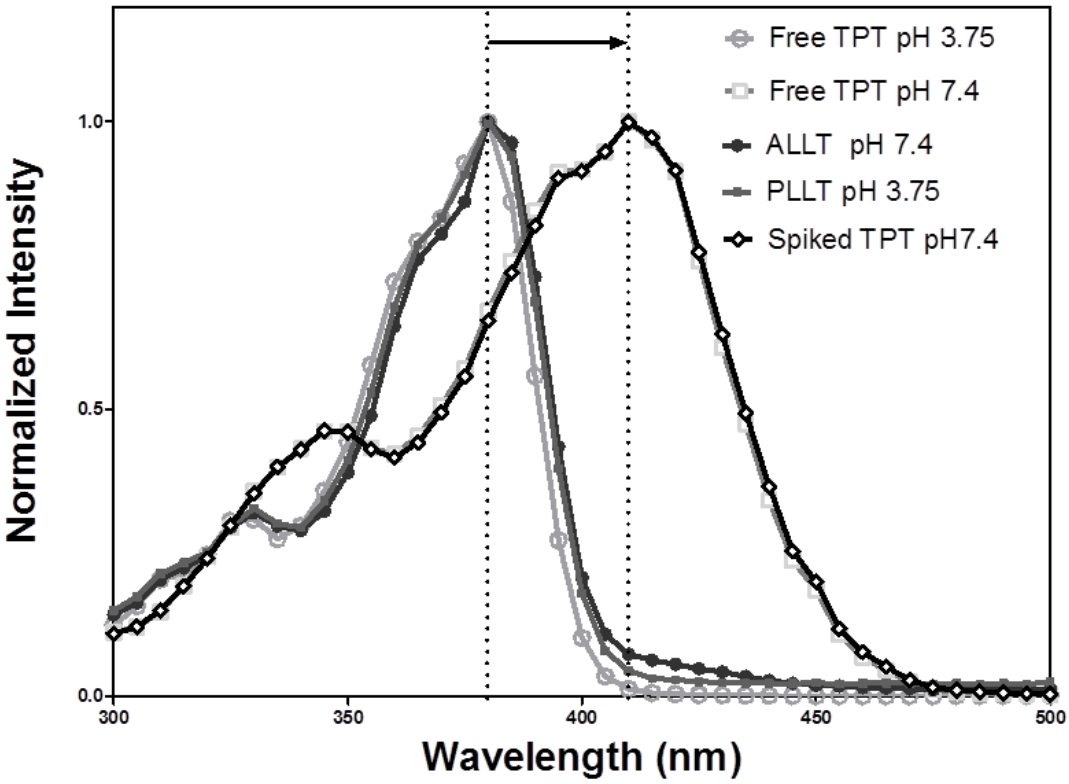

Figure 5.1. Illustration of differences in normalized excitation spectra between free and entrapped TPT at 37 °C. Excitation spectra of free TPT at pH 3.75, passively-loaded liposomal TPT (PLLT) at the same pH, and actively-loaded liposomal TPT (ALLT) suspensions in pH 7.4 buffer have identical spectra, indicating an acidic intraliposomal pH within ALLT.. At pH 7.4, spectra of free TPT solutions and suspensions of blank liposomes spiked with free TPT (i.e., spiked TPT pH 7.4) exhibit a red shift in the excitation spectrum (denoted by the arrow). The identical spectra of spiked and free TPT indicates that drug binding to the outer bilayer leaflet or particle scattering have no effect on the spectra of extravesicular TPT. All the spectra displayed contained total TPT concentrations of ~ 2.5 μM. The lipid concentration in liposome suspensions was ~ 37 μg lipid/mL.

Calibration curves for quantifying extravesicular TPT were constructed from excitation spectra at varying concentrations (0.2-5 μM) of TPT in pH 7.4 PBS, human plasma, and plasma ultrafiltrate. Fluorescence intensity versus TPT concentration was nearly linear

with slight quenching of fluorescence at higher concentrations (~ 5 μM). This quenching was due to TPT dimerization and accounted for in the calibration curve (see Methods).[138] Quantitation of intravesicular TPT was not possible due to self-association and collisional quenching effects at the high intravesicular TPT concentrations (~ 15 mM) present as a consequence of the active loading process.

5.3.2 TPT degradation in the presence and absence of ammonia

TPT degradation was monitored by HPLC at pH 7.4 and 37 °C in PBS and PBS containing 60 μM NH_4Cl (data not shown). The degradation was first-order and independent of the presence of ammonia. The rate constant for degradation was determined to be 1.15 ± 0.08 x 10^{-2} hr^{-1} (95% CI). This value was incorporated into the models used to fit release data.

5.3.3 Comparison of fluorescence and HPLC methods to monitor release

Release studies were conducted in PBS with or without added ammonia and analyzed by HPLC and fluorescence methods to validate the use of fluorescence for determining release. Degradation of topotecan at pH 7.4 limited the time frame for release studies by fluorescence to ~ 24 h. However, because longer times were necessary to establish equilibrium, both HPLC and fluorescence release data in PBS with and without ammonia were fit simultaneously to determine values for K ($T_i / f_L T_o$ at equilibrium). The resulting fits indicated that K decreases with the addition of extravesicular ammonia to the release media.

While K was assumed to be independent of the method of analysis, separate km values were determined for each method and condition. The values obtained are shown in Table 5.1, and the resulting fits of the data from both methods are illustrated in Figure 5.2. Half-lives to equilibrium, $t_{1/2}^{eq}$, were also calculated for easier comparison. This $t_{1/2}^{eq}$ is defined by the equation below.

$$t_{1/2}^{eq} = \frac{\ln(2)}{k_m(1+Kf_L)} \quad (6)$$

Both methods show similar trends in km, with faster release in PBS containing 60 μM NH_4Cl than that in PBS alone. In PBS containing 60 μM NH_4Cl, the 95% confidence limits of the km values determined from both methods overlapped. However, in PBS without ammonia km values differed significantly depending on the monitoring method, with TPT release monitored by fluorescence being faster than that obtained by HPLC. This was attributed to the lower concentration of liposomes in the experiments monitored by HPLC which resulted in more ammonia release. Reduction in the intravesicular concentration of ammonia lowered the intravesicular pH, thus slowing TPT release.[125] A detailed analysis of the differences in ammonia release and subsequent effects on intravesicular pH is provided in a later section.

Table 5.1. Release parameters obtained from HPLC and fluorescence methods.[b]

	PBS only		PBS w/ 60 μM NH_4Cl		Plasma &
Constant	HPLC	Fluorescence	HPLC	Fluorescence	Ultrafiltrate
k_m(hr $^{-1}$)	0.037 ± 0.004	0.053 ± 0.008	0.15 ± 0.02	0.18 ± 0.04	1.5 ± 0.4
K	4.1 ± 0.6		0.5 ± 0.2		0
$t_{1/2}^{eq}$(hr)	10 ± 1	6.9 ± 0.9	4.6 ± 0.6	3.8 ± 0.8	0.54 ± 0.2
k_d(hr $^{-1}$)	0.0115	0.0115	0.0115	0.0115	0.1

[b] ± 95 % confidence intervals

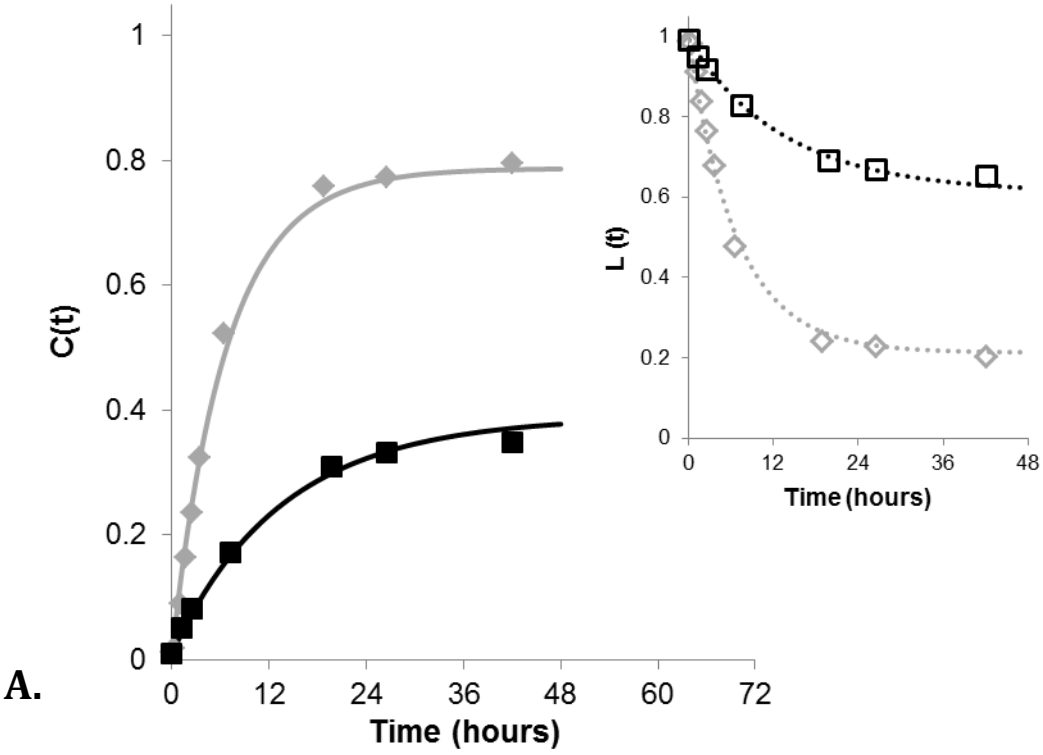

A.

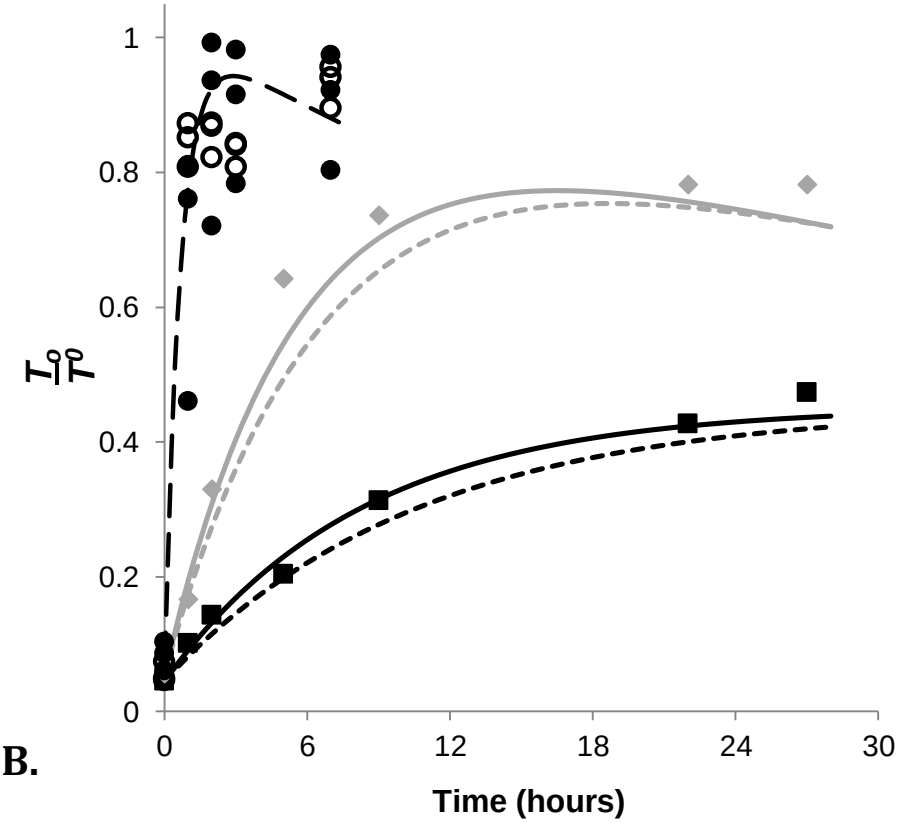

B.

Figure 5.2. Comparison of release profiles obtained by HPLC and fluorescence methods. A) Changes in the fraction of TPT carboxylate versus time obtained by HPLC in release studies at 37 °C in pH 7.4 PBS with 60 μM NH_4Cl and without ammonia (◆ and ■, respectively) are shown along with fits of the carboxylate fraction to the release model (— and —). The open symbols in the inset reflect the change in the fraction of lactone over the same time frame with ···· and ···, reflecting their respective fits to the release model. B) The fraction of TPT in the extravesicular compartment relative to the initial total suspension concentration of TPT (T_o/T^0) versus time determined by the fluorescence method in pH 7.4 PBS in the presence or absence of ammonia (◆ and ■, respectively). Solid lines (— and —) represent fits to the release model . The short-dashed lines (····· and ·····) reflect simulated profiles using the parameters obtained from release data monitored by HPLC for comparison. Release rates were accelerated to the same degree in plasma (●) and plasma ultrafiltrates (○). The long-dashed line (– –) is representative of the simultaneous fits of all six data sets (i.e. plasma and plasma ultrafiltrate from three separate donors) from which the parameters listed in Table 5.1 were obtained.

5.3.4 Release experiments in human plasma and plasma ultrafiltrate

Red shifts in excitation spectra were also observed during release studies in plasma. These shifts were again used to monitor TPT release. This is illustrated in Figure 5.3. Rate constants for release in plasma were ~30-fold greater than in PBS (Figure 5.2b and Table 5.1) alone. To assess possible contributions of colloidal lipoprotein particles that might participate in lipid exchange with the lipid bilayer or protein effects such as opsonization,[93, 156, 166-168] plasma samples were ultrafiltered and the ultrafiltrates were then used in release experiments. TPT release in plasma ultrafiltrates was indistinguishable from the plasma release profiles (see Figure 5.2b) and the release rate constants in both plasma and plasma ultrafiltrates were ~10-fold greater than in PBS containing 60 μM NH_4Cl. These observations provided motivation to measure ammonia concentrations in plasma to

determine whether the accelerated release rates seen in plasma and plasma ultrafiltrates were related to higher ammonia concentrations in these samples. The ammonia concentrations, analyzed using an ammonia selective electrode, were 180, 185, and 355 μM for these three plasma samples (each from a different donor) and their respective ultrafiltrates. These levels were much higher than those reported in normal human blood (15-60 μM). [163, 164] These higher levels were likely due to protein degradation during storage, even under the -20 °C temperatures employed.[169]

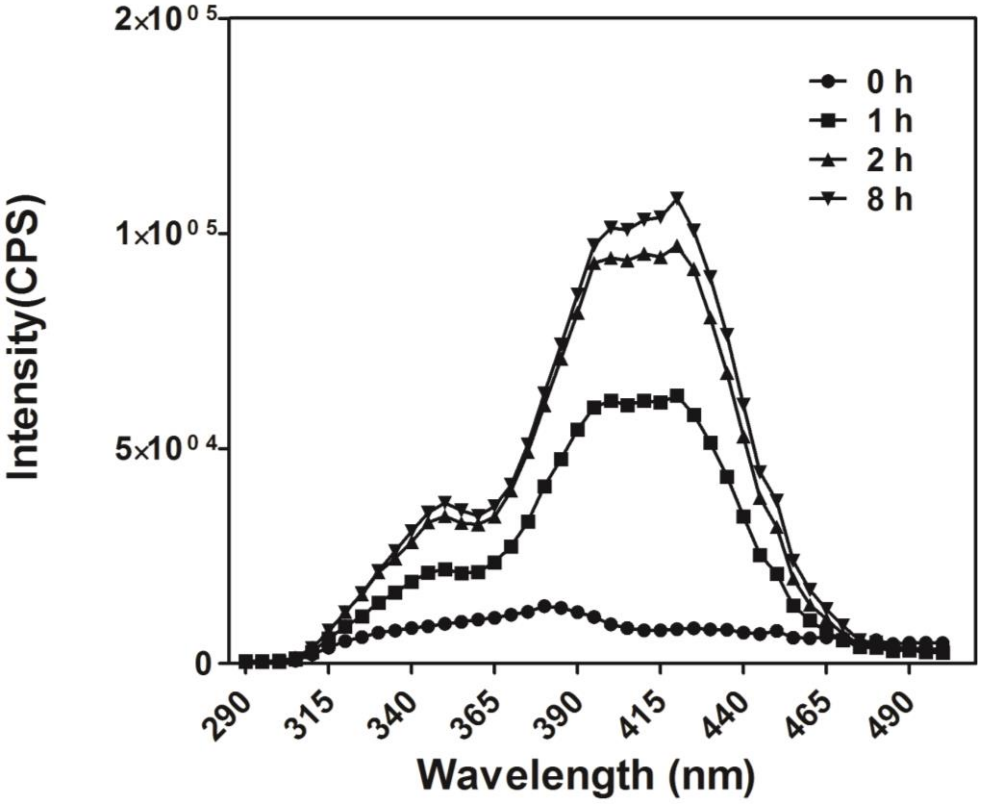

Figure 5.3. Fluorescence excitation spectra of ALLT in plasma over time. The change in fluorescence at 420 nm was used to monitor extravesicular TPT and subsequently liposomal release kinetics.

5.4 Discussion

5.4.1 Differences in liposome concentration led to changes in intravesicular ammonia, pH, and subsequent release kinetics

While attempts were made to keep the release media consistent between experiments analyzed by HPLC and fluorescence, the liposome suspension concentrations differed between the two methods. This was necessary for maintaining TPT concentrations in an optimal range for quantification by each method. Simulations indicated that this seemingly minor difference could be important.

A preliminary estimate of the intravesicular pH under the different conditions in these experiments was obtained by simulating the effects of ammonia transport across the bilayer. The first-order rate constant for ammonia bilayer transport, $k_{m,n}$, is related to the permeability coefficient for ammonia transport, $P^m_{NH_3}$, and liposome diameter d:[50]

$$k_{m,n} = \frac{6\,P^m_{NH_3}}{d} \tag{7}$$

The differential equations that govern ammonia transport are then:

$$\frac{dN_i}{dt} = -k_{m,n}(NH_{3,i} - NH_{3,o}) \tag{8a}$$

$$\frac{dN_o}{dt} = f_v k_{m,n}(NH_{3,i} - NH_{3,o}) \tag{8b}$$

Because the free base form of ammonia is the permeable species,[170] the rates of change in the total concentration of ammonia in the intra- and extra-vesicular compartments (N_i and N_o respectively) are dependent on the concentration gradient between neutral ammonia in the intra- and extra-vesicular compartments ($NH_{3,i}$ and $NH_{3,o}$ respectively), the rate constant for neutral ammonia transport ($k_{m,n}$), and the ratio of liposomally-entrapped to

unentrapped volume (f_v). The latter quantity, f_v, can be calculated from the particle size and lipid content in the liposome suspension with knowledge of the lipid surface density.[50] NH3,I and NH3,o may be written in terms of Ni and No by solving for the fractions of neutral ammonia in the intra- and extra-vesicular phases (f_i^N and f_o^N):

$$f_i^N = \frac{K_{AN}}{H_i^+ + K_{AN}} \tag{9a}$$

$$f_o^N = \frac{K_{AN}}{H_o^+ + K_{AN}} \tag{9b}$$

These fractions are dependent on the acid dissociation constant for ammonia, K_{AN}, and the acidity or hydrogen ion concentrations in the intra-or extra-vesicular compartments (H_i^+ and H_o^+, respectively). Using these fractions, equations 8a and b can be rewritten to yield:

$$\frac{dN_i}{dt} = -k_{m,n}(f_i^N N_i - f_o^N N_o) \tag{10a}$$

$$\frac{dN_o}{dt} = f_v k_{m,n}(f_i^N N_i - f_o^N N_o) \tag{10b}$$

The pH in the intravesicular compartment decreases as ammonia release causes deprotonation of ammonium to replenish the released ammonia. This process governs the acidity of the intravesicular compartment by satisfying the charge balance equation:

$$H_i^+ = B^- + OH_i^- - (NH_{4,i}^+ + TPTH_i^+) \tag{11}$$

where B^- is the ammonium salt counterion (besylate) concentration and $TPTH_i^+$ is the concentration of the cationic form of topotecan. The ammonium ($NH_{4,i}^+$) and $TPTH_i^+$ concentrations can be expressed in terms of total intravesicular concentration of ammonia (N_i) and topotecan (T_i) while OH_i^- can be rewritten in terms of H_i^+ and the ion product of water, K_w.

$$H_i^+ = B^- + {K_w}/{H_i^+} - [(1 - f_i^N)N_i + f_i^T T_i] \quad (12)$$

At low pH, the fraction of intravesicular TPT in its protonated form, f_i^T, is a function of H_i^+ and the TPT phenol acid dissociation constant, K_{A1}:

$$f_i^T = \frac{H_i^+}{H_i^+ + K_{A1}} \quad (13)$$

Simulations were performed using these equations and the values in Table 5.2 to calculate H_i^+ concentration versus time when the extravesicular solution initially contained either no ammonia (Figure 5.4A) or 60 μM of NH_4Cl (Figure 5.4B) using the lipid concentrations measured in this study. From these simulations, it is apparent that the entrapped volume can have a significant impact on intravesicular pH depending on the concentration of extravesicular ammonia present. In solutions that initially contained no buffer, the higher lipid concentration (i.e. large entrapped volume) allows more ammonia release while the intravesicular ammonia is depleted to a lesser extent. Because of the resulting higher intravesicular ammonia concentration, the increase in H_i^+ is less for the liposome suspensions used in the fluorescence method. TPT release is pH-dependent and slower as H_i^+ increases.[125] The higher rate of TPT release determined by the fluorescence method compared to that observed by HPLC is consistent with this difference in H_i^+.

This effect, however, is not apparent in the release studies conducted in PBS solutions which initially had ammonia present. At 60 μM NH_4Cl, the extravesicular concentration of ammonia is sufficiently high and the volume entrapped low enough that the extravesicular concentration essentially remained constant. This normalized the ammonia concentration gradient to be the same and independent of the entrapped volume (Figure 5.5b). This results in nearly identical H_i^+ profiles for both methods and subsequently the same release kinetics for both methods.

For these simulations, the initial H_i^+ was calculated assuming a 1:1 exchange between ammonia and TPT during the active loading process (i.e. $N_o(0) = 0.3 - T_i$). While this can only be a rough estimation of the initial H_i^+, simulations at a higher or lower initial H_i^+ (10-2.5 and 10-5.5 or pH of 2.5 and 5.5, respectively) also resulted in similar trends in the terminal H_i^+ simulated in Figure 5.4.

Table 5.2. Parameters used to simulate H_i^+ profiles at different lipid concentrations

Parameters	Values
$k_{m,n}$	$2.88 \times 10^4\ s^{-1}$ [c]
K_{A1}	2.8×10^{-7} [d]
K_{AN}	9.40×10^{-10} [e]
K_w	2.12×10^{-14} [e]
H_o	$3.98 \times 10^{-8} M$
T_i	$1.45 \times 10^{-2} M$
B_i	$0.3\ M$
f_v – HPLC conditions (6.4 µg lipid/mL)	1.66×10^{-5} [f]
f_v – Fluorescence conditions (19.2 µg lipid/mL)	5.19×10^{-5} [f]

[c] Calculated from a previously reported ammonia permeability coefficient of $P_{NH_3}^m = 48 \times 10^{-3}\ cm/s$ [171]

[d] Obtained from a previous study[125]

[e] Values adjusted to reflect conditions at 37 °C and 0.3 I

[f] Calculated based on particle size, lipid content, and lipid surface density calculations previously reported[50, 135]

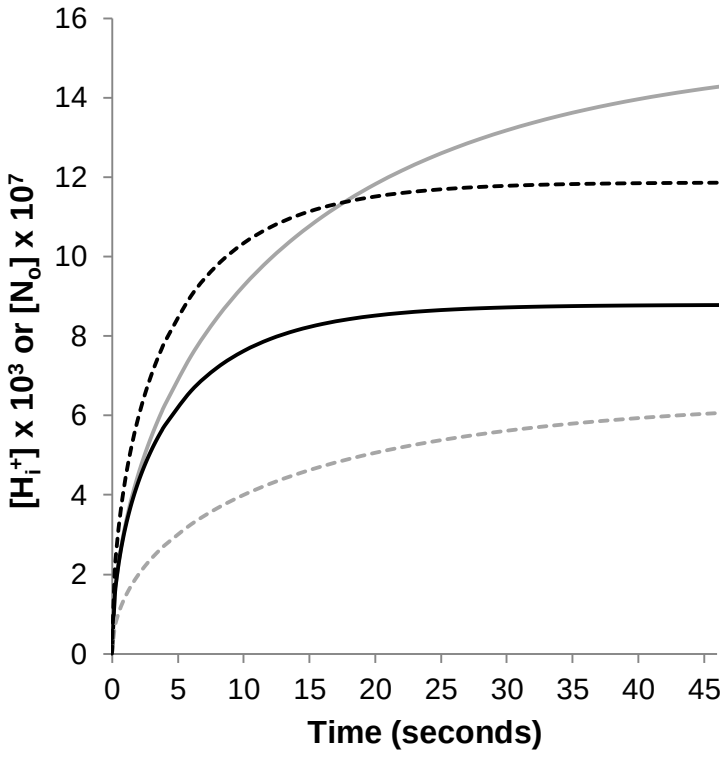
16
14
12
10
8
6
4
2
0
0
5
10
15
20
25
30
35
40
45
Time (seconds)
[H+i] x 10^3 or [No] x 10^7

A.

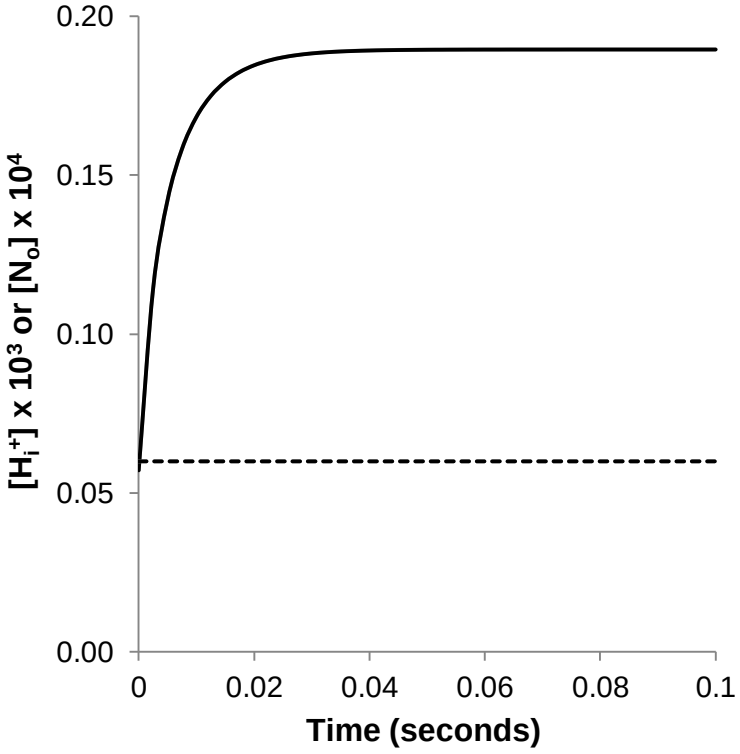
0.20
0.15
0.10
0.05
0.00
0
0.02
0.04
0.06
0.08
0.1
Time (seconds)
[H+i] x 10^3 or [No] x 10^4

B.

Figure 5.4. The simulated profiles of $[H_i^+]$ and $[N_o]$ versus time in pH 7.4 PBS release media that initially contained no extravesicular ammonia (A) or 60 μM NH_4Cl (B). $[H_i^+]$ simulations shown are at the lipid concentrations at which release studies by HPLC (—) and fluorescence methods (—) were conducted. The dotted lines of corresponding color reflect the total extravesicular ammonia present over this time period for HPLC and fluorescence methods, respectively.

5.4.2 Effects of ammonia concentration in physiological samples and implications on liposomal TPT release

Initial simulations of intravesicular pH showed that the presence of extravesicular ammonia in the release media partially dissipated the pH gradient. Such an effect may also be possible in the release studies in plasma and plasma ultrafiltrates as relatively high levels of ammonia were detected in these samples. This was explored further in simulations of the intravesicular pH after accounting for the extravesicular ammonia present in the various release media studied (buffer, plasma, or plasma ultrafiltrate). These simulations, shown in Figure 5.5, indicate a negative correlation between the release half-life and the intravesicular pH. This relationship provides further evidence that the presence of extravesicular ammonia raises intravesicular pH, given the pH-sensitive release of liposomal TPT previously reported.[125]

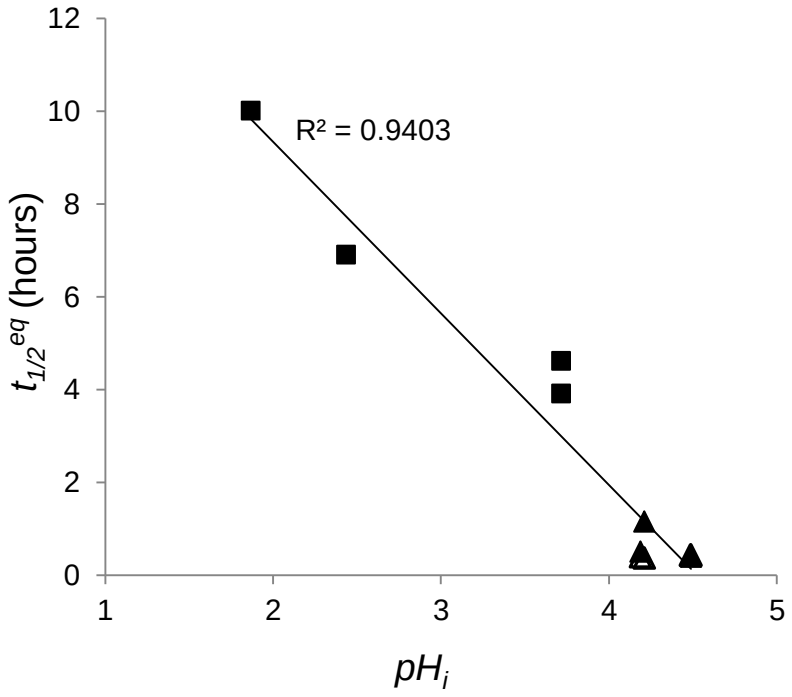

Figure 5.5. The relationship between TPT release half-life and simulated intravesicular pH. Release studies performed in PBS (■), plasma (▲), and ultrafiltrate obtained from plasma (Δ) are shown. In some instances, the plasma ultrafiltrate data are difficult to observe due to overlap with data points from plasma studies. The resulting trend line along with its R^2 are shown to illustrate the negative correlation between TPT retention and intravesicular pH.

While further studies are necessary to fully understand the effect of ammonia transport on actively-loaded liposomal systems (e.g. in formulations with drug precipitation/complexation within the intravesicular environment), the potential implications are considerable. Many liposomal drug loading strategies rely on the generation of a pH gradient using ammonia,[62, 73] an ionophore,[64, 96, 97] or another highly permeable amine (e.g. di- or tri-methylamine).[21, 42] In all of these strategies, the pH gradients generated to stabilize drug encapsulation are susceptible to the influx of ammonia or other highly permeable basic species present in physiological tissue or fluid. The intravesicular pH in these formulations should be calculable using an equation based on a

charge balance similar to Equation 11 with appropriate modifications to account for precipitation, self-association, etc. Under *in vivo* conditions, the much larger volume of physiological fluids, in comparison with the entrapped volume of administered liposomes, would also provide constant extravesicular ammonia levels, similar in manner to the conditions studied within this chapter.

While it is likely that ammonia is the primary basic-permeable species present in physiological fluids and tissues, other low molecular weight amines (e.g. di- and tri-methylamine) are also present at levels which vary from patient to patient.[172-174] Other effects have been suggested to account for variability of liposomal release kinetics in plasma such as destabilization of the bilayer due to protein interactions.[32, 55, 57, 166, 167, 175] However, these theories could not explain the effects seen here as release kinetics obtained in plasma would have been significantly different from release kinetics obtained in studies performed in an ultrafiltrate of the same plasma (which was not the case).

Lastly, the storage conditions and history of the plasma may also have a considerable effect on release rates from actively loaded liposomes. Previous reports on the production of ammonia under a wide variety of conditions typically encountered during the processing and storage of plasma are considerable.[169, 173] Furthermore, these studies indicate that ammonia production is significant at room temperature and even when samples have been frozen. This may account for the higher ammonia levels in these plasma studies than those reported in the literature for fresh plasma and blood samples.[163, 164] Such an issue could lead to overestimations of drug release *in vivo*. Characterization of the ammonia content and possibly other protein degradants in release studies performed in plasma should be considered. Furthermore, ammonia generation during release studies may also affect release kinetics. In the present study, ammonia levels in plasma after a 48 hour release

experiment were considerably higher (approximately two-fold) than the initial ammonia levels. This is yet another scenario that could lead to possible overestimation of drug release based on characterization studies in plasma, as renal excretion of ammonia would typically prevent such high levels in patients. In contrast, however, patients suffering from hyperammonemia could present much higher ammonia concentrations (~1 mM).[176, 177] This condition may be quite relevant in cancer patients with diminished liver function,[178] either as a result of the cancer's pathophysiology, a side effect of a previous treatment,[178-181] or a preexisting condition (e.g. cirrhosis).[178] In such cases, further acceleration in liposomal drug release may be seen.

5.4.3 Adaptation of method for other nanoparticles and drugs

In the field of nanotechnology-based drug delivery systems, analytical methods to quantify in vivo drug release from nanoparticles are needed to develop in vitro-in vivo release rate correlations and to ultimately relate anti-tumor efficacy to drug exposure. Described herein is a fluorescence technique to non-invasively distinguish free TPT from liposomally entrapped drug in tissue (human plasma). The release profiles generated were analyzed using mathematical models to probe the effects of critical experimental variables affecting release rates. The combination of a non-invasive method to analyze liposomal drug release and mechanism-based mathematical modeling to interpret release profiles represents a powerful new approach for understanding actively-loaded liposomal drug release that may ultimately contribute to improved liposomal drug therapy.

For these studies, fluorescence spectroscopy is used; however, the general validation scheme could be applied to other spectroscopic techniques depending on the spectrometric properties of the particular drug and/or nanoparticle. While qualitative comparisons of spectrometric data are initially made to distinguish free from entrapped drug, quantitative

analysis and validation of release kinetics requires a mathematical model describing release kinetics.

5.5 Conclusion

Reliable methods to monitor drug release in physiological fluids and tissues could improve predictions of in vivo performance of liposomal drug delivery systems. To this end, a non-invasive method was developed to monitor liposomal release kinetics of TPT. This method utilizes the pH-dependent shift in the excitation spectra of TPT to distinguish between drug entrapped at the low intravesicular pH in actively-loaded liposomal formulations from released drug. Release kinetics obtained by fluorescence were consistent with results using an HPLC method to monitor release.

Accelerated liposomal TPT release kinetics were observed in human plasma. Additional experiments in plasma that was ultrafiltered to remove protein and lipid components that have previously been theorized to alter release kinetics indicated similar accelerated release rates. When release studies were performed in PBS buffer at pH 7.4, the addition of ammonia to the buffer was also found to dramatically increase release rates. Analyses of ammonia concentrations in the plasma samples employed in release studies were therefore undertaken. Model-based simulations were used to estimate the intravesicular pH in the presence or absence of extravesicular ammonia. The intravesicular pH increased with increasing concentrations of extravesicular ammonia. A significant correlation was found between TPT release rates and intravesicular pH simulated based on the extravesicular ammonia present in the plasma, plasma ultrafiltrates, or PBS buffer in which release studies were conducted. These findings may account for the accelerated release rates typically experienced in physiological fluids and potentially some of the preclinical variability

observed from ALLTs[23] and likely present for other actively-loaded, weakly basic drugs (e.g. doxorubicin, irinotecan, and vincristine).[21, 73, 95, 96, 112, 182]

Because extensive processing of sample is not required to analyze drug release, the non-invasive fluorescence method developed in this work has potential applications for analyzing release kinetics in real-time for physiological samples. One such application may include analysis of free and entrapped drug in blood samples taken for PK studies. This would allow for both particle clearance and liposomal release kinetics of drug in systemic circulation to be analyzed simultaneously. Currently, adaptation of this method is under investigation using two-photon fluorescence for intratumoral imaging of release kinetics in mouse xenografts equipped with a dorsal window. This method may also be adaptable to other molecules that exhibit pH dependent fluorescence spectra.

CHAPTER SIX

Mechanistic Evaluation of Self-association, Ion-pairing, Ammonia, and Precipitation Effects on Active Loading and Release of Liposomal Topotecan

6.1 Introduction

Nanoparticle formulations of anticancer agents are studied intensively for drug delivery applications due to their unique ability to passively or actively target their payloads of anticancer agents to the tumor site. Such targeting has the potential to lower systemic toxicity while increasing intratumoral concentrations of the pharmaceutical agent of interest.[6, 7, 42] Liposomes constitute a class of nanoparticles that has shown additional benefits in chemotherapy delivery due to their slow systemic clearance allowing greater accumulation of the particles (and consequently, the drug) at the tumor site.[30, 111, 183, 184]

Many of the well-studied liposomal formulations incorporate a weakly basic anticancer agent due to their ability to achieve high drug-to-lipid ratios[21, 42, 62, 73, 94, 95] . This result is beneficial for a variety of reasons including: increased API solubility, smaller infusion volume for patients, higher encapsulation efficiency (i.e. high drug loading) resulting in less waste of valuable API, and altered exposure profiles of said API due to liposomal release kinetics. While high loading efficiency is desirable, understanding its effect on *in vivo* performance (i.e. release kinetics) has yet to be adequately characterized.

Mechanistic modeling constitutes a means to provide such understanding by distinguishing physicochemical release characteristics intrinsic to the drug/particles system from artifacts of the release environment (i.e. kinetic or thermodynamic effects attributable to the particular medium that release is studied within).[49, 60, 63, 124, 126, 130] With mechanistic models, optimization of drug release profiles may be achieved by rationally selecting the proper drug loading conditions (e.g. drug suspension concentration, pH,

temperature, counter-ions in solution, etc.). A model capable of providing predictable release rates under a variety of in vitro conditions could be adapted to incorporate physiological variables which affect release *in vivo*. Such modeling would allow a formulator to reasonably predict *in vivo* formulation performance from *in vitro* release studies and reduce the need for costly preclinical testing.

One of the anticancer agents extensively researched as an actively-loaded liposomal formulation is the anticancer agent topotecan (TPT). TPT is a camptothecin analogue known for its topoisomerase-I inhibitory activity[185] and has demonstrated increased anti-tumorigenic efficacy as a liposomal formulation.[62, 158, 159] Many liposomal TPT formulations utilize active loading of the anticancer agent via the establishment of a pH gradient. Generating an acidic intravesicular environment relative to the extravesicular loading solution preserves the active lactone form of the drug while achieving high drug loading efficiencies. Furthermore, this active loading strategy has been shown to result in prolonged retention in release studies conducted in aqueous solution.[62, 64] Unfortunately, these same formulations have shown accelerated release in plasma.[62] Understanding what underlying mechanisms lead to these differences, whether physiological or physicochemical, requires rigorous studies of the active loading process of liposomal TPT. Understanding the kinetic and thermodynamic factors that drive loading will not only allow for optimization of the active loading process, but also help decipher the subsequent release of TPT from these formulations.

This study develops and evaluates several models to describe active loading of TPT based on physicochemical properties of the drug and the liposomal environment. All of these models accounted for the generation of low intravesicular pH in addition to other factors, including TPT self-association and/or ion-pairing transport across the bilayer. The

validity of these models was assessed by fitting experimentally observed uptake profiles of TPT undergoing active loading into liposomes containing ammonium besylate [$NH_4C_6H_6SO_3$] or sulfate [$(NH_4)_2SO_4$]. A loading model which incorporated ion-paired transport of cationic TPT with chloride and TPT dimerization was found to describe drug loading best. Further validation of this model was performed by assessing the model's ability to predict TPT release under varying chloride conditions. Lastly, the influence of chloride on TPT loading at higher temperature was also demonstrated experimentally, showing much higher encapsulation efficiencies and slower release than formulations loaded at lower temperatures. These effects were rationalized by the development of a mechanistic release model which suggests the prolonged release from these high-temperature-loaded liposomes was due to the precipitation of intravesicular TPTHCl. These findings suggest that tunable drug release of liposomal TPT could be achieved through manipulation of chloride during active loading. This work also provides a general approach for mechanistically characterizing active loading and release kinetics of liposomal formulations.

6.2 Materials and methods

6.2.1 Materials

Powders of 1,2-distearoyl-sn-glycero-3-phosphatidylcholine (DSPC, >99% purity) and 1,2-distearoyl-sn-glycero-3-phosphoethanolamine-N-[methoxy(polyethyleneglycol)-2000] (m-PEG DSPE, MW = 2806, >99% purity) were purchased from Avanti Polar Lipids (Alabaster, AL). Topotecan hydrochloride was purchased from AK Scientific (Union City, CA). Benzene sulfonic acid sodium salt (sodium besylate) was purchased from Spectrum Chemicals. Millipore ultrafiltration cartridges (Amicon® Ultra 0.5 mL centrifugal filter device with 30,000 MWCO Ultracel® membrane), Nuclepore polycarbonate membranes

(0.1 μm), Dowex 50Wx8-200 resin in the H^+ form, solvents, and buffer salts were purchased from Fisher Scientific (Florence, KY). All solvents were HPLC grade.

6.2.2 Liposome preparation and characterization

Large unilamellar liposomes were prepared based on previously reported methods.[49, 50, 60, 118, 124, 130] Briefly, powders of DSPC and DSPE-PEG2K were dissolved in chloroform at a ratio of 95:5 mol:mol, then dried under nitrogen, then under vacuum (- 30 in Hg) at 35 °C for 6 hours. After drying, the films were hydrated with ammonium besylate solutions (0.3 M), 0.3 M $(NH_4)_2SO_4$, or a solution of 50 uM TPT in pH 4.1 50 mM sodium formate (adjusted to an ionic strength of 0.3 with NaCl) to make 30 mg/mL lipid suspensions. These suspensions were vortexed at 60 °C, then extruded through 2, 100 nm polycarbonate membranes 10 times at 40 psig and 60 °C to yield ammonium besylate or sulfate-containing liposomes (ABL*s* and ASL*s* respectively) for active loading and passively-loaded TPT liposomes (PLLT), for separate release studies. Liposome particle size was determined with dynamic light scattering (DLS) as reported previously,[126, 130] yielding diameters (with 95% CI of 6 independent readings) of 100 ± 4 and 103 ± 2 nm before active loading and release studies, respectively. Lipid content was also determined (see HPLC analyses) for calculations of entrapped volume and TPT loading efficiency.

The ammonium besylate solutions used for ABL hydration were prepared by passing solutions of sodium besylate (0.6 M) through an ion exchange column made of Dowex 50Wx8-200 resin in the H^+ form. The eluted solutions were subsequently titrated with ammonium hydroxide (3.0 M) to the equivalence point and diluted to the desired concentration as previously reported for several other amino-based salts.[21, 42]

6.2.3 Active loading of TPT

Previous studies have shown that active loading of weakly basic drugs results in high encapsulation efficiency and possibly longer drug retention *in vitro* and *in vivo*. Active loading was performed by generating low intravesicular pH via an ammonia gradient.[62, 73] Establishing an ammonia (or another small-MW amine) gradient is typically accomplished via removal of extravesicular ammonia upon elution of the suspension through a size exclusion column.[21, 42, 62, 73, 95] In this study, 0.4 mL of the ABL or ASL suspension was passed through a Sephadex G-25 column equilibrated with 100 mM 2-(*N*-morpholino)ethanesulfonic acid (MES) pH 5.5 buffer containing 0.25 M NaCl to maintain an isotonic state between the intra-and extra-vesicular solutions. The first 5 mL of eluted suspension was collected for loading studies.

Next, 1.5 mL of the eluted suspension was added to an equal volume of TPT dissolved in the same pH 5.5 buffer to achieve a total TPT suspension concentration of 60, 130, or 180 μM and lipid concentration of 0.92 mg lipid/mL. Loading either occurred over a 72 hour period within a 37 °C incubator or over 30 min in a 60 °C oven as previously reported.[62] Loading kinetics was monitored at 37 °C by isolating intravesicular TPT with a previously validated ultrafiltration method.[126, 130] After ultrafiltration, the obtained suspensions of intravesicular TPT were dissolved in chilled (-20 °C) acidified (0.001 N HCl) methanol to convert all drug to its lactone form for monitoring of loading with HPLC (see HPLC analyses). The levels of released ammonia were also monitored during loading studies. This was achieved by ultrafiltering 0.4 mL of the liposome suspension and analyzing ammonia levels in the ultrafiltrate with an ammonia selective ion probe (see ammonia analyses section).

6.2.4 Release of passively-loaded TPT

Passively-loaded liposomal release was used to assess transport of cationic TPT via ion-pairing with chloride. This was examined by performing TPT release studies where the cationic form of TPT was dominant (pH 4.1) and by examining three different chloride conditions including: 1) an excessive amount of chloride present in both the intra- and extravesicular compartments, 2) only chloride from the TPTHCl salt present in the intravesicular compartment and no chloride present in the extravesicular compartment and 3) only Cl from the TPTHCl salt present in the intravesicular compartment with a large concentration of chloride in the extravesicular compartment. These conditions were achieved using passively-loaded liposomes made in solutions of 50 μM TPTHCl in pH 4.1 50 mM sodium formate buffer with either 0.25 M NaCl or 0.167 M Na_2SO_4 to achieve isotonic conditions. Release was monitored after removal of extravesicular TPT by passing 0.35 mL of the liposomal suspensions through a Sephadex column. For liposomes made with 0.25 M NaCl solutions, the same buffer was used in the Sephadex column. For liposomes made in the presence of sulfate, the suspensions were passed through columns equilibrated with either the same formate buffer or the buffer with 0.25 M NaCl. After 1.5 mL of buffer had been passed through the column, liposomal TPT was eluted in the next 3.5 mL and collected to achieve a final suspension concentration of 135 nM TPT and 0.9 mg lipid/mL. At various time points, 150 uL aliquots of the suspension were collected. Release was monitored by isolating intravesicular TPT using ultrafiltration. After ultrafiltration, intravesicular TPT was dissolved in chilled acidified methanol and analyzed by HPLC.

6.2.5 Release of actively-loaded TPT in the presence of extravesicular ammonia

Release of liposomal TPT in the presence of extravesicular ammonia may be particularly important, as it is present in physiological fluids and tissues and may have an effect on intravesicular pH and subsequently alter release kinetics (as already illustrated in Chapter 5). To observe this effect, release studies of actively loaded TPT in ABLs and ASLs were conducted at 37 °C in pH 7.4, phosphate buffered saline (PBS) solution and in PBS which also contained 12 or 60 μM of NH_4Cl. Removal of extravesicular buffer and any unloaded drug from the loading phase was accomplished by applying 0.5 mL of actively-loaded liposome suspensions to a Sephadex G-25 column equilibrated with PBS similar to previous reports.[60, 63] The first 2.5 mL fraction eluted from the column was discarded and the next 2.5 mL fraction was collected and used in release studies. Release studies were performed by diluting 0.2 mL of the actively-loaded liposomal suspension of TPT obtained from Sephadex to a final volume of 4 mL using PBS with NH_4Cl to achieve final concentrations of 0, 12, or 60 μM. The resulting TPT suspension concentrations ranged between 240 and 600 nM and had a lipid concentration of 6.4 μg/mL. Over time, 150 μL aliquots were withdrawn from the suspension and diluted with chilled methanol (-20 °C) to disrupt the liposomes and quench the lactone/carboxylate ratio of TPT. These samples were immediately injected and analyzed by HPLC to monitor release.

6.2.6 Isolation of intravesicular TPT by ultrafiltration

A previously validated ultrafiltration method was used to separate extravesicular from entrapped TPT[126, 130] for passively-loaded release studies and active-loading at 37 °C. Briefly, an Amicon® Ultra 0.5 mL centrifugal filter device with 30,000 MWCO Ultracel®

membrane containing sample was centrifuged at 14,000 rpm for 10 minutes in an Eppendorf 5417R maintained at 4 °C.

For the analysis of intravesicular TPT, samples were diluted to 0.45 mL with chilled (4 °C) buffer identical to that of the extravesicular solution to quench loading or release before centrifugation. After centrifugation, the resulting concentrate (25 μL) containing the liposome suspension was recovered by inverting the cartridge and centrifuging at 2000 rpm for another 2 minutes. Recovered concentrate was resuspended in another 400 μL of chilled buffer and the process was repeated. The final concentrate was dissolved in acidified methanol and diluted within the calibration range for HPLC analysis of TPT.

Extravesicular ammonia released during loading at 37 °C was also separated with this method with some modification. Here, liposomal suspensions (0.45 mL) were centrifuged through the same ultrafiltration cartridges; however, only one cycle of centrifugation (with the same conditions used to isolate intravesicular TPT) was used. After centrifugation, 0.35 mL of the ultrafiltrate was recovered and used for ammonia analysis.

6.2.7 HPLC analyses

Both the lactone and carboxylate forms of TPT were monitored with HPLC using a previous method with slight modifications.[130] Briefly, a Waters Alliance 2695 separation system running mobile phase (11.5% acetonitrile: 88.5% (v/v) of 5% (pH = 5.5) triethylamine acetate, 50 mM tetrabutylammonium hydrogen sulfate (TBAHS) buffer) at a flow rate of 1 mL/min used a Waters Symmetry® C18 column (3.9×150 mm, 5 μm) and guard column (3.9 x 20 mm) to separate lactone and carboxylate TPT in samples. A Waters fluorescence detector (M474) (operating at excitation and emission wavelengths of 380 and 560 nm, respectively) was used to analyze the fractions of lactone and carboxylate TPT after separation. Standards containing TPT in its lactone and carboxylate forms were prepared

in chilled, acidified methanol (-20 °C) and 10 mM sodium carbonate buffer (pH 10.1), respectively. Standards ranged from 20-200 nM. Lactone and carboxylate retention times were 6.1 and 2.7 min, respectively.

Lipid content was also monitored by HPLC using an evaporative light scattering detector (ELSD). Using the same separations module as mentioned above, an Allsphere (Alltech Associates, Inc., Deerfield, IL) silica column (4 x 150 mm, 5 μm) and guard column (20 x 4.0 mm, 5 μm) with a mobile phase consisting of 80% of solvent A (80% chloroform:19.5% methanol:0.5%(v/v) NH_4OH) and 20% of solvent B (80% methanol:19.5% water:0.5% (v/v) NH_4OH) at a flow rate of 1 mL/min were used to quantify DSPC using an ELSD (Sedere, Inc., Lawrenceville, NJ) operated at 40 psig and 40 °C. Logarithms of peak areas of DSPC standards in mobile phase A (0.05 – 0.3 mg DSPC/mL) were linear with respect to the logarithm of concentration. Samples (100 – 250 μL) were dried at room temperature under N_2, then dissolved in chilled solvent A before analysis.

6.2.8 Ammonia analyses

Potentiometric measurements of ammonia released during loading at 37 °C employed an Orion ammonia ion selective electrode in conjunction with a Thermo Scientific Orion Star A214 pH, ISE, mV, temperature meter. Ammonia standards were prepared between 0.01-0.3 ppm in Milli-Q H_2O. Immediately before the ammonia analyses, NaOH reagent was added to 10 mL of ammonia standards or samples diluted in Milli-Q H_2O (10 – 15 mL total volume) at a ratio of 0.01:1 (v/v) to raise pH and convert any ammonium to ammonia. Solutions were allowed to equilibrate for 3-5 minutes under mild stirring and the final voltage was recorded. A Nernst relationship between ammonia concentration and electric potential (mV) was observed and used to make a standard curve for estimation of ammonia concentration in these samples. Blank solutions of MES buffer diluted with Milli-Q H_2O in

the same manner as ammonia samples were found to have no effect on the baseline voltage and therefore no corrections were necessary.

6.2.9 Loading and release models of liposomal TPT

Models describing the pH-dependent release kinetics of ionizable drugs from liposomes exist;[49, 60, 124, 127, 128, 130] however, only a few have been experimentally tested[49, 60, 124, 130] and even fewer have been tested under conditions in which a pH gradient was established via transport of another small, highly permeable acid/base entrapped within the intravesicular compartment.[60, 124] To our knowledge, this is the first mechanistic model used to examine active loading of a weakly basic drug. Furthermore, this model also explores the incorporation of drug self-association, ion-pairing, and precipitation to characterize the active loading process and subsequent release from these actively-loaded formulations. An illustration of these factors and others already shown to affect the release of liposomal TPT[130] can be found in Scheme 6.1.

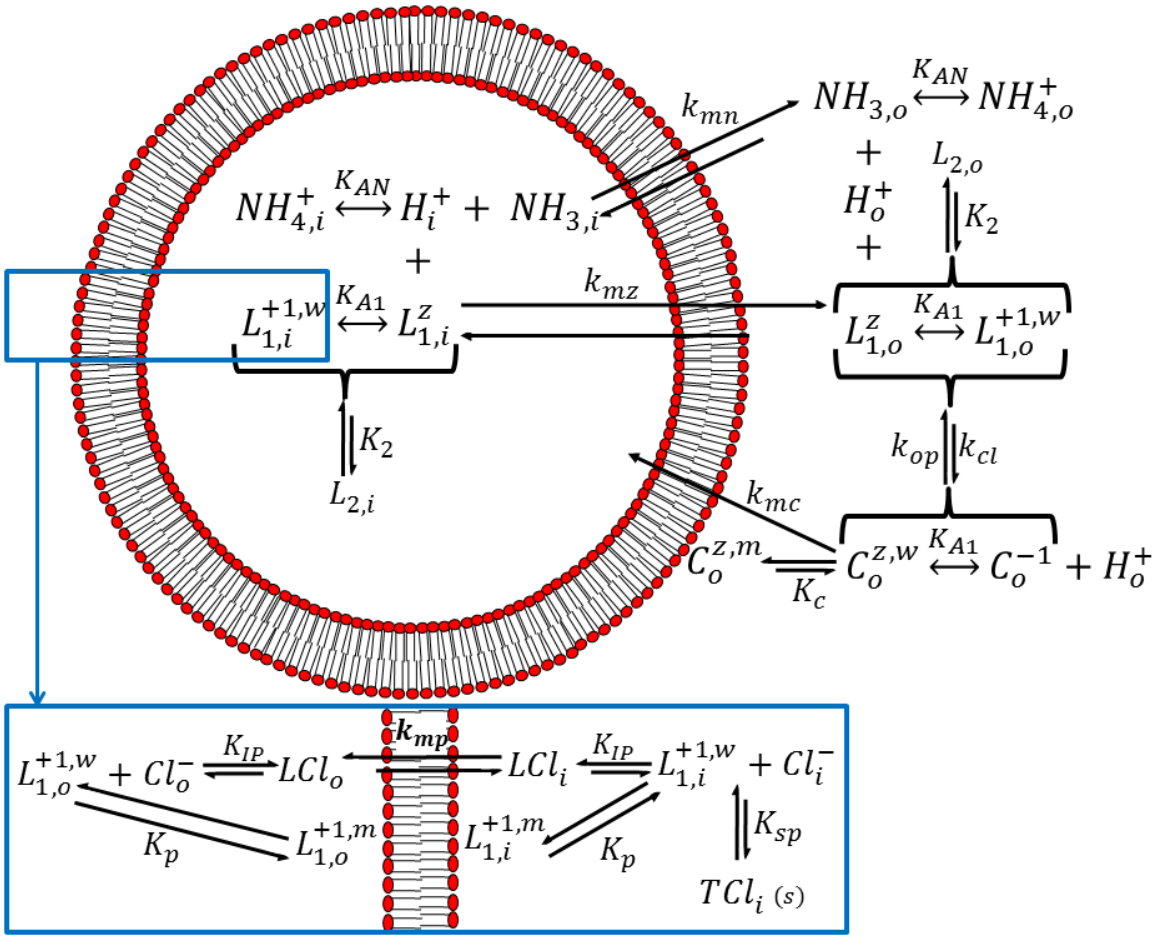

Scheme 6.1. A mechanistic illustration of the equilibria and kinetic processes that govern active loading of TPT in the presence of pH and chloride gradients. Intravesicular pH (i.e. negative logarithm of the proton concentration, H_i^+) is lowered as ammonia permeates the lipid bilayer. This is governed by ammonia's release rate constant, k_{mn}, and the concentration gradient between intra- and extravesicular ammonia ($NH_{3,i}$ and $NH_{3,o}$, respectively). Similar release rate constants governing the transport of the zwitterionic lactone ($L_{1,i}^z$and $L_{1,o}^z$) and carboxylate ($C_o^{z,w}$) forms of TPT as well as its ion-pair with chloride (LCl_i and LCl_o) are represented by k_{mz}, k_{mc}, and k_{mp}, respectively. Equilibria governing dimerization of TPT (K_2), partitioning of cationic lactone and zwitterionic carboxylate TPT to the bilayer/solution interface (K_p and K_c„ respectively), and the ionization state of TPT lactone and carboxylate (K_{A1}) are shown along with the rate constants governing ring-opening and closing of TPT

(k_{op} and k_{cl}, respectively). The inset at the bottom depicts the ion-pair transport of TPT-Cl across the bilayer which is dependent on the association constant of the ion-pair (K_{ip}) in addition to k_{mp}. A TPTHCl salt may also form in the intravesicular compartment (TCl_i) during or after the loading process as governed by the salt's solubility product, K_{sp}.

6.2.9.1 TPT rate equations governing loading kinetics

The rate equations governing transport of TPT may contain multiple terms to account for the permeable species in the intra- and extravesicular compartments (from this point on, the subscript "*i*" and "*o*" will refer to chemical species in the intra- and extra-vesicular compartments respectively.) This is expressed by Equations 1a and b.

$$\frac{dT_i}{dt} = \frac{dL_i^z}{dt} + \frac{dLCl_i}{dt} \tag{1a}$$

$$\frac{dT_o}{dt} = \frac{dL_o^z}{dt} + \frac{dLCl_o}{dt} + \frac{dC_o}{dt} \tag{1b}$$

Here, the rates of change of total intra- and extra-vesicular TPT (T_i and T_o, respectively) are a sum of the transport rates of the lactone forms (L_i and L_o, respectively), the TPT-Cl ion-pair (LCl_i andLCl_o, respectively), and extravesicular carboxylate (C_o). Intravesicular carboxylate may be ignored as the intravesicular pH is sufficiently low that essentially no carboxylate exists inside the liposome as shown in CH. 5.[92, 130]

The rates governing transport may be described by pseudo steady-state Fickian diffusion through a membrane[49, 50, 60, 124, 130] of each drug species (or complex) permeable to the bilayer. These terms are incorporated into the rate equations governing intravesicular transport of TPT below.

$$\frac{dT_i}{dt} = -k_{mz}\left(L_{1,i}^z - L_{1,o}^z\right) - k_{mp}(LCl_i - LCl_0) + k_{mc}C_o^{z,w} \tag{2}$$

The concentration gradient governing Fickian diffusion across the membrane is between the monomeric forms of the lactone zwitterion ($L_{1,i}^z$and $L_{1,o}^z$). Because

intravesicular carboxylate is negligible at low pH, only unbound extravesicular carboxylate zwitterion ($C_o^{z,w}$) contributes to transport. In previous studies, such transport was also assumed for L^{+1}. However, those studies were performed in dilute concentrations of TPT and high chloride concentrations in both the intra- and extra-vesicular compartments. Such conditions are not present during active loading. Because several gradients now exist in active loading (e.g., pH, TPT, chloride, and ammonia), a more complex process may become apparent.

This complexity regarding the transport of L^{+1} was hypothesized to proceed through ion-pairing of the cationic lactone form of TPT with chloride since it is the smallest and most abundant anion present in the extravesicular (i.e. loading) solution. Transport across the bilayer is governed by the release rate constant k_{mp}, and the concentration gradient of the TPT-Cl ion pair formed in the intra- and extra-vesicular compartments (LCl_i and LCl_o, respectively).

The rate equation governing the extravesicular compartment is similar to that for the intravesicular compartment and shown below.

$$\frac{dT_o}{dt} = f_v\left[k_{mz}\left(L_{1,i}^z - L_{1,o}^z\right) + k_{mp}\left(LCl_i - LCl_0\right) - k_{mc}C_{n,o}^u\right] \quad (3)$$

Here, the ratio of entrapped volume to extravesicular volume ($f_v = \frac{V_i}{V_o}$) is used to maintain mass balance between the intra-and extra-vesicular compartments. The calculation of f_v is possible with the aid of lipid surface area densities, particle size, and the concentration of lipid as previously defined elsewhere.[50, 126, 130, 135]

Accounting for chloride transport is also necessary due to ion-pairing. This is achieved with rate equations governing intra- and extra-vesicular chloride ($Cl_{T,i}$ and $Cl_{T,o}$, respectively) as shown below.

$$\frac{dCl_{T,i}}{dt} = -k_{mp}(LCl_i - LCl_0) \quad (4a)$$

$$\frac{dCl_{T,o}}{dt} = f_v k_{mp}(LCl_i - LCl_0) \quad (4b)$$

Initial conditions are required to solve this system of differential equations. These initial conditions are shown by the equations below for loading studies.

$$T_i(0) = Cl_{T,i}(0) = 0 \quad (5a \text{ \&b})$$

$$Cl_{T,o}(0) = 0.25M \quad (5c)$$

$$T_i^b(0) = LS \quad (5d)$$

Here, *LS* is the concentration of TPT in the loading suspension which was varied to examine self-association and its effect on loading efficiency.

Derivation of the concentrations of monomeric species of TPT in terms of T_i and T_o are required to model drug transport during the active loading process. These derivations will be described in the subsequent sections for the different loading models examined.

6.2.9.2 Generation of pH gradient

The release of neutral ammonia from the intravesicular compartment generates a low intravesicular pH (pH_i).[170] This is governed by the rate equations below.

$$\frac{dN_i}{dt} = -k_{mn}(NH_{3,i} - NH_{3,o}) \quad (6a)$$

$$\frac{dN_o}{dt} = f_v k_{mn}(NH_{3,i} - NH_{3,o}) \quad (6b)$$

The rates of change in the total concentration of ammonia in the intra- and extra-vesicular compartments (N_i and N_o respectively) are dependent on the concentration gradient between neutral ammonia in the intra- and extra-vesicular compartments ($NH_{3,i}$ and $NH_{3,o}$,, respectively), the rate constant for neutral ammonia transport (k_{mn}), and f_v. $NH_{3,i}$ and $NH_{3,o}$

may be written in terms of N_i and N_o by solving for the fractions of neutral ammonia in the intra- and extra-vesicular compartments (f_i^N and f_o^N):

$$f_i^N = \frac{K_{AN}}{H_i^+ + K_{AN}} \tag{7a}$$

$$f_o^N = \frac{K_{AN}}{H_o^+ + K_{AN}} \tag{7b}$$

These fractions are dependent on the acid dissociation constant for ammonia, K_{AN}, and the acidity or hydrogen ion concentrations in the intra-or extra-vesicular compartments (H_i^+ and H_o^+, respectively). Using these fractions, Equations 6a and b can be rewritten to yield:

$$\frac{dN_i}{dt} = -k_{m,n}(f_i^N N_i - f_o^N N_o) \tag{8a}$$

$$\frac{dN_o}{dt} = f_v k_{m,n}(f_i^N N_i - f_o^N N_o) \tag{8b}$$

The pH in the intravesicular compartment decreases as ammonia release causes deprotonation of ammonium to replenish the released ammonia. This process governs the acidity of the intravesicular compartment by satisfying the overall charge balance expressed by the following equation:

$$H_i^+ = \frac{K_w}{H_i^+} + Cl_i^- + B_i^- - NH_{4,i}^+ - L_i^{+n} \tag{9}$$

The dissociation of water, K_w, is included along with free chloride, Cl_i^-, and besylate, B_i^-, in the intravesicular compartment. The concentration of intravesicular ammonium, $NH_{4,i}^+$, may be rewritten in terms of N_i as shown below.

$$NH_{4,i}^+ = (1 - f_i^N)N_i \tag{10}$$

Solving for total cationic TPT, L_i^{+n}, will be discussed in the next section.

6.2.9.3 Loading Model #1: TPT dimerization and ion-pairing

TPT has been shown to self-associate in solution to form dimers[137, 138] The equilibrium expression for TPT dimerization may be expressed with the constant K_2 and the expression below relating the unbound lactone monomer, L_1^w, and dimer, L_2, species.

$$K_2 = \frac{L_2}{(L_1^w)^2} \tag{11}$$

Only the lactone form of TPT is considered to self-associate as previous studies have suggested the carboxylate conformation does not lend itself to stacking.[137]

With this information, the total concentration of TPT in both the intra-and extra-vesicular compartments (T_i and T_o, respectively) may be rewritten in terms of the various species present in solution. These overall mass balances are written in terms of concentration using corrections for the differences in volumes of the various compartments.

$$T_i = a\left(L_{1,i}^w + 2L_{2,i}\right) \tag{12a}$$

$$T_o = c\left(L_{1,o}^w + 2L_{2,o} + C_o^u\right) + dC_o^m \tag{12b}$$

These corrections relate aqueous to total volumes of the intra- and extravesicular compartments (a and c, respectively) and the membrane volume of the outer bilayer leaflet to total extra-vesicular volume (d) as defined in previous studies of liposomal transport of TPT.[126, 130]

Previous studies also indicated the lactone zwitterion of TPT does not bind to the bilayer while its cationic form does;[126, 130] however, the high intravesicular TPT concentrations achieved during active loading (>1 mM) and the small surface area-to-volume ratio of the membrane in the external compartment make binding of the cationic species negligible in both compartments. This is supported by previous studies which show only the monomeric species binds, and the cationic species follows the Gouy Chapman

theory of diminished binding as the charge on the membrane increases.[126, 141] These assumptions make intravesicular TPT only a function of the monomer and dimer forms of lactone TPT.

Using Equation 11, Equation 12a can be rewritten solely in terms of $L_{1,i}^{w}$ and T_i,[136, 186] resulting in the equations below.

$$T_i = a\left(L_{1,i}^{w} + 2{L_{1,i}^{w}}^{2}\right) \tag{13a}$$

$$L_{1,i}^{w} = \frac{-1+\sqrt{1+8K_2T_i/a}}{4K_2} \tag{13b}$$

At the extravesicular pH at which loading studies were conducted, extravesicular carboxylate TPT in solution, C_o^u, and bound to the membrane, C_o^m, must be considered. This makes solving for $L_{1,o}^{w}$ more complex. Eqn. 12b can be rewritten in terms of $L_{1,o}^{w}$ and takes on the general form of a quadratic equation which is illustrated below:

$$L_{1,o}^{w} = \frac{-\beta+\sqrt{\beta^2-4\alpha\gamma}}{2\alpha} \tag{14}$$

where $\beta = c(H_o^+ + K'_{A2}) + dK'_C K'_{A2}$, $\alpha = 2cH_o^+ K_2$, and $\gamma = H_o^+ T_o$. In these terms, the carboxylate species may be rewritten in terms of $L_{1,o}^{w}$ using the apparent acid dissociation constant for the equilibrium between the lactone and carboxylate forms, K'_{A2} and the apparent binding coefficient for carboxylate, K'_C, in addition to other constants already defined. The value of K'_C is pH dependent and may be determined using the intrinsic binding constant of the zwitterionic carboxylate, K_c, and the dissociation constant of TPT's phenol, K_{A1}. These conditions are incorporated into the following equation based on the equilibria scheme described for TPT in Chapter 4.[130]

$$K'_C = \frac{H_o^+ K'_{A2} K_c}{{H_o^+}^2 + H_o^+ K_{A1} + K_{A1} K'_{A2}} \tag{15}$$

While total monomer may now be expressed in terms of total drug in both compartments, the determination of each permeable species is still required. This may be accomplished using the mass balances below for the aqueous monomeric species in both intra- and extra-vesicular compartments.

$$L_{1,i}^{w} = L_{1,i}^{z} + L_{1,i}^{+1,w} + LCl_i \tag{16a}$$

$$L_{1,o}^{w} = L_{1,o}^{z} + L_{1,o}^{+1,w} + LCl_o \tag{16b}$$

Since LCl_i and LCl_o also contain chloride, a mass balance for chloride must be considered for each compartment.

$$Cl_{T,i} = Cl_i^- + LCl_i \tag{17a}$$

$$Cl_{T,o} = Cl_o^- + LCl_o \tag{17b}$$

It is easiest to first solve for $L_{1,i}^{+1,w}$ by combining equations 16a_and 17a in addition to the expressions governing the equilibrium constants K_{IP} and K_{A1}. The resulting equation is shown below.

$$L_{1,i}^{w} = \frac{K_{A1}}{H_i^+} L_{1,i}^{+1,w} + L_{1,i}^{+1,w} + \frac{K_{IP} Cl_{T,i} L_{1,i}^{+1,w}}{1 + K_{IP} L_{1,i}^{+1,w}} \tag{18}$$

This equation is quadratic in nature and takes on the general form below when solved for $L_{1,i}^{+1,w}$:

$$L_{1,i}^{+1,w} = \frac{-B_i + \sqrt{B_i^2 - 4A_i C_i}}{2A_i} \tag{19}$$

where $B_i = K_{A1} + H_i^+(1 + K_{IP} Cl_{T,i} - K_{IP} L_{1,i}^{w})$, $A_i = K_{IP}(H_i^+ + K_{A1})$, and $C_i = -H_i^+ L_{1,i}^{w}$. A similar expression for $L_{1,o}^{+1,w}$ may be written where $B_o = K_{A1} + H_o^+(1 + K_{IP} Cl_{T,o} - K_{IP} L_{1,o}^{w})$, $A_o = K_{IP}(H_o^+ + K_{A1})$, and $C_o = -H_o^+ L_{1,o}^{w}$.

With $L_{1,i}^{+1,w}$ and $L_{1,o}^{+1,w}$ solved, solutions for $L_{1,i}^{z}$, $L_{1,o}^{z}$, LCl_i, and LCl_o are straightforward and shown below.

$$L_{1,i}^{z} = \frac{K_{A1}}{H_i^+} L_{1,i}^{+1,w} \tag{20a}$$

$$LCl_i = \frac{K_{IP} Cl_{T,i} L_{1,i}^{+1,w}}{1 + K_{IP} L_{1,i}^{+1,w}} \tag{20b}$$

Similar equations for $L_{1,i}^{+1,w}$ and $L_{1,i}^{z}$ use H_i^+ and $L_{1,i}^{w}$ instead of H_o^+ and $L_{1,o}^{w}$.

$$L_{1,o}^{z} = \frac{K_{A1}}{H_o^+} L_{1,o}^{w} \tag{21a}$$

$$LCl_o = \frac{K_{IP} Cl_{T,o} L_{1,o}^{+1,w}}{1 + K_{IP} L_{1,o}^{+1,w}} \tag{21b}$$

And the solution for $C_o^{z,w}$ is simply the following expression.

$$C_o^{z,w} = \frac{K'_{A2}}{H_o^+ + K_{A1}} L_{1,o}^{w} \tag{21c}$$

Equations 20a-b and 21a-c can be substituted back into Equations 13 and 14, respectively, so the transport equations governing loading and release of TPT may be written in terms of T_i and T_o, respectively, and of $Cl_{T,i}$ and $Cl_{T,o}$, respectively. These equations are also used for the transport equations governing chloride.

The following equation was used to express the total concentration of intravesicular cationic TPT, L_i^{+n}, for the calculation of intravesicular pH during the loading process

$$L_i^{+n} = \frac{H_i^+ (T_i - LCl_i)}{a(H_i^+ + K_{A1})} \tag{22}$$

while Cl_i^- was simply calculated with the rearrangement of Eqn. 17a (shown below).

$$Cl_i^- = Cl_{T,i} - LCl_i \tag{23}$$

6.2.9.4 Loading Model #2: Ion-pairing without dimerization

Without dimerization, $aL_{1,i}^{w} = T_i$and the subsequent equations solving for the different intravesicular species of TPT (Eqns. 18-19b) may be used for this model. The equations governing the extravesicular compartment require more explanation as T_o is now expressed by the following equation.

$$T_o = c(L_o^w + C_o^u) + dC_o^m \tag{24}$$

Now L_o^w may be expressed using K'_{A2} and K'_C yielding the following equation for L_o^w in terms of T_o.

$$L_o^w = \frac{H_o^+ T_o}{aH_o^+ + aK'_{A2} + bK'_{A2}K'_C} \tag{25}$$

From this point, Eqns. 19 (substituting L_o^w and H_o^+ for L_i^w and H_i^+, respectively) and 20a-c can be used to determine the concentrations of $L_{1,o}^{+1,w}$, $L_{1,o}^{z}$, $L_{1,o}^{z}$, and $C_o^{z,w}$, respectively. Lastly, the calculation of intravesicular pH can be made assuming $L_{1,i}^{+1,w} = L_i^{+n}$.

6.2.9.5 Loading Model #3: Dimerization with no ion-pairing

The rate equations governing TPT transport are the same if one substitutes $L_{1,i}^{+1,w}$ and $L_{1,o}^{+1,w}$ for LCl_i and LCl_o, respectively, and neglects the transport equations for Cl. Solving for the monomeric species is the same as Equations 13 and 14 so solving for $L_{1,i}^{+1,w}$, and $L_{1,i}^{z,w}$ becomes straightforward, resulting in the equations below.

$$L_{1,i}^{+1,w} = \frac{H_i^+}{H_i^+ + K_{A1}} L_{1,i}^{w} \tag{26a}$$

$$L_{1,i}^{z,w} = \frac{K_{A1}}{H_i^+ + K_{A1}} L_{1,i}^{w} \tag{26b}$$

The equations for $L_{1,o}^{+1,w}$, and $L_{1,o}^{z,w}$ are the same as 24 a & b aside from using H_o^+ instead of H_i^+.

6.2.9.6 Equations describing PLLT release

The equations describing TPT transport and model #1 were used to simulate the release of PLLT. This is achieved by setting $H_i^+ = H_o^+ = 10^{-4.1}$ and setting the initial conditions to reflect the concentrations of TPT and chloride present in the solution used to hydrate these passively-loaded liposomes. For all PLLT studies, the initial conditions for TPT were the same and shown below.

$$T_i(0) = 50\ \mu M \tag{27a}$$

$$T_o(0) = 0 \tag{27b}$$

The initial conditions for chloride, however, were varied. In two release studies, $Cl_i^-(0) = T_i(0)$ since its HCl salt was used to make the solutions. In one of these studies, the extravesicular solution contained no chloride ($Cl_i^-(0) = 0$) while the other suspension did have chloride ($Cl_i^-(0) = 0.25M$) present. The other PLLT suspension contained Cl on both sides. Its initial conditions were $Cl_o^-(0) = Cl_i^-(0) = 0.25M$. The rate equations governing ammonia transport were unnecessary since it was not present in any of the buffers used in PLLT studies.

6.2.9.7 Equations describing release of liposomal TPT loaded at 37 °C

Equilibrium between the lactone and carboxylate forms of TPT was assumed in loading studies as ring-opening/closing kinetics for TPT and other camptothecins have been shown to be acid-catalyzed at the pH of the loading solution.[92] Because the intravesicular compartment retains its low pH, carboxylate is still negligible and Equations 2a and b may be used to describe intravesicular transport of TPT. However, this interconversion has previously been shown to have an effect on liposomal TPT release at physiological pH (7.4).[130] This effect requires the differential equation governing extravesicular TPT (Eqn. 3) to be modified as shown below.

$$\frac{dL_o}{dt} = f_v\left[k_{mz}\left(L_{1,i}^z - L_{1,o}^z\right) + k_{mp}(LCl_i - LCl_0) - k_{mc}C_{n,o}^u\right] - k_{op}OH_o^- L_o + k_{cl}OH_o^- f_{COOH}C_o \quad (28)$$

This equation now reflects the interconversion kinetics previously reported with rate constants governing base-catalyzed ring-opening and closing kinetics (k_{op} and k_{cl}, respectively).[92, 130] Since the carboxylic acid form of TPT is the only ring-opened species involved in ring-closing,[92] the term f_{COOH} is introduced to account for this fraction of ring-opened TPT.[130]

$$f_{COOH} = \frac{H_o^+}{H_o^+ + K_{COOH}} \quad (29)$$

The ionization of the carboxylic acid to form carboxylate TPT is pH-sensitive and governed by K_{COOH}.

One should notice that Equation 28 only governs the rate of change of L_o due to non-instantaneous interconversion. A differential equation governing C_o is required.

$$\frac{dC_o}{dt} = -f_v k_{mc} C_o^{z,w} + k_{op}OH_o^- L_o - k_{cl}OH_o^- f_{COOH}C_o \quad (30)$$

The permeable, zwitterionic form of carboxylate TPT unbound to the membrane, $C_o^{z,w}$, may be defined in terms of C_o. This is shown in the equation below.

$$C_o^{z,w} = \frac{H_o^+ C_o}{(H_o^+ + K_{A1})(c + dK_C)} \quad (31)$$

In loading studies, the permeability of chloride alone was not considered since its influx into the liposome through this pathway would be much slower than through the ion pair. During release studies however, the influx of chloride from the extravesicular solution[187-189] would alter the amount of drug released as it would continue to provide more chloride for transport of LCl_i. Accounting for this effect requires a release rate constant for chloride, k_{mCl}, and modification of the transport equations governing chloride. These equations are shown below.

$$\frac{dCl_{T,i}}{dt} = -k_{mp}(LCl_i - LCl_0) - k_{mCl}(Cl_i^- - Cl_0^-) \quad (32a)$$

$$\frac{dCl_{T,o}}{dt} = f_v[k_{mp}(LCl_i - LCl_0) + k_{mCl}(Cl_i^- - Cl_0^-)] \quad (32b)$$

The concentration gradient is between the anionic forms of intra- and extra-vesicular chloride (Cl_i^- and Cl_0^-, respectively). These concentrations may be expressed in terms of $Cl_{T,i}$ and $Cl_{T,o}$ using the ion-pairing constant and the equations below.

$$Cl_i^- = \frac{Cl_{T,i}}{1+K_{IP}L_{1,i}^{+1,w}} \quad (33a)$$

$$Cl_o^- = \frac{Cl_{T,o}}{1+K_{IP}L_{1,o}^{+1,w}} \quad (33b)$$

While the equations above imply that chloride permeability soley involves the chloride anion, the identity of this permeable species is a point of contention. Cl^- permeability has been argued to behave as an ion-pair, typically suggested to be the HCl pair since protons are much smaller than any other cations in solution. This assumption would indicate Cl^- flux to be pH-dependent as a pKa exists for the HCl pair and its dissociated ions, and a pH-dependence in Cl^- permeability has been observed.[187, 190] However, a pH-independent pathway has also been observed.[187, 190] This pH-independent pathway suggests Cl^- to be the permeable species and is supported by molecular dynamics simulations (arguing several different transport mechanisms) which illustrate anion transport.[153, 188, 191, 192] Because a mechanistic evaluation of Cl^- was beyond the scope of this study, Cl- co-transport was assumed. Under this assumption, Cl^- transport was pH-independent and proton conduction across the bilayer was assumed to be fast enough to maintain electroneutrality and prevent the generation of an electrical potential across the membrane. While proton transport equations are not used, they are implicitly expressed mathematically by assuming charge is conserved within the intravesicular compartment. This was previously expressed mathematically by Equation 9 and in the subsequent calculation of intravesicular pH.

Finally, the concentrations obtained from this release model must be transformed to illustrate the fraction of lactone and carboxylate TPT (*L(t)* and *C(t)*, respectively) in solution at each time point. This is shown by the following equations.

$$L(t) = \frac{f_v L_i + L_o}{f_v L_i + L_o + C_o} \quad (34a)$$

$$C(t) = \frac{C_o}{f_v L_i + L_o + C_o} \quad (34b)$$

The initial conditions for the various differential equations for the transport of each permeable molecule are shown in Table 6.4 while those of the extravesicular compartment were determined based on the concentrations calculated at the end of loading studies.

6.2.9.8 Equations describing release of liposomal TPT loaded at 60 °C

At 60 °C, DSPC bilayers are in a more permeable liquid crystalline state as opposed to their rigid gel phase below 54 °C.[135, 193] Under these conditions, the permeabilities of both the zwitterion and ion-paired form of TPT may be much faster and increased to different extents, resulting in altered Cl: TPT ratios. Further alteration of this ratio may be due to the the relative change in chloride permeability as well. These effects may ultimately lead to much higher Cl: TPT ratios and possibly supersaturate the intravesicular compartment at this higher temperature, resulting in precipitate formation upon cooling.

The formation of precipitate in the intravesicular aqueous compartment is governed by an apparent solubility product, K'_{sp}, as illustrated by the following equation:

$$K'_{sp} = T_{i(aq)} Cl_{i(aq)} \quad (35)$$

where $T_{i(aq)}$ and $Cl_{i(aq)}$ are the concentrations of TPT and chloride still solubilized in solution. Only these soluble species may be considered in the equation used to calculate pH. Furthermore, these species along with the precipitate, $TCl_{i(s)}$, must be incorporated into the

rate equations governing drug and chloride transport. Equations 1a and 4a may be modified to reflect these stipulations as shown below.

$$\frac{dT_i}{dt} = \frac{dL_{1,i}^{z}}{dt} + \frac{dLCl_i}{dt} + \frac{dTCl_{i(s)}}{dt} = \frac{dT_{i(aq)}}{dt} + \frac{dTCl_{i(s)}}{dt} \tag{36a}$$

$$\frac{dCl_{T,i}}{dt} = \frac{dLCl_i}{dt} + \frac{dCl_i^-}{dt} + \frac{dTCl_{i(s)}}{dt} = \frac{dCl_{i(aq)}}{dt} + \frac{dTCl_{i(s)}}{dt} \tag{36b}$$

Since both TPT and chloride leave in a 1:1 ratio via transport of their ion pair, the rate of precipitate dissolution is simply equal to that of the rate of ion-pair transport as shown by the following equation.

If: $K'_{sp} \geq T_{i(aq)}Cl_{i(aq)}$ $\qquad \frac{dTCl_{i(s)}}{dt} = \frac{dLCl_i}{dt} = k_{mp}(LCl_i - LCl_0)$ (37a)

When $K'_{sp} < T_{i(aq)}Cl_{i(aq)}$, changes in the amount of $TCl_{i(s)}$ will be governed by the flux of free chloride as illustrated by the expression below.

If: $K'_{sp} < T_{i(aq)}Cl_{i(aq)}$ $\qquad \frac{dTCl_{i(s)}}{dt} = -k_{mCl}(Cl_i^- - Cl_0^-)$ (37b)

With these rate equations, the rate equations already derived for the extravesicular compartment during ALLT release, and the expressions already derived for the various aqueous TPT and chloride species, these differential equations may be modeled once the initial conditions (i.e. how much drug and chloride are in the aqueous and solid phases) are determined for the intravesicular compartment. For this calculation, the mass balances for TPT and total chloride in the intravesicular compartment, M_{TPT} and M_{Cl} respectively, are necessary and shown below.

$$M_{TPT} = M_{TPT(aq)} + M_{TCl(s)} \tag{38a}$$

$$M_{Cl} = M_{Cl(aq)} + M_{TCl(s)} \tag{38b}$$

Assuming the intravesicular volume remains constant, the masses for the aqueous species of TPT and Cl may be rewritten in terms of the concentrations used in the rate equations (Eqns. 36a and b) as illustrated by the following equations.

$$T_i = T_{i(aq)} + TCl_{i(s)} \tag{39a}$$

$$Cl_{T,i} = Cl_{i(aq)} + TCl_{i(s)} \tag{39b}$$

This system of equations may be used along with the equation for K'_{sp} to solve for $TCl_{i(s)}$ in terms of the initial amount of total intravesicular TPT and Cl, $T_i(0)$ and $Cl_{T,i}(0)$ respectively. The resulting solution is expressed below as the initial condition for $TCl_{i(s)}$

$$TCl_{i(s)}(0) = \frac{T_i(0) + Cl_{T,i}(0) - \sqrt{[T_i(0) + Cl_{T,i}(0)]^2 - 4(T_i(0)Cl_{T,i}(0) - K'_{sp})}}{2} \tag{40a}$$

while the initial conditions for $T_{i(aq)}$ and $Cl_{i(aq)}$ simply become the following expressions.

$$T_{i(aq)}(0) = T_i(0) - TCl_{i(s)}(0) \tag{40b}$$

$$Cl_{i(aq)}(0) = Cl_{T,i}(0) - TCl_{i(s)}(0) \tag{40c}$$

HPLC analysis of carboxylate and lactone forms of TPT can again be used to monitor release by modifying the Eqns. 34a and b to the form below.

$$L(t) = \frac{f_v[T_{i(aq)} + TCl_{i(s)}] + L_o}{f_v[T_{i(aq)} + TCl_{i(s)}] + L_o + C_o} \tag{41a}$$

$$C(t) = \frac{C_o}{f_v[T_{i(aq)} + TCl_{i(s)}] + L_o + C_o} \tag{41b}$$

This model was used to determine both K'_{sp} and $Cl_{T,i}(0)$ from the release profiles obtained after active loading of TPT into liposomes at 60 °C.

All data fitting to the models described above was performed with MicroMath® Scientist® non-linear regression software in conjunction with the values supplied in Tables 6.1 and 6.2 for the various parameters used in these models.

Table 6.1. Parameters used to model release and loading kinetics of liposomal TPT that are independent of the experiment

Parameters	Values
k_{mn}	$2.88 \times 10^4\ s^{-1}$ [a]
k_{mz}	$43\ hr^{-1}$ [b]
k_{mc}	$5.6\ hr^{-1}$ [b]
K_c	42 [b]
K'_{A1}	2.8×10^{-7} [b]
K_{AN}	9.40×10^{-10} [c]
K_w	2.12×10^{-14} [c]
B_i	$0.3\ M$
a	0.15 [d]
b	0.85 [d]

[a] Calculated from a previously reported ammonia permeability coefficient of $P^m_{NH_3} = 48 \times 10^{-3}\ cm/s$ [171]

[b] Obtained from a previous study[125]

[c] Values adjusted to reflect conditions at 37 °C and 0.3 I

[d] Calculated based on particle size, lipid content, and lipid surface density calculations previously reported[50, 135]

Table 6.2. Parameters used to model release and loading kinetics of liposomal TPT that are experiment-specific*

Param-eters	Values		
	Active Loading #1 (19.2 µg lipid/mL)	PLLT (19.2 µg lipid/mL)	ALLT release (6.4 µg lipid/mL)
K'_{A2}	2.66×10^{-7} [b]	2.66×10^{-7} [b]	N/A
k_{cl}	N/A	N/A	7.4×10^8 $mol^{-1}hr^{-1}$ [b]
k_{op}	N/A	N/A	1.4×10^6 $mol^{-1}hr^{-1}$ [b]
f_v	2.40×10^{-3} [d]	2.40×10^{-3} [d]	1.66×10^{-5} [d]
c	0.9997 [d]	0.9997 [d]	0.9999 [d]
d	3.44×10^{-4} [d]	3.44×10^{-4} [d]	2.58×10^{-6} [d]
H_o^+	$3.16 \times 10^{-6} M$	$7.94 \times 10^{-5} M$	$3.98 \times 10^{-8} M$

* Superscripts same as those used in Table 6.1.

6.3 Results

6.3.1 Active loading of TPT at 37 °C

Multiple loading models were explored and the estimated values for the fitted parameters are shown for each model in Table 6.3. The values for the parameters are quite revealing. The model selection criterion (MSC) generated by the non-linear regression software provides an indication of the goodness-of-fit for each model to the data obtained from fitting the profiles of TPT during active loading at 37 °C. The MSC for model #3 is drastically lower than the other models as it does not account for ion-pairing effects. This result suggests the importance of ion-pairing transport during active loading of TPT. The differences between the MSC for model #1 and #2 are less drastic; however, closer examination of the fitted parameters in Table 6.3 provides further evidence of the validity of model #1. The confidence limits for these parameters are far better for model #1, which is in agreement upon comparison of the fitted models to the loading data illustrated by Figures 6.1a and b. Furthermore, the value of k_{mp} is nearly identical to the value of k_{mz}. This is reasonable considering the ion-pair is likely not much larger than the TPT zwitterion (i.e. similar diffusivity through the bilayer). This value is much more reasonable than the k_{mp} obtained from model # 2 which is 70 fold higher than that of the zwitterion rate constant. Figure 6.1c shows the predicted profile of ammonia release from model #1 has a similar trend as that experimentally observed for each of the loading conditions studied. While the trends are similar, it does appear that ammonia release is over- and under-predicted at the loading conditions using 180 and 60 μM of TPT in the extravesicular solution, respectively. This is likely due to a couple of factors. The first is using an average ratio of entrapped volume to extravesicular volume (f_v) to calculate uptake rather than an individual f_v for each suspension. The average f_v was 4.6 % lower and 2.6 % higher than the actual values determined from uptake in the 180 and 60 μM TPT loading solutions, respectively. The

respective over and under-estimations of f_v would consequently lead to under- and over-estimations in the amount of ammonia released similar to that shown in Figure 6.1c. With this consideration and the high sensitivity of the ammonia probe's response to different buffers and ions in solution (attempts were made to keep the solution composition of ammonia standards as similar as possible to the samples), the differences in observed and predicted ammonia release appear to correlate well. Using the ammonia release in conjunction with the chloride and TPT loaded into the intravesicular compartment, the profile of intravesicular pH was also calculated and is illustrated by Figure 6.1d. This drop in intravesicular pH agrees with that expected during the active loading process.

Table 6.3. Values of release parameters and goodness-of-fit for the various loading models developed[a]

Loading Model	K_2 (M^{-1}) [b]	K_{IP}	k_{mp} (hr^{-1})	Model Selection Criterion (MSC)
Model #1	6700	0.9 ± 0.7	49 ± 7	5.2
Model #2	NA	0.1 ± 2	3400 ± 2000	2.9
Model #3	6700	NA	0.65[c]	0.8

[a] ± 95% confidence intervals

[b] Previously determined in another study.[126]

[c] Based on a previously reported value of 0.51 hr^{-1} which assumed k_{mp} referred to transport of the cation without a counterion. This value was altered to reflect the fraction of monomer being 0.78 in that study.[130]

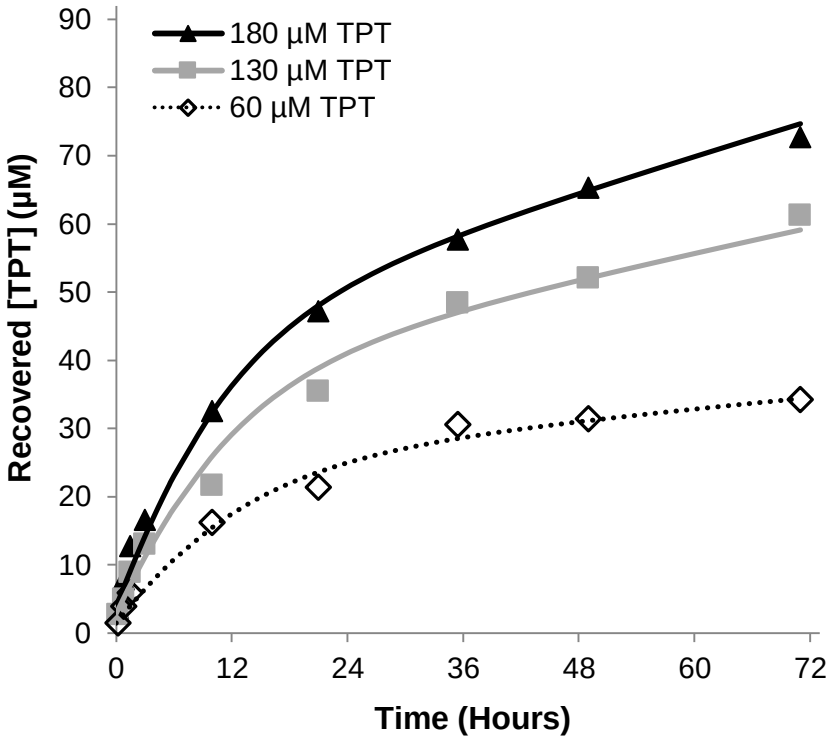
180 µM TPT
130 µM TPT
60 µM TPT
Recovered [TPT] (µM)
Time (Hours)
0
10
20
30
40
50
60
70
80
90
0
12
24
36
48
60
72

A.

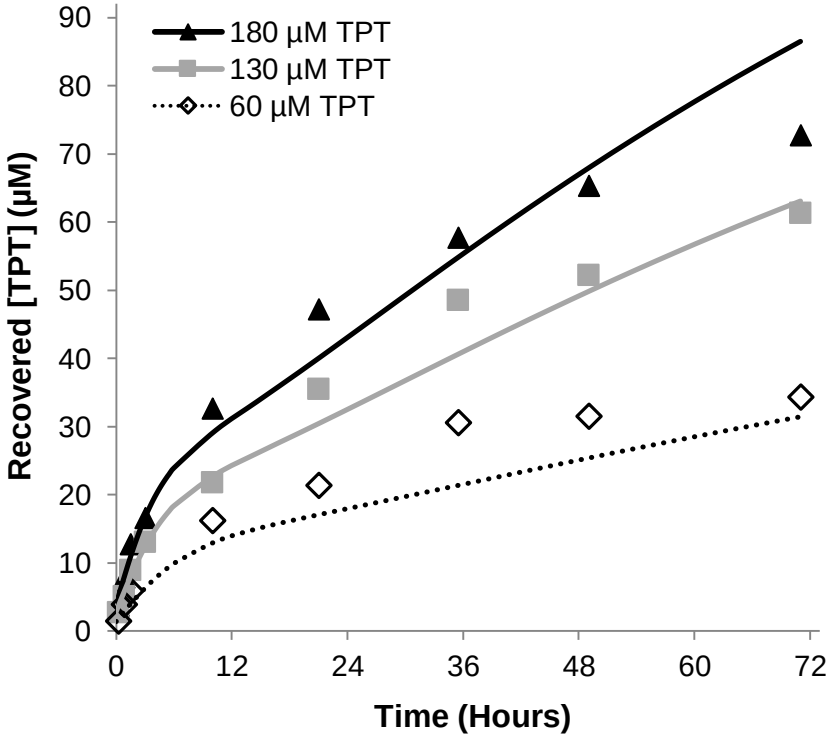
180 µM TPT
130 µM TPT
60 µM TPT
Recovered [TPT] (µM)
Time (Hours)
0
10
20
30
40
50
60
70
80
90
0
12
24
36
48
60
72

B.

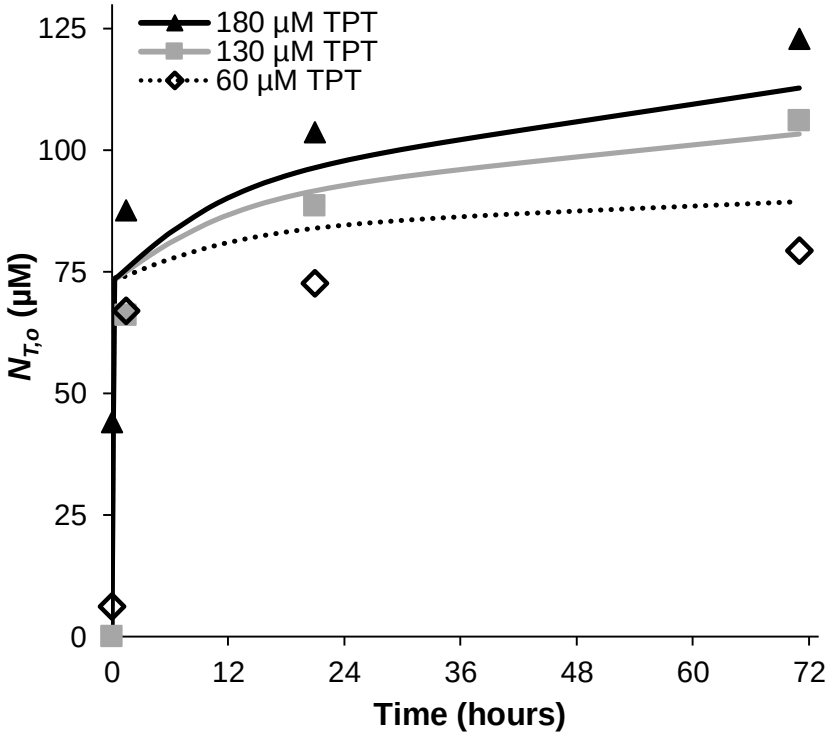
180 µM TPT
130 µM TPT
60 µM TPT
125
100
75
50
25
0
$N_{T,o}$ (µM)
0
12
24
36
48
60
72
Time (hours)

C.

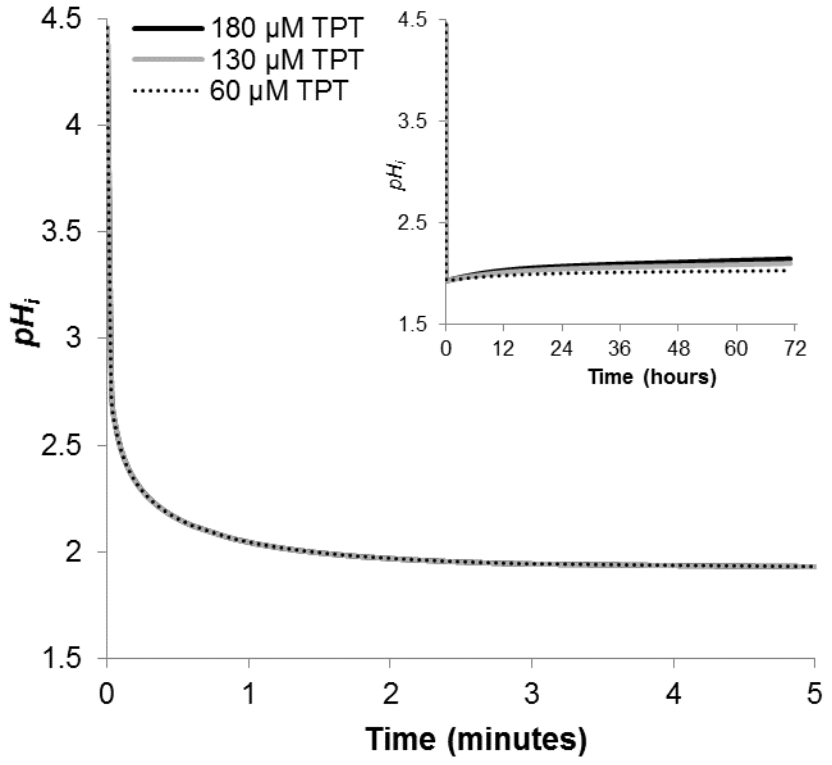
180 µM TPT
130 µM TPT
60 µM TPT
4.5
4
3.5
3
2.5
2
1.5
pH_i
0
1
2
3
4
5
Time (minutes)
4.5
3.5
2.5
1.5
pH_i
0
12
24
36
48
60
72
Time (hours)

D.

Figure 6.1. Loading profiles at 37 °C with TPT loading concentrations of 60, 130, and 180 μM in the extravesicular compartment with lines indicating simulated profiles obtained from the fit of loading models #1 (A) and #2 (B). A comparison of the fit of these two models to the studied loading conditions shows TPT dimerization and ion-pairing affects loading kinetics. Profiles of ammonia released during the loading process were also observed experimentally and shown along with the profiles of ammonia release predicted by model #1 (C). Using the amount of ammonia released and TPT and Cl loaded based on loading model #1, the intravesicular pH during the time course of the loading experiments could be calculated (D) and shows the initial drop in pH_i is rapid and slowly increases during uptake as illustrated in the legend.

It should also be noted that during the course of fitting models considering ion-pairing, the dissociation constant of TPT's phenol, $K_{A!}$, was allowed to change during regression in accordance with K_{IP}. This consideration was made due to the high levels of chloride present in previous studies would result in the measurement of an effective dissociation constant, K'_{A1}, for TPT if ion-pairing was present in those solutions.[130] The effect of ion-pairing on K'_{A1} is illustrated with the equation below.

$$K'_{A1} = \frac{H^+ L_1^z}{L_1^+ + LCl} \tag{42}$$

The value for $K_{A!}$ can be used to calculate $K_{A!}$ to be used during regression of the loading studies. This is done using the following equation.

$$K_{A1} = \frac{K'_{A1}}{1 + K_{IP} Cl_T} \tag{43}$$

The equation above assumes TPT dimerization is negligible and that very little chloride is consumed to form the ion-pair ($Cl_T \cong Cl^-$) as solutions used to spectrometrically determined K'_{A1} contained 500 nM TPT and 225 mM chloride.[130] With this correction and K_{IP} determined with loading model #1, K_{A1} was determined to be 3.3 x 10^{-7}.

6.3.2 PLLT release studies

PLLT release studies were conducted at 37 °C in pH 4.1 buffer containing 50 uM TPTHCl. The concentration of intra- and extra-vesicular Cl was altered and the resulting release profiles of TPT are shown below in Figure 6.2. The release studies in which no excess Cl was added to the intravesicular buffer agreed well with the profile predicted by the parameters obtained from loading studies. The release profile of TPT in the presence of excess Cl (0.25 M) in the intravesicular compartment is over 4 times faster than that of these other release profiles. This supports the hypothesis of bilayer transport via the TPT-Cl ion pair.

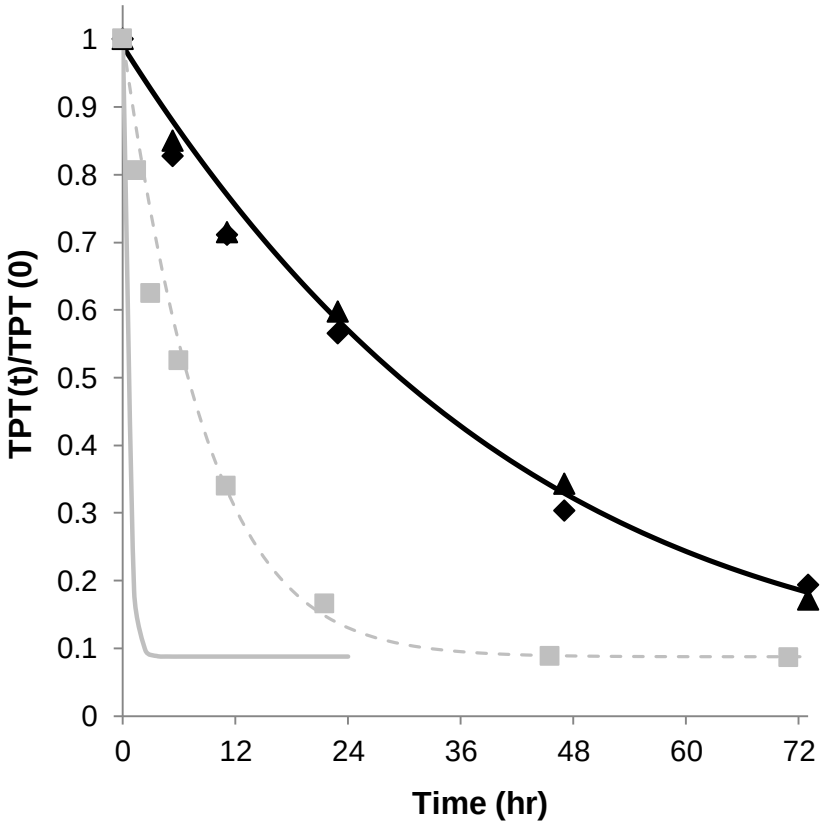

Figure 6.2. Comparison of release profile of PLLT in the presence or absence of chloride at 37 °C. Release when chloride was not added to intravesicular buffer and either none (◆) or 0.25 M Cl was added to the extravesicular buffer (▲) are

shown. The profiles predicted based on the fitted values obtained from loading studies were the same and are both represented by (—). Release when Cl_T was 0.25 M in both intra- and extra-vesicular compartments was also observed (■) and compared with the profiles predicted by the loading model under these chloride conditions (—) and when $Cl_{i,T}$ was fitted to be 1.1 mM (.....).

While TPT release is faster in the presence of 0.25 M Cl, one may also notice that the release profile predicted by the values obtained from loading experiments would suggest much faster release in the presence of that much Cl. Part of this discrepancy may be due to the method employed to monitor release as the fastest release half-life monitored before with this method was ~0.5 hrs.[130] The ionic strengths of the two intravesicular solutions used in these release studies, while different (0.3 vs. 0.55), are sufficiently high that differences in chloride activity would be minimal and therefore an unlikely factor in the discrepancy between predicted and observed release kinetics. Previous reports of chloride binding to other gel phosphatidylcholine bilayers would reduce the driving force for ion-pair formation and release.[194] Ion-pairing of chloride with sodium in the aqueous phase or at the interface of the bilayer solution could also hinder ion-pair transport of TPT.

A more likely explanation for the slower release at these high Cl concentrations may be related to the differences in PEG density between the intra- and extra-vesicular compartments. The higher PEG density within the aqueous core may create an aqueous two-phase system. Such systems are routinely used for milder separations of more hydrophobic solutes by their partitioning into the PEG phase.[195] Partitioning of TPT into this PEG phase would reduce ion-pair transport in two ways: 1) the amount of TPT available to ion-pair with Cl in the aq. salt phase near the bilayer would be reduced and subsequently lower the effective driving force for ion-pair transport,[196] and 2) the rate of TPT transfer from the PEG-phase to the aq. salt phase may become partially rate-limiting to bilayer transport due to the increased viscosity (i.e. reduced TPT diffusivity) of the PEG-phase.[195]

This effect would only be present within the intravesicular compartment since the PEG density near the bilayer would be much higher due to curvature effects inherent to the spherical shape of liposomes. Furthermore, NaCl was never present in the intravesicular compartments of liposomal formulations used in active loading studies. Since drug partitioning and liquid viscosity are highly dependent upon the concentration and type of salt(s) present in the PEG-salt system,[195, 196] it is plausible that the ammonium salts and the lower, model-calculated intravesicular Cl concentrations of the actively-loaded systems would likely not suffer the same effects during release studies.

6.3.3 ALLT release studies

6.3.3.1 Effect of chloride permeability on ALLT release

After loading at 37 °C, ALLT release was monitored in pH 7.4 PBS at 37 °C with the changes in the lactone and carboxylate fractions of TPT in solution. Simulations of these release profiles were made using the fitted values obtained from loading experiments. The initial conditions used in these studies were obtained from the final concentrations of total intravesicular chloride, ammonia, and TPT calculated from the loading model and are found below in Table 6.4. Initial simulations did not predict the extent of release seen in the later phase of release of these ALLT formulations. This was likely due to the slight but significant permeability of chloride that was not a factor during loading. With this rationale, these ALLT release profiles were used to fit a chloride release rate constant, k_{mCl}, and resulted in the fit shown in Figures 6.4a and b. Based on this fit, k_{mCl} was estimated to be 3.8 ± 0.4 x 10^{-4} hr^{-1}. Based on the 100 nm diameter of these liposomal formulations, the permeability of the chloride anion, $P_m^{Cl^-}$, can be estimated by the following equation.

$$P_m^{Cl^-} = \frac{d}{6} k_{mCl} \tag{44}$$

The resulting permeability coefficient for chloride is 1.8 ± 0.2 x 10^{-13} cm/s. This value is lower than other values reported for chloride permeability through phosphatidylcholine (PC) liposomes and is expected due to the greater rigidity of DSPC bilayers over the PC bilayers studied by Toyoshima and Thompson.[187] In those studies, PC liposomes were a mixture of DSPC and shorter saturated fatty acids that tend to provide less resistance to transport and higher permeabilities.[50, 53, 187]

Table 6.4 Initial conditions used for modeling ALLT release

	Ammonium Besylate ALLT					$(NH_4)_2SO_4$ ALLT
Loading Temp	37 °C			60 °C		60 °C
Loading TPT	60 µM	130 µM	180 µM	60 µM	180 µM	130 µM
$T_i(0)$ (mM)[a]	13.7	23.4	29.5	24.6	61.2	42.6
$Cl_{T,i}(0)$ (mM)	5.52[b]	7.09[b]	9.12[b]	68 ± 8[c]	250± 60[c]	140 ± 60[c]
$N_i(0)$ (mM)[b]	263	257	253	255	220	453
$Cl_{T,o}(0)$ (mM)	0.13					
$N_o(0)$ (µM)	0, 12, or 60					

[a] Values calculated based on initial amount of TPT observed in release study and entrapped volume ($L_i(0) = {}^{T_{Total}(0)}/_{f_v}$)

[b] Value obtained from loading model simulation of final experimental loading time point.

[c] Fitted value from release profile with 95% CI.

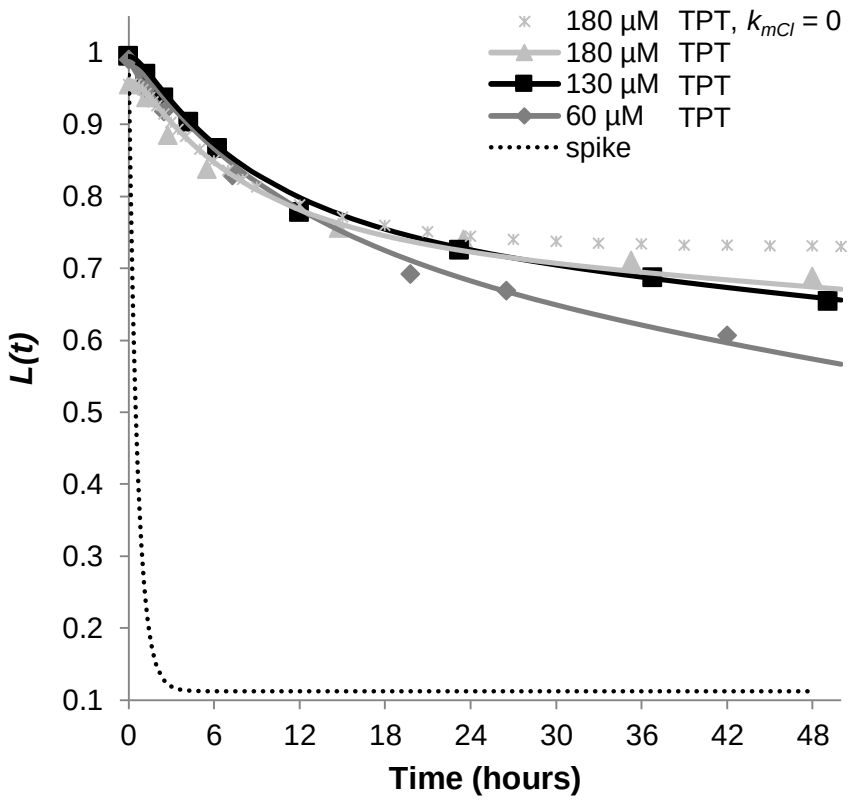
180 µM TPT, k_{mCl} = 0
180 µM TPT
130 µM TPT
60 µM TPT
spike
L(t)
Time (hours)

A.

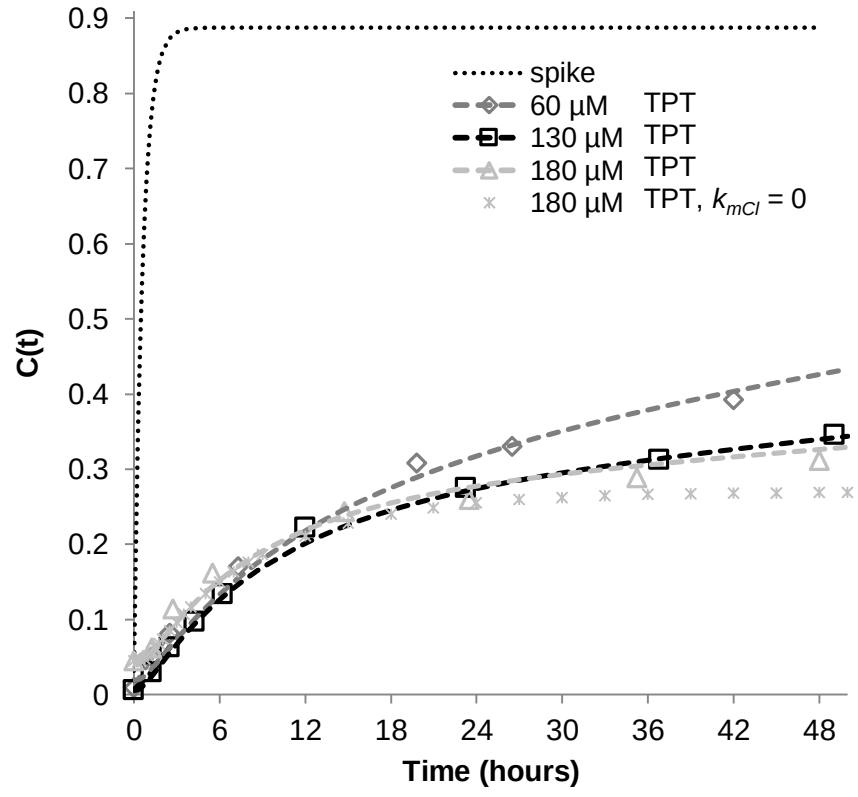
spike
60 µM TPT
130 µM TPT
180 µM TPT
180 µM TPT, k_{mCl} = 0
C(t)
Time (hours)

B.

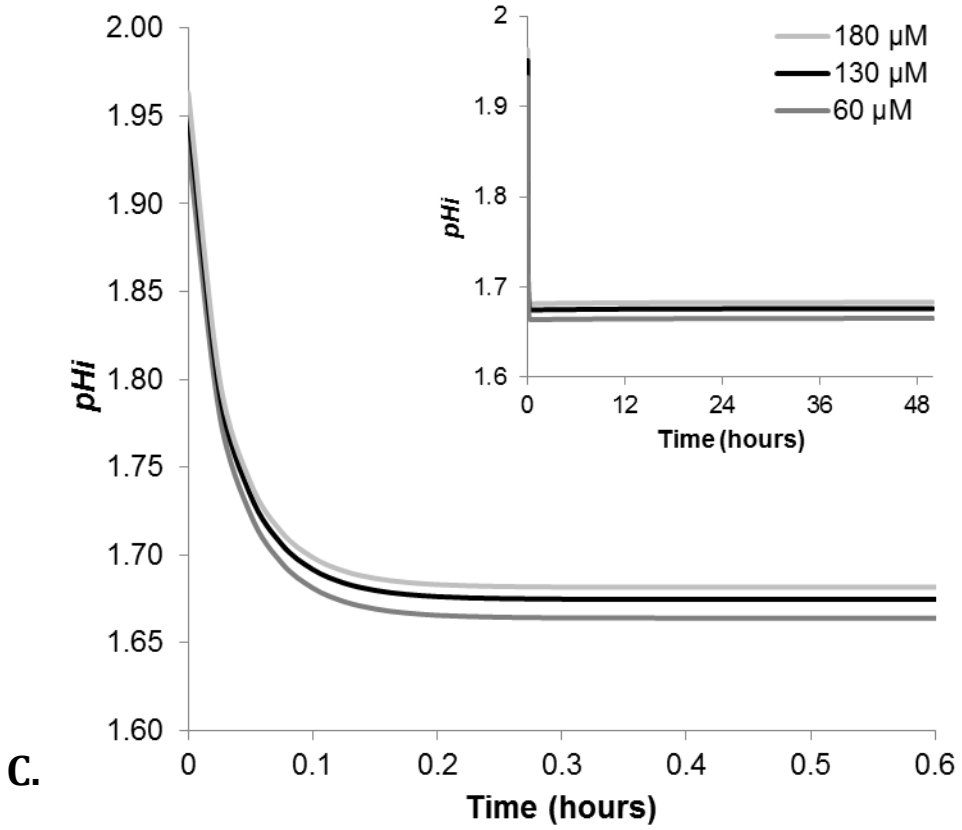

Figure 6.3. Release at 37 °C in PBS of ALLT formulations loaded at 37 °C. Release was monitored by the changes in the fractions of lactone (A) and carboxylate (B) TPT (*L(t)* and *C(t)*, respectively) for TPT actively loaded into ABLs (loaded with TPT suspension concentrations of 60, 130, and 180 μM TPT as designated in the legend). The lines through the data points represent the fits of the profiles to the ALLT release model accounting for chloride permeability. Simulations of the interconversion of pure lactone TPT spiked in the pH 7.4 buffer is also shown to emphasize the retardation in ring-opening due to liposomal release kinetics while ALLT loaded in the presence of a 180 μM TPT was simulated assuming no Cl permeability to illustrate its effect on release. The intravesicular pH was also calculated to reiterate the low intravesicular pH maintained during these release studies (C).

6.3.3.2 Effect of ammonia transport on ALLT release

Preliminary simulations from Chapter 5 indicated the concentration of extravesicular ammonia in release media could alter the intravesicular pH and subsequently accelerate release with higher ammonia concentrations. In Figure 6.3c, the intravesicular pH remains low as ammonia is continuously released because no ammonia was present in the PBS buffer. The profiles in Figure 6.4, however, show the effect of ammonia influx on intravesicular pH and subsequently release kinetics. As more NH_4Cl is added to the pH 7.4 PBS release media, the rate and extent of release also increases. Simultaneous fitting of release profiles in PBS with varying concentrations of NH_4Cl were conducted for ALLT suspensions using 60 uM TPT in the loading solution (Figures 6.4a and b). Fitting these profiles identified a shift in the pK_A for intravesicular ammonia which was estimated to be 1.49 ± 0.05. The change in intravesicular pH due to ammonia influx can be calculated and shows the considerable increase in pH resulting in accelerated release (Figure 6.4c). This change in the pK_A allows prediction of the release kinetics in the presence of 60 μM NH_4Cl for the other ALLT formulations studied (Figures 6.4d & e).

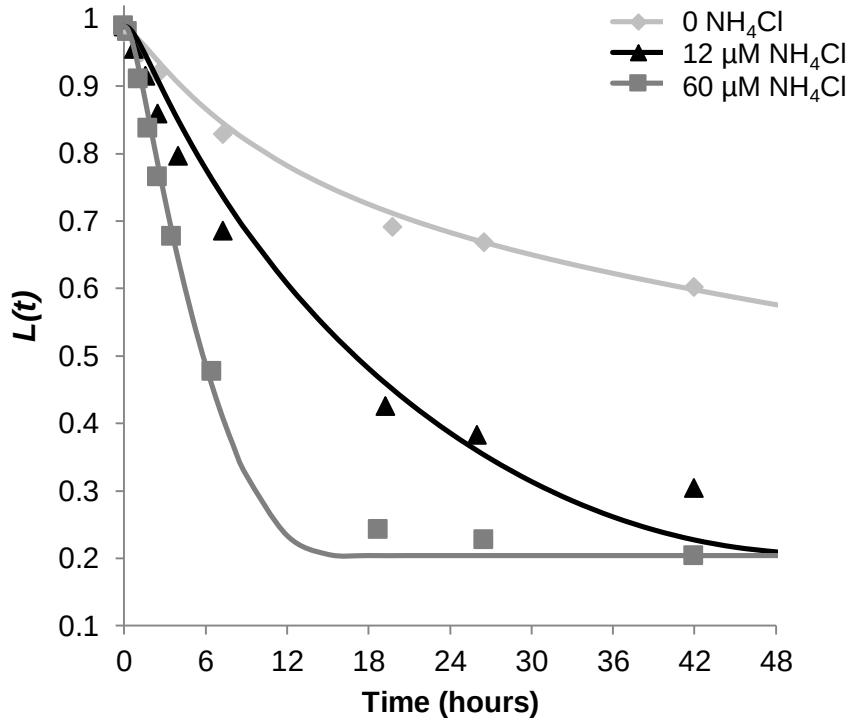
0 NH4Cl
12 µM NH4Cl
60 µM NH4Cl
L(t)
Time (hours)
1
0.9
0.8
0.7
0.6
0.5
0.4
0.3
0.2
0.1
0
6
12
18
24
30
36
42
48

A.

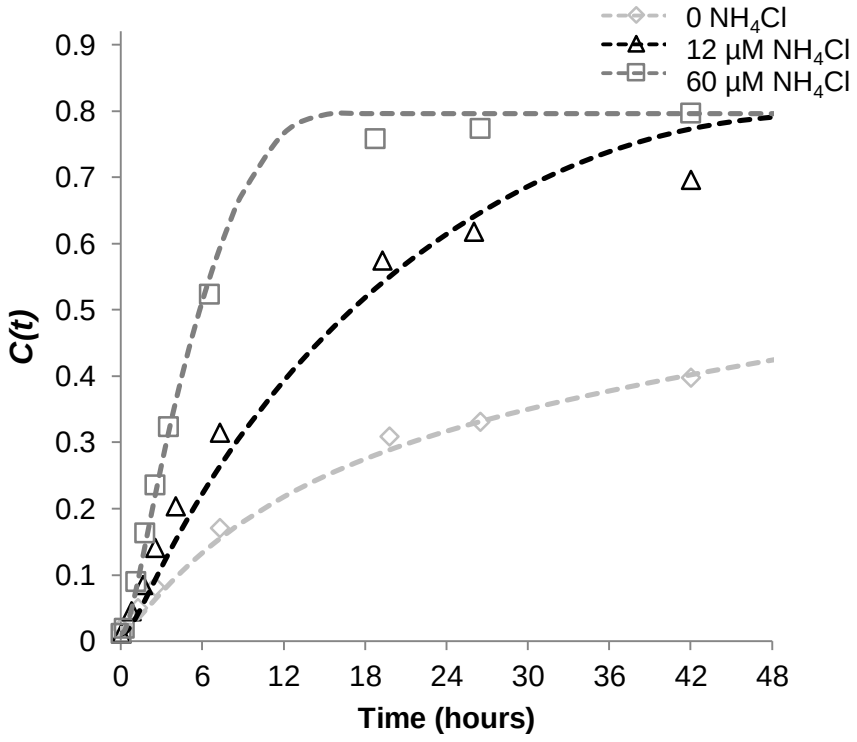
0 NH4Cl
12 µM NH4Cl
60 µM NH4Cl
C(t)
Time (hours)
0.9
0.8
0.7
0.6
0.5
0.4
0.3
0.2
0.1
0
0
6
12
18
24
30
36
42
48

B.

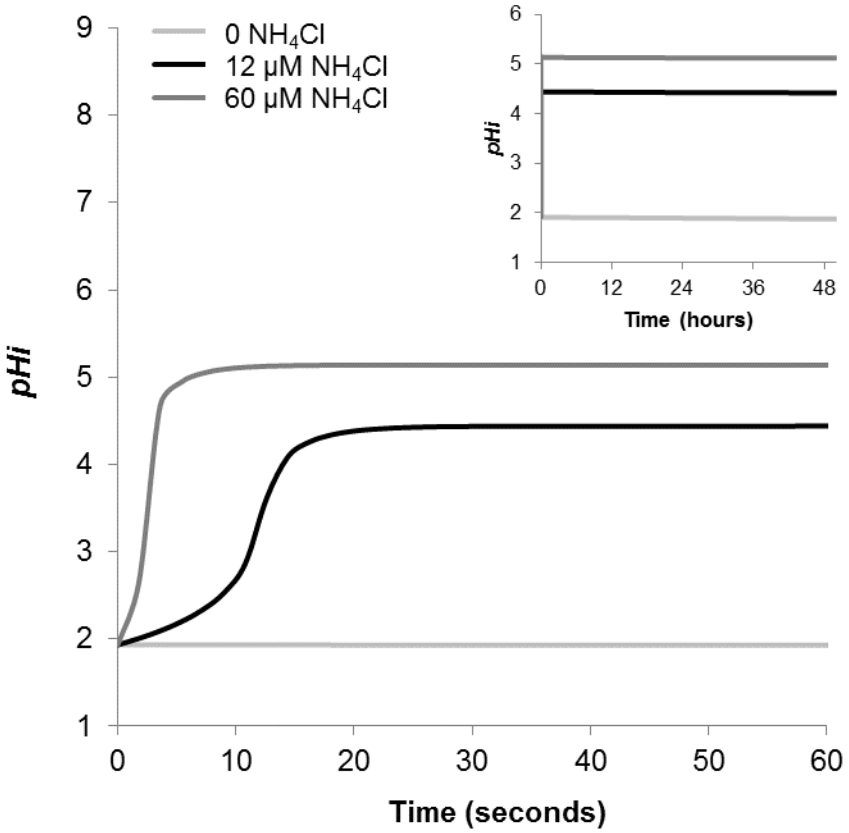
0 NH4Cl
12 µM NH4Cl
60 µM NH4Cl
pHi
Time (seconds)
pHi
Time (hours)

C.

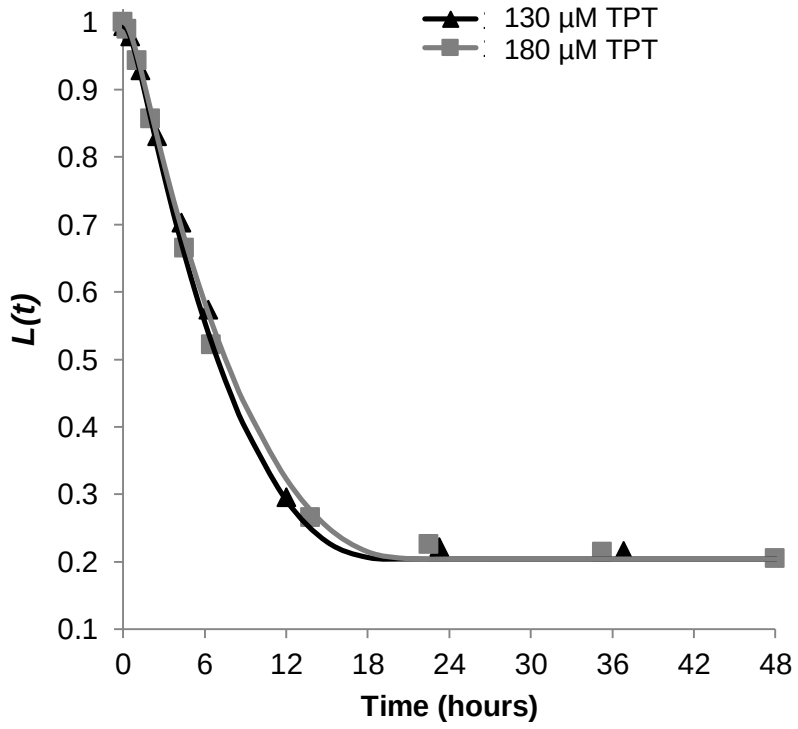
130 µM TPT
180 µM TPT
L(t)
Time (hours)

D.

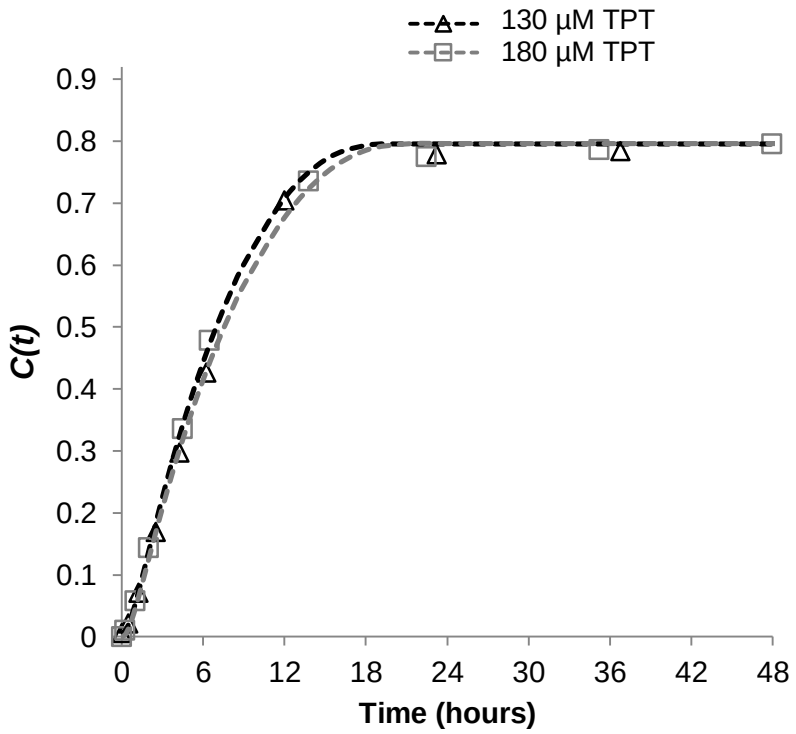
130 µM TPT
180 µM TPT
C(t)
0.9
0.8
0.7
0.6
0.5
0.4
0.3
0.2
0.1
0
0
6
12
18
24
30
36
42
48
Time (hours)

E.

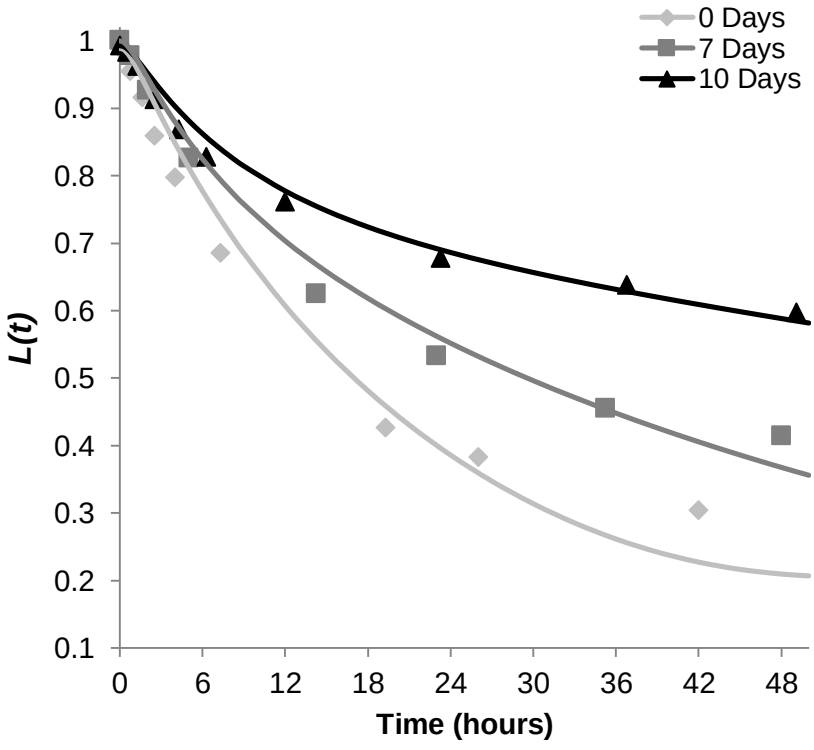
0 Days
7 Days
10 Days
L(t)
1
0.9
0.8
0.7
0.6
0.5
0.4
0.3
0.2
0.1
0
6
12
18
24
30
36
42
48
Time (hours)

F.

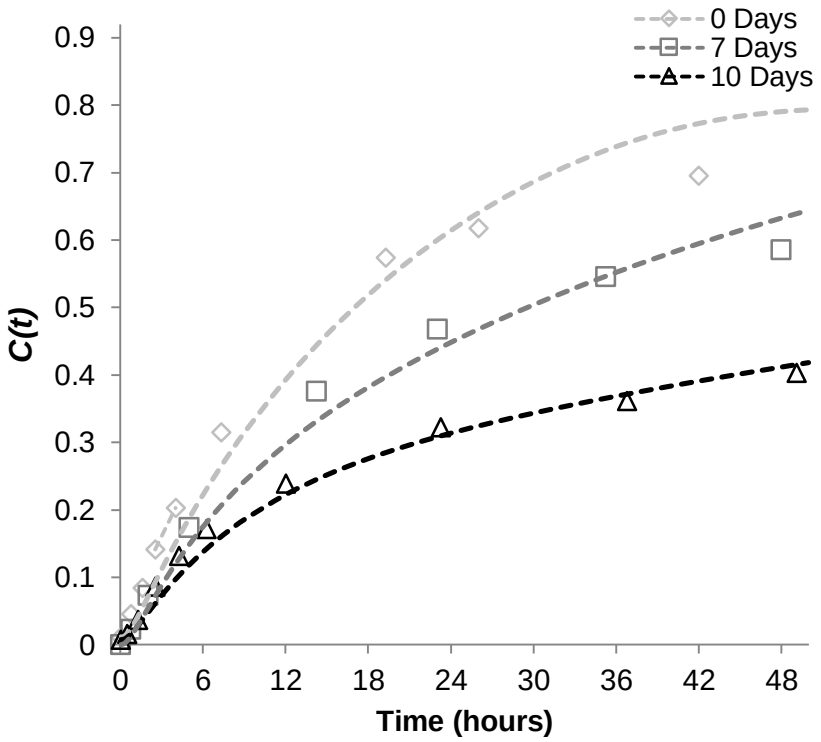
0 Days
7 Days
10 Days
C(t)
0.9
0.8
0.7
0.6
0.5
0.4
0.3
0.2
0.1
0
0
6
12
18
24
30
36
42
48
Time (hours)

G.

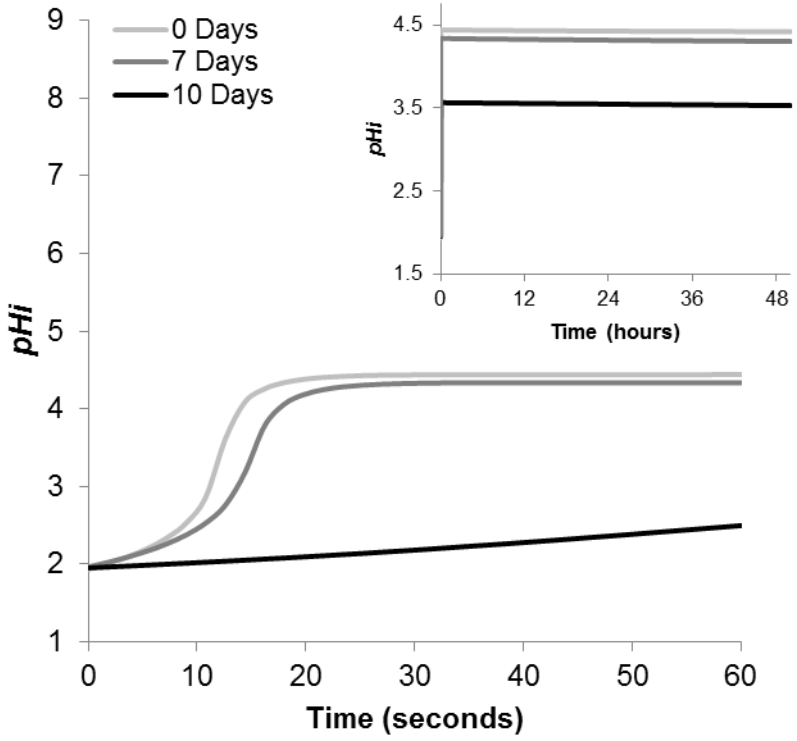
0 Days
7 Days
10 Days
pHi
9
8
7
6
5
4
3
2
1
0
10
20
30
40
50
60
Time (seconds)
4.5
3.5
2.5
1.5
0
12
24
36
48
Time (hours)

H.

Figure 6.4. The effect of ammonia transport on ALLT release at pH 7.4 (PBS) and 37 °C. After active loading in a 60 μM TPT suspension using ABLs, TPT release was monitored in PBS with the NH_4Cl concentrations displayed in the legend. The changes in *L(t)* and *C(t)* are used to monitor release and shown in (A) and (B) respectively while intravesicular pH is shown to illustrate the effect of ammonia influx (C). The shift in ammonia pK_A fit to these release profiles is shown by the plotted lines. This shift in pK_A was able to predict the release profiles in 60 μM NH_4Cl for the ALLT formulations listed in the legends of (D) and (E). Because ammonia may evaporate over time from solutions, the release kinetics of can slow over time as shown in (F) and (G). The loss of ammonia from the PBS buffer over time reduces the influx of ammonia and lessens the increase of intravesicular pH (H).

Another factor which may impact release profiles is the evaporation of ammonia during release studies. Even through rubber stoppers were used to seal the suspension vials during release studies, the gaseous form of ammonia may fill the air space in the vial and possibly diffuse through the rubber stopper, and be released when the vials are open for sampling. This appears to have some effect on the release profile of ALLT in the presence of PBS with 12 μM NH_4Cl (Figure 6.4a & b). The model expects more TPT to be released than that observed at later time points. Ammonia evaporation could cause such an effect as it would effectively lower the intravesicular pH as extravesicular ammonia is depleted. Further evidence of ammonia evaporation from the PBS with 12 μM NH_4Cl is illustrated by the release profiles in Figure 6.4g and h. Release studies were repeated in the same buffer 7 and 10 days after it was initially made, clearly showing slower release the longer the buffer has aged. Fitting of the initial extravesicular ammonia concentration for these release profiles estimated these concentrations to be 8.6 ± 1 and 1.9 ± 0.6 μM NH_4Cl in the buffer after 7 and 10 days of aging respectively, further supporting the likelihood of ammonia evaporation altering release kinetics.

6.3.3.3 Effect of loading at high temperature (60 °C) on ALLT release

Loading for 30 minutes at 60 °C achieved higher TPT loading efficiencies than loading for 72 hrs at 37 °C (see Figure 6.5). This is expected due to the bilayer existing in its more permeable liquid crystalline phase rather than its more rigid gel phase.[135] The ALLT's made with the 60 μM TPT loading solution had the highest encapsulation efficiency, which was similar to previous reports of TPT loading with $(NH_4)_2SO_4$ liposomes.[62]

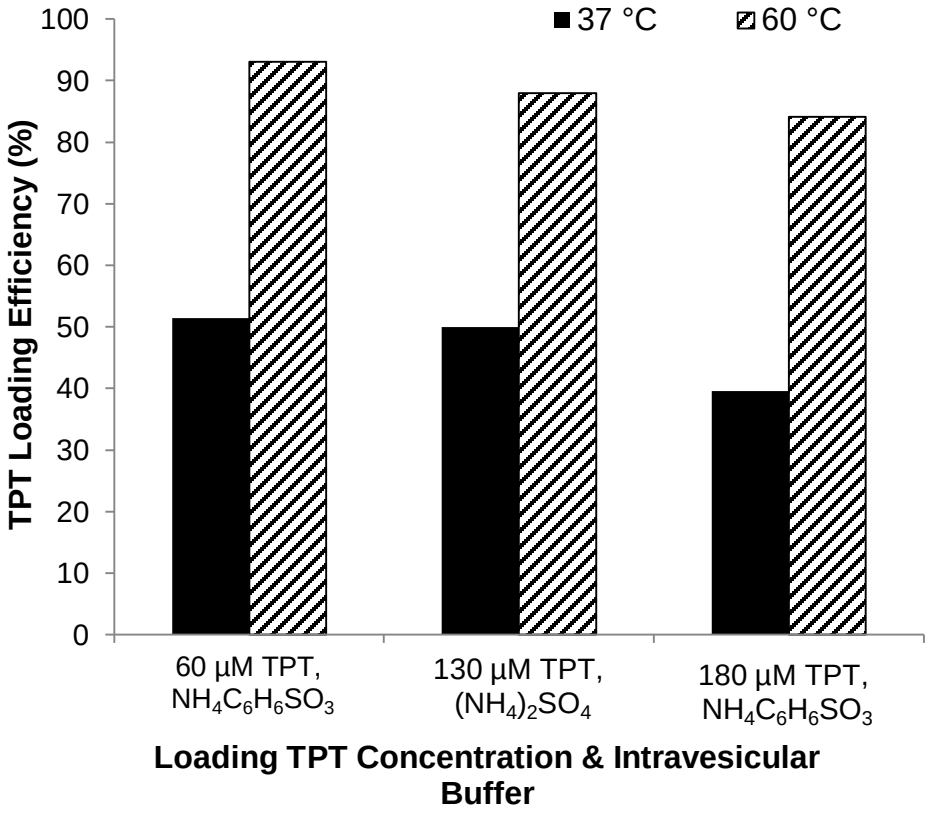

Figure 6.5 Comparison of the loading efficiencies of TPT at different temperatures and suspension conditions. Experimental values were calculated based on the quotient of the initial TPT suspension concentration and ratio of volume entrapped ($L_i(0) = {}^{T_{Total}(0)}/_{f_v}$, determined by HPLC) compared to that if the entire amount of TPT in the loading suspension had been entrapped in the intravesicular volume.

Modeling release used the initial conditions in Table 6.4. Initially, release studies for these formulations were conducted in PBS without any NH_4Cl; however, no significant release was observed (> 96% still lactone after 72 hours). Release was then studied in PBS containing 60 μM NH_4Cl to increase release, resulting in the profiles of lactone and carboxylate TPT in Figure 6.6a and b respectively. As expected, the intravesicular pH is raised due to the influx of ammonia (Figure 6.6c) to increase release. The simulation in Figure 6.6d of the precipitate dissolution occurring during release from these formulations reveals the unique profile of release seen due to the high loading temperatures. Initially, $T_{i(aq)}Cl_{i(aq)} \leq K'_{sp}$ and dissolution of precipitate occurs. Meanwhile, the influx of chloride is occurring in the ALLT formulations loaded using solutions of 60 and 130 μM TPT and liposomes with aqueous cores containing $NH_4C_6H_6SO_3$ and $(NH_4)_2SO_4$ respectively. The initial concentration of $Cl_{i(aq)}$ in the formulations was calculated to be 45 and 96 mM, respectively. These concentrations are lower than that of the extravesicular compartment ($Cl_{T,o}$ of 0.13 M) which remains relatively constant during release studies due to the small fraction of encapsulated volume. As precipitate is dissolved and $T_{i(aq)}Cl_{i(aq)} > K'_{sp}$ is satisfied, release is halted by this chloride influx. In the case of the ALLT formulation loaded with a loading solution of 180 μM TPT and liposomes containing $NH_4C_6H_6SO_3$, $Cl_{i(aq)}$ is initially 190 mM, higher than $Cl_{T,o}$, so TPT release continues to release due to efflux of chloride after $T_{i(aq)}Cl_{i(aq)} > K'_{sp}$.

The K'_{sp} determined for each release profile required correction for the fraction of total aqueous intravesicular TPT in the monomeric (f_1), cationic (f^+) state. This correction can be calculated using the equation below.

$$K_{sp} = f_1 f^+ K'_{sp} = \frac{H_i^+(-1+\sqrt{1+8K_2T_{i(aq)}})}{4K_2T_{i(aq)}(H_i^+ + K_{A1})} K'_{sp} \quad (45)$$

The importance of this correction is illustrated by Figure 6.6e. A plot of $T_{i(aq)}$ against $Cl_{i(aq)}^{-1}$ is not linear while linearity is quite apparent when $f_1 f^+ T_{i(aq)}$ is plotted against $Cl_{i(aq)}^{-1}$. This linearity is expected as the slope should be K_{sp}^{-1}. Using these corrections, the average K_{sp} was determined to be 1.39 ± 0.08 x 10^{-5}. Figure 6.6e also demonstrates that the K_{sp} is independent of the ammonium salt, $NH_4C_6H_6SO_3$ or $(NH_4)_2SO_4$, used to achieve active loading. This provides further evidence supporting the hypothesis that the precipitate formed is the chloride salt rather than a besylate or sulfate salt of TPT.

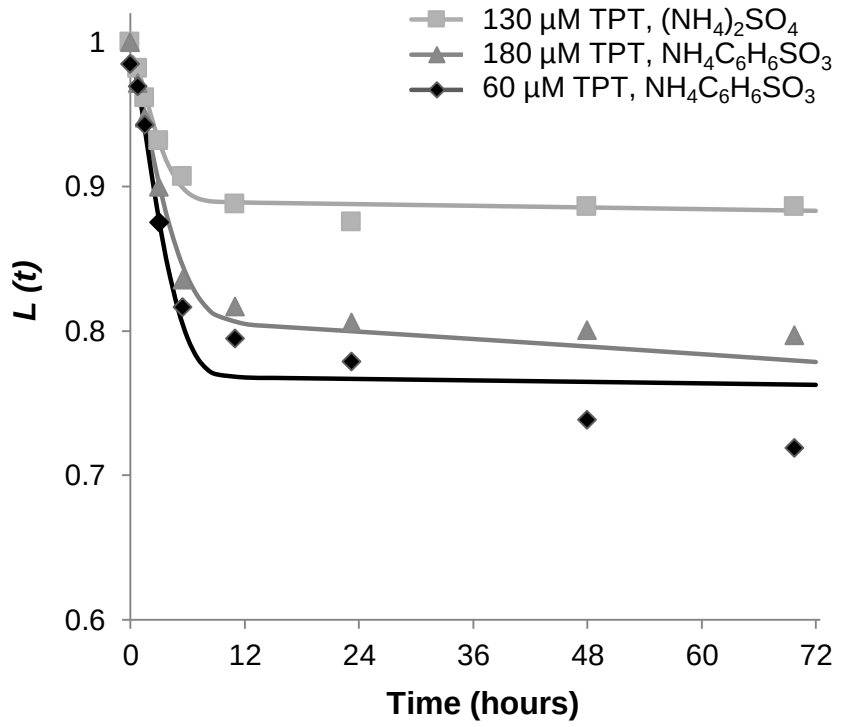

A.

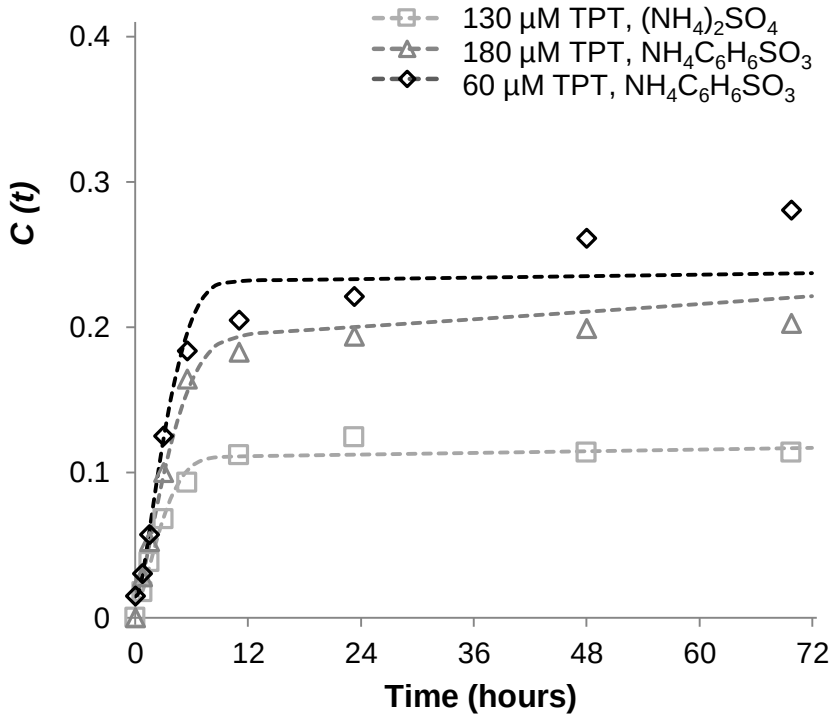
130 µM TPT, $(NH_4)_2SO_4$
180 µM TPT, $NH_4C_6H_6SO_3$
60 µM TPT, $NH_4C_6H_6SO_3$
C (t)
0.4
0.3
0.2
0.1
0
0
12
24
36
48
60
72
Time (hours)

B.

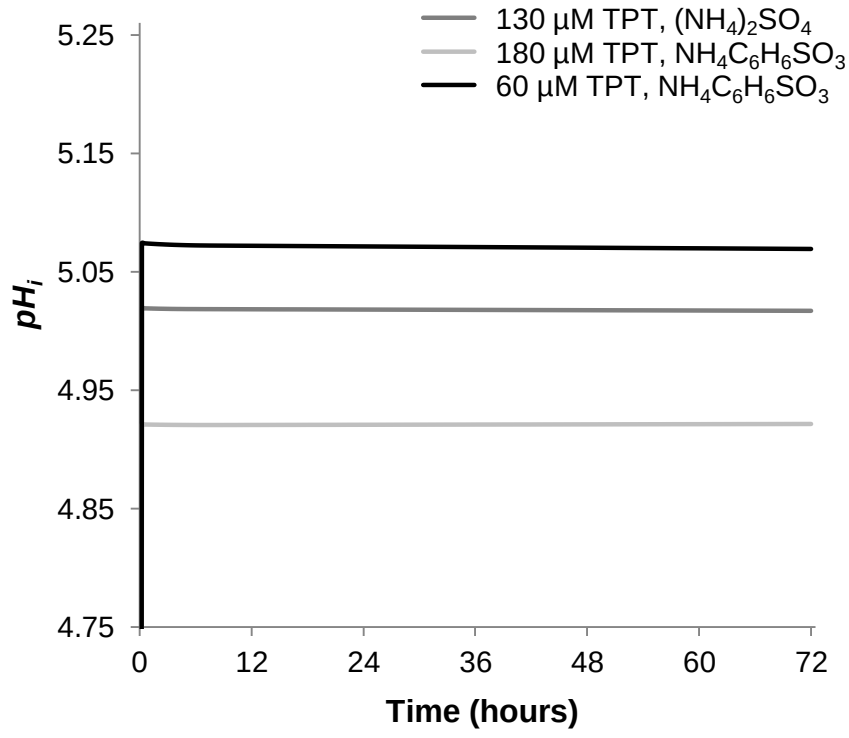
130 µM TPT, $(NH_4)_2SO_4$
180 µM TPT, $NH_4C_6H_6SO_3$
60 µM TPT, $NH_4C_6H_6SO_3$
pH_i
5.25
5.15
5.05
4.95
4.85
4.75
0
12
24
36
48
60
72
Time (hours)

C.

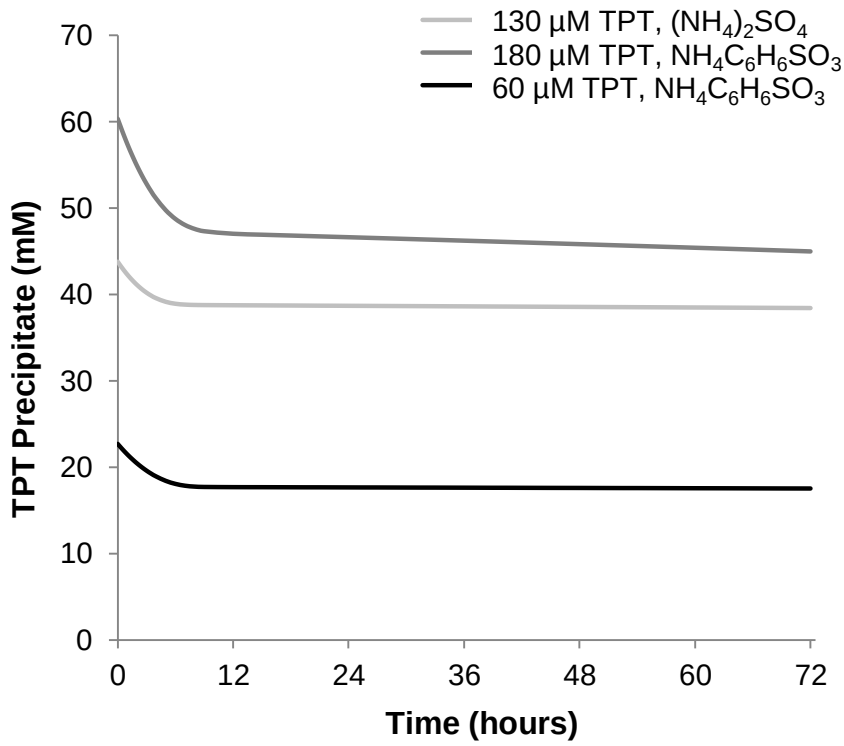

D.

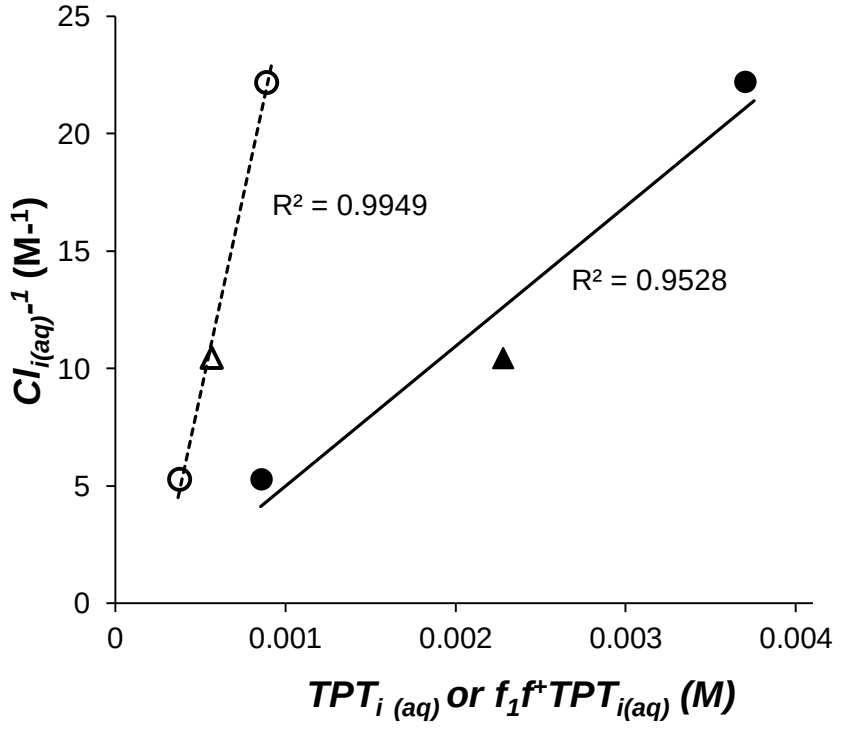

E.

Figure 6.6 The effect of high temperature loading (60 °C) on ALLT release in pH 7.4 PBS at 37 °C. The fractions of lactone (A) and carboxylate (B) TPT were

monitored from ALLT formulations loaded using different concentrations of TPT and liposomes containing the ammonium salts described in the legend. The lines represent the profile obtained after fitting the release model which accounts for the formation of TPT precipitate within the liposomes. The effect of ammonia influx on intravesicular pH is shown (C) to illustrate that the initial phase of release is a result of this increased pH while the dissolution of drug precipitate is shown (D) to illustrate the point at which $T_{i(aq)}Cl_{i(aq)} > K'_{sp}$ is reached and TPT release is greatly reduced as it becomes governed by the flux of chloride. Because a K'_{sp} was fit for each release profile, corrections for dimerization and pH were required (E). Without these corrections, the relationship between $T_{i(aq)}$ and $Cl^{-1}_{i(aq)}$ (filled-in symbols) exhibits poor linearity. These corrections were incorporated by plotting $f_1 f^+ T_{i(aq)}$ against $Cl^{-1}_{i(aq)}$ (empty symbols). The trend is linear even though the data represent liposomal formulations containing besylate (circles) and sulfate (triangles) anions within the aqueous core.

6.4 Discussion

6.4.1 Effect of TPT ion-pairing, dimerization, and intravesicular pH on active loading and subsequent release kinetics

The significance of ion-pairing and dimerization become apparent upon simulation of the variables these factors significantly influence. These factors are shown in Figure 6.7. In 6.7a, the uptake rates corresponding to those of the zwitterion ($\frac{dL_i^z}{dt} = r_{z,i}$) and ion-pair ($\frac{dLCl_i}{dt} = r_{ip,i}$) clearly illustrate biphasic uptake as the ion-pair is rapidly taken up in the initial phase of release until enough chloride accumulates within the intravesicular compartment. At this point, the influx of zwitterionic TPT dominates uptake and provides enough additional TPT to stimulate efflux of the ion pair from the intravesicular compartment, further slowing uptake at later times.

Dimerization affects loading in drastically different ways between the intra-and extra-vesicular compartments. Both of these effects are illustrated by Figure 6.7b. Focusing on the extravesicular compartment first, the fraction of the initial amount of lactone TPT still present in the loading solution (i.e. $f_{T,o}^{0} = L_o/L_o(0)$) decreases faster than the fraction of initial monomer ($f_{1,o}^{0} = L_{1,o}/L_{1,o}(0)$ still present in the loading solution. This illustrates the ability of TPT dimerization to prolong the faster uptake phase. Dimerization also affects the intravesicular compartment by greatly reducing the effective concentration of the permeable species within the intravesicular compartment. This is represented with the fraction of intravesicular TPT in the monomeric form (i.e. $f_{1,i} = T_1/T_i$)

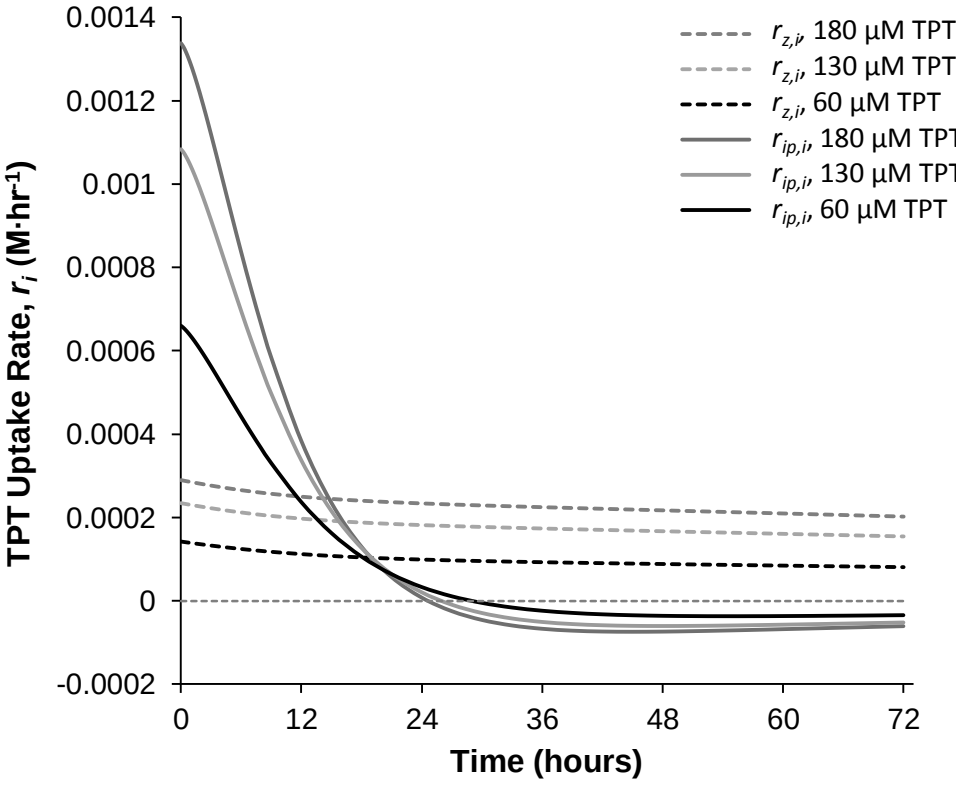

A.

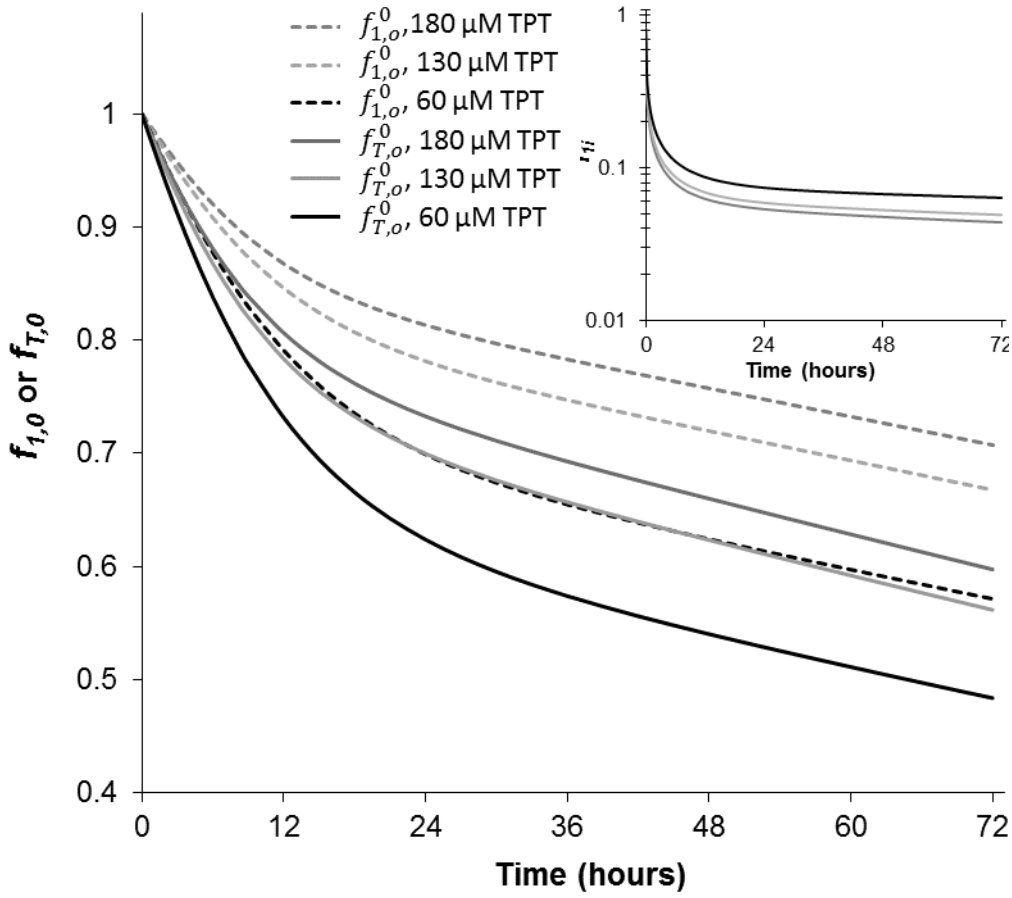

B.

Figure 6.7 The effects of ion pairing and dimerization on TPT active loading at 37 °C. (A) The uptake rates of TPT as its zwitterion, $r_{z,i}$, and ion-pair, $r_{ip,I}$, forms are shown to illustrate each species' contribution to the uptake profiles observed during active loading at the concentrations of TPT used in the loading solution (see legend). (B) Dimerization prolongs the initial phase of rapid uptake as the change in monomer concentration over time (represented by $f^0_{1,o}$) is slowed relative to the change in total TPT concentration in the loading solution (illustrated here with the profile of $f^0_{T,o}$). Meanwhile, the fraction of total intravesicular drug in the monomeric form, $f_{1,i}$, is shown to be greatly reduced in the inset at the top right.

Similar effects are present for ALLT release and are shown in Figure 6.8. In Figure 6.8a, the rate of ion-pair release is shown to be far greater than the rates of zwitterion release or chloride influx when there is no extravesicular ammonia initially present in the buffer. Under these conditions, zwitterion permeablity is negligible and release is greatly slowed

after the concentration of ion-pair is depleted over 90%. This is illustrated by Figure 6.8b. At the same time, however, total intravesicular TPT is only depleted by ~ 50 %.

Upon the additon of ammonia to the extravesicular release media, the influx of ammonia and subsequently the increase in intravesicular pH (see Figure 6.4c) has a dramatic effect on the rate of zwitterion release. This is illustrated by Figure 6.8c. For the ABL formulations loaded in the presence of a 60 μM solution of TPT, $r_{z,i}$ increases over 1000-fold after the addition of 60 μM NH_4Cl. With the zwitterion dominating release under these conditions, release proceeds to completion at this higher intravesicular pH (see Figure 6.8b). Figure 6.8c also shows this effect is independent of the concentration range of TPT studied here.

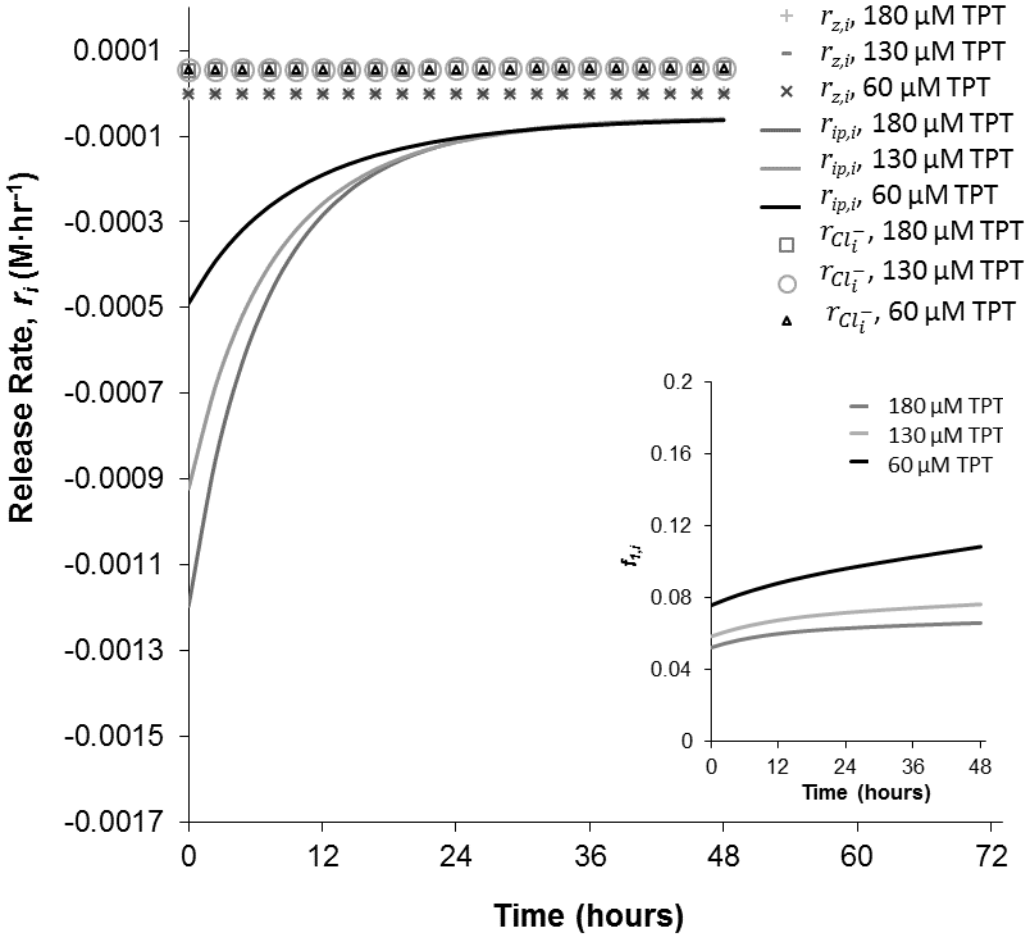

A.

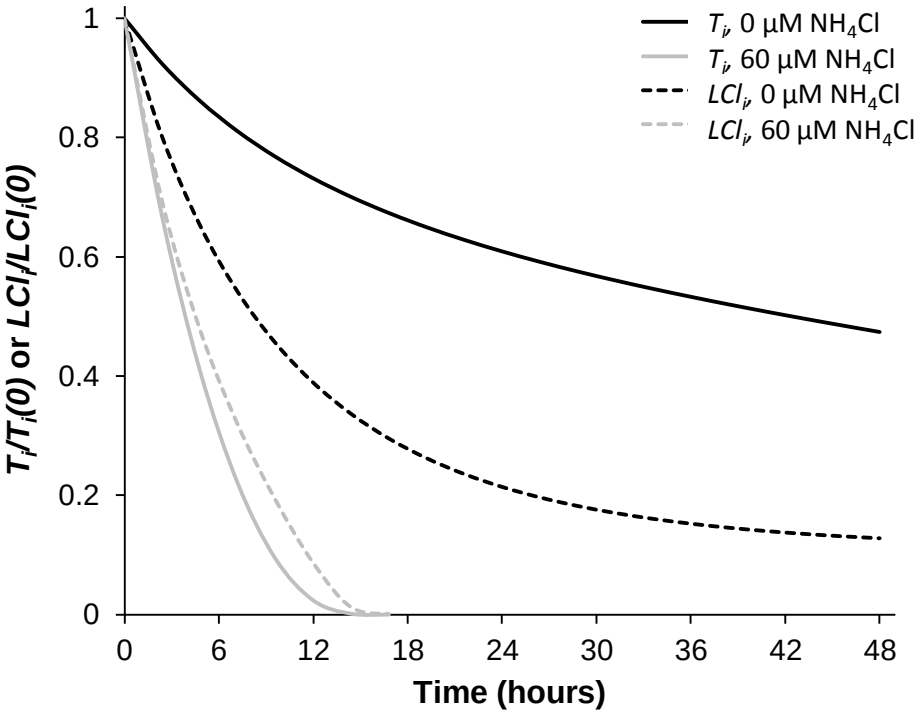
T_i, 0 µM NH_4Cl
T_i, 60 µM NH_4Cl
LCl_i, 0 µM NH_4Cl
LCl_i, 60 µM NH_4Cl
$T_i/T_i(0)$ or $LCl_i/LCl_i(0)$
Time (hours)

B.

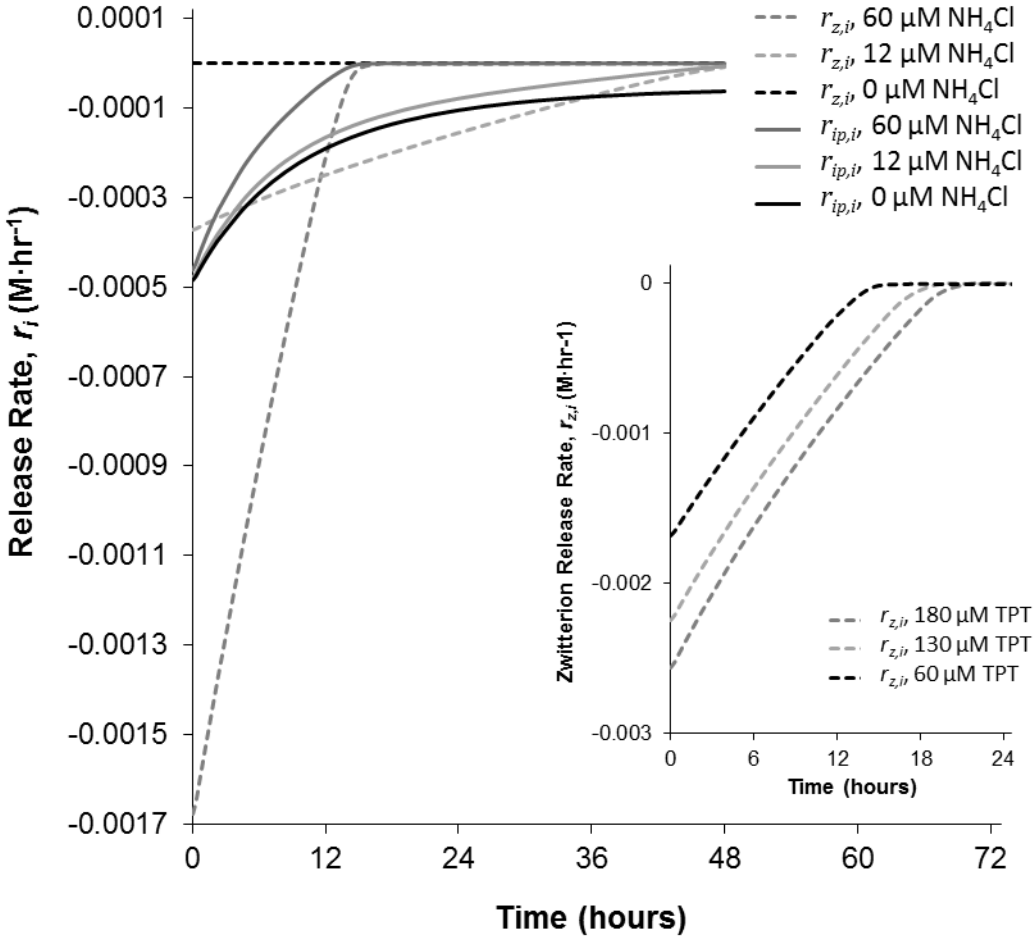
$r_{z,i}$, 60 µM NH_4Cl
$r_{z,i}$, 12 µM NH_4Cl
$r_{z,i}$, 0 µM NH_4Cl
$r_{ip,i}$, 60 µM NH_4Cl
$r_{ip,i}$, 12 µM NH_4Cl
$r_{ip,i}$, 0 µM NH_4Cl
Release Rate, r_i (M·hr^{-1})
Time (hours)
Zwitterion Release Rate, $r_{z,i}$ (M·hr-1)
$r_{z,i}$, 180 µM TPT
$r_{z,i}$, 130 µM TPT
$r_{z,i}$, 60 µM TPT
Time (hours)

C.

Figure 6.8 The effects of ion-pairing, dimerization, and pH on ALLT release at 37 °C. (A) Simulated rates of TPT release attributed to its zwitterionic, $r_{z,i}$, and ion-paired, $r_{ip,i}$, forms are shown to illistrate the ion-pair is the dominant species governing release when the extravesicular buffer does not contain NH_4Cl. (B) The slow terminal phase of release seen under the conditions in A is the result of ion-pair depletion well before that of total TPT. This is illustrated for the ALLT loaded in the presence of 60 μM TPT by normalizing with respect to the intial amount of ion-pair and total TPT in the intravesicular compartment ($LCl_i(0)$ and $T_i(0)$, respectively). (C) The release rates due to increases in intravesicular pH are shown for ALLT loaded in the presence of 60 μM TPT, illustrating $r_{z,i}$ increases dramatically and drives release to completion as ammonia concentrations are increased in the extravesicular buffer. The inset shows similar rates (i.e. much greater) of zwitterion release in PBS with 60 μM NH_4Cl for all the loading conditions employed. The legends in A and the insets refer to the concentration of TPT used during acive loading while the legends for B and C refer to the amount of NH_4Cl added to the extravesicular buffer.

6.4.2 Significance of loading temperature and precipitate identity

Due to the rapid uptake of TPT at 60 °C, direct experimental observations of the loading kinetics of TPT could not be achieved. Furthermore, assuming the increases in the species' permeabilities would be proportional would not be appropriate since the temperature dependence of their water partition coefficients are unknown and the mechanism of transport for ion-pairs and small anions is highly debated.[44, 153, 188, 189] Even so, several inferences can be made upon comparison of the values estimated by the loading and release models used during data regression. Figure 6.9a illustrates such a comparison with the Cl:TPT ratios estimated from these models to be present at the end of loading at 37° and 60 °C. While more TPT is present than Cl after loading at 37 °C, the opposite is the case based on the precipitation model used to fit the release profiles of the high temperature-loaded ALLTs. Furthermore, extrapolations from the 37 °C loading model would predict a decrease rather than an increase in the Cl:TPT ratio based on the amount of entrapped TPT observed

after loading at 60 °C (see Figure 6.9b). This suggests that the relative changes in species' permeability are not proportional (i.e. have different activation energies). Based on these ratios being >1:1 and the observation that the initial chloride concentrations reported in Table 6.4 are ≤ that of the loading solution ($Cl_{T,o} = 0.25\ M$), it is also likely that chloride transport is greatly dependent upon Cl^- as well as the ion pair. This conclusion is based on the observation that the maximum Cl:TPT ratio achievable by ion-pair transport would be 1 while the total amount of intravesicular Cl loaded would be $\geq Cl_{T,o}$ if Cl^- permeability was the main driving force behind Cl transport.

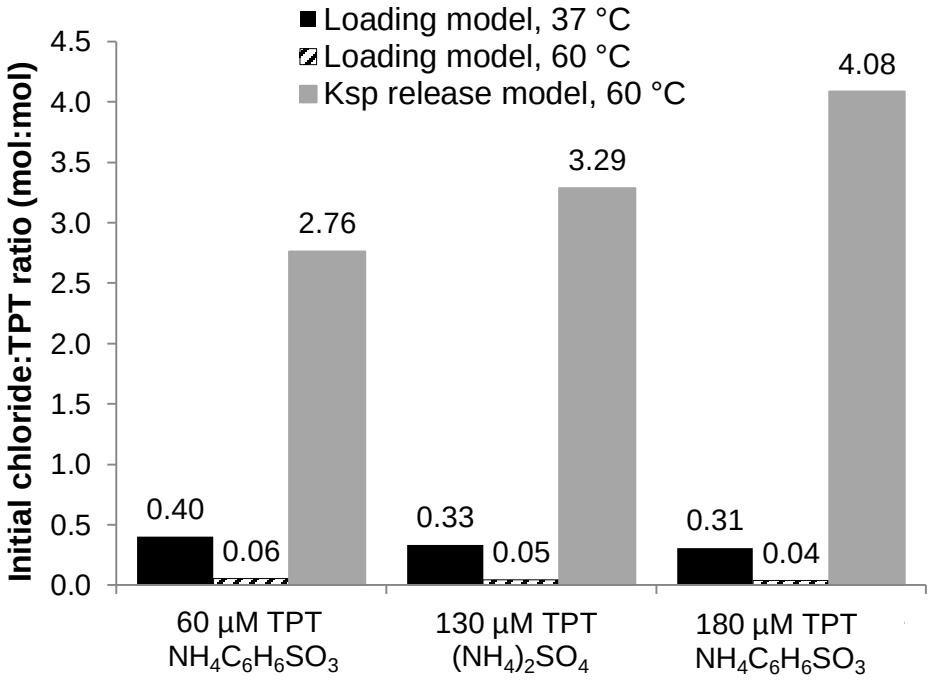

A.

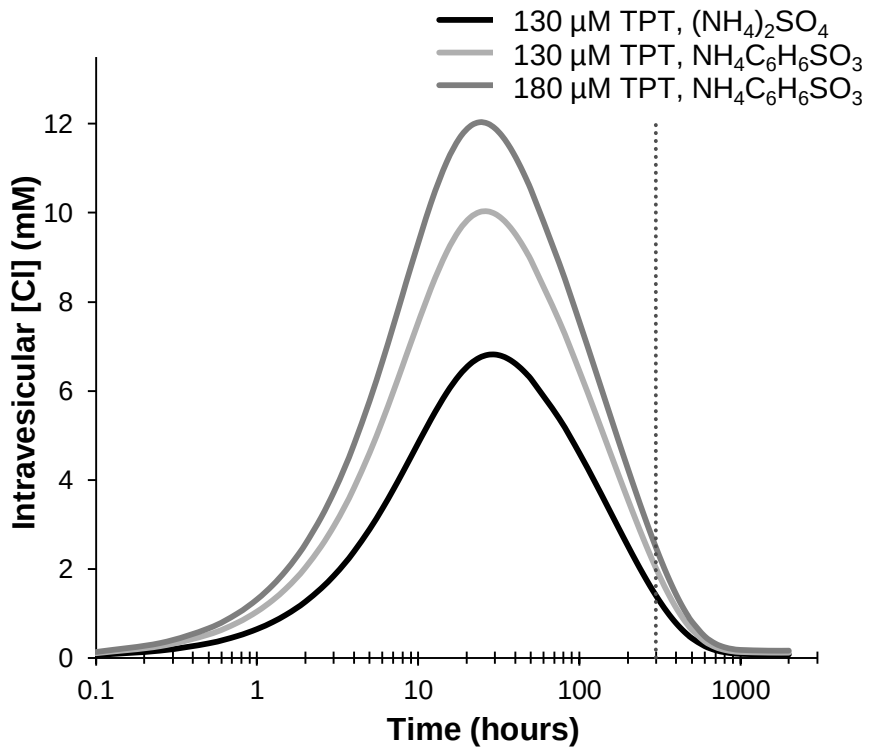

B.

Figure 6.9. Changes in the intravesicular Cl:TPT ratio provide insight on the mechanism of TPT uptake at 60 °C. (A) Three different ratios of intravesicular Cl:TPT are shown for three ALLT formulations with varying combinations of TPT loading concentrations and ammonium salts. The three Cl:TPT ratios for each formulation are estimated based on the 37 °C loading model after 72 hrs of uptake, the 37 °C loading model after 300 hrs of uptake to achieve the intravesicular concentrations observed from loading at 60 C°, and the release model which accounts for TPTHCl precipitate. (B) The uptake profile of intravesicular Cl simulated by the 37 °C loading model for the three TPT loading concentrations studied (see legend). The vertical line indicates the point at which this model achieves the same intravesicular TPT concentration as that determined after loading for 30 min at 60 °C.

In addition to these possible changes to the mechanism of uptake at higher temperature, these higher intravesicular chloride concentrations are biased due to the model assuming the K_{sp} governs precipitation of TPTHCl rather than anion of the ammonium salt used for loading. This assumption is necessary because of the unique condition of ion-pair transport

across the bilayer. The transport of both drug and the counterion of its precipitated salt, chloride, is necessary to account for the burst phase of release observed with ALLT formulations loaded at 60 °C. This effect is better illustrated by comparing simulations of release profiles when another anion forms the TPT salt.

Under these conditions, the transport equations governing the extravesicular compartment (Eqns. 28, 30 and 32) and intravesicular TPT in the presence of precipitate (Eqn. 36a) do not change while intravesicular chloride transport reverts back to Eqn. 32a. In the case of a monovalent anion (benzene sulfonate for the purpose of these simulations), the rate of precipitate dissolution follows the following condition:

$$\text{If: } K'_{sp} \leq T_{i(aq)} B_{i(aq)} \qquad \frac{dTB_{i(s)}}{dt} = -\frac{dT_{i(aq)}}{dt} \tag{46}$$

where $B_{i(aq)}$ and $TB_{i(s)}$ are the concentrations of benzene sulfonate in the intravesicular solution and the TPT salt respectively. In the instance where $K'_{sp} > T_{i(aq)} B_{i(aq)}$, there should be no precipitate left, $TB_{i(s)} = 0$, and intravesicular TPT transport follows Eqn. 28. With a rate equation for $TB_{i(s)}$, $B_{i(aq)}$ can simply be expressed with the following mass balance.

$$B_{i(aq)} = B_T - TB_{i(s)} \tag{47}$$

where B_T is the total concentration of benzene sulfonate. The pH equation (Eqn. 9) may be satisfied by substituting $B_{i(aq)}$ for B_i^-. Lastly, the initial conditions to define the amount of precipitate and soluble drug and counterion must be solved. This can be performed with Eqns. 40a and b by substituting B_T (0.3 M) for $Cl_{T,i}(0)$. Using these equations, release in the presence of TPT-besylate salt was simulated at varying fractions of total drug precipitated ($f_s = TB_{i(s)}(0)/T_i(0)$) and compared to the observed release profile and fit to the precipitate model which assumes TPTHCl is the salt. This is illustrated in Figure 6.10.

These simulations show very different release profiles than those observed experimentally due to the presence of intravesicular Cl in both ammonium sulfate and besylate ALLTs. This proposed mechanism of ion-paired TPT-Cl loading and precipitation at high temperatures may also explain the presence of TPT salts within liposomal TPT formulations containing various intravesicular solutions. This effect was illustrated in a study by Abraham et. al which showed intravesicular precipitates formed after TPT loading in liposomes containing $(NH_4)_2SO_4$, Mn SO_4, citrate, and $MnCl_2$.[64].

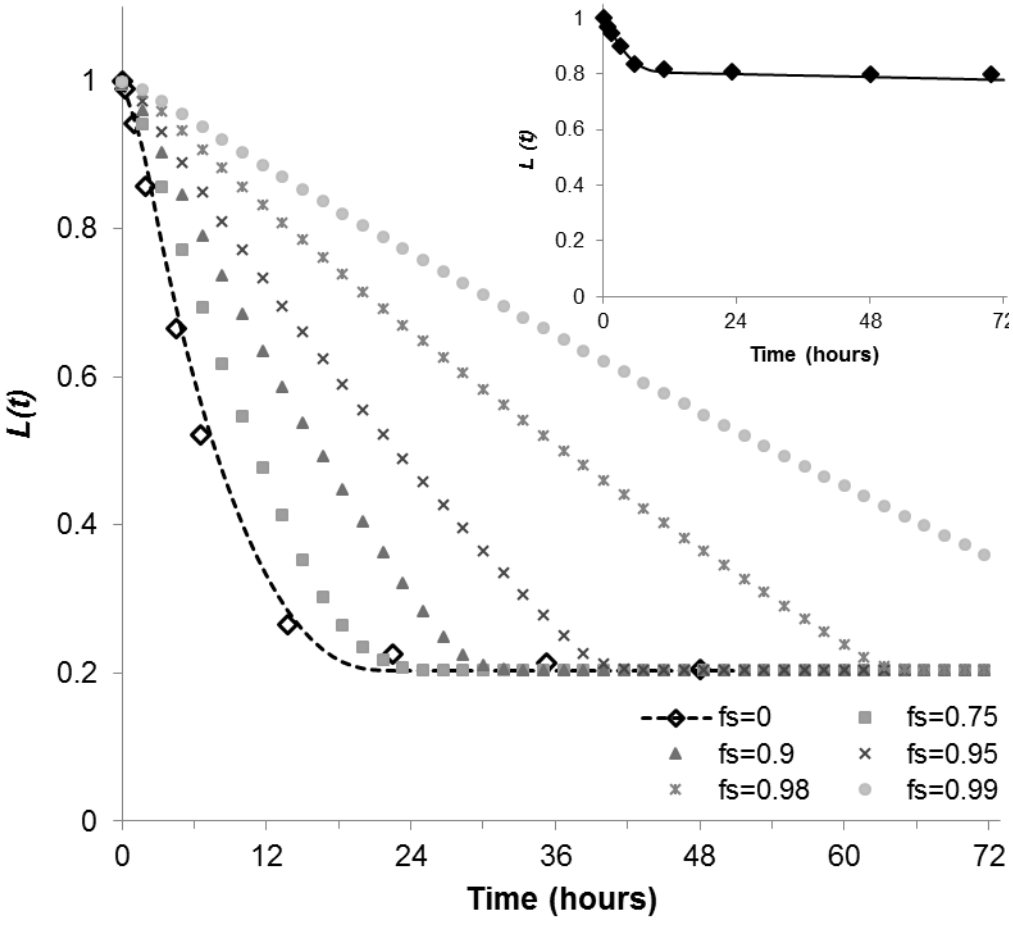

A.

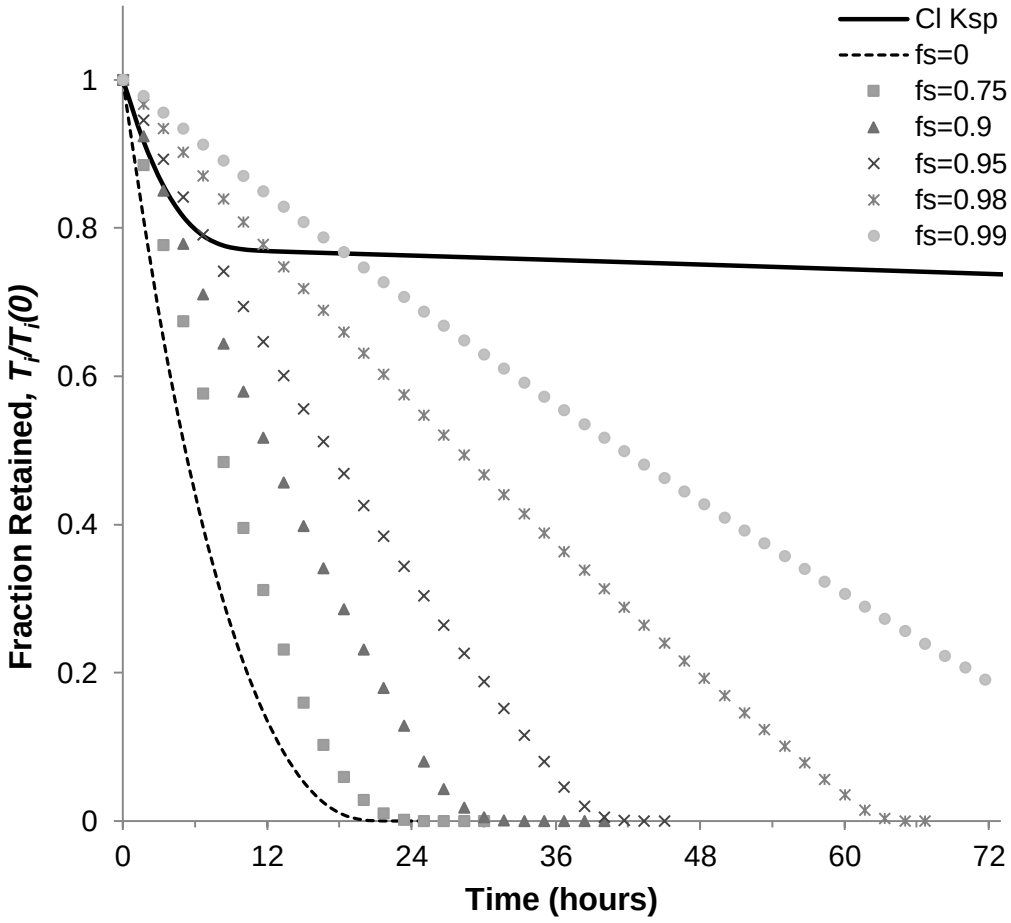

B.

Figure 6.10 The identity of TPT salt affects release. (A) The change in lactone was simulated for ALLTs loaded using a 180 μM solution of TPT. The simulations assumed TPT was precipitaed as a besylate salt and the resulting changes in *L(t)* are shown at varying fractions of TPT initially precipitated, f_s (see legend), while the inset shows the data and fitted model which assumes a TPTHCl salt. The points at $f_s=0$ are data from the ALLT formulation loaded at 37 °C (using 180 μM TPT), and the dotted line indicates the profile generated from the code used to simulate this precipitation model. B) The simulations in A were normalized to fraction retained to illustrate the release profiles more clearly. The solid line shown in the resulting simulation uses the TPTHCl precipitate model used for the inset of A. The simulations for the TPT-besylate precipitation model used the initial conditions for ALLTs loaded at 37 °C and 60 μM NH_4Cl in the release media. Varying these initial conditions resulted in accelerated or slowed release profiles but showed the same trends as a function of precipitate present.

6.4.3 Implications of loading conditions on optimizing release kinetics

The effect of chloride on loading and release of TPT is considerable based on the results of this study. These effects could be exploited for controlling release kinetics by simply altering the amount of chloride contained in the loading solution. This would be especially advantageous at high loading temperatures where intravesicular TPTHCl precipitate is formed. Further studies are needed to use this chloride effect as an advantage in formulation development. The current findings were only able to indicate that ion-pairing and Cl^- permeabilities both contribute to TPT active loading at higher temperature since direct measurement of their respective permeabilities was not possible under these conditions. Without these permeabilities, predicting how much chloride would need to be added to the loading solution is not possible. Even so, the potential to alter the relative ratio of fast-to-slow release phases of TPT in these liposomal formulations is worth further exploration as a tunable drug release system.

6.5 Conclusions

The results of this study provide a mechanistic understanding of the factors governing the active loading process for liposomal TPT. The loading model developed herein combined with experimental observations reveals TPT transport across the lipid bilayer is achieved in part by ion-pairing with chloride and affected by the drug's dimerization in solution. To the author's knowledge, this is the first report demonstrating significant bilayer transport of a large cationic molecule due to ion-pairing. Furthermore, subsequent release studies conducted with these liposomes of actively-loaded TPT were used to develop a mechanistic release model which incorporated the effect of drug precipitation on liposomal release kinetics. Mathematical modeling also identified the TPTHCl as the precipitated salt rather than the other anions present in the intravesicular core of the

liposome. The mechanistic underpinnings identified here for active loading of TPT and its subsequent release will be useful in future studies which aim to optimize the TPT loading process to provide tunable drug release kinetics via manipulations of the chloride-to-TPT ratio. The mathematical principles and mechanistic methodology used here should also be applicable to developing loading and release models for other liposomal formulations of pharmaceutical agents.

CHAPTER SEVEN

Mechanistic Modeling Provides Insights on Doxorubicin Release, Partitioning, and Conjugation Stability in Polymeric Micelles

7.1 Introduction

Nanoparticles such as dendrimers, liposomes, and polymeric micelles have been heavily explored as drug carriers for the treatment of various human diseases including infection and cancer.[2-4] These nanoparticulate systems are attractive for pharmaceutical applications for two main reasons: 1) their ability to entrap and release drug payloads in a manner capable of altering drug pharmacokinetics via increased drug solubility or modulated drug release from the particle[3, 5] and 2) their unique size and multitudes of surface chemistry may potentially aid in reducing systemic toxicity through passive and active targeting respectively.[3-5, 10-13] While many types of nanoformulations have been developed to take advantage of these properties, few have had clinical success. Part of this low success rate may be attributable to differences in release rates observed during *in vitro* characterization studies and those which occur *in vivo*.

There have been many methods used to characterize drug release kinetics from nanoparticles;[115-117] however, stringent validation of these *in vitro* methods is necessary as many environmental effects *in vitro* may alter observed drug release kinetics. Part of this validation requires mechanistic models which deconvolute these environmental effects from the intrinsic release parameters governing drug release.[118, 197] With models capable of mechanistically describing nanoparticle drug release, incorporation of *in vivo* conditions would be possible and ultimately lead to accurate *in vitro/in vivo* correlations. Such correlations would reduce much of the costs incurred during preclinical development due to extensive animal testing and unguided formulation optimization. To this end, considerable efforts have been made to establish mechanistic drug release models for

liposomal formulations;[118, 130] however, similar models have yet to be developed for other nanoparticles. The construction of such models for other nanoparticles will require the unique physicochemical properties of the drug, particle, and those of the drug-particle system to be considered.

One of these systems which has received considerable attention is polymeric nano-assemblies.[5, 65] These self-assembled nanoparticles are unique structures which provide a plethora of characteristics that may be exploited for altering drug release (e.g. particle size, charge, hydrophobicity, and conjugation sites for drug). While these may be advantageous to altering drug release kinetics, they may also result in a complicated drug release mechanism. For example, block copolymer micelles are generally composed of a hydrophilic shell and a hydrophobic core. Drug payloads can partition into the core of the micelle typically due to the drug's affinity for the particle's hydrophobic or highly-charged core.[5, 65, 66] Over time, drug is released from these polymeric micelles due to a combination of kinetic factors (i.e. drug diffusion and/or stability of drug-polymer linkage) and thermodynamic factors (i.e. complexation/absorption to the micelle core, CMC) intrinsic to the drug/polymer system and independent of the release environment.

Further complexity is added when nanoparticles are engineered to respond to external stimuli such as heat, electromagnetic waves, enzymatic activity, or pH.[5, 63, 65, 71-79] Chemically conjugating drugs to the block copolymers is another way to alter drug release kinetics and adds another dimension to the mechanism of drug release. In several instances, these drug-conjugated micelles exhibit a biphasic drug release pattern (i.e. burst drug release followed by an extremely slow drug release phase) that varies depending on the pH of release medium.[80-83]

In this study, a mathematical was developed to describe hydrazone-conjugated doxorubicin (DOX) release from block copolymer micelles. The block copolymers were

composed of 12 kDa poly(ethylene-glycol) (PEG) and 16 hydrophobic repeating units and conjugated with DOX using a hydrazone linkage. Because hydrazone bonds have been shown to be pH-sensitive (i.e. responsive to lysosomal pH),[80, 81, 198] multiple drug release studies were performed at pH 5.0 and pH 7.4. Spacer insertion prior to the hydrazone moiety was previously shown to alter drug release. [80, 82, 83, 102, 199-201] As such, block copolymer micelles with glycine (GLY) or methyl 4-aminobenzoate (ABZ) spacers and another formulation without a spacer (HYD) were studied to assess how spacer modification mechanistically altered DOX release. Dynamic dialysis was used as the primary method to monitor release. The dynamic dialysis setting provided an additional physical barrier (i.e. dialysis membrane) to the removal of released, unconjugated DOX from the micellar solution. The kinetics of drug transport across the dialysis membrane were incorporated to isolate its effects on observed drug release profiles and generate intrinsic kinetic release rate constants for drug release from the block copolymer micelles. Initial modeling indicated instability of the hydrazone bond during prolonged storage and was confirmed with subsequent experiments. Additionally, a non-sink release method previously developed to determine both release kinetics and drug partitioning[197] was adapted to determine the extent of free DOX partitioning into the HYD micelle formulations and validate the mechanistic model. Using this mechanistic model, release parameters were generated to identify the factors governing the pH-sensitive release of DOX observed by these micelle formulations. This approach and the subsequent findings from this study will provide useful guidance to drug release analysis for future polymeric micelle drug carriers.

7.2 Materials and methods

7.2.1 Materials

L-aspartic acid β-benzyl ester, anhydrous hydrazine, benzene, N,N'-diisopropylcarbodiimide (DIC), 4-(dimethylamino) pyridine (DMAP), N-Hydroxysuccinimide (NHS), N,N-dimethylformamide, anhydrous N,Ndimethylformamide (DMF), anhydrous dimethylsulfoxide (DMSO), ethanolamine, anhydrous ethyl ether, anhydrous hexane, anhydrous tetrahydrofuran (THF), triphosgene, acetate buffer solution, phosphate buffer solution, methyl 4-aminobenzoate, O-Benzotriazole-N,N,N',N'-tetramethyl-uronium-hexafluoro-phosphate (HBTU), sodium hydroxide (NaOH) were purchased from Sigma-Aldrich (USA). Glycine-OMe is from Novabiochem (SUI). α-Methoxy-ω-amino poly(ethylene glycol) (PEG-NH2, MW=12,266) was purchased from NOF Corporation (Japan). Doxorubicn hydrochloride was purchased from LC Laboratories (USA). Slide-A-Lyzer® dialysis cassettes with 10,000 MWCO, Sephadex LH-20 gels, potassium biphthalate sodium hydroxide buffer solution, potassium phosphate monobasic buffer solution, and 96-well plates were purchased from Fisher Scientific (USA). Amicon-Ultra centrifugal ultrafiltration devices with MWCO 10,000 were purchased from Millipore (USA).

7.2.2 Preparation and characterization of polymeric micelles

Block copolymers of PEG-polyasparte (PEG-pAsp) were synthesized by Dr. Ponta using a method previously reported.[83] The synthesis involved the following steps: preparation of β-Benzyl-L-aspartate N-carboxy anhydride monomer (BLA-NCA), block copolymer synthesis of PEG-poly(16 β-benzyl-L-aspartate BLA) (PEG-pBLA), formation of PEG-poly-aspartate [PEG-p(Asp)] with hydrazide [PEG-p(Asp-Hyd)] or with a glycine (Gly) or methyl 4-aminobenzoate (Abz) spacer between the aspartate and hydrazide (PEG-p(Asp-Gly-Hyd) and PEG-p(Asp-Abz-Hyd) respectively) followed by DOX conjugation via a hydrazone bond.

7.2.2.1 BLA-NCA monomer synthesis

BLA-NCA was prepared by adding triphosgene (2.88 g, 9.7 mmol) to β-benzyl –L-aspartaten (5.0 g, 22.4 mmol) in dry THF (100 mL). The reaction proceeded at 45°C under a N_2 atmosphere. Once the solution became clear, anhydrous hexane was slowly added until NCA crystals appeared, then rapidly disappeared. Crystallization of BLA-NCA was achieved after storage in −20°C.

7.2.2.2 PEG-pBLA synthesis

These BLA-NCA crystals were used for synthesis of PEG-pBLA block copolymers via ring-opening polymerization of BLA-NCA. Using the terminal primary amine of PEG-NH_2 as the initiator, block copolymers containing 16 BLAs per PEG molecule were synthesized by dissolving BLA-NCA (183 μmol) monomers and PEG (7.67 μmol) in separate flasks to achieve 50 mg material/mL anhydrous DMSO under a N_2 atmosphere. Polymerization was performed at 45°C for 2 days after the dissolved monomers were added to the PEG solution. Purification of the resulting block copolymers were was achieved by ether precipitation then freeze drying from benzene. From this purified PEG-pBLA, three types of PEG-pAsp block copolymers were synthesized with or without an additional spacer between the polymer aspartate side chain and the DOX-hydrazone linkage.

7.2.2.3 PEG-p(Asp-Hyd) functionalization

Freeze-dried PEG-p(BLA) (56.42 μmol) was dissolved in dry DMF, and anhydrous hydrazine (9034 μmol) was added to the solution. PEG-p(Asp-Hyd) was produced after anhydrous hyrdrazine (9034 μmol) was added to the PEG-pBLA solution and allowed to react for one hour at 40°C under a N_2 atmosphere and constant stirring. The block copolymers were collected by ether precipitation and subsequent freeze drying.

7.2.2.4 Synthesis of PEG-p(Asp-Gly-Hyd) and PEG-p(Asp-Abz-Hyd) block copolymers

Purified PEG-pBLA was subjected to 01. N NaOH to deprotect its side chains and subsequently yielded PEG-p(Asp) block copolymers. Spacer modification was performed by dissolving freeze dried PEG-p(Asp) (12 μmol) in THF and reacting the block copolymer with glycine methyl ester (GlyOMe) (400 μmol) and methyl 4-aminobenzoate (AbzOMe) (450 μmol) using HBTU at 40°C overnight. Precipitates were removed through filtration at the end of the reaction. Ether precipitation followed by dialysis in a deionized water: methanol (50:50) solution was used to remove any unreacted GlyOMe and AbzOMe from the side-chain modified block copolymers. Hydrazide (Hyd) functionalization of PEG-p(Asp-GlyOME) and PEG-p(Asp-AbzOMe) was by removal of the methy esters and amide formation. This was performed by adding excess hydrazine with respect to number of repeating units (490 μmol, and 515 μmol for the GlyOMe and AbzOMe modified block copolymers, respectively) to PEG-p(Asp-GlyOMe) (6.5 μmol) and PEG-p(Asp-AbzOMe) (6.8 μmol) in DMF and reacting at 40°C for 1 h to obtain PEG-p(Asp-Gly-Hyd) and PEG-p(Asp-Abz-Hyd) block copolymers, respectively. The block copolymers were purified and recovered by repeated ether precipitation and freeze drying.

7.2.2.5 DOX conjugation via hydrazone bond

DOX was conjugated to each of the three block copolymers via a hydrozone linkage between the aspartate side change and the 13 position ketone on DOX. The reaction between DOX and PEG-p(Asp-Hyd) (750 mg, 53 μmol), PEG-p(Asp-Gly-Hyd) (899 mg, 59 μmol), or PEG-p(Asp-Abz-Hyd) (824 mg, 50 μmol) occurred in DMSO over two days under gentle shaking at 40°C to produce PEG-p(Asp-Hyd-DOX), PEG-p(Asp-Gly-Hyd-DOX), or PEG-p(Asp-Abz-Hyd-DOX) respectively. Physically-entrapped DOX and DMSO were initially removed by ether precipitation. The block copolymers were then dissolved in methanol and eluted through a Sephadex LH-20 column for further purification. After elution, the

block copolymers were dissolved in deionized water and filtered using a 0.22 μm filter. The final product was obtained after freeze-drying and stored as solids at -20°C.

7.2.2.6 Block copolymer micelle characterization

Once purified, PEG-p(Asp-Hyd-DOX), PEG-p(Asp-Gly-Hyd-DOX), and PEG-p(Asp-Abz-Hyd-DOX) block copolymers were added to DI water to form HYD, GLY, and ABZ micelles respectively. Characterization of the block copolymer synthesis is reported elsewhere.[83, 202] For the purpose of these release studies, micelle particle size and ζ-potential were determined using Zetasizer Nano-ZS (Malvern, UK). Block copolymers were suspended in DI water to a concentration of 2.0 mg copolymer/mL in triplicate for both analyses (six samples total). Particle size analysis was based on the average diameter obtained from number distribution analysis.

DOX loading for the three micelle formulations and subsequent DOX release was determined from DOX absorption spectra by Dr. Ponta.[83, 202] Briefly, standards of DOX varying in concentration between 0.98 and 250 μM were analyzed by a SpectraMax M5 (Molecular Devices, USA) equipped with variable spectrum filters. Absorbance was found to be linear at 485 nm over this concentration range. Spectra of DOX conjugated to micelles was found not to differ from free DOX in solution.[202] This allowed DOX concentrations to be calculated in micelle suspensions during drug release studies from free DOX standards.

7.2.3 Drug release studies

All drug release studies were performed by Dr. Ponta using the particles he developed above. Release studies were performed at both pH 5.0 and 7.4 using Potassium biphthalate sodium hydroxide (pH 5.0, 0.01 M ionic strength) and potassium phosphate monobasic buffer solution (pH 7.4, 0.02 M ionic strength) buffers respectively for all three copolymer

formulations of micelles. All release conditions were conducted in triplicate for all three micelle formulations.

7.2.3.1 DOX release monitored by dynamic dialysis: sink conditions

Micelle suspensions of 0.1, 0.5, and 1 mg copolymer/mL were used to fill 3 mL dialysis cassettes (10,000 MWCO). These cassettes were then dialyzed against reservoirs of the same buffers used to suspend the micelles at a reservoir: cassette ratio of 5,000:9 (v:v). The reservoirs were continuously stirred throughout the duration of release studies. During dialysis, release was monitored over a 72 hour period by withdrawing 0.1 mL samples from within the dialysis cassettes and analyzing the concentration of DOX using the colorimetric method already described.

Additional dialysis studies were also conducted to examine DOX transport across the dialysis membrane along with partitioning of free DOX into the micelle particles. For these determination of DOX transport across the dialysis membrane, free DOX (0.12 mg/mL) solutions were put into to dialysis cassettes and dialyzed under the same conditions used above for DOX-loaded micelle suspensions. Lastly, 0.5 mg copolymer/mL suspensions of HYD, GLY, and ABZ micelles which had already undergone release for 72 hours were spiked with free DOX (0.1 mg/mL, 0.17 – 0.25 mg total DOX/mL) and thoroughly mixed. These suspensions were dialyzed against the same reservoir conditions used in micelle release studies to observe if partitioning of unconjugated, free DOX into the micelle had any effect on observed DOX transport across the dialysis membrane.

7.2.3.2 DOX release monitored by ultrafiltration: non-sink conditions

Non-sink studies were performed based on an ultrafiltration method previously developed in Chapter 3 for use in liposomal release studies. The method was modified by Dr. Ponta for use with HYD, GLY, and ABZ micelles. Briefly, micelle suspensions (3 mL, 0.5

mg copolymer/mL) were transferred to scintillation vials and placed in a 37 °C incubator and gently shaken. At various time points, aliquots (250 µL) of the micelle suspension was withdrawn and diluted with methanol to 500 µL. The samples were transferred to an Amicon® Ultra 0.5 mL centrifugal filter cartridge with 10,000 MWCO Ultracel® membrane. Ultrafiltration was achieved by centrifugation of these cartridges at 14,000 rpm for 10 min. After centrifugation, the remaining supernatant was recovered and diluted to 500 µL with methanol and the process was repeated twice more. Validation of free DOX removal was performed by ultrafiltration of DOX solutions and by comparison of DOX concentration in copolymer suspensions spiked with free DOX before and after ultrafiltration.

7.2.4 Determination of unconjugated drug produced during storage

Because of the elapsed time between release studies (approx. 15 months), degradation of the hydrazone bond may be significant and should be accounted for during modeling. Two techniques were used to validate the % of unconjugated DOX generated during storage that was estimated by the mathematical model. Ultrafiltration using the same procedure described in the non-sink release section was performed on micelle suspensions immediately after reconstitution. The amount of DOX present in the sample before and after ultrafiltration was analyzed to calculate the % of DOX conjugated in the suspension. Secondly, micelle suspensions were passed through a Sephadex LH-20 column and the drug loading in the eluted volume pertaining to the MW of the copolymer was compared to drug load before Sephadex calculate the % of DOX conjugated.

7.2.5 Model Development

Several models have been developed for liposomal nanoparticles in which release is governed mainly by drug permeability through their phospholipid membrane.[50, 60, 63, 124, 127, 128, 130] Other models describing drug release from novel pharmaceutical formulations have

been developed and to incorporate effects such as Fickian diffusion, particle/drug dissolution, and polymer degradation/swelling;[203, 204] however, these models have not been applied to nanoparticle formulations. To our knowledge, no such model has been developed for a micelle formulation in which the drug has been conjugated to the copolymer scaffold of the micelle. Such a mechanistic model is developed here in collaboration with Dr. Ponta. The model incorporates two-phase release kinetics attributable to hydrazone bond hydrolysis of conjugated DOX as well as partitioning of unconjugated DOX into the micelle. These properties are illustrated by Scheme 7.1. For these studies, dynamic dialysis and ultrafiltration studies were used to probe and confirm DOX partitioning was a factor in release studies. The math for both types of release studies are described in the following sections.

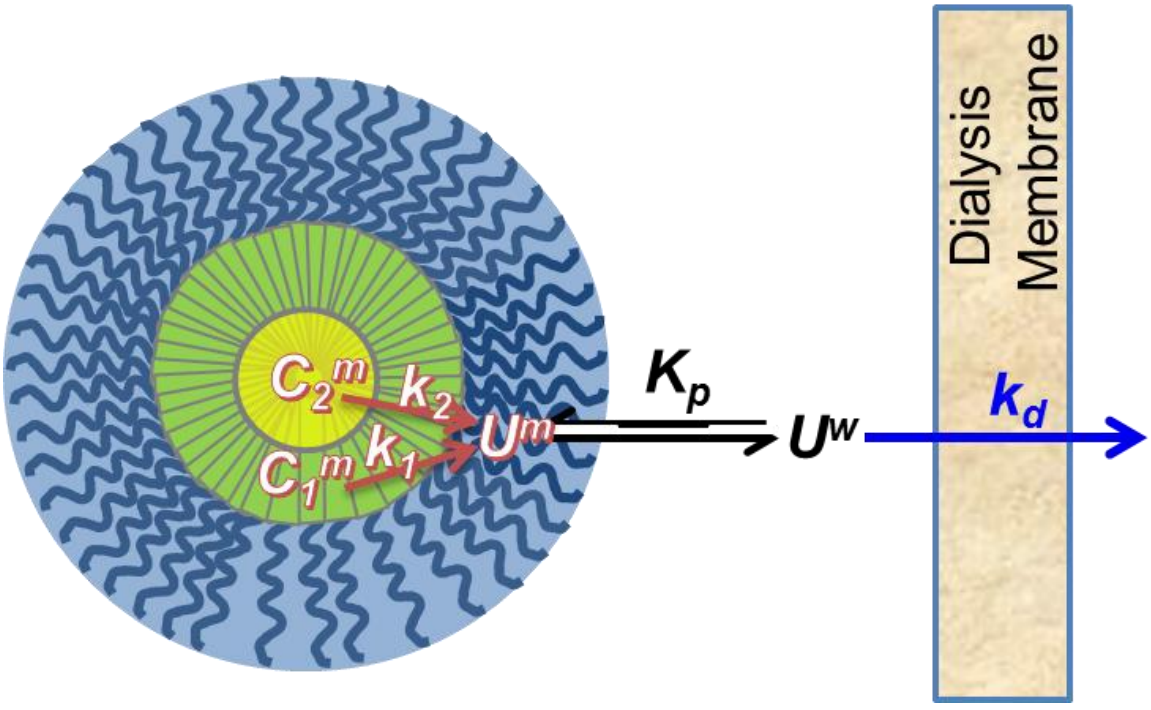

Scheme 7.1. An illustrated schematic of the mathematical model used to describe DOX release from the three different micelle formulations studied. Here, the hydrophilic PEG shell (blue) surrounds the polyaspartate core. In the

core, two populations of conjugated DOX are shown. These populations correspond to fast (C_1^m, green) and slow (C_2^m, yellow) hydrolysis of the hydrazone bond and their hydrolysis is governed by rate constants k_1 and k_2 respectively. After hydrolysis, unconjugated DOX may stay partitioned in the micelle nanoenvironment (U^m) or reside in the aqueous phase (U^w). This equilibrium is governed by the partition coefficient K_p. In dynamic dialysis studies, DOX transport though the dialysis membrane is governed by the rate constant k_d and concentration of U^w.

Drug release profiles for all three types of micelles and both pH conditions studied were fit using Micromath Scientist non-linear regression software using a weight factor or two.

7.2.5.1 Release studies monitored by ultrafiltration: non-sink conditions

In release studies monitored by ultrafiltration, the various species of DOX within the sample vial may be expressed by the mass balance below.

$$M_T = M_1^c + M_2^c + M_m^u + M_w^u \quad (1)$$

Here, M_T, M_1^c, M_2^c, M_m^u, and M_w^u, refer to the total amount of DOX in solution, conjugated DOX which undergoes fast hydrazone hydrolysis, conjugated DOX which undergoes slow hydrazone hydrolysis, and unconjugated DOX partitioned into the micelle and aqueous phases respectively. These terms may be rewritten as the concentrations of total DOX (D_T), conjugated DOX undergoing fast hydrolysis kinetics (C_1^m), conjugated DOX undergoing slow hydrolysis kinetics (C_2^m), and unconjugated DOX in micelle (U^m) and aqueous (U^w) phases can be related as described by equation 2.

$$D_T = bC_1^m + bC_2^m + bU^m + aU^w \quad (2)$$

Here, the volume fractions of aqueous and micellar phases (a and b respectively) are used to relate the total volume of the solution, V_T, to the volume of aqueous and micelle phases (V^w and V^m respectively). This is expressed by equations 3a and b.

$$a = \frac{V^w}{V_T}; b = \frac{V^m}{V_T} \quad \text{(3a \& b)}$$

In these studies, the density of the micelles was not known and assumed to be similar to that of water which allowed the weight fraction of micelle to be used for volume calculations. The values used for the different concentration of micelle solutions studied are found below in Table 7.1.

Table 7.1. Volume parameters used for mathematical modeling of DOX release from block copolymer micelles

Micelle Concentration	a	b
1.0 mg copolymer/mL	0.9990	0.0010
0.5 mg copolymer/mL	0.9995	0.0005
0.1 mg copolymer/mL	0.9999	0.0001

The differential equations which incorporate two-phase hydrazone hydrolysis kinetics and govern DOX release are shown below.

$$\frac{dC_1^m}{dt} = -k_1 C_1^m \quad \text{(4a)}$$

$$\frac{dC_2^m}{dt} = -k_2 C_2^m \quad \text{(4b)}$$

$$\frac{dU}{dt} = b(k_1 C_1^m + k_2 C_2^m) \quad \text{(4c)}$$

This system of differential equations may only be solved by defining the initial conditions for each equation. These conditions must incorporate the initial fraction of total DOX conjugated to the copolymer (f_c), the initial fraction of conjugated DOX in the fast hydrolysis phase (f) in relation to the total concentration of DOX initially present in solution ($C_{T,0}$). With these parameters, the initial conditions for equations 4a-c can be expressed.

$$C_1^m(0) = f_c \frac{f}{b} C_{T,0} \quad \text{(5a)}$$

$$C_2^m(0) = f_c\frac{(1-f)}{b}C_{T,0} \quad (5b)$$

$$U(0) = (1 - f_c)C_{T,0} \quad (5c)$$

Lastly, the concentration profile of DOX obtained by ultrafiltration (D^u) must defined. This was done by assuming D^u was composed of both conjugated DOX and DOX partitioned into the membrane. This is expressed by equation 6.

$$D^u = b(C_1^m + C_2^m + U^m) \quad (6)$$

Solving for U^m in terms of U is required to fit D^u. This may be performed by first defining a DOX partition coefficient as shown below.

$$K_p = \frac{U^m}{U^w} \quad (7)$$

Using this equilibrium expression and the mass balance relating U^m and U^w to the concentration of total unconjugated DOX, U^T (see equation 8),

$$U^T = aU^w + bU^m \quad (8)$$

U^m can be solved in terms of U as illustrated by the following equation.

$$U^m = \frac{K_pU}{a+bK_p} \quad (9)$$

Upon substitution into equation 6, the final equation for D^u is the result and shown below by equation 10.

$$D^u = b(C_1^m + C_2^m + \frac{K_pU}{a+bK_p}) \quad (10)$$

7.2.5.2 Release studies monitored by dynamic dialysis: sink conditions

Typically, dynamic dialysis is believed to maintain a "sink" for drug release if an adequately large reservoir volume is used to maintain the driving force for release and depletion of released drug from the compartment within the dialysis cassette. However, the rate of drug transport across the membrane may alter observed release kinetics if initial

drug release from the nanoparticle formulation is faster, similar,[49, 118, 197] or if a significant fraction of released drug binds to the dialysis membrane or the nanoparticle itself.[49, 118]

If one considers the compartment within the dialysis cassette in a context similar to that already defined in the ultrafiltration studies, the same differential equations governing C_1^m and C_2^m and the mass balances developed there (Equations 1 – 4b) may be used. However, the differential equation governing unconjugated drug (Equation 4c) must be rewritten to include DOX diffusion through the dialysis membrane and accumulation in the reservoir compartment. These events are expressed by equations 11a and b with the parts in **red** indicating the features unique to dynamic dialysis.

$$\frac{dU}{dt} = b(k_1 C_1^m + k_2 C_2^m) - k_d(aU^w - R) \tag{11a}$$

$$\frac{dR}{dt} = k_d f_R(aU^w - R) \tag{11b}$$

Here, R accounts for DOX concentration in the reservoir compartment and f_R is the volume ratio of dialysis tube to reservoir (9/5000). With such a large reservoir volume relative to the dialysis cassette volume ($f_R \rightarrow 0$), the reservoir concentration can be assumed to be negligible ($R \cong 0$), $\frac{dR}{dt}$ may be ignored, and equation 11a may be simplified to the following equation:

$$\frac{dU}{dt} = b(k_1 C_1^m + k_2 C_2^m) - ak_d U^w \tag{12}$$

Based on this equation, removal of unconjugated DOX from the dialysis cassette is dependent upon a rate constant for DOX transport across the dialysis membrane, k_d, and the concentration of unconjugated drug in the aqueous phase, U^w. Using Equations 7 and 8, U^w may be rewritten in terms of U and substituted back into equation 12. This is shown by equations 13a and b.

$$U^w = \frac{U}{a+bK_p} \tag{13a}$$

$$\frac{dU}{dt} = b(k_1 C_1^m + k_2 C_2^m) - k_d \frac{aU}{a+bK_p} \tag{13b}$$

The initial conditions for this system of differential equations are identical to those used in the ultrafiltration equations (5a-c).

As a control, spike experiments were also conducted to monitor the effect DOX partitioning had on the disappearance of unconjugated DOX. This was accomplished by dialyzing the micelle solution for 72 hours in release medium to minimize the amount of conjugated DOX before spiking with free DOX. The differential equations are the same for these experiments as those used for release studies utilizing conjugated DOX (Equations 3a, 3b, and 13b). The initial conditions for spike experiments, however, required the concentration of conjugated DOX left after 72 hours of dialysis to be accounted for in the initial conditions. These corrections are reflected in Equations 14a-c where the terms in **blue** indicate the parameters unique to the spike experiments.

$$C_1^m(0) = f_c \frac{f}{b} C_{T,0} e^{-72k_1} \tag{14a}$$

$$C_2^m(0) = f_c \frac{(1-f)}{b} C_{T,0} e^{-72k_2} \tag{14b}$$

$$U(0) = C_{ST,0} \tag{14c}$$

In addition to the terms present in the initial conditions already introduced by Equations 5a-c (f_c, f, and $C_{T,0}$), the time the micelle solutions were already dialyzed against release medium used a monoexponential decay for both the fast and slow compartments (with rate constants k_1 and k_2 respectively). Because the solution was spiked with DOX solution, the concentration of this unconjugated DOX, $C_{ST,0}$, was used in equation 14c.

Lastly, dialysis of DOX solutions was also conducted to accurately estimate the rate of unconjugated DOX transport across the dialysis membrane. Since no micelle material is

present in these studies, the release of total DOX concentration, D_T, may be expressed by equation 15a and its initial conditions are simply the initial concentration of dissolved DOX in solution (Equation 15b).

$$\frac{dD_T}{dt} = -k_d D_T \quad (15a)$$

$$D_T(0) = C_{T,0} \quad (15b)$$

7.3 Results

7.3.1 Micelle characterization

Characterization of the DOX-conjugated copolymers was reported elsewhere by Dr. Ponta.[202] Upon addition to aqueous solution, these copolymers formed micelles with drug loading of 26 ± 1.6, 17 ± 1.5, and 26 ± 1.1% by weight while the particle size obtained from dynamic light scattering resulted in hydrodynamic diameters of 117 ± 37, 54 ± 12, and 58 ± 11 nm for the HYD, ABZ, and GLY micelles respectively. Measurements of ζ-potential were also taken and found to be 13 ± 0.2, -4.0 ± 0.6, and 0.5 ± 1.5 mV for the HYD, ABZ, and GLY micelles respectively. Values reported here are averages of triplicate measurements along with the resulting standard deviation.

7.3.2 Validation of free DOX removal for methods used to monitor release

Both release methods employed in this study have unique conditions which may affect analysis of release kinetics from observed release profiles.[118, 130, 197] In the case of dynamic dialysis, significant drug binding or absorption may dominate the kinetics observed during release studies and skew the determination of rate constants and other parameters intrinsic to the nanoparticle/drug system.[118] To assess this factor, free DOX solutions (pH 5.0 and 7.4) were dialyzed under the same conditions used in the micelle release studies. During these studies, the biphasic release anticipated if DOX binding to the dialysis membrane was

not evident, indicating the use of a rate constant for DOX transport across the dialysis membrane was sufficient for modeling purposes.

Analysis of ultrafiltration studies is affected by incomplete removal of unconjugated drug during the centrifugation and washing steps.[130, 197] In the context of these release studies, ultrafiltration must remove unconjugated DOX in the aqueous phase from the DOX remaining in the micelle. This was validated two ways. First, free DOX was dissolved in a 50% methanol:water mixture and underwent the ultrafiltration process described in the methods section. After the ultrafiltration process, spectrometric analysis determined that no DOX was present in the concentrate. The second confirmation used two identical block copolymer solutions. The ultrafiltration was performed on three micelle solutions and three more solutions that were spiked with free DOX. Comparison of DOX present in the concentrate after ultrafiltration confirmed complete DOX removal as there was no statistical difference between the group of solutions that was or was not spiked with free DOX.

7.3.3 Model-predicted micelle instability during storage confirmed by other experimental methods

Initial modeling of the release profiles of DOX required a fraction of DOX to be unconjugated, f_c, at the beginning of the release studies for the 0.1 and 0.5 mg micelle/mL solutions unlike the 1.0 mg micelle/mL solutions which indicated 100% of DOX was initially conjugated. While the DOX release studies at 1.0 mg micelle/mL solutions were conducted shortly after synthesis (within two weeks), the other micelle solutions were constituted from freeze-dried block copolymer material that had been stored at -20 °C for approximately 15 months.

Hydrdazone degradation during storage seemed like a plausible explanation; however, such degradation has not been previously reported for these micelle systems and was

unexpected. Confirmation that the model-predicted degradation was indeed a factor in the discrepancies seen in release profiles at different micelle concentrations was confirmed experimentally by comparing the DOX concentrations before and after ultrafiltration. Analysis of drug loading before and after running the stored copolymer material through a Sephadex column to separate free DOX from the DOX-conjugated copolymer was also performed as a second validation. Values of the percentage of conjugated DOX ($f_c \times 100\%$) calculated from the results of these methods along with those from mathematical modeling were similar as illustrated by Figure 7.1. Averaging the values obtained from all four methods for all three micelle formulations resulted in an average percent of DOX conjugated of 63 ± 3% (95 % CI) after 15 months of storage. For further regression analysis, this parameters was fixed for the value obtained from size exlculsion experiments (67, 68, and 69 % for HYD, ABZ, and GLY, respectively) to increase the statistical strength of the fitted release parameters.

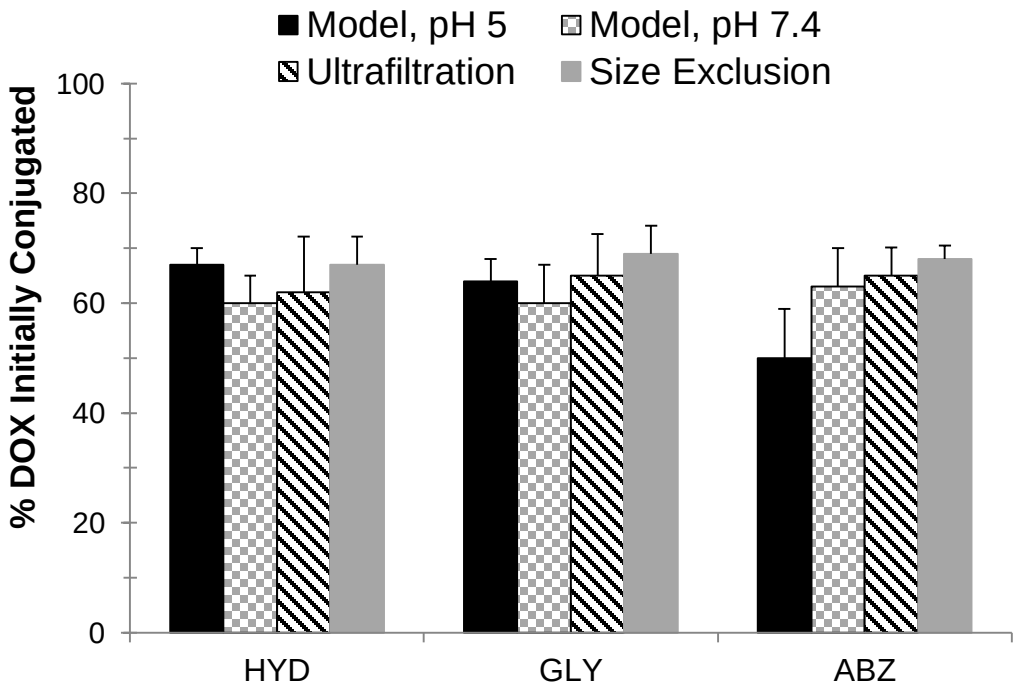

Figure 7.1. The graph above displays the % of DOX conjugated ($f_c \times 100\%$) after 15 months of storage determined by mathematical modeling (under both pH conditions DOX release was monitored) and two other experimental methods (see legend at the top). Error bars represent 95% confidence intervals.

7.3.4 Characterization of release kinetics of HYD DOX-conjugated block copolymer micelles

For the HYD micelles, both release profiles obtained from ultrafiltration and dynamic dialysis (including all three micelle concentrations, spike experiments, and dialysis of free DOX only) were simultaneously fit to the mathematical release models described in the model development section. By fitting these profiles, the effects of DOX transport through the dialysis membrane and the % of unconjugated DOX present due to hydrazone degradation during storage could be separated from the intrinsic parameters to be estimated for the DOX/HYD system. The experimental release profiles along with the resulting profiles obtained by the model-fitted release parameters (see Table 7.2) are shown below in Figure 7.2a and b for release in pH 5.0 and 7.4 medium respectively. Based on the values reported in Table 7.2, the main parameters affected by pH are not the rate constants, but partitioning (K_p) and the fraction of conjugated DOX in the phase fast phase (f) at each pH.

Table 7.2. Values of release parameters fitted to mathematical model to describe DOX release from micelle formulations at pH 5.0 and 7.4

Micelle	pH	k_1 (hr^{-1})	$k_2 \times 10^2$ (hr^{-1})	k_d (hr^{-1})	$K_p \times 10^{-3}$	f
HYD	7.4	0.24 ± 0.1	0.55 ± 0.1	0.81 ± 0.03	2.5 ± 0.6	0.38 ± 0.06
ABZ	7.4	0.27 ± 0.2	0.36 ± 0.1	0.79 ± 0.03	1.1 ± 0.8	0.34 ± 0.06
GLY	7.4	0.30 ± 0.1	0.46 ± 0.1	0.80 ± 0.03	2.2 ± 1	0.25 ± 0.04
HYD	5.0	0.29 ± 0.05	0.45 ± 0.1	0.80 ± 0.03	0.62 ± 0.2	0.68 ± 0.03
ABZ	5.0	≥ 1.15*	0.59 ±0. 2	0.78 ± 0.03	0	0.36 ± 0.05
GLY	5.0	0.64 ± 0.5	0.82 ± 0.1	0.77 ± 0.02	0	0.20 ± 0.05

Values are reported along with 95% confidence intervals

*Value used for generation of statistics as release of fast phase was rate-limited by DOX transport through the dialysis membrane

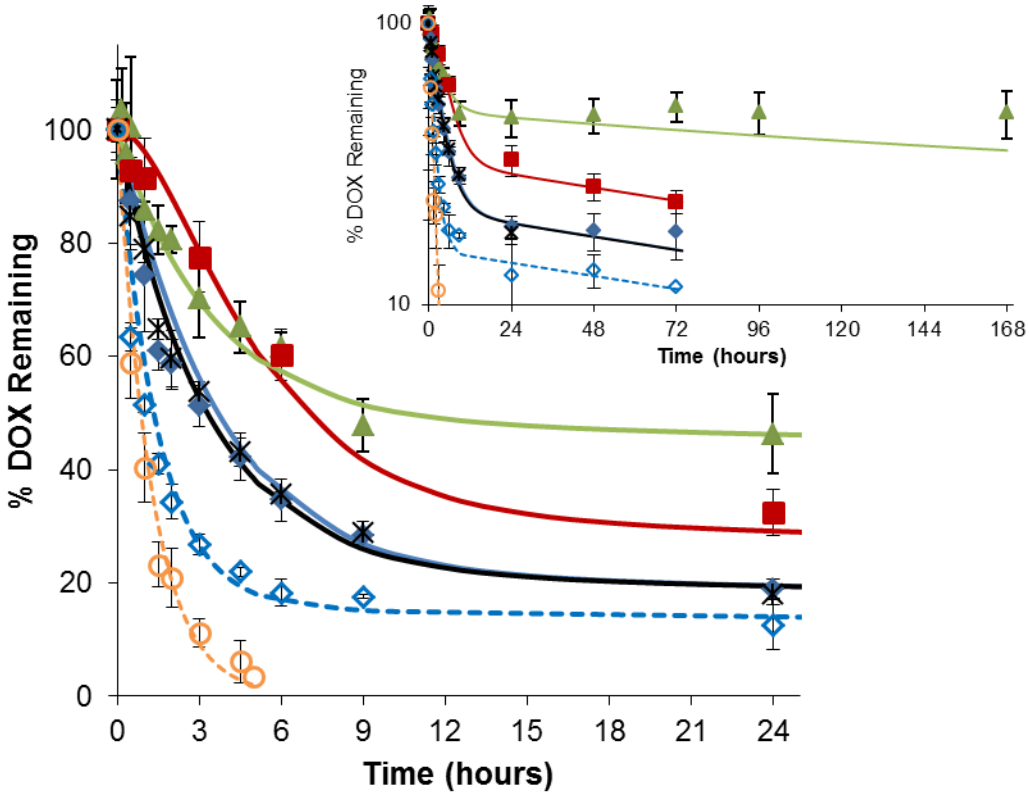

A.

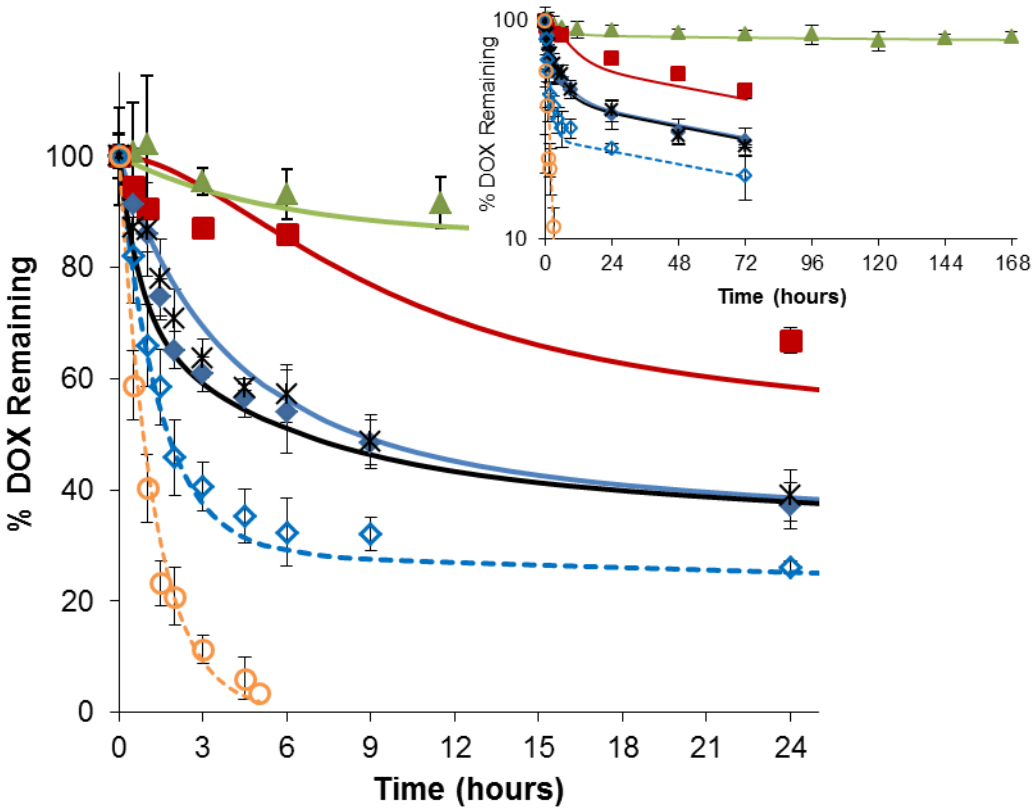

B.

Figure 7.2. DOX release profiles at pH 5.0 (A) and 7.4 (B) obtained for HYD micelles. The same symbols are used to describe the micelle concentrations and methods at both pH conditions. The release profile obtained by ultrafiltration of a 0.5 mg copolymer/mL solution is shown (▲) in addition to release profiles obtained by dynamic dialysis of micelle solutions composed of 1.0 (■), 0.5 (◆), and 0.1 (×) mg copolymer/mL. Additionally, the profile of free DOX (0.12 mg/mL) allowed to dialyze from the cassette (○) and the DOX release profile obtained by dynamic dialysis of a 0.5 mg copolymer/mL solution (which had been dialyzed for 72 hours in release media to remove conjugated DOX) spiked with 0.1 mg/mL of free DOX (◇) are also shown to reflect DOX transport across the dialysis membrane and the effect DOX partitioning to the micelle has on DOX transport out of the dialysis cassette respectively. The lines of corresponding color to the symbols represent the simulated release profiles at those conditions generated by the fitted parameters reported in Table 7.2 using the mathematical model developed. The inset at the top right of each plot reflects the entire time course release was monitored while the initial phase of release is shown in the

main plot. Error bars indicate the standard deviation of triplicate release studies at each time point.

Using both ultrafiltration and dynamic dialysis methods to monitor release, DOX partitioning could be identified and shown to affect DOX release profiles. Based on the success of this mechanistic model to describe DOX release from HYD, the same model was applied to the GLY and ABZ formulations to generate constants which described their release profiles.

7.3.5 Characterization of release kinetics of DOX-conjugated block copolymer micelles with GLY and ABZ spacers

Release studies of GLY and ABZ micelles showed similar biphasic release profiles as those observed with HYD by the dynamic dialysis method. This is illustrated by the release profiles in Figure 7.3. However, release profiles could not be obtained by the ultrafiltration method for these micelles. This was likely due to the smaller amount present in the fast phase for these solutions at pH 5.0 and then worsened by the added effect of DOX partitioning at pH 7.4. Because ultrafiltration was not possible with these formulations, DOX partitioning was dependent upon the initial (fast) phase of release in conjunction with the multiple concentrations studied.

Based on the values reported in Table 7.2, several comparisons can be made between these spacer-modified micelles and the HYD micelles which lack such a spacer. Like the HYD micelles, DOX partitioning, K_p, is higher at pH 7.4 than at pH 5.0; however, comparing the values of each formulation to each other is difficult due the large variability indicated by the confidence intervals. This is not unexpected as K_p is mainly determined in the fast phase of release observed during dynamic dialysis. In these micelles, this fast phase is the minor phase of release. Furthermore, this section of the release profile is also complicated by the

effects of free DOX present in the 0.1 and 0.5 mg copolymer/mL micelle solutions. Unlike the HYD micelles however, the fraction of DOX release in the fast phase, *f*, was similar for release studied at pH 5.0 and 7.4 for both the GLY and ABZ micelles. In addition, the rate constants of fast hydrazine hydrolysis, k_1, also appear to be pH-sensitive in contrast to the HYD micelles. For GLY, the value of k_1 is higher at pH 5.0 than at pH 7.4, but the variability of this value is high. This is not surprising as the value estimated is similar to the rate constant of DOX diffusion through the dialysis membrane (k_d) and again its estimation is complicated due to the significant amount of unconjugated DOX released in the profiles obtained from the 0.5 and 0.1 mg copolymer/mL solutions. This effect essentially results in a triphasic release profile in which the phase governed by k_1 is reduced due to the fast phase represented by unconjugated DOX initially present. For the ABZ micelles at pH 5.0, the exact value of k_1 could not be determined as the fast phase of release was rate-limited by DOX transport. During modeling, it was determined that k_1 needed to be at least 1.15 hr^{-1} to adequately fit the release profiles. This value is only a lower limit for k_1 for for hydrazone hydrolysis of ABZ under pH 5.0 conditions which indicates that release at pH 5.0 for ABZ is the fastest of the micelle formulations.

The terminal phase (i.e. slow hydrzazone hydrolysis phase) was similar for all three micelle formulations at both pH conditions studied. Only DOX release from GLY micelles at pH 5.0 was different, resulting in a hydrazone hydrolysis rate constant of the slow phase, k_2, to be nearly twice as fast that from the HYD micelles and was statistically different.

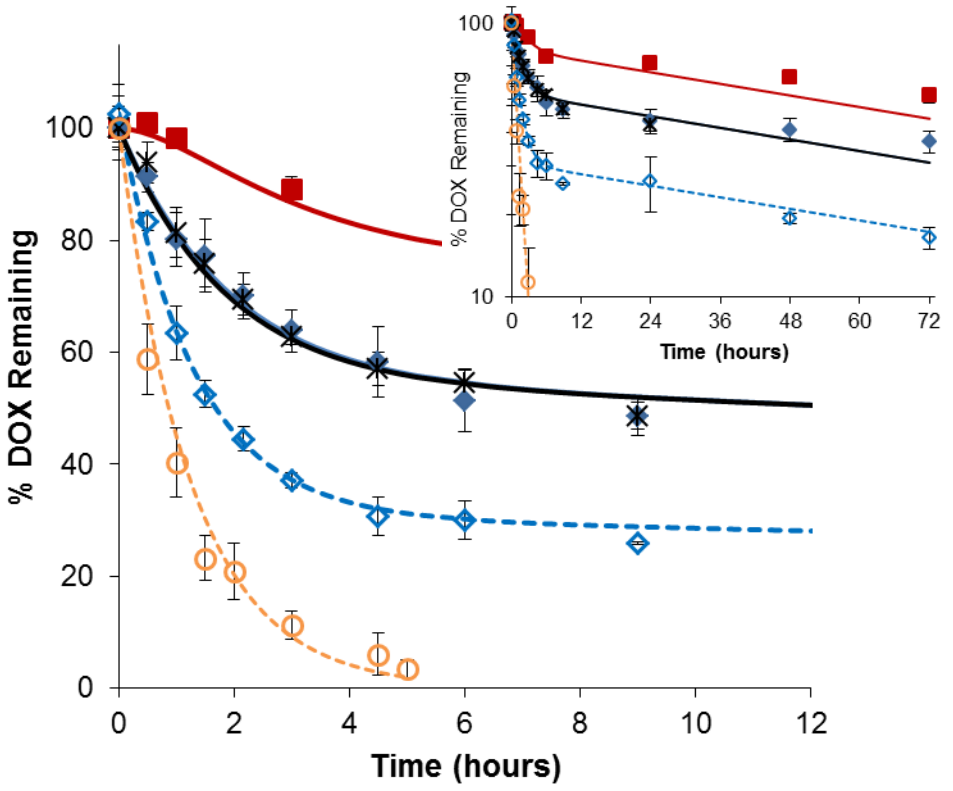
% DOX Remaining
Time (hours)
0
20
40
60
80
100
0
2
4
6
8
10
12
% DOX Remaining
Time (hours)
10
100
0
12
24
36
48
60
72

A.

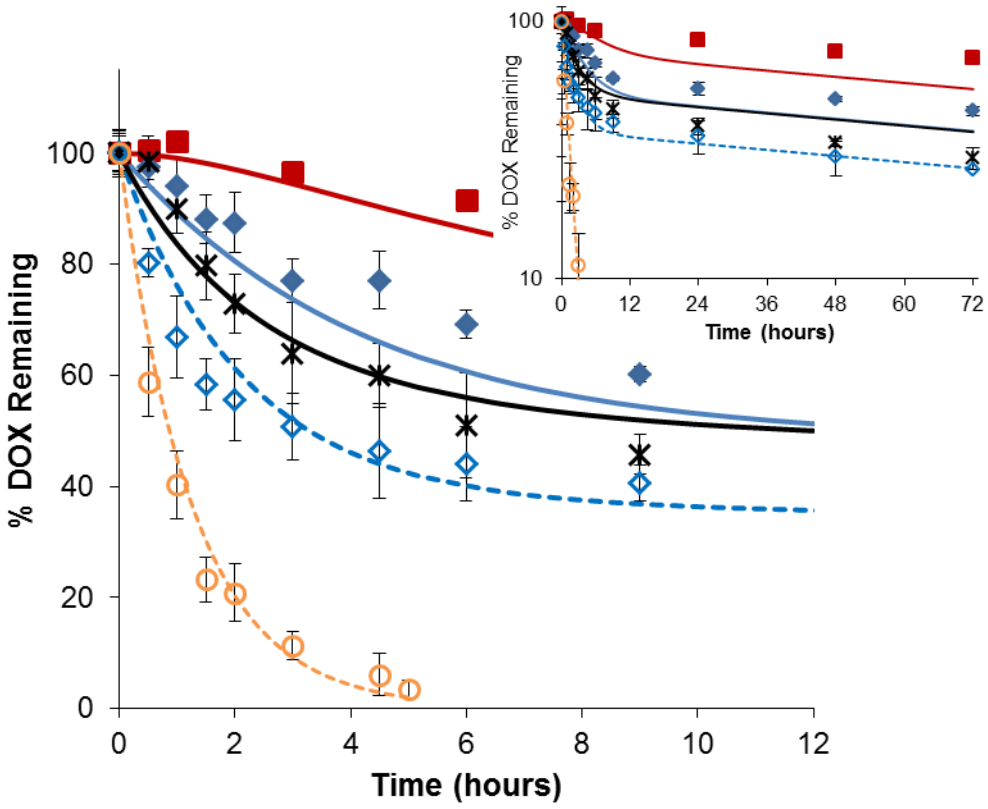
% DOX Remaining
Time (hours)
0
20
40
60
80
100
0
2
4
6
8
10
12
% DOX Remaining
Time (hours)
10
100
0
12
24
36
48
60
72

B.

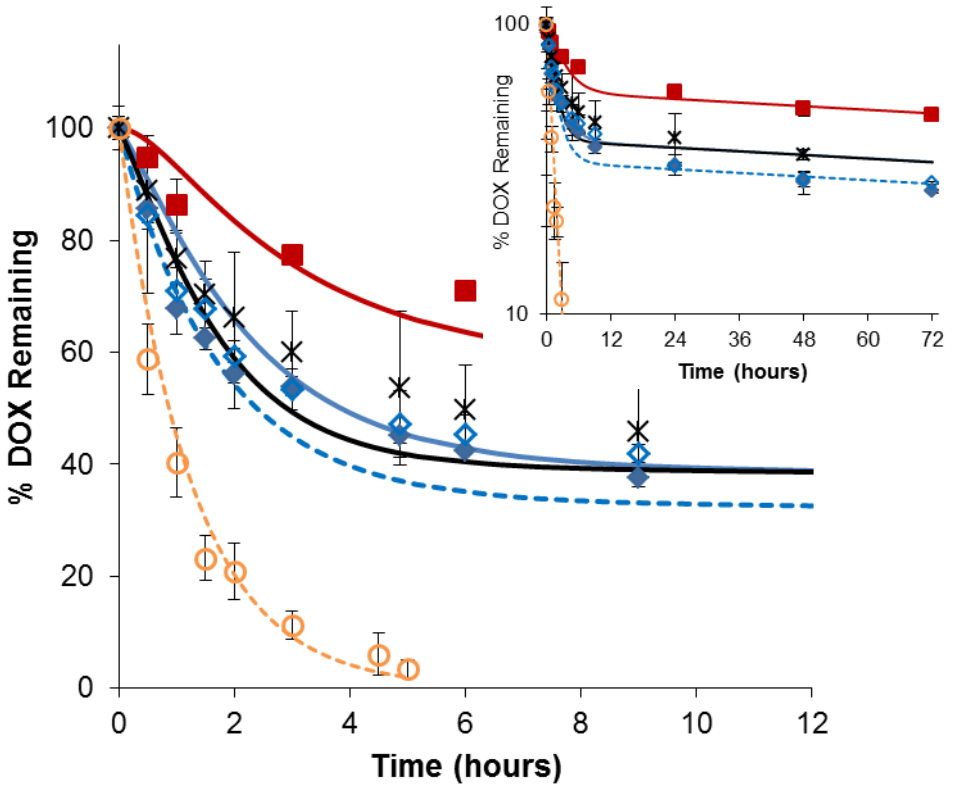
% DOX Remaining
Time (hours)
100
80
60
40
20
0
0
2
4
6
8
10
12
% DOX Remaining
Time (hours)
100
10
0
12
24
36
48
60
72

C.

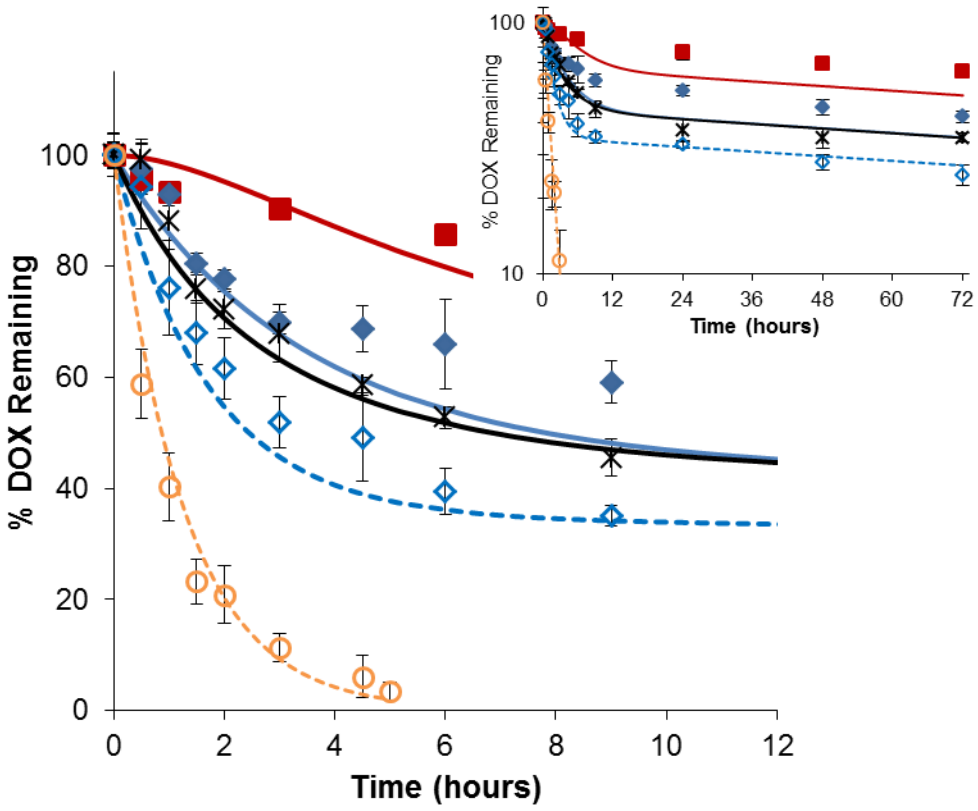
% DOX Remaining
Time (hours)
100
80
60
40
20
0
0
2
4
6
8
10
12
% DOX Remaining
Time (hours)
100
10
0
12
24
36
48
60
72

D.

Figure 7.3. DOX release profiles obtained for GLY micelles at pH 5.0 (A) and 7.4 (B) along with those obtained for ABZ micelles at pH 5.0 (C) and 7.4 (D). The symbols used here indicate the same conditions as those used in Figure 7.2. The release profiles obtained by dynamic dialysis of GLY and ABZ micelle solutions composed of 1.0 (■), 0.5 (◆), and 0.1 (×) mg copolymer/mL are shown. The profiles of free DOX (0.12 mg/mL) allowed to dialyze from the cassette (○) and the DOX release profile obtained by dynamic dialysis of a 0.5 mg copolymer/mL solution solution (which had been dialyzed for 72 hours in release media to remove conjugated DOX) spiked with 0.1 mg/mL of free DOX (◇) are also shown to reflect DOX transport across the dialysis membrane and the effect DOX partitioning to the micelle has on DOX transport out of the dialysis cassette respectively. The lines of corresponding color to the symbols represent the simulated release profiles at those conditions generated by the fitted parameters reported in Table 7.2. The inset at the top right of each plot reflects the entire time course release was monitored while the initial phase of release is shown in the main plot. Error bars indicate the standard deviation of triplicate release studies at each time point.

7.4 Discussion

7.4.1 Strengths and limitations of micelle release model and methods used

7.4.1.1 Instability of hydrazone bond under storage conditions identified with mathematical modeling

DOX degradation under the specified storage conditions was unprecedented and illustrates a prime example of the usefulness of mathematical modeling of drug release in nanoparticle systems. Without such modeling, the instability of the hydrazone linkage would likely not have been identified until much later in the development process if at all.

In addition to identifying this instability, the fact that a single value of f_c could be fit to both fast and slow release phases indicates that the structure of the copolymer material in

its freeze-dried state does not possess the same domains or microenvironments as those of the micellar structure formed in solution.

While modeling was able to identify hydrazone degradation, the mechanism behind degradation was beyond the scope of the model. However, several possible modes of degradation could be hypothesized. First, DOX could have been hydrolyzed during the freeze-drying process prior to storage. This is unlikely since all the material was freeze-dried (including the material used for drug release studies at a 1.0 mg/mL block copolymer concentration) before any analysis on DOX content was performed. According to modeling, the percent of DOX conjugated was 100% for the 1.0 mg copolymer/mL release studies performed shortly after synthesis. If DOX degraded during freeze-drying, the percent of conjugated DOX would have been similar to that observed by release studies performed with copolymer material that had been stored for 15 months.

The next logical explanation would be degradation due to trace amounts of water still present or introduced after the freeze drying process. In a previous study, hydrazone degradation of a DOX conjugate was shown to undergo degradation after lyophilization during storage at cooler temperatures (2 – 8 °C).[198] In that study, the amount of water in lyophilized samples was approximately 2% and resulted in 20% degradation of the hydrazone bond after 12 months. Storage of the copolymer material in this study, however, was stored over a longer period of time but at colder temperatures. Because PEG is hydrophilic, the PEG chains here may have retained more water residue than the samples in this earlier study. Increased water residue in the lyophilized cake could lead to increased hydrazone degradation. This was surmised to be the most likely scenario but additional studies are required to elucidate the conditions attributing to degradation.

7.4.1.2 Probing contributions of DOX partitioning and DOX hydrolysis kinetics on release using sink and non-sink conditions

The terminal phase of release in these profiles is quite slow and could be the result of slow hydrolysis kinetics of the DOX-hydrazone bond, DOX partitioning, or a combination of these effects. Distinguishing these effects using only dynamic dialysis or ultrafiltration methods to monitor release is problematic. By using both methods for the HYD release studies, the effects of partitioning and slow DOX release become apparent as the % of DOX removed is greater in all release profiles obtained from dynamic dialysis (at both pH conditions studied) than the extent of DOX release monitored by ultrafiltration. This observation indicates partitioning of unconjugated DOX into the micelle is present for both micelle formulations but not the sole contributor to the terminal release phase as reflected by the values in Table 7.2.

7.4.1.3 Concentration effects of conjugated and unconjugated DOX on partitioning

While both methods provide the ability to ascertain hydrazone hydrolysis kinetics and partitioning effects, the simple model used here is still limited in its description of the entire release profile due to the complexity of the micelle system. Because DOX is conjugated and initially a large percentage of the micelle (i.e. high drug loading),[83] it is reasonable to expect that in addition to pH, *Kp* is also a function of the amount of DOX conjugated and the concentration of unconjugated, partitioned DOX. Such an effect was previously proposed in liposomal studies for a different drug and was attributed to self-association effects.[197] In the case of micelles however, these high DOX concentrations (conjugated or unconjugated) may alter the properties (e.g. charge, hydrophobicity) of the micelle environment itself. This is evident in both Figures 7.2a and b where the fitted release profiles systematically predict slower release than that seen at several conditions release studies were performed. This aging effect is revealed because the K_p estimated from the ultrafiltration profiles relies more

heavily on the terminal phase of release. At this stage in the release study, significant hydrolysis (i.e. release) has occurred as opposed to dynamic dialysis in which the effects of K_p are more pronounced during the initial burst phase of release. In Figure 7.2b, the release profiles of DOX at 0.5 and 0.1 mg micelle/mL are initially faster as the amount of DOX conjugated is much higher; however, the spike profile is simulated well. This supports the notion of aging effects as the micelle samples used in spike experiments had already undergone significant DOX release and were ultimately more reflective of the micelle environment at the end of the ultrafiltration studies.

In the release studies conducted with GLY at pH 7.4 (Figure 7.3b), errors in the initial phase of release are also present; however, it is not the systematic error of slow release seen in HYD release studies since ultrafiltration studies were not possible with these formulations and do not share in this bias. In these release studies, K_p is ultimately determined by the initial phase of DOX release observed in each profile. This is well illustrated by the pH 7.4 release profiles where DOX partitioning was indicated to be significant. In the GLY studies, the initial phase of release observed in the spike experiment is predicted to be slower by the model due to the slower release seen in this initial phase at 0.5 and 0.1 mg micelle/mL concentrations. This would suggest that DOX partitioning may become diminished at later time points after significant amounts of DOX have been released. Similar trends are seen to a lesser extend in the ABZ pH 7.4 release profiles as K_p is lower for these micelles than the K_p estimated for GLY. Such an explanation also explains the high error in K_p values since it is averaging micelle formulations with different aging effects.

7.4.2 Effect of unconjugated DOX partitioning into micelle on observed drug release under non-sink and sink conditions

The amount of drug released in non-sink studies will vary depending upon the partitioning of unconjugated DOX into the micelle (K_p). This effect is shown by Figure 7.4 by comparing the release profile observed for HYD release at pH 5.0 with a simulation of the profile if no binding occurred.

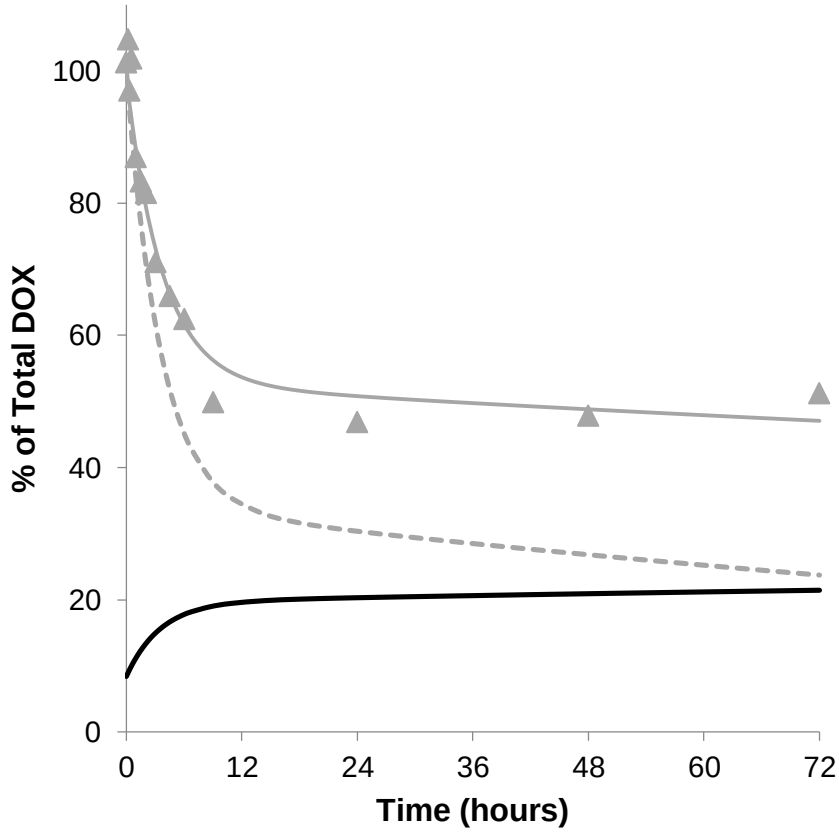

Figure 7.4. Simulation of HYD pH 5.0 release profile under non-sink conditions. Using the rate constants provided in Table 7.2. The % of DOX remaining in the ultrafiltered samples analyzed during release (▲) along with the fit using the mechanistic model developed (—) are shown and compared to a simulation of that profile if there was no partitioning of unconjugated DOX ($K_p=0$) into the micelle (- - -). Based on the values in Table 7.2, the amount of unconjugated DOX that partitioned into the micelle was also simulated as a % of total DOX present in the solution (—).

This partitioning effect in conjunction with the rate of DOX transport through the dialysis membrane has implications on the pH-sensitive nature of the initial phase of release observed from dynamic dialysis. This is illustrated by Figure 7.5. Here, the release profile of 1 mg/mL GLY at pH 7.4 was simulated based on the values reported in Table 7.2 and compared to the simulated profile of drug remaining in the dialysis tube still conjugated to the block copolymer micelles. It is evident that the lag seen in DOX release is due to the accumulation of free DOX. This is expected based on previous reports of a similar lag in drug release seen with liposomal nanoparticles using dynamic dialysis.[63, 118, 197] This effect is exaggerated at pH 7.4 where all formulations have a higher K_p. The high partitioning of DOX at pH 7.4 reduces the rate DOX is able to leave the dialysis cassette and thus contributes to the slower release seen at pH 7.4. This is clearly illustrated by Figure 7.5 which compares the release profile of 1 mg/mL GLY at pH 7.4 with a simulation of this profile if K_p were zero (i.e. no partitioning). If DOX partitioning was not present, observed release would be faster. This is also apparent by the rate of unconjugated DOX accumulation in the dialysis cassette, $\frac{dU}{dt}$, (also shown in Figure 7.5). Here, the accumulation phase (when the rate is positive) lasts much longer than it would if there was no binding of unconjugated DOX.

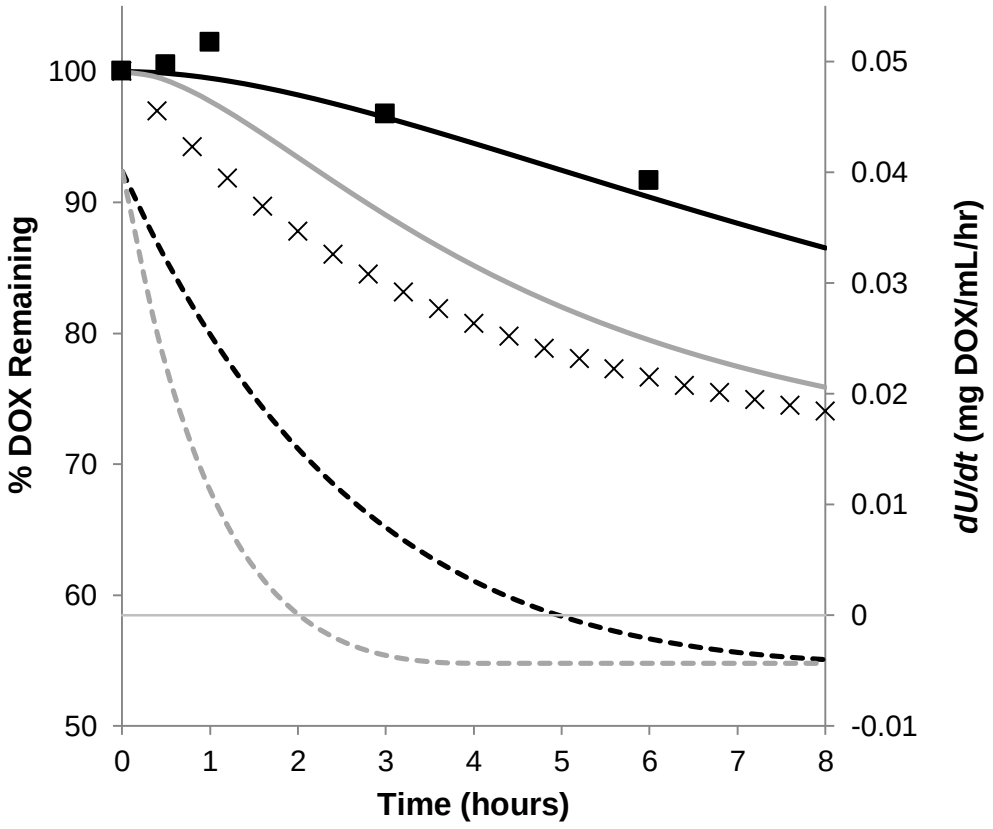

Figure 7.5. The effect of unconjugated DOX partitioning is illustrated for dynamic dialysis release studies. Here, the initial portion of the DOX release profile from a 1.0 mg GLY/mL solution at pH 7.4 (■) is shown along with the profile generated by the mathematical model (⎯⎯) using the values listed in Table 7.2. This is compared to a simulation of the expected release profile if only conjugated DOX was monitored (×). This comparison indicates significant accumulation of released DOX within the dialysis cassette during the initial phase of release. Furthermore, when the observed release profile is compared to the simulated profile which assumes K_p is zero (⎯⎯), the initial phase of release is shown to be further slowed by DOX partitioning. This is also supported by the differences in the rate of accumulation and depletion of unconjugated DOX in the dialysis cassette ($\frac{dU}{dt}$) during dynamic dialysis of the micelle formulation. The accumulation phase (positive values) of unconjugated DOX in the dialysis cassette when binding is considered (- - -) is over double that if there were no binding (- - -).

These effects can be can be better understood by thinking of the effective rate constant for DOX transport out of the dialysis cassette as:

$$k'_d = \frac{ak_d}{a+bK_p} \tag{16}$$

which takes into the account the fraction of unconjugated drug that is in the aqueous phase. The equation uses the volume coefficients of the aqueous and micelle phases (a and b respectively) and the DOX partitioning coefficient, K_p. These effects on k'_d and subsequently the effective half-life of DOX transport out of the dialysis cassette in the presence of block copolymers ($t_{1/2} = \frac{\ln(2)}{k'_d}$) was simulated in Figure 7.6a and b respectively for several micelle concentrations. Based on the parameters generated by the mathematical model, k'_d and $t_{1/2}$ are also plotted for the micelles studies at the two pH conditions employed. As these figures show, increases in K_p and micelle concentration both decrease k'_d and increase the half-life of free DOX transport from the dialysis cassette.

Both of these effects can be considered simultaneously by calculating the free fraction in the aqueous phase, $f^w = \frac{a}{a+bK_p}$. Using f^w, a general trend can be surmised for k'_d and $t_{1/2}$ for all micelle concentrations employed. These trends are illustrated by Figure 7.6c.

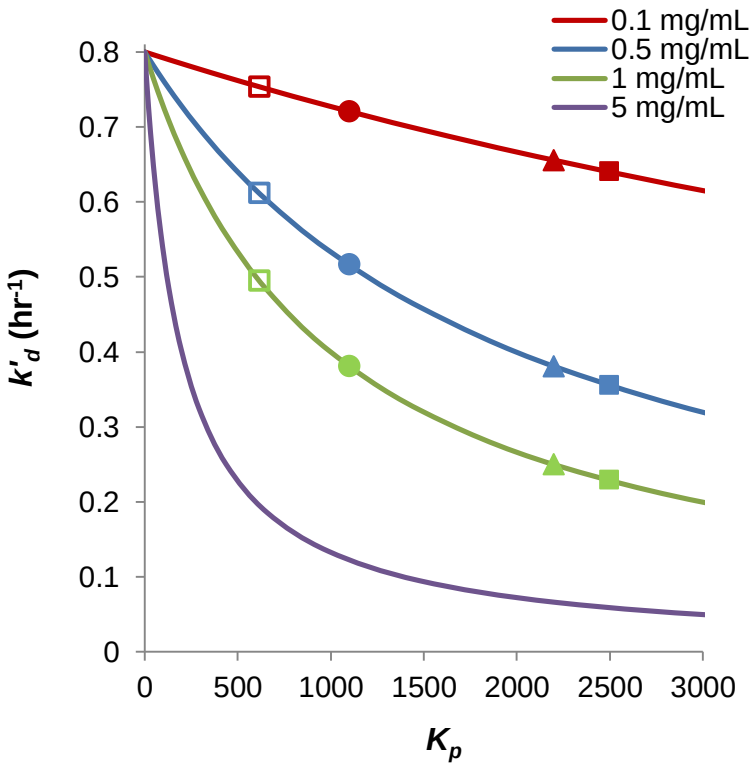
0.1 mg/mL
0.5 mg/mL
1 mg/mL
5 mg/mL
0.8
0.7
0.6
0.5
0.4
0.3
0.2
0.1
0
k'd (hr-1)
0
500
1000
1500
2000
2500
3000
Kp

A.

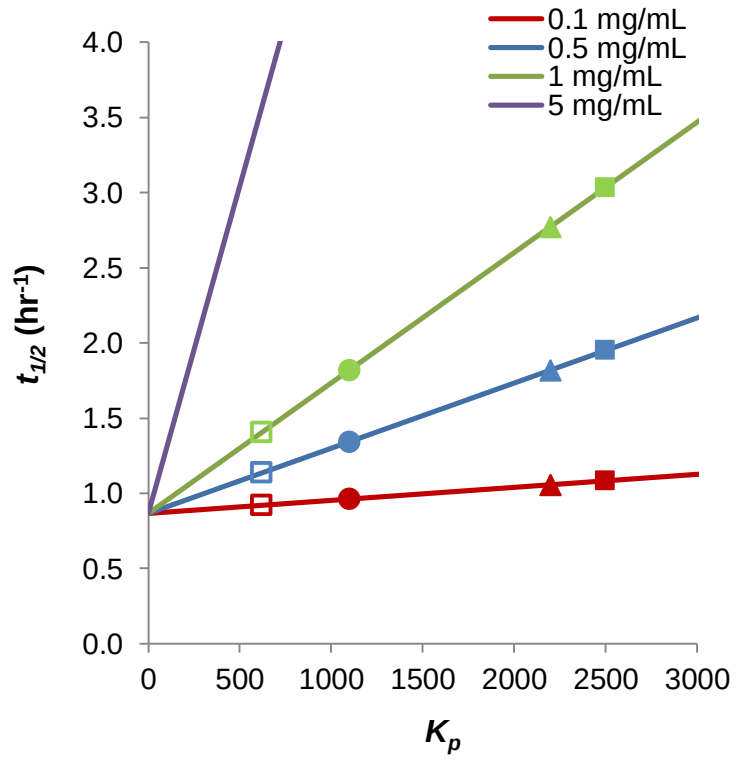
0.1 mg/mL
0.5 mg/mL
1 mg/mL
5 mg/mL
4.0
3.5
3.0
2.5
2.0
1.5
1.0
0.5
0.0
t1/2 (hr-1)
0
500
1000
1500
2000
2500
3000
Kp

B.

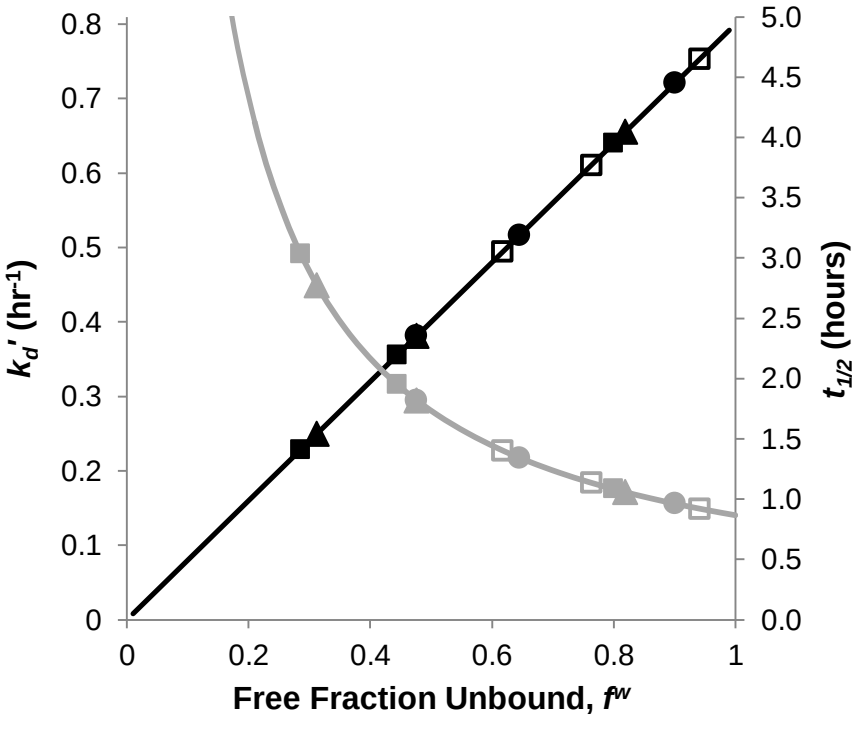

C.

Figure 7.6. The effect of micelle concentration and partioning of unconjugated DOX (K_p) on the effective rate constant, k'_d, (A) and half-life, $t_{1/2}$, (B) of unconjugated DOX transport from the dialysis cassette. Lastly, micelle concentration and K_p can be used to determine the fraction of unconjugated DOX unbound to the micelle, f^w (C). The use of f^w results in a more general trend with k'_d (—) and $t_{1/2}$ (—). In these plots, the symbols ■, ▲, and ● refer to the values calcualted for HYD, GLY, and ABZ at pH 7.4 based on the parameters generated in Table 7.2. Their color corresponds to the conditions designated by the trend line they are related with. The opened symbols of the same shape correspond to values calculated from pH 5.0 release parameters.

7.4.3 Intrinsic factors governing micellar DOX release

7.4.3.1 pH-dependent DOX partitioning

The effects of DOX partitioning on observed drug release has already been explained; however the reason why partitioning is higher for all micelles at higher pH is also significant

and should be addressed. The partitioning seen here may be due to change DOX speciation as a function of pH. This is illustrated below in Scheme 7.2. DOX is a weak base with a pKa of 8.2.[107] As the pH is increased over the region studied, the fraction of DOX in its neutral base from increases over 200 fold. If only the neutral form contributed to binding, the partitioning DOX in GLY and ABZ micelles at pH 5.0 would be 10 and 5. These values are too small to affect release kinetics at the micelle concentrations employed in dynamic dialysis studies, making this a plausible explanation for the considerable difference in DOX partitioning between pH 5.0 and 7.4 studies.

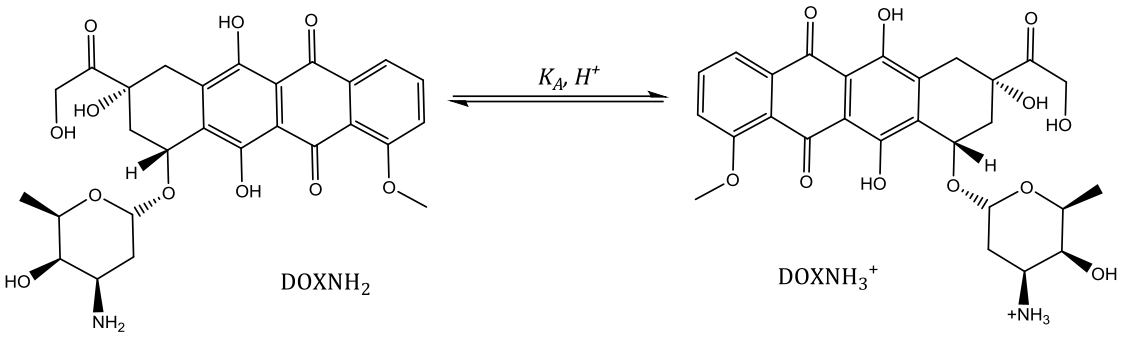

Scheme 7.2. The ionization states of DOX are governed by its acid dissociation constant (K_A) and the pH of the solution. At higher pH, the neutral base form ($DOXNH_2$) dominates while its cationic form ($DOXNH_3^+$) dominates at lower pH.

7.4.3.2 Biphasic hydrazone hydrolysis kinetics

Biphasic drug release has been observed for many micelle systems, but a consensus has not been reached on the cause of the two phases.[16, 99, 104, 205, 206] The exact reason behind the biphasic release seen herein has not been confirmed, but the most likely hypothesis relates to the ability of water/hydronium ion to penetrate the micelle core. Due to the hydrophobic nature of the core, the penetration of water (and subsequently hydronium ions) would not be a favorable interaction, but is required for acid-catalyzed hydrolysis of the hydrazone bond used to conjugate DOX to the micelle core. Based on this line of thinking, most of the

water/hydronium likely resides at the interface of the micelle core and PEG shell. The hydrophilic nature of PEG would reduce the hydrophobic effect at this interface relative to the core of the micelle. Conjugated DOX near this interface is relatively free to interact with water/hydronium because conjugation occurs on the side chains of the polyaspartate core rather than the backbone of the copolymer scaffold (i.e. more rotational freedom of DOX). Due to the high surface-area to volume ratio associated with spherical geometries, the fraction of conjugated DOX susceptible to fast release, *f*, would only require the shell/core interface to extend to 7-15% of the total radial distance of the micelle's core for values of *f* ranging from 0.2 – to 0.38. Even the value of 0.68 obtained for HYD micelles at pH 5.0 would only extend the interface to cover approximately 30% of the core's total radial distance. The slow phase of hydrazone hydrolysis kinetics also supports this theory as the core of the micelle (which is sufficiently removed from the core/shell interface) has less water to achieve hydrolysis. With less water in this region, the rate constant of this phase, k_2, should be much slower and be less sensitive to changes in pH than that expected by hydrolysis kinetics in bulk solution over the pH range studied here.[198] This is reflects the trends observed in all three formulations in regards to k_2.

Such a theory also explains the fast hydrolysis kinetics observed for ABZ and GLY micelles as *f* nearly remains constant while k_1 increases at lower pH. This observation is consistent with acid-catalyzed hydrazone hydrolysis.[198] The HYD micelles however, do not show an increase in k_1 but an increase in *f*. This would suggest penetration of water increases but the activity of hydronium does not within the micelle environment as pH is lowered. While not as straightforward as the ABZ and GLY micelles, HYD micelles may still conform to the above theory if acid supplied locally by unreacted hydrazide side chains of the polyaspartate core dominate acid catalysis.

7.5 Conclusions

DOX release from HYD, ABZ, and GLY micelles was analyzed in both acidic and neutral conditions. Irrespective of drug release conditions and formulation, micelles exhibited biphasic DOX release. A drug release model accounting for biphasic release was developed and parameters were estimated through mathematical modeling. Modeling results identified a stability issue with the hydrazone linkage used to conjugate DOX to the block copolymers stored after freeze drying. This stability issue was confirmed by two other independent methods. The impact of such a finding is significant as researchers considering the use of drug conjugation strategies employing a hydrazone linkage should be cognoscente of these stability issues and give careful consideration to validation of conjugation stability at the storage conditions selected. Failure to do so could lead to poor efficacy results in preclinical testing if particles with this stability issue are administered after a period of time in which drug conjugation has started to degrade.

In addition to the stability issue, mathematical modeling also revealed pH-sensitive DOX partitioning was present in all three micelle formulations. Due to the complexity of the micelle system, this partitioning effect also appeared to be dependent upon particle aging. This was evident because partitioning effects in the initial phase of release observed by dynamic dialysis of freshly-constituted micelle solutions was different than the partitioning captured in micelle samples used in ultrafiltration and spike experiments. (i.e. conditions where significant amounts of conjugated DOX had already been released at the point in which DOX partitioning was estimated). Future studies which can capture the change in DOX partitioning with micelle aging may be useful in the development of *in vitro/in vivo* correlations for drug release from micelle formulations.

While the variability in partition coefficient estimation was high, its effect on drug release kinetics was observed. As the fast hydrazone hydrolysis rate constants for all micelle formulations were within the same magnitude as rate constant of free DOX transport across the dialysis membrane, the initial phase of release was slowed due to the reduction in the fraction of unconjugated DOX available to permeate the dialysis membrane. This reduction driving force of DOX transport from the dialysis cassette exaggerated the initial lag in DOX release in a manner similar to that previously reported when monitoring release kinetics from liposomal formulations using dynamic dialysis.[49, 118, 197]

In addition to partitioning, hydrazone hydrolysis kinetics were quantified for all three micelle formulations and shown to be biphasic. This was attributed to the likely scenario of higher water penetration at interface of the PEG shell and micelle core than at the center of the hydrophobic core. The insertion of spacers appeared to keep the fraction of conjugated DOX that underwent fast hydrolysis similar between release studies conducted at pH 5.0 and 7.4. The spacers also appeared to have an effect on the hydrolysis rate constant within the fast phase of release. This was most evident for DOX release from ABZ micelles at pH 5.0. Hydrazone hydrolysis kinetics of DOX in the fast phase was too fast to be determined due to rate-limiting DOX transport across the dialysis membrane.

These results illustrate the usefulness of mechanistic mathematical models in the development process of micellar nanoparticles. The approach used to here develop a mechanistically-based mathematical that accounts for method-specific effects on observed drug release profiles should prove to be a useful guide for assessing release characteristics intrinsic to a particular drug/nanoparticle system.

CHAPTER EIGHT

Conclusions and Future Directions

Unlocking the full potential of nanoparticles as drug delivery vehicles requires developing rationally-design formulations with predictable properties *in vivo*. A paradigm shift from the current trial-by-error approach used to design nanoparticle formulations to a more methodical approach will only be facilitated with fundamental knowledge of the critical physicochemical properties and physiological mechanisms affecting nanoparticle performance (i.e. drug release kinetics). Mechanistic mathematical models supported by experimental studies provide a means to study these effects. The studies conducted within this thesis provide several examples of identifying physicochemical properties and environmental (sometimes even physiological) conditions through mechanistic modeling of experiments rationally designed to identify such effects. More importantly, these studies demonstrate a methodical approach for future nanoparticle formulation design and development.

The non-sink ultrafiltration method developed in chapter three provided a way to both quantify drug permeability and binding constants for liposomal drug delivery systems. This study also provided a quantitative example of the differences in release profiles due to the presence of non-sink or sink conditions. The interplay of both kinetic and thermodynamics effects on liposomal release kinetics are clearly illustrated by this study and stresses the importance for nanoparticle formulators to consider both effects when evaluating characterization studies of drug release from nanoparticulate drug delivery systems.

The results of chapter four demonstrated the applicability of the non-sink method to observe the pH-sensitivity of both liposomal topotecan release kinetics and interfacial binding at the bilayer surface. This study is also the first attempt to develop an extensive

mechanistic model for topotecan release. Developing this model required further studies to evaluate the ionization state (i.e. pKa) and kinetics of reversible, pH-dependent, ring-opening/closing of topotecan. Adaptation of the model to incorporate opening/closing of topotecan's lactone ring identified the rate-limiting effect of ring-closing on release kinetics and the observed pH permeability profile. The constants estimated by this mathematical model also laid a foundation for future studies of liposomal topotecan intended to probe effects on more sophisticated, and commonly studied, liposomal formulations of the drug.

Chapter five probed the effect of ammonia on liposomal release kinetics of actively-loaded (i.e. low intravesicular pH driven loading) topotecan. In the course of this study, a spectroscopic fluorescence method was developed to monitor liposomal release kinetics and validated with the aid of mathematical modeling. Consequently, modeling showed increases in the rate of release with increasing ammonia concentrations. The increase in release correlated with increases in intravesicular pH due to ammonia influx from the extravesicular solution. These simulations combined with the ammonia levels measured in the various release media studied (solutions or plasma) identified a correlation between accelerated release and increases in intravesicular pH rather than some other physiological effect present in the plasma samples. The implications of this observation are significant. Many liposomal delivery systems are actively-loaded and take advantage of low intravesicular pH to increase loading efficiencies and slow release. Any of these formulations will also be sensitive to ammonia influx. This study also warns of the great care that should be taken when using plasma to study release as its stability can have undue effects (i.e. acceleration) on release kinetics.

Chapter six built upon the physicochemical properties identified in Chapters 3- 5 to develop a mechanistic model capable of explaining loading and subsequent release kinetics

from actively-loaded formulation of liposomal topotecan. Mathematical modeling of active loading kinetics at 37 °C suggested uptake of cationic topotecan across the bilayer occurred as an ion-pair with chloride present in the loading solution. This prediction was confirmed with release studies which showed slower release in the absence of chloride. Using the transport mechanism suggested by modeling these loading experiments, the effect of loading temperature on topotecan release was evaluated. A mechanistic model incorporating the precipitation of a topotecan HCl salt within the liposome led to the extended release kinetics observed from topotecan loaded at 60 °C. The mechanism of transport identified for actively-loaded liposomal topotecan will aid in formulation optimization. These results suggest alterations in the levels of chloride during loading could provide a rational way to tune liposomal release kinetics of topotecan.

Lastly, chapter seven extended the approach used to mechanistically model liposomal drug release to the development of mechanistic models for the characterization of drug release from polymeric micelle nanoparticles. Experimental release studies of doxorubicin conjugated to block copolymers via a pH-sensitive hydrazone linkage were mechanistically modeled. The model-predicted instability of doxorubicin conjugation during storage was experimentally confirmed. This finding is considerable to the field of nanoparticle drug delivery systems as because many polymer-based formulations use a similar conjugation strategy, making them potentially susceptible to this stability issue. Such stability issue could greatly alter the *in vivo* performance of these nanoparticle formulations if significant storage has been incurred between synthesis and preclinical studies. In addition to stability issues, further modeling of doxorubicin release kinetics using sink and non-sink conditions revealed biphasic release and partitioning of unconjugated doxorubicin into the micelle phase. While the stability and partitioning effects complicated the interpretation of release

kinetics, these studies were still able to illustrate the kinetic and thermodynamic factors affecting release kinetics under sink and non-sink release conditions.

While the developed models within this thesis sometimes become quite complex, the same initial approach was used for the development of each model. This approach is generalized by the equation below:

$$\sum_i \frac{dM_i}{dt} = \sum_i \left[\sum_j k_j(t, r, \sum M_i\,, \sum G_i)\, M_{i,j} \right]$$

essentially, any drug species, *i*, that may undergo transport into or out of the nanoparticle must be expressed by their respective rate of change, $\frac{dM_i}{dt}$, with their sum yielding the net transport of drug from the nanoparticle. These rates are governed by the sum of kinetic processes, *j*, with each process described by a rate constant for that particular driving force, k_j, which contribute to the rates affecting the release of drug species, M_i. In some cases, this is strictly diffusion, but other kinetic factors (e.g. drug interconversion, degradation kinetics, convection) may also be incorporated as was successfully demonstrated in several chapters of this thesis. These rate constants may be a function of time, position (denoted by the variable, *r*), other drug species in solution ($\sum M_i$), as well as other excipients or solutes in solution ($\sum G_i$). In addition to these rate constants, the driving force may also be dependent upon the amount of species *i* that is susceptible to the kinetic process k_j (which is denoted by $M_{i,j}$). Two clear examples of this effect relate to the transport of only drug species unbound to the bilayer driving drug diffusion through the bilayer and the driving force governing drug transport through dialysis membranes in both liposomal and micellar drug release studies. Equilibrium constants were used throughout these chapters to solve for $M_{i,j}$ in terms of M_i. These mathematical manipulations also illustrate the mechanistic

aspect of modeling release kinetics via the incorporation of thermodynamic coefficients governing drug speciation.

While the terms comprising k_j appear to be complex functions in the generalized equation above, they can usually be simplified and assumed to be constant depending upon the conditions in which they are evaluated. Much of this work assumes constant release rate constants for the evaluation of these release studies; however, exploration of their dependence on environmental factors and consequently their dependence upon some of the variables mentioned above may be of relevance in the future development of nanoformulations. In the case of liposomal formulations, factors which alter the barrier properties of the lipid bilayer are of key importance to extending the predictability of release kinetics under *in vivo* conditions. In the actively-loaded formulations studied here, the low intravesicular pH calculated in these formulations may alter bilayer properties as lipid degradation is acid-catalyzed. The resulting lysolipids, other degradation products, or the loss of PEG over time may alter partitioning, drug diffusivity through the bilayer, interfacial drug binding, or a combination of these properties. The first three of these factors would directly alter drug permeability while the last would alter the concentration gradient of unbound drug driving drug release. Such changes may be particularly important for liposomal formulations in which release occurs over several days and remain in systemic circulation over a similar period of time. Under these circumstances, liposomal drug release may be more dependent on bilayer degradation due to many of the factors illustrated to slow release (e.g. self-association, precipitation) within this thesis.

The high concentrations of intravesicular drug observed during active-loading (in these studies and typically present in other formulations that employ a similar loading process) may also alter bilayer properties. This was partially illustrated in chapter three which

illustrated the effect of charge buildup upon the bilayer surface diminishing binding as drug concentrations increased. In this case, the driving force increases as higher drug loading is achieved. A similar scenario may also occur for neutral, highly lipophilic compounds which may exhibit much higher binding constants than topotecan. Such compounds may exhibit saturable binding if high enough intravesicular concentrations are achieved. Furthermore, the binding of pharmaceutical agents may alter the structure of the bilayer itself. One can understand this best by considering such an effect on bilayer chain ordering. Incorporation of enough drug may have effects similar to the incorporation of cholesterol on bilayer chain ordering and surface density calculations. The diffusivity of drug as well as the volume contributions of the membrane and aqueous volume may be significantly altered if enough drug is incorporated into the bilayer. Such effects may become important and require further study for liposomal formulations that incorporate more lipophilic agents. Lastly, these high intravesicular drug concentrations may also increase osmotic stress on the bilayer. Considerable effort was made to maintain isotonic conditions during release studies, but the effect of high intravesicular concentrations of drug were problematic to address as release or uptake during studies could conceivably alter intravesicular osmolality throughout the experiment. While these stresses did not seem to change particle size significantly (which would have suggested ruptured or shriveled vesicles), significant counter-transport of water across the bilayer may have occurred to compensate for the changes in intravesicular osmolality due to solute transport. The transport of water across the bilayer (and consequently its presence within the bilayer) may also alter bilayer properties and may enhance the partitioning of a TPT-Cl ion-pair within the bilayer. Enhancing ion-pair partitioning of topotecan and Cl would consequently promote its transport across the bilayer.

Developing more mechanistic approaches to modeling drug release for other nanoparticle formulations should also be explored. For polymeric micelles, identifying the factors which affect the hydrolysis kinetics of drug conjugated to the copolymers comprising the micelle may be advantageous. It may also be helpful to perform additional studies that probe the mechanism governing partitioning of unconjugated drug to the micelle core and/or its surface. Developing rational ways to test the mechanisms of drug release in other nanoformulations should also be possible if one is cognizant of the general transport equation above and correctly identifies the factors likely to govern drug transport from the nanoparticle under consideration.

As more variables affecting release kinetics are incorporated, evaluating the validity of these mechanistic mathematical models will also be of greater importance. During the course of these studies, most of the effort given to regression analysis of these mechanistic models concerned the achievement of the global minimum for the objective function and reducing correlation coefficients. Confidence in achieving the global minimum can be quite difficult when multiple data sets and parameters are fit simultaneously (as was the case in nearly every chapter of this thesis) due to a high probability of multiple local minima existing under these scenarios. Such a challenge is best addressed by careful consideration of the initial values provided for parameters to be evaluated by regression. Sensical initial values can sometimes be determined by preliminary simulations of the model using a range of parameter values. Sometimes, logical reasoning based on previous studies in the lab or from values reported in the literature (e.g. properties of similar particles or drugs) can be used to provide reasonable estimates for these initial values. At other times, especially in the case of more complex models, regression may fail when multiple parameters have similar mathematical (but mechanistically distinct) effects on fitting the data. Chapter four contains a good example of this situation as changes in both ring-opening kinetics and the

pKa of topotecan's phenol could provide similar effects on the drug's liposomal release profile. This is one of the main reasons why separate experiments were required to validate the constants for both topotecan's phenol ionization and ring-opening/closing interconversion kinetics. Further evidence of the relationship of these parameters was also observed by the correlation coefficients obtained during model fitting of these parameters.

Correlation coefficients aid in understanding the limitations of using a particular data set to provide high statistical confidence for parameters evaluated by regression. High positive or negative correlation (values approaching 1 or -1, respectively) between multiple fitted parameters will also result in poor confidence limits for those parameters in most cases. This issue may require additional experiments to isolate one or more of these parameters (as already mentioned for chapter four). Another way of circumventing this issue may be mathematical transformation of the equation or parameters of interest. Rewriting the rate constants for ring opening and closing in chapter four in terms of the ring closing rate constant and an equilibrium constant between the ring-opened and closed forms is an example of such a transformation.

Sometimes mathematical transformations may also allow the removal of bias when parameters from previous studies are used. Such was the case in chapter six. Here, an expression for topotecan's true pKa was rewritten in terms of the previously determined pKa and its ion pairing association constant with Cl. This effort was made to remove any bias ion-pairing with Cl may have contributed during the previous study which determined TPT's pKa. While such considerations remove some bias, one can argue that any of these previously determined values (whether from other studies performed by the experimenter or reported in the literature) are still only a sample mean of a population and therefore must have a measure of the variance of the sample data too. Fixing certain parameters in

this manner may lead to underestimates in the uncertainty of those parameters that are fitted. Perhaps simultaneous regression of those data sets along with the new data sets (e.g. release profiles) would provide a better assessment of the values of interest for the population. Currently, however, many of the data fitting software packages available are not capable of handling multiple data sets during regression analysis. Hopefully, further advancements in software and processing will allow such a global fit of data to be achievable.

Perhaps advancements in regression software will also provide a better statistic to determine the validity of these complex models. Most regression software packages do have some indicator of the model's ability to fit the data set. This indicator is illustrated in chapter six by the Model Selection Criterion (MSC) as it is the calculation made by the regression program used for these studies to assess goodness-of-fit. MSC, like similar values reported by other software programs, is only useful as a relative scale in the determination of whether one model or another is a better fit of a certain data set. It cannot, however, provide an absolute statistic indicating the probability that the fitted model accurately explains the data. In this thesis, the validity of a model has been handled to an extent by using parameters generated by one data set to predict the outcomes of separate experiments performed under different conditions. Another future test for model validity might be the analysis of residuals between experimental and predicted values from the fitted model. Such an analysis would speak to the scatter of data and identify systematic deviations in the data. Both of these approaches, however, only provide a qualitative demonstration of the model's validity. One possible solution may be a lack-of-fit test performed as part of the analysis of the multiple conditions fitted to the developed models during regression. This test, however, requires the ability to determine the sum of square errors attributable to the lack-of-fit (S_L) and noise of the experimental method (S_E).

Calculation of these variables, however, requires repeated experiments at the same conditions to isolate $S_{E.}$, which was not done in many of these studies. It would appear reasonable for future studies which aim to utilize such a statistical test to have at least one condition repeated to assess this error and calculate the lack-of-fit F-statistic. Assessing the sensitivity of this statistic, however, is a more complicated issue. The F-statistic calculated by the lack-of-fit test (as well as the critical F-value used to judge the probability of a lack-of-fit) is highly dependent upon the degrees of freedom associated with the model-evaluated data set. More specifically, the number of parameters, study conditions (e.g. release studies at different conditions), and total number of observations will alter the magnitude of both the experimental and critical F-values of the study. High critical F-values are an indication that the number of fitted parameters is too high for the number of conditions evaluated in the study (i.e. a statistical false negative would result). Under this scenario, the lack-of-fit test would be too insensitive for a meaningful evaluation of the model's ability to explain the data set in question. Use of this test for the evaluation of future models will thus require careful consideration of the statistical power necessary for a meaningful lack-of-fit test.

While this work provides insights that will aid in the optimization of the nanoparticle formulations studied herein, future work is still necessary to probe the issues mentioned above. Such studies will aid in the eventual prediction of *in vivo* nanoparticle drug delivery systems from *in vitro* characterization studies. Even so, these studies illustrate the advantages of a combined experimental and mechanistic modeling approach to characterize the physicochemical properties governing release in nanoparticle drug delivery systems. The studies discussed in this dissertation will provide examples for future approaches to analyzing drug release kinetics and developing models capable of predicting drug release.

References

1. Kehrer, D. F. S.; Soepenberg, O.; Loos, W. J.; Verweij, J.; Sparreboom, A. Modulation of camptothecin analogs in the treatment of cancer: a review. *Anticancer. Drugs* **2001,** *12*, 89-105.
2. Barenholz, Y. Doxil (R) - The first FDA-approved nano-drug: Lessons learned. *J. Controlled Release* **2012,** *160*, 117-134.
3. Drummond, D. C.; Noble, C. O.; Hayes, M. E.; Park, J. W.; Kirpotin, D. B. Pharmacokinetics and in vivo drug release rates in liposomal nanocarrier development. *J. Pharm. Sci.* **2008,** *97*, 4696-4740.
4. Ferrari, M., Cancer nanotechnology: opportunities and challenges. In *Nat. Rev. Cancer*, Nature Publishing Group: 2005; 'Vol.' 5, pp 161-171.
5. Torchilin, V. P. Structure and design of polymeric surfactant-based drug delivery systems. *J. Controlled Release* **2001,** *73*, 137-172.
6. Maeda, H.; Nakamura, H.; Fang, J. The EPR effect for macromolecular drug delivery to solid tumors: Improvement of tumor uptake, lowering of systemic toxicity, and distinct tumor imaging in vivo. *Adv. Drug Delivery Rev.* **2013,** *65*, 71-79.
7. Brigger, I.; Dubernet, C.; Couvreur, P. Nanoparticles in cancer therapy and diagnosis. *Adv. Drug Delivery Rev.* **2012,** *64, Supplement*, 24-36.
8. Maeda, H. The enhanced permeability and retention (EPR) effect in tumor vasculature: the key role of tumor-selective macromolecular drug targeting. *Adv. Enzyme Regul.* **2001,** *41*, 189-207.
9. Maeda, H.; Wu, J.; Sawa, T.; Matsumura, Y.; Hori, K. Tumor vascular permeability and the EPR effect in macromolecular therapeutics: a review. *J. Controlled Release* **2000,** *65*, 271-284.
10. Nagayasu, A.; Uchiyama, K.; Kiwada, H. The size of liposomes: a factor which affects their targeting efficiency to tumors and therapeutic activity of liposomal antitumor drugs. *Adv. Drug Delivery Rev.* **1999,** *40*, 75-87.
11. Campbell, R. B. Tumor Physiology and Delivery of Nanopharmaceuticals. *Anticancer Agents Med. Chem.* **2006,** *6*, 503-512.
12. Constantinides, P. P.; Chaubal, M. V.; Shorr, R. Advances in lipid nanodispersions for parenteral drug delivery and targeting. *Adv. Drug Delivery Rev.* **2008,** *60*, 757-767.
13. Holback, H.; Yeo, Y. Intratumoral Drug Delivery with Nanoparticulate Carriers. *Pharm. Res.* **2011,** *28*, 1819-1830.
14. Zhang, C.; Jugold, M.; Woenne, E. C.; Lammers, T.; Morgenstern, B.; Mueller, M. M.; Zentgraf, H.; Bock, M.; Eisenhut, M.; Semmler, W.; Kiessling, F. Specific Targeting of Tumor Angiogenesis by RGD-Conjugated Ultrasmall Superparamagnetic Iron Oxide Particles Using a Clinical 1.5-T Magnetic Resonance Scanner. *Cancer Res.* **2007,** *67*, 1555-1562.
15. Minko, T.; Pakunlu, R. I.; Wang, Y.; Khandare, J. J.; Saad, M. New Generation of Liposomal Drugs for Cancer. *Anticancer Agents Med. Chem.* **2006,** *6*, 537-552.
16. Guo, X.; Shi, C.; Wang, J.; Di, S.; Zhou, S. pH-triggered intracellular release from actively targeting polymer micelles. *Biomaterials* **2013,** *34*, 4544-4554.
17. Gao, Z.; Zhang, L.; Sun, Y. Nanotechnology applied to overcome tumor drug resistance. *J. Controlled Release* **2012,** *162*, 45-55.

18. Zhang, X.; Guo, S.; Fan, R.; Yu, M.; Li, F.; Zhu, C.; Gan, Y. Dual-functional liposome for tumor targeting and overcoming multidrug resistance in hepatocellular carcinoma cells. *Biomaterials* **2012,** *33*, 7103-7114.
19. Zhang, W.; Shi, Y.; Chen, Y.; Ye, J.; Sha, X.; Fang, X. Multifunctional Pluronic P123/F127 Mixed Polymeric Micelles Loaded With Paclitaxel for the Treatment of Multidrug Resistant Tumors. *Biomaterials* **2011,** *32*, 2894-2906.
20. Venditto, V. J.; Szoka Jr, F. C. Cancer nanomedicines: So many papers and so few drugs! *Adv. Drug Delivery Rev.* **2013,** *65*, 80-88.
21. Kirpotin, D. B.; Drummond, D. C.; Shao, Y.; Shalaby, M. R.; Hong, K.; Nielsen, U. B.; Marks, J. D.; Benz, C. C.; Park, J. W. Development of a Highly Active Nanoliposomal Irinotecan Using a Novel Intraliposomal Stabilization Strategy. *Cancer Res.* **2006,** *66*, 6732.
22. Noble, C. O.; Krauze, M. T.; Drummond, D. C.; Yamashita, Y.; Saito, R.; Berger, M. S.; Kirpotin, D. B.; Bankiewicz, K. S.; Park, J. W. Novel Nanoliposomal CPT-11 Infused by Convection-Enhanced Delivery in Intracranial Tumors: Pharmacology and Efficacy. *Cancer Res.* **2006,** *66*, 2801-2806.
23. Patankar, N.; Waterhouse, D.; Strutt, D.; Anantha, M.; Bally, M. Topophore C: a liposomal nanoparticle formulation of topotecan for treatment of ovarian cancer. *Invest. New Drugs* **2013,** *31*, 46-58.
24. Ramsay, E. C.; Anantha, M.; Zastre, J.; Meijs, M.; Zonderhuis, J.; Strutt, D.; Webb, M. S.; Waterhouse, D.; Bally, M. B. Irinophore C: A Liposome Formulation of Irinotecan with Substantially Improved Therapeutic Efficacy against a Panel of Human Xenograft Tumors. *Clin. Cancer Res.* **2008,** *14*, 1208-1217.
25. Laverman, P.; Carstens, M. G.; Boerman, O. C.; Dams, E. T. M.; Oyen, W. J.; van Rooijen, N.; Corstens, F. H.; Storm, G. Factors affecting the accelerated blood clearance of polyethylene glycol-liposomes upon repeated injection. *J. Pharmacol. Exp. Ther.* **2001,** *298*, 607-612.
26. Caron, W.; Song, G.; Kumar, P.; Rawal, S.; Zamboni, W. Interpatient pharmacokinetic and pharmacodynamic variability of carrier-mediated anticancer agents. *Clin. Pharmacol. Ther.* **2012**.
27. Zamboni, W. C.; Torchilin, V.; Patri, A. K.; Hrkach, J.; Stern, S.; Lee, R.; Nel, A.; Panaro, N. J.; Grodzinski, P. Best practices in cancer nanotechnology: perspective from NCI nanotechnology alliance. *Clin. Cancer Res.* **2012,** *18*, 3229-3241.
28. Xiang, T. X.; Anderson, B. D. Development of a combined NMR paramagnetic ion-induced line-broadening/dynamic light scattering method for permeability measurements across lipid bilayer membranes. *J. Pharm. Sci.* **1995,** *84*, 1308-1315.
29. Korstanje, L. J.; van Faassen, E. E.; Levine, Y. K. Reorientational dynamics in lipid vesicles and liposomes studied with ESR: effects of hydration, curvature and unsaturation. *Biochim. Biophys. Acta, Biomembr* **1989,** *982*, 196-204.
30. Charrois, G. J. R.; Allen, T. M. Rate of biodistribution of STEALTH® liposomes to tumor and skin: influence of liposome diameter and implications for toxicity and therapeutic activity. *Biochim. Biophys. Acta, Biomembr* **2003,** *1609*, 102-108.
31. Yuan, F.; Leunig, M.; Huang, S. K.; Berk, D. A.; Papahadjopoulos, D.; Jain, R. K. Mirovascular Permeability and Interstitial Penetration of Sterically Stabilized (Stealth) Liposomes in a Human Tumor Xenograft. *Cancer Res.* **1994,** *54*, 3352-3356.
32. Chonn, A.; Semple, S. C.; Cullis, P. R. Association of blood proteins with large unilamellar liposomes in vivo. Relation to circulation lifetimes. *J. Biol. Chem.* **1992,** *267*, 18759-18765.
33. Gabizon, A. A. Liposomal Drug Carrier Systems in Cancer Chemotherapy: Current Status and Future Prospects. *J. Drug Target.* **2002,** *10*, 535-538.
34. O'Brien, S.; Schiller, G.; Lister, J.; Damon, L.; Goldberg, S.; Aulitzky, W.; Ben-Yehuda, D.; Stock, W.; Coutre, S.; Douer, D.; Heffner, L. T.; Larson, M.; Seiter, K.; Smith, S.; Assouline, S.; Kuriakose, P.; Maness, L.; Nagler, A.; Rowe, J.; Schaich, M.; Shpilberg, O.; Yee, K.; Schmieder,

G.; Silverman, J. A.; Thomas, D.; Deitcher, S. R.; Kantarjian, H. High-Dose Vincristine Sulfate Liposome Injection for Advanced, Relapsed, and Refractory Adult Philadelphia Chromosome–Negative Acute Lymphoblastic Leukemia. *J. Clin. Oncol.* **2013,** *31*, 676-683.
35. Batist, G.; Gelmon, K. A.; Chi, K. N.; Miller, W. H.; Chia, S. K. L.; Mayer, L. D.; Swenson, C. E.; Janoff, A. S.; Louie, A. C. Safety, Pharmacokinetics, and Efficacy of CPX-1 Liposome Injection in Patients with Advanced Solid Tumors. *Clin. Cancer Res.* **2009,** *15*, 692-700.
36. Montanari, M.; Fabbri, F.; Rondini, E.; Frassineti, G. L.; Mattioli, R.; Carloni, S.; Scarpi, E.; Zoli, W.; Amadori, D.; Cruciani, G. Phase II trial of non-pegylated liposomal doxorubicin and low-dose prednisone in second-line chemotherapy for hormone-refractory prostate cancer. *Tumori* **2012,** *98*, 696-701.
37. Koudelka, S.; Turanek, J. Liposomal paclitaxel formulations. *J Control Release* **2012,** *163*, 322-34.
38. Deeken, J. F.; Slack, R.; Weiss, G. J.; Ramanathan, R. K.; Pishvaian, M. J.; Hwang, J.; Lewandowski, K.; Subramaniam, D.; He, A. R.; Cotarla, I.; Rahman, A.; Marshall, J. L. A phase I study of liposomal-encapsulated docetaxel (LE-DT) in patients with advanced solid tumor malignancies. *Cancer Chemother. Pharmacol.* **2013,** *71*, 627-33.
39. Kaspers, G. J.; Zimmermann, M.; Reinhardt, D.; Gibson, B. E.; Tamminga, R. Y.; Aleinikova, O.; Armendariz, H.; Dworzak, M.; Ha, S. Y.; Hasle, H.; Hovi, L.; Maschan, A.; Bertrand, Y.; Leverger, G. G.; Razzouk, B. I.; Rizzari, C.; Smisek, P.; Smith, O.; Stark, B.; Creutzig, U. Improved outcome in pediatric relapsed acute myeloid leukemia: results of a randomized trial on liposomal daunorubicin by the International BFM Study Group. *J. Clin. Oncol.* **2013,** *31*, 599-607.
40. Mamot, C.; Ritschard, R.; Wicki, A.; Stehle, G.; Dieterle, T.; Bubendorf, L.; Hilker, C.; Deuster, S.; Herrmann, R.; Rochlitz, C. Tolerability, safety, pharmacokinetics, and efficacy of doxorubicin-loaded anti-EGFR immunoliposomes in advanced solid tumours: a phase 1 dose-escalation study. *Lancet Oncol.* **2012,** *13*, 1234-41.
41. Toy, R.; Hayden, E.; Camann, A.; Berman, Z.; Vicente, P.; Tran, E.; Meyers, J.; Pansky, J.; Peiris, P. M.; Wu, H.; Exner, A.; Wilson, D.; Ghaghada, K. B.; Karathanasis, E. Multimodal In Vivo Imaging Exposes the Voyage of Nanoparticles in Tumor Microcirculation. *ACS Nano* **2013,** *7*, 3118-3129.
42. Drummond, D. C.; Noble, C. O.; Guo, Z.; Hayes, M. E.; Connolly-Ingram, C.; Gabriel, B. S.; Hann, B.; Liu, B.; Park, J. W.; Hong, K.; Benz, C. C.; Marks, J. D.; Kirpotin, D. B. Development of a highly stable and targetable nanoliposomal formulation of topotecan. *J. Controlled Release* **2010,** *141*, 13-21.
43. Abraham, M. H.; Acree, W. E. Linear free-energy relationships for water/hexadec-1-ene and water/deca-1,9-diene partitions, and for permeation through lipid bilayers; comparison of permeation systems. *New J. Chem.* **2012,** *36*, 1798-1806.
44. Xiang, T.-X.; Anderson, B. D. Liposomal Drug Transport: A molecular Perspective From Molecular Dynamics Simulations in Lipid Bilayers. *Adv. Drug Delivery Rev.* **2006,** *58*, 1357-1378.
45. Bemporad, D.; Luttmann, C.; Essex, J. W. Behaviour of small solutes and large drugs in a lipid bilayer from computer simulations. *Biochim. Biophys. Acta, Biomembr* **2005,** *1718*, 1-21.
46. Mayer, P.; Xiang, T.-X.; Anderson, B. Independence of substituent contributions to the transport of small-molecule permeants in lipid bilayer. *AAPS PharmSci* **2000,** *2*, 40-52.
47. Overton, E. Ueber die allgemeinen osmotischen Eigenschaften der Zelle, ihre vermutlichen Ursachen und ihre Bedeutung für die Physiologie. *Vierteljahrsschr. Naturforsch. Ges. Zurich* **1899,** *44*, 88-135.

48. Overton, E. Ueber die osmotischen Eigenschaften der Zelle in ihrer Bedentung für die Toxicologie und Pharmakologie. *Vierteljahrsschr. Naturforsch. Ges. Zuerich* **1896,** *41*, 383-406.
49. Joguparthi, V.; Xiang, T.-X.; Anderson, B. D. Liposome Transport of Hydrophobic Drugs: Gel Phase Lipid Bilayer Permeability and Partitioning of the Lactone Form of a Hydrophobic Camptothecin, DB-67. *J. Pharm. Sci.* **2008,** *97*, 400-420.
50. Xiang, T.-X.; Anderson, B. D. Permeability of acetic acid across gel and liquid-crystalline lipid bilayers conforms to free-surface-area theory. *Biophys. J.* **1997,** *72*, 223-237.
51. Xiang, T. X.; Xu, Y. H.; Anderson, B. D. The Barrier Domain for Solute Permeation Varies With Lipid Bilayer Phase Structure. *J. Membr. Biol.* **1998,** *165*, 77-90.
52. Xiang, T.-X.; Anderson, B. D. Influence of Chain Ordering on the Selectivity of Dipalmitoylphosphatidylcholine Bilayer Membranes for Permeant Size and Shape. *Biophys. J.* **1998,** *75*, 2658-2671.
53. Modi, S.; Anderson, B. Bilayer Composition, Temperature, Speciation Effects and the Role of Bilayer Chain Ordering on Partitioning of Dexamethasone and its 21-Phosphate. *Pharm. Res.* **2013**, 1-16.
54. Yoshimura, T.; Maezawa, S.; Kameyama, K.; Takagi, T. Fusion of phospholipid-vesicles induced by clathrin - modulation of fused liposome size. *J. Biochem.* **1994,** *115*, 715-723.
55. Efremova, N. V.; Bondurant, B.; O'Brie, D. F.; Leckband, D. E. Measurements of Interbilayer Forces and Protein Adsorption on Uncharged Lipid Bilayers Displaying Poly(ethylene glycol) Chains†. *Biochemistry (Mosc.)* **2000,** *39*, 3441-3451.
56. Dos Santos, N.; Allen, C.; Doppen, A.-M.; Anantha, M.; Cox, K. A. K.; Gallagher, R. C.; Karlsson, G.; Edwards, K.; Kenner, G.; Samuels, L.; Webb, M. S.; Bally, M. B. Influence of poly(ethylene glycol) grafting density and polymer length on liposomes: Relating plasma circulation lifetimes to protein binding. *Biochim. Biophys. Acta, Biomembr* **2007,** *1768*, 1367-1377.
57. Ahl, P. L.; Bhatia, S. K.; Meers, P.; Roberts, P.; Stevens, R.; Dause, R.; Perkins, W. R.; Janoff, A. S. Enhancement of the in vivo circulation lifetime of -[alpha]-distearoylphosphatidylcholine liposomes: importance of liposomal aggregation versus complement opsonization. *Biochim. Biophys. Acta, Biomembr* **1997,** *1329*, 370-382.
58. Yoshikawa, W.; Akutsu, H.; Kyogoku, Y. Light-scattering properties of osmotically active liposomes. *Biochim. Biophys. Acta, Biomembr* **1983,** *735*, 397-406.
59. White, G.; Pencer, J.; Nickel, B. G.; Wood, J. M.; Hallett, F. R. Optical changes in unilamellar vesicles experiencing osmotic stress. *Biophys. J.* **1996,** *71*, 2701-2715.
60. Joguparthi, V.; Anderson, B. D. Liposomal Delivery of Hydrophobic Weak Acids: Enhancement of Drug Retention Using a High Intraliposomal pH. *J. Pharm. Sci.* **2008,** *97*, 433-454.
61. Maurer-Spurej, E.; Wong, K. F.; Maurer, N.; Fenske, D. B.; Cullis, P. R. Factors Influencing Uptake and Retention of Amino-Containing Drugs in Large Unilamellar Vesicles Exhibiting Transmembrane pH Gradients. *Biochim. Biophys. Acta, Biomembr.* **1999,** *1416*, 1-10.
62. Liu, J.-J.; Hong, R.-L.; Cheng, W.-F.; Hong, K.; Chang, F.-H.; Tseng, Y.-L. Simple and Efficient Liposomal Encapsulation of Topotecan by Ammonium Sulfate Gradient: Stability, Pharmacokinetic and Therapeutic Evaluation. *Anticancer. Drugs* **2002,** *13*, 709-717.
63. Joguparthi, V.; Feng, S.; Anderson, B. D. Determination of Intraliposomal pH and its Effect on Membrane Partitioning and Passive Loading of a Hydrophobic Camptothecin, DB-67. *Int. J. Pharm.* **2008,** *352*, 17-28.
64. Abraham, S. A.; Edwards, K.; Karlsson, G.; Hudon, N.; Mayer, L. D.; Bally, M. B. An Evaluation of Transmembrane Ion Gradient-Mediated Encapsulation of Topotecan Within Liposomes. *J. Controlled Release* **2004,** *96*, 449-461.

65. Batrakova, E. V.; Kabanov, A. V. Pluronic block copolymers: Evolution of drug delivery concept from inert nanocarriers to biological response modifiers. *J. Controlled Release* **2008,** *130*, 98-106.
66. Kozlov, M. Y.; Melik-Nubarov, N. S.; Batrakova, E. V.; Kabanov, A. V. Relationship between Pluronic Block Copolymer Structure, Critical Micellization Concentration and Partitioning Coefficients of Low Molecular Mass Solutes. *Macromolecules* **2000,** *33*, 3305-3313.
67. Wei, Z.; Hao, J.; Yuan, S.; Li, Y.; Juan, W.; Sha, X.; Fang, X. Paclitaxel-loaded Pluronic P123/F127 mixed polymeric micelles: Formulation, optimization and in vitro characterization. *Int. J. Pharm.* **2009,** *376*, 176-185.
68. Wang, Y.; Li, Y.; Zhang, L.; Fang, X. Pharmacokinetics and biodistribution of paclitaxel-loaded pluronic P105 polymeric micelles. *Arch. Pharm. Res.* **2008,** *31*, 530-538.
69. Bromberg, L. Polymeric micelles in oral chemotherapy. *J. Controlled Release* **2008,** *128*, 99-112.
70. Batrakova, E. V.; Li, S.; Li, Y.; Alakhov, V. Y.; Elmquist, W. F.; Kabanov, A. V. Distribution kinetics of a micelle-forming block copolymer Pluronic P85. *J. Controlled Release* **2004,** *100*, 389-397.
71. Frimpong, R. A.; Fraser, S.; Zach Hilt, J. Synthesis and temperature response analysis of magnetic-hydrogel nanocomposites. *Journal of Biomedical Materials Research Part A* **2007,** *80A*, 1-6.
72. Lu, D.-X.; Wen, X.-T.; Liang, J.; Zhang, X.-D.; Gu, Z.-W.; Fan, Y.-J. Novel pH-Sensitive Drug Delivery System Based on Natural Polysaccharide for Doxorubicin Release. *Chin. J. Polym. Sci.* **2008,** *26*, 369-374.
73. Haran, G.; Cohen, R.; Bar, L. K.; Barenholz, Y. Transmembrane ammonium sulfate gradients in liposomes produce efficient and stable entrapment of amphipathic weak bases. *Biochim. Biophys. Acta* **1993,** *1151*, 201-15.
74. Gaber, M. H.; Wu, N. Z.; Hong, K.; Huang, S. K.; Dewhirst, M. W.; Papahadjopoulos, D. Thermosensitive liposomes: Extravasation and release of contents in tumor microvascular networks. *International Journal of Radiation Oncology*Biology*Physics* **1996,** *36*, 1177-1187.
75. Kong, G.; Dewhirst, M. W., Review Hyperthermia and liposomes. In *Int. J. Hyperthermia*, Taylor & Francis Ltd: 1999; 'Vol.' 15, pp 345-370.
76. Ono, A.; Takeuchi, K.; Sukenari, A.; Suzuki, T.; Adachi, I.; Ueno, M. Reconsideration of Drug Release from Temperature-Sensitive Liposomes. *Biol. Pharm. Bull.* **2002,** *25*, 97-101.
77. Tai, L.-A.; Tsai, P.-J.; Wang, Y.-C.; Wang, Y.-J.; Lo, L.-W.; Yang, C.-S. Thermosensitive liposomes entrapping iron oxide nanoparticles for controllable drug release *Nanotechnology* **2009,** *20*, 9.
78. Thomas, C. R.; Ferris, D. P.; Lee, J.-H.; Choi, E.; Cho, M. H.; Kim, E. S.; Stoddart, J. F.; Shin, J.-S.; Cheon, J.; Zink, J. I. Noninvasive Remote-Controlled Release of Drug Molecules in Vitro Using Magnetic Actuation of Mechanized Nanoparticles. *J. Am. Chem. Soc.* **2010,** *132*, 10623-10625.
79. Amstad, E.; Kohlbrecher, J.; Müller, E.; Schweizer, T.; Textor, M.; Reimhult, E. Triggered Release from Liposomes through Magnetic Actuation of Iron Oxide Nanoparticle Containing Membranes. *Nano Lett.* **2011,** *11*, 1664-1670.
80. Bae, Y.; Fukushima, S.; Harada, A.; Kataoka, K. Design of environment-sensitive supramolecular assemblies for intracellular drug delivery: Polymeric micelles that are responsive to intracellular pH change. *Angew. Chem. Int. Ed.* **2003,** *42*, 4640-4643.
81. Bae, Y.; Nishiyama, N.; Fukushima, S.; Koyama, H.; Yasuhiro, M.; Kataoka, K. Preparation and Biological Characterization of Polymeric Micelle Drug Carriers with Intracellular pH-Triggered Drug Release Property: Tumor Permeability, Controlled Subcellular Drug Distribution, and Enhanced in Vivo Antitumor Efficacy. *Bioconjug. Chem.* **2005,** *16*, 122-130.

82. Bae, Y.; Kataoka, K. Intelligent polymeric micelles from functional poly(ethylene glycol)-poly(amino acid) block copolymers. *Adv Drug Deliver Rev* **2009,** *61*, 768-784.
83. Ponta, A.; Bae, Y. PEG-poly(amino acid) block copolymer micelles for tunable drug release. *Pharm. Res.* **2010,** *27*, 2330-42.
84. Seelig, A.; Seelig, J. Dynamic Structure of Fatty Acyl Chains in a Phospholipid Bilayer Measured by Deuterium Magnetic Resonance. *Biochemistry (Mosc.)* **1974,** *13*, 4839-4845.
85. Potter, S. L.; Berg, S.; Ingle, A. M.; Krailo, M.; Adamson, P. C.; Blaney, S. M. Phase 2 clinical trial of intrathecal topotecan in children with refractory leptomeningeal leukemia: a Children's Oncology Group trial (P9962). *Pediatr. Blood Cancer* **2012,** *58*, 362-5.
86. Rose, P. G.; Sill, M. W.; McMeekin, D. S.; Ahmed, A.; Salani, R.; Yamada, S. D.; Wolfson, A. H.; Fusco, N.; Fracasso, P. M. A phase I study of concurrent weekly topotecan and cisplatin chemotherapy with whole pelvic radiation therapy in locally advanced cervical cancer: a gynecologic oncology group study. *Gynecol. Oncol.* **2012,** *125*, 158-62.
87. McGonigle, K. F.; Muntz, H. G.; Vuky, J.; Paley, P. J.; Veljovich, D. S.; Greer, B. E.; Goff, B. A.; Gray, H. J.; Malpass, T. W. Combined weekly topotecan and biweekly bevacizumab in women with platinum-resistant ovarian, peritoneal, or fallopian tube cancer: results of a phase 2 study. *Cancer* **2011,** *117*, 3731-40.
88. NCI Cancer Drug Information : Topotecan Hydrochloride. http://www.cancer.gov/cancertopics/druginfo/topotecanhydrochloride
89. Pommier, Y.; Pourquier, P.; Fan, Y.; Strumberg, D. Mechanism of action of eukaryotic DNA topoisomerase I and drugs targeted to the enzyme. *Biochimica et Biophysica Acta (BBA) - Gene Structure and Expression* **1998,** *1400*, 83-105.
90. Kearney, A. S.; Patel, K.; Palepu, N. R. Preformulation studies to aid in the development of a ready-to-use injectable solution of the antitumor agent, topotecan. *Int. J. Pharm.* **1996,** *127*, 229-237.
91. Patel, K.; Kearney, A. S.; Palepu, N. R. Investigation of new degradation products arising from the encapsulation of an oil-based suspension formulation of topotecan. *Int. J. Pharm.* **1997,** *151*, 7-13.
92. Fassberg, J.; Stella, V. J. A kinetic and mechanistic study of the hydrolysis of camptothecin and some analogues. *J. Pharm. Sci.* **1992,** *81*, 676-684.
93. Mi, Z.; Malak, H.; Burke, T. G. Reduced Albumin Binding Promotes the Stability and Activity of Topotecan in Human Blood. *Biochemistry (Mosc.)* **1995,** *34*, 13722-13728.
94. Burke, T. G.; Gao, X. Stabilization of topotecan in low pH liposomes composed of distearoylphosphatidylcholine. *J. Pharm. Sci.* **1994,** *83*, 967-969.
95. Mayer, L. D.; Tai, L. C. L.; Bally, M. B.; Mitilenes, G. N.; Ginsberg, R. S.; Cullis, P. R. Characterization of liposomal systems containing doxorubicin entrapped in response to pH gradients. *Biochim. Biophys. Acta, Biomembr* **1990,** *1025*, 143-151.
96. Ramsay, E.; Alnajim, J.; Anantha, M.; Taggar, A.; Thomas, A.; Edwards, K.; Karlsson, G.; Webb, M.; Bally, M. Transition Metal-Mediated Liposomal Encapsulation of Irinotecan (CPT-11) Stabilizes the Drug in the Therapeutically Active Lactone Conformation. *Pharm. Res.* **2006,** *23*, 2799-2808.
97. Taggar, A. S.; Alnajim, J.; Anantha, M.; Thomas, A.; Webb, M.; Ramsay, E.; Bally, M. B. Copper–topotecan complexation mediates drug accumulation into liposomes. *J. Controlled Release* **2006,** *114*, 78-88.
98. NCI Cancer Drug Information: Doxorubicin hydrochloride. http://www.cancer.gov/cancertopics/druginfo/doxorubicinhydrochloride
99. Kwon, G.; Naito, M.; Yokoyama, M.; Okano, T.; Sakurai, Y.; Kataoka, K. Block copolymer micelles for drug delivery: loading and release of doxorubicin. *J. Controlled Release* **1997,** *48*, 195-201.

100. Alakhov, V.; Klinski, E.; Li, S.; Pietrzynski, G.; Venne, A.; Batrakova, E.; Bronitch, T.; Kabanov, A. Block copolymer-based formulation of doxorubicin. From cell screen to clinical trials. *Colloids and Surfaces B: Biointerfaces* **1999,** *16*, 113-134.
101. Needham, D.; Anyarambhatla, G.; Kong, G.; Dewhirst, M. W. A New Temperature-sensitive Liposome for Use with Mild Hyperthermia: Characterization and Testing in a Human Tumor Xenograft Model. *Cancer Res.* **2000,** *60*, 1197-1201.
102. Etrych, T.; Chytil, P.; Jelinkova, M.; Rihova, B.; Ulbrich, K. Synthesis of HPMA copolymers containing doxorubicin bound via a hydrazone linkage. Effect of spacer on drug release and in vitro cytotoxicity. *Macromol. Biosci.* **2002,** *2*, 43-52.
103. Krauze, M. T.; Noble, C. O.; Kawaguchi, T.; Drummond, D.; Kirpotin, D. B.; Yamashita, Y.; Kullberg, E.; Forsayeth, J.; Park, J. W.; Bankiewicz, K. S. Convection-enhanced delivery of nanoliposomal CPT-11 (irinotecan) and PEGylated liposomal doxorubicin (Doxil) in rodent intracranial brain tumor xenografts. *Neuro-oncol.* **2007,** *9*, 393-403.
104. Lee, S. J.; Bae, Y.; Kataoka, K.; Kim, D.; Lee, D. S.; Kim, S. C. In vitro release and in vivo anti-tumor efficacy of doxorubicin from biodegradable temperature-sensitive star-shaped PLGA-PEG block copolymer hydrogel. *Polymer Journal* **2008,** *40*, 171-176.
105. Pommier, Y.; Leo, E.; Zhang, H.; Marchand, C. DNA Topoisomerases and Their Poisoning by Anticancer and Antibacterial Drugs. *Chem. Biol.* **2010,** *17*, 421-433.
106. Tewey, K. M.; Chen, G. L.; Nelson, E. M.; Liu, L. F. Intercalative antitumor drugs interfere with the breakage-reunion reaction of mammalian DNA topoisomerase II. *J. Biol. Chem.* **1984,** *259*, 9182-7.
107. Sturgeon, R. J.; Schulman, S. G. Electronic absorption spectra and protolytic equilibria of doxorubicin: direct spectrophotometric determination of microconstants. *J. Pharm. Sci.* **1977,** *66*, 958-61.
108. Carvalho, F. S.; Burgeiro, A.; Garcia, R.; Moreno, A. J.; Carvalho, R. A.; Oliveira, P. J. Doxorubicin-Induced Cardiotoxicity: From Bioenergetic Failure and Cell Death to Cardiomyopathy. *Med. Res. Rev.* **2014,** *34*, 106-135.
109. Singal, P. K.; Iliskovic, N.; Li, T.; Kumar, D. Adriamycin cardiomyopathy: pathophysiology and prevention. *The FASEB Journal* **1997,** *11*, 931-6.
110. Richardson, D. S.; Johnson, S. A. Anthracyclines in haematology: preclinical studies, toxicity and delivery systems. *Blood Rev.* **1997,** *11*, 201-223.
111. Gabizon, A.; Catane, R.; Uziely, B.; Kaufman, B.; Safra, T.; Cohen, R.; Martin, F.; Huang, A.; Barenholz, Y. Prolonged circulation time and enhanced accumulation in malignant exudates of doxorubicin encapsulated in polyethylene glycol-coated liposomes. *Cancer Res.* **1994,** *54*, 987-92.
112. Mayer, L. D.; Cullis, P. R.; Bally, M. B. The Use of Transmembrane pH Gradient-Driven Drug Encapsulation in the Pharmacodynamic Evaluation of Liposomal Doxorubicin. *J. Lipos. Res.* **1994,** *4*, 529-553.
113. Gabizon, A.; Shmeeda, H.; Barenholz, Y. Pharmacokinetics of Pegylated Liposomal Doxorubicin: Review of Animal and Human Studies. *Clin. Pharmacokinet.* **2003,** *42*, 419-436.
114. Lotem, M.; Hubert, A.; Lyass, O.; et al. Skin toxic effects of polyethylene glycol–coated liposomal doxorubicin. *Arch. Dermatol.* **2000,** *136*, 1475-1480.
115. Domingo, C.; Saurina, J. An Overview of the Analytical Characterization of Nanostructured Drug Delivery Systems: Towards Green and Sustainable Pharmaceuticals: A Review. *Anal. Chim. Acta* **2012,** *744*, 8-22.
116. Mehnert, W.; Mäder, K. Solid lipid nanoparticles: Production, characterization and applications. *Adv. Drug Delivery Rev.* **2012,** *64, Supplement*, 83-101.
117. Cho, E. J.; Holback, H.; Liu, K. C.; Abouelmagd, S. A.; Park, J.; Yeo, Y. Nanoparticle Characterization: State of the Art, Challenges, and Emerging Technologies. *Mol. Pharm.* **2013,** *10*, 2093-2110.

118. Modi, S.; Anderson, B. D. Determination of Drug Release Kinetics from Nanoparticles: Overcoming Pitfalls of the Dynamic Dialysis Method. *Mol. Pharm.* **2013,** *10*, 3076-3089.
119. Gajbhiye, V.; Ganesh, N.; Barve, J.; Jain, N. K. Synthesis, Characterization and Targeting Potential of Zidovudine Loaded Sialic Acid Conjugated-Mannosylated poly(Propyleneimine) Dendrimers. *Eur. J. Pharm. Sci.* **2013,** *48*, 668-679.
120. Liko, F.; Erdoğan, S.; Özer, Y. A.; Vural, I. In vitro Studies on 5-Florouracil-Loaded DTPA-PE Containing Nanosized Pegylated Liposomes for Diagnosis and Treatment of Tumor. *J. Lipos. Res.* **2013,** *23*, 61-69.
121. Tejwani, R. W.; Anderson, B. D. Influence of Intravesicular pH Drift and Membrane Binding on the Liposomal Release of a Model Amine-Containing Permeant. *J. Pharm. Sci.* **2008,** *97*, 381-399.
122. Chen, Y.; Bose, A.; Bothun, G. D. Controlled Release from Bilayer-Decorated Magnetoliposomes via Electromagnetic Heating. *ACS Nano* **2010,** *4*, 3215-3221.
123. Babincová, M.; Cicmanec, P.; Altanerová, V.; Altaner, C.; Babinec, P. AC-magnetic field controlled drug release from magnetoliposomes: design of a method for site-specific chemotherapy. *Bioelectrochemistry* **2002,** *55*, 17-19.
124. Modi, S.; Xiang, T.-X.; Anderson, B. D. Enhanced Active Liposomal Loading of a Poorly Soluble Ionizable Drug Using Supersaturated Drug Solutions. *J. Controlled Release* **2012,** *162*, 330-339.
125. Fugit, K. D.; Anderson, B. D. The role of pH and ring-opening hydrolysis kinetics on liposomal release of topotecan. *J. Control. Release* **2014,** *174*, 88-97.
126. Fugit, K. D.; Anderson, B. D. Dynamic, Non-sink Method for the Simultaneous Determination of Drug Permeability and Binding Coefficients in Liposomes. *Mol. Pharm.* **2014,** *11*, 1314-1325.
127. Čeh, B.; Lasic, D. D. A Rigorous Theory of Remote Loading of Drugs Into Liposomes. *Langmuir* **1995,** *11*, 3356-3368.
128. Čeh, B.; Lasic, D. D. A Rigorous Theory of Remote Loading of Drugs into Liposomes: Transmembrane Potential and Induced pH-Gradient Loading and Leakage of Liposomes. *J. Colloid Interface Sci.* **1997,** *185*, 9-18.
129. Tejwani, R. W.; Stouch, T. R.; Anderson, B. D. Substituent Effects on the Ionization and Partitioning of p-(Aminoethyl)Phenols and Structurally Related Compounds: Electrostatic Effects Dependent on Conformation. *J. Pharm. Sci.* **2009,** *98*, 4534-4544.
130. Fugit, K. D.; Anderson, B. D. The Role of pH and Ring-Opening Hydrolysis Kinetics on Liposomal Release of Topotecan. *J. Controlled Release* **2014,** *174*, 88-97.
131. Franzen, U.; Østergaard, J. Physico-Chemical Characterization of Liposomes and Drug Substance–Lliposome Interactions in Pharmaceutics Using Capillary Electrophoresis and Electrokinetic Chromatography. *J. Chromatogr. A* **2012,** *1267*, 32-44.
132. Park, J.; Cho, Y.; Son, Y.; Kim, K.; Chung, H.; Jeong, S.; Choi, K.; Park, C.; Park, R.-W.; Kim, I.-S.; Kwon, I. Preparation and Characterization of Self-Assembled Nanoparticles Based on Glycol Chitosan Bearing Adriamycin. *Colloid Polym. Sci.* **2006,** *284*, 763-770.
133. Ferraretto, A.; Sonnino, S.; Soria, M. R.; Masserini, M. Characterization of Biotinylated Liposomes Sensitive to Temperature and pH: New Tools for Anti-Cancer Drug Delivery. *Chem. Phys. Lipids* **1996,** *82*, 133-139.
134. Atyabi, F.; Farkhondehfai, A.; Esmaeili, F.; Dinarvand, R. Preparation of Pegylated Nano-Liposomal Formulation Containing SN-38: In vitro Characterization and in vivo Biodistribution in Mice. *Acta. Pharmaceut.* **2009,** *59*, 133.
135. Huang, C. H. A 13C and 2H Nuclear Magnetic Resonance Study of Phosphatidylcholine/Cholesterol Interactions: Characterization of Liquid-Gel Phases. *Biochemistry (Mosc.)* **1993,** *32*, 11.

136. Bocian, W.; Kawecki, R.; Bednarek, E.; Sitkowski, J.; Pietrzyk, A.; Williamson, M. P.; Hansen, P. E.; Kozerski, L. Multiple Binding Modes of the Camptothecin Family to DNA Oligomers. *Chem.-Eur. J.* **2004,** *10*, 5776-5787.
137. Strel'tsov, S.; Oleinikov, V.; Ermishov, M.; Mochalov, K.; Sukhanova, A.; Nechipurenko, Y.; Grokhovsky, S.; Zhuze, A.; Pluot, M.; Nabiev, I. Interaction of Clinically Important Human DNA Topoisomerase I Poison, Topotecan, With Double-Stranded DNA. *Biopolymers* **2003,** *72*, 442-454.
138. Strel'tsov, S. A.; Grokhovskii, S. L.; Kudelina, I. A.; Oleinikov, V. A.; Zhuze, A. L. Interaction of Topotecan, DNA Topoisomerase I Inhibitor, with Double-Stranded Polydeoxyribonucleotides. 1. Topotecan Dimerization in Solution. *Mol. Biol.* **2001,** *35*, 365-373.
139. Clerc, S.; Barenholz, Y. A Quantitative Model for Using Acridine Orange as a Transmembrane pH Gradient Probe. *Anal. Biochem.* **1998,** *259*, 104-111.
140. Zucker, D.; Marcus, D.; Barenholz, Y.; Goldblum, A. Liposome Drugs' Loading Efficiency: A Working Model Based on Loading Conditions and Drug's Physicochemical Properties. *J. Controlled Release* **2009,** *139*, 73-80.
141. Austin, R. P.; Barton, P.; Davis, A. M.; Manners, C. N.; Stansfield, M. C. The Effect of Ionic Strength on Liposome–Buffer and 1-Octanol–Buffer Distribution Coefficients. *J. Pharm. Sci.* **1998,** *87*, 599-607.
142. Grit, M.; Crommelin, D. J. A. Chemical Stability of Liposomes: Implications for Their Physical Stability. *Chem. Phys. Lipids* **1993,** *64*, 3-18.
143. Grit, M.; Crommelin, D. J. A. The Effect of Aging on the Physical Stability of Liposome Dispersions. *Chem. Phys. Lipids* **1992,** *62*, 113-122.
144. Grit, M.; de Smidt, J. H.; Struijke, A.; Crommelin, D. J. A. Hydrolysis of Phosphatidylcholine in Aqueous Liposome Dispersions. *Int. J. Pharm.* **1989,** *50*, 1-6.
145. Romiti, A.; Cox, M. C.; Sarcina, I.; Rocco, R.; D'Antonio, C.; Barucca, V.; Marchetti, P. Metronomic chemotherapy for cancer treatment: a decade of clinical studies. *Cancer Chemother. Pharmacol.* **2013**, 1-21.
146. Santana, V. M.; Zamboni, W. C.; Kirstein, M. N.; Tan, M.; Liu, T.; Gajjar, A.; Houghton, P. J.; Stewart, C. F. A Pilot Study of Protracted Topotecan Dosing Using a Pharmacokinetically Guided Dosing Approach in Children with Solid Tumors. *Clin. Cancer Res.* **2003,** *9*, 633-640.
147. Brigger, I.; Dubernet, C.; Couvreur, P. *Adv. Drug Delivery Rev.* **2002**, 631.
148. Xiang, T.-x.; Anderson, B. D. Stable Supersaturated Aqueous Solutions of Silatecan 7-t-Butyldimethylsilyl-10-Hydroxycamptothecin via Chemical Conversion in the Presence of a Chemically Modified β-Cyclodextrin. *Pharm. Res.* **2002,** *19*, 1215-1222.
149. Kodati, V. R.; Lafleur, M. Comparison between orientational and conformational orders in fluid lipid bilayers. *Biophys. J.* **1993,** *64*, 163-170.
150. Zuidam, N. J.; Crommelin, D. J. A. Chemical hydrolysis of phospholipids. *J. Pharm. Sci.* **1995,** *84*, 1113-1119.
151. di Nunzio, M. R.; Wang, Y.; Douhal, A. Structural Spectroscopy and Dynamics of Inter- and Intramolecular H-Bonding Interactions of Topotecan, a Potent Anticancer Drug, in Organic Solvents and in Aqueous Solution. *The Journal of Physical Chemistry B* **2012,** *116*, 7522-7530.
152. Epstein, J.; Michel, H. O.; Rosenblatt, D. H.; Plapinger, R. E.; Stephani, R. A.; Cook, E. Reactions of Isopropyl Methylphosphonofluoridate with Substituted Phenols. II. *J. Am. Chem. Soc.* **1964,** *86*, 4959-4963.
153. Heimburg, T. Lipid ion channels. *Biophys. Chem.* **2010,** *150*, 2-22.
154. Shirai, O.; Yoshida, Y.; Kihara, S. Voltammetric study on ion transport across a bilayer lipid membrane in the presence of a hydrophobic ion or an ionophore. *Anal. Bioanal. Chem.* **2006,** *386*, 494-505.

155. Shirai, O.; Yoshida, Y.; Kihara, S.; Ohnuki, T.; Uehara, A.; Yamana, H. Ion transport across a bilayer lipid membrane facilitated by gramicidin A - Effect of counter anions on the cation transport. *J. Electroanal. Chem.* **2006,** *595*, 53-59.
156. Burke, T. G.; Gao, X. Stabilization of topotecan in low pH liposomes composed of distearoylphosphatidylcholine. *J. Pharm. Sci.* **1994,** *83*, 967-9.
157. Bergers, G.; Hanahan, D. Modes of resistance to anti-angiogenic therapy. *Nat. Rev. Cancer* **2008,** *8*, 592-603.
158. Subramanian, D.; Muller, M. T. Liposomal encapsulation increases the activity of the topoisomerase I inhibitor topotecan. *Oncol. Res.* **1994,** *7*, 461-469.
159. Tardi, P.; Choice, E.; Masin, D.; Redelmeier, T.; Bally, M.; Madden, T. D. Liposomal encapsulation of topotecan enhances anticancer efficacy in murine and human xenograft models. *Cancer Res.* **2000,** *60*, 3389-3393.
160. Hao, Y. L.; Deng, Y. J.; Chen, Y.; Hao, A. J.; Zhang, Y.; Wang, K. Z. In-vitro cytotoxicity, in-vivo biodistribution and anti-tumour effect of PEGylated liposomal topotecan. *J. Pharm. Pharmacol.* **2005,** *57*, 1279-1287.
161. Patankar, N. A.; Waterhouse, D.; Strutt, D.; Anantha, M.; Bally, M. B. Topophore C: a liposomal nanoparticle formulation of topotecan for treatment of ovarian cancer. *Invest. New Drugs* **2013,** *31*, 46-58.
162. Errington, R. J.; Ameer-Beg, S.; Vojnovic, B.; Patterson, L. H.; Zloh, M.; Smith, P. J. Advanced microscopy solutions for monitoring the kinetics and dynamics of drug–DNA targeting in living cells. *Adv. Drug Delivery Rev.* **2005,** *57*, 153-167.
163. Huizenga, J. R.; Tangerman, A.; Gips, C. H. Determination of ammonia in biological fluids. *Ann. Clin. Biochem.* **1994,** *31*, 529-543.
164. Diaz, J.; Tornel, P. L.; Martinez, P. Reference intervals for blood ammonia in healthy subjects, determined by microdiffusion. *Clin. Chem.* **1995,** *41*, 1048.
165. Hao, Y.-L.; Deng, Y.-J.; Chen, Y.; Wang, X.-M.; Zhong, H.-J.; Suo, X.-B. *In Vitro* & *In Vivo* Studies of Different Liposomes Containing Topotecan. *Arch. Pharm. Res.* **2005,** *28*, 626-635.
166. Kirby, C.; Gregoriadis, G. Plasma-induced release of solutes from small unilamellar liposomes is associated with pore formation in the bilayers. *Biochem. J.* **1981,** *199*, 251-254.
167. Harashima, H.; Ochi, Y.; Kiwada, H. Kinetic modeling of liposome degradation in serum: effect of size and concentration of liposomes in vitro. *Biopharm. Drug Dispos.* **1994,** *15*, 217-25.
168. Harashima, H.; Hiraiwa, T.; Ochi, Y.; Kiwada, H. Size dependent liposome degradation in blood: in vivo/in vitro correlation by kinetic modeling. *J. Drug Targeting* **1995,** *3*, 253-61.
169. Barsotti, R. J. Measurement of ammonia in blood. *J. Pediatr.* **2001,** *138*, S11-9;discussion S19-20.
170. Walter, A.; Gutknecht, J. Permeability of small nonelectrolytes through lipid bilayer membranes. *J. Membr. Biol.* **1986,** *90*, 207-17.
171. Antonenko, Y. N.; Pohl, P.; Denisov, G. A. Permeation of ammonia across bilayer lipid membranes studied by ammonium ion selective microelectrodes. *Biophys. J.* **1997,** *72*, 2187-2195.
172. daCosta, K.-A.; Vrbanac, J. J.; Zeisel, S. H. The measurement of dimethylamine, trimethylamine, and trimethylamine N-oxide using capillary gas chromatography-mass spectrometry. *Anal. Biochem.* **1990,** *187*, 234-239.
173. Chobanyan, K.; Mitschke, A.; Gutzki, F.-M.; Stichtenoth, D. O.; Tsikas, D. Accurate quantification of dimethylamine (DMA) in human plasma and serum by GC–MS and GC–tandem MS as pentafluorobenzamide derivative in the positive-ion chemical ionization mode. *J. Chromatogr. B Biomed. Appl.* **2007,** *851*, 240-249.

174. Teerlink, T.; W.T. Hennekes, M.; Mulder, C.; Brulez, H. F. H. Determination of dimethylamine in biological samples by high-performance liquid chromatography. *J. Chromatogr. B Biomed. Appl.* **1997,** *691*, 269-276.
175. Harashima, H.; Kume, Y.; Yamane, C.; Kiwada, H. Kinetic modeling of liposome degradation in blood circulation. *Biopharm. Drug Dispos.* **1993,** *14*, 265-70.
176. Brusilow, S., *Determination of urine orotate and orotidine and plasma ammonium*. Wiley-Liss: New York, 1991; Vol. 345, p 357.
177. Brusilow, S. W.; Maestri, N. E. Urea cycle disorders: diagnosis, pathophysiology, and therapy. *Adv. Pediatr.* **1995,** *43*, 127-170.
178. Willson, K. J.; Nott, L. M.; Broadbridge, V. T.; Price, T. Hepatic encephalopathy associated with cancer or anticancer therapy. *Gastrointest Cancer Res* **2013,** *6*, 11-6.
179. Nakamura, M.; Kobashikawa, K.; Tamura, J.; Takaki, R.; Ohshiro, M.; Matayoshi, R.; Hirata, T.; Kinjyo, F.; Fujita, J. A case of 5-fluorouracil-induced hyperammonia after chemotherapy for metastatic colon cancer. *Nippon Shokakibyo Gakkai Zasshi* **2009,** *106*, 1744-1750.
180. Aihara, A.; Terasawa, M.; Furukawa, S.; Kasai, R.; Ito, T.; Ochiai, T.; Kumagai, Y.; Iida, M.; Yamazaki, S. [Two cases of hyperammonemic patients treated by chemotherapy for colorectal cancer]. *Gan To Kagaku Ryoho* **2012,** *39*, 839-42.
181. Nott, L.; Price, T. J.; Pittman, K.; Patterson, K.; Young, R.; Fletcher, J. Hyperammonaemic encephalopathy associated with rituximab-containing chemotherapy. *Intern. Med. J.* **2008,** *38*, 800-803.
182. Webb, M. S.; Harasym, T. O.; Masin, D.; Bally, M. B.; Mayer, L. D. Sphingomyelin-cholesterol liposomes significantly enhance the pharmacokinetic and therapeutic properties of vincristine in murine and human tumour models. *Br. J. Cancer* **1995,** *72*, 896-904.
183. Papahadjopoulos, D.; Allen, T. M.; Gabizon, A.; Mayhew, E.; Matthay, K.; Huang, S. K.; Lee, K. D.; Woodle, M. C.; Lasic, D. D.; Redemann, C. Sterically stabilized liposomes: improvements in pharmacokinetics and antitumor therapeutic efficacy. *Proc. Natl. Acad. Sci. U. S. A.* **1991,** *88*, 11460-11464.
184. La-Beck, N.; Zamboni, B.; Gabizon, A.; Schmeeda, H.; Amantea, M.; Gehrig, P.; Zamboni, W. Factors affecting the pharmacokinetics of pegylated liposomal doxorubicin in patients. *Cancer Chemother. Pharmacol.* **2012,** *69*, 43-50.
185. Bergers, G.; Hanahan, D. Modes of resistance to anti-angiogenic therapy. *Nat. Rev. Cancer* **2008,** *8*, 592-603.
186. Baxter, N. J.; Williamson, M. P.; Lilley, T. H.; Haslam, E. Stacking interactions between caffeine and methyl gallate. *J. Chem. Soc., Faraday Trans.* **1996,** *92*, 231-234.
187. Toyoshima, Y.; Thompson, T. E. Chloride flux in bilayer membranes. Chloride permeability in aqueous dispersions of single-walled, bilayer vesicles. *Biochemistry (Mosc.)* **1975,** *14*, 1525-1531.
188. Paula, S.; Volkov, A. G.; Deamer, D. W. Permeation of Halide Anions through Phospholipid Bilayers Occurs by the Solubility-Diffusion Mechanism. *Biophys. J.* **1998,** *74*, 319-327.
189. Vorobyov, I.; Olson, Timothy E.; Kim, Jung H.; Koeppe Ii, Roger E.; Andersen, Olaf S.; Allen, Toby W. Ion-Induced Defect Permeation of Lipid Membranes. *Biophys. J.* **2014,** *106*, 586-597.
190. Gutknecht, J.; Walter, A. Transport of protons and hydrochloric acid through lipid bilayer membranes. *Biochim. Biophys. Acta, Biomembr* **1981,** *641*, 183-188.
191. Vácha, R.; Jurkiewicz, P.; Petrov, M.; Berkowitz, M. L.; Böckmann, R. A.; Barucha-Kraszewska, J.; Hof, M.; Jungwirth, P. Mechanism of Interaction of Monovalent Ions with Phosphatidylcholine Lipid Membranes. *The Journal of Physical Chemistry B* **2010,** *114*, 9504-9509.

192. Wodzinska, K.; Blicher, A.; Heimburg, T. The thermodynamics of lipid ion channel formation in the absence and presence of anesthetics. BLM experiments and simulations. *Soft Matter* **2009,** *5*, 3319-3330.
193. Blume, A. Apparent molar heat capacities of phospholipids in aqueous dispersion. Effects of chain length and head group structure. *Biochemistry (Mosc.)* **1983,** *22*, 5436-5442.
194. Satoh, K. Determination of binding constants of Ca2+, Na+, and Cl− ions to liposomal membranes of dipalmitoylphosphatidylcholine at gel phase by particle electrophoresis. *Biochim. Biophys. Acta, Biomembr* **1995,** *1239*, 239-248.
195. Asenjo, J. A.; Andrews, B. A. Aqueous two-phase systems for protein separation: Phase separation and applications. *J. Chromatogr. A* **2012,** *1238*, 1-10.
196. Ferreira, L. A.; Teixeira, J. A.; Mikheeva, L. M.; Chait, A.; Zaslavsky, B. Y. Effect of salt additives on partition of nonionic solutes in aqueous PEG–sodium sulfate two-phase system. *J. Chromatogr. A* **2011,** *1218*, 5031-5039.
197. Fugit, K. D.; Anderson Bradley, D. A Dynamic, Non-sink Method for the Simultaneous Determination of Drug Permeability and Binding Coefficients in Liposomes. *Mol. Pharm.* **2014**, *In submission*.
198. Barbour, N.; Paborji, M.; Alexander, T.; Coppola, W.; Bogardus, J. Stabilization of Chimeric BR96-Doxorubicin Immunoconjugate. *Pharm. Res.* **1995,** *12*, 215-222.
199. Baker, M. A.; Gray, B. D.; OhlssonWilhelm, B. M.; Carpenter, D. C.; Muirhead, K. A. Zyn-Linked colchicines: Controlled-release lipophilic prodrugs with enhanced antitumor efficacy. *J. Controlled Release* **1996,** *40*, 89-100.
200. West, K. R.; Otto, S. Reversible covalent chemistry in drug delivery. *Curr. Drug Discovery Technol.* **2005,** *2*, 123-160.
201. Lee, H. J.; Bae, Y. Pharmaceutical differences between block copolymer self-assembled and cross-linked nanoassemblies as carriers for tunable drug release. *Pharm. Res.* **2013,** *30*, 478-88.
202. Ponta, A. G. Polymer Micelles for Tunable Drug Release and Enhanced Antitumor Efficacy. Dissertation, Univeristy of Kentucky, Lexington, KY, 2013.
203. Rice, R. G.; Do, D. D. Dissolution of a solid sphere in an unbounded, stagnant liquid. *Chem. Eng. Sci.* **2006,** *61*, 775-778.
204. Siepmann, J.; Siepmann, F. Mathematical modeling of drug delivery. *Int. J. Pharm.* **2008,** *364*, 328-343.
205. Li, F.; Danquah, M.; Mahato, R. I. Synthesis and characterization of amphiphilic lipopolymers for micellar drug delivery. *Biomacromolecules* **2010,** *11*, 2610-20.
206. Sutton, D.; Wang, S. H.; Nasongkla, N.; Gao, J. M.; Dormidontova, E. E. Doxorubicin and beta-lapachone release and interaction with micellar core materials: Experiment and modeling. *Exp. Biol. Med.* **2007,** *232*, 1090-1099.

VITA

Kyle Daniel Fugit

Birthplace: Huntsville, Alabama

Education

The University of Alabama, 2008	Bachelor of Science, with Honors
Chemical Engineering	Summa Cum Laude

Awards and Honors

UK College of Pharmacy March Publication Highlight	2014
NIH Cancer Nanotechnology Training Award	2011-2016
NSF Integrative Graduate Education and Research Training Award	2008-2011
Randall Undergraduate Research Award	2008
Tau Beta Pi Outstanding Senior Award	2008
McWane Undergraduate Research Fellowship	2007-2008
Eagle Scout	2002

Publications

Fugit, K.D. and Anderson, B.D**.** *"*The Role of pH and Ring-opening Hydrolysis Kinetics on Liposomal Release of Topotecan.*"* Journal of Controlled Release **174** (2014) 88-97.

Fugit, K.D. and Anderson, B.D**.** "Dynamic, Non-sink Method for the Simultaneous Determination of Drug Permeability and Binding Coefficients in Liposomes." Molecular Pharmaceutics **11** (2014) 1314-1325.

Fugit, K.D.; Jyoti, A.; Upreti, M.; and Anderson, B.D**. "**Insights into accelerated liposomal release of topotecan in plasma monitored by a non-invasive fluorescence spectroscopic method." Journal of Controlled Release – *in submission.*

Ponta, A. G.; **Fugit, K. D.**; Anderson, B. D.; and Bae, Y. "Mechanistic Modeling Provides Insights on Doxorubicin Release, Partitioning, and Particle Stability of Polymeric Micelles." Journal of Controlled Release – *in submission.*

Sewell, M.K.; **Fugit, K.D.**; Ankareddi, I.; Zhang, C.; Hampel, M.L.; Kim, D.H.; Brazel, C.S. "Magnetothermally-triggered drug delivery using hydrogels with imbedded cobalt ferrite, iron platinum or manganese ferrite nanoparticles." PMSE Preprints **98** (2008) 694-695.

Invited Talks

Fugit, K.D. and Anderson, B.D. "Modeling Release of Liposomal Topotecan: the Roles of Ring-Opening Hydrolysis Kinetics and pH." Pharmaceutical Graduate Student Research Meeting, University of Iowa, June 2013.

Fugit, K.D. and Anderson, B.D. "pH-Dependent Release of Liposomal Topotecan." NCI Alliance for Nanotechnology in Cancer Principle Investigators' meeting, Houston, TX, November 2012.

Fugit, K.D. and Anderson, B.D. "Characterization of Liposomal Release Kinetics of Topotecan for the Improvement of Chemotherapeutic Efficacy." Society of Medical Engineers – UA Chapter meeting, Tuscaloosa, AL, November 2012.

Fugit, K.D.; Hilt, J.Z.; and Anderson, B.D. "Methods for Characterizing Paramagnetic Nanoparticle-Loaded Liposomes for Remote Controlled Drug Release in Solid Tumors." AIChE National Convention, Nashville, TN, November 2009.